CARDIFF UNIVERSITY

Electrosurgical Vessel Sealing

by

Hayley Wyatt

A thesis submitted in partial fulfilment for
the degree of Doctor of Philosophy

Institute of Medical Engineering and Medical Physics
School of Engineering

2014

Abstract

Electrosurgical vessel sealing devices have been demonstrated to reduce patient blood loss and operative time during surgery. Whilst the benefits of such devices are widely reported there is still a large variation in the quality of the seal produced, with factors such as vessel size known to effect seal quality. The study aimed to investigate parameters affecting device performance and improve the seal quality.

The burst pressure test was used to assess the seal quality and tissue adhesion was measured using a peel test. Additionally histology techniques were used to quantify vessel morphology and found that with an increase in elastin content there was a reduction in seal quality. A number of device modifications were made, testing a selection of non-stick coatings and surface features of the shims. No coating reduced the level of tissue adhesion to the device, but results found that with a greater level of adhesion there was a reduction in seal quality. Considering the different surface features one design, a combination of longitudinal and transverse grooves, resulted in a seal failure rate of 0.0%, a significant improvement in device performance.

Two FEM's were produced to further investigate the device modifications; one in FEBio investigating the mechanical aspects of vessel sealing and the second a multiphysics model to investigate the thermal aspects of vessel sealing. Results from both FEM's showed a difference in shim performance, with the addition of surface features effecting the stress distribution within the vessel wall and the heat distribution.

Additionally DIC was used to capture the vessel sealing process, with results showing each seal was produced in a different way with different levels of tissue contraction. Research conducted demonstrated a number of significant relationships between seal quality and vessel properties, but did not find an explanation for all variation occurring.

Declaration of Authorship

This work has not been submitted in substance for any other degree or award at this or any other university or place of learning, nor is being submitted concurrently in candidature for any degree or other award.

Signed …………………………………………… (candidate)   Date…………………………………

STATEMENT 1

This thesis is being submitted in partial fulfilment of the requirements for the degree of PhD.

Signed …………………………………………… (candidate)   Date…………………………………

STATEMENT 2

This thesis is the result of my own independent work / investigation, except where otherwise stated. Other sources are acknowledged by explicit references. The views expressed are my own.

Signed …………………………………………… (candidate)   Date…………………………………

STATEMENT 3

I hereby give consent for my thesis, if accepted, to be available for photocopying and for inter-library loan, and for the title and summary to be made available to outside organisations.

Signed …………………………………………… (candidate)   Date…………………………………

STATEMENT 4

I hereby give consent for my thesis, if accepted, to be available for photocopying and for inter-library loans after expiry of a bar on access previously approved by the Academic Standards and Quality Committee.

Signed …………………………………………… (candidate)   Date…………………………………

I dedicate this to my parents, my brothers, my family and my friends

who have provided unconditional support, encouragement

and distractions throughout

Acknowledgements

Contents

List of Figures

List of Tables

List of Abbreviations

FEM	Finite element modelling
FEA	Finite element analysis
RF	Radio frequency
DIC	Digital image correlation
OA	Opening angle
BP	Burst pressure
S_G	Shim gap
C/E	Collagen / Elastin ratio
FDA	Food and drug administration
IQR	Inter quartile range
TiN	Titanium Nitride
CrN	Chromium Nitride
DLC	Diamond – like – Carbon
WS_2	Tungsten Disulphide
OD	Outer diameter
RMS	Root mean square
HiLis	High intensity LED illumination system
LED	Light emitting diode
DCO	Displacement control object
SD	Standard deviation
AC	Alternating current
DC	Direct current

Nomenclature

Statistics	
s	Correlation Coefficient
p	Calculate probability, significance value 0.05
N	Number of samples
Surface roughness calculations	
R_a	Roughness average
R_{rms}	Root mean square roughness
y_i	Vertical distance from the mean line to the ith data point
n	Number of samples
Material properties and models	
$\mu\varepsilon$	Principal strain, micro strain
λ	Stretch
μ	Ogden constant
α	Ogden constant
C_1	Material constant, neo-Hookean and Mooney-Rivlin Model
C_2	Material constant, neo-Hookean and Mooney-Rivlin Model
I_1	First invariant
I_2	Second invariant
c	Material constant, Holzapfel-Gasser model
k_1	Material constant, Holzapfel-Gasser model
k_2	Material constant, Holzapfel-Gasser model
G	Instantaneous shear modulus
M1	Ogden constant, α, within FEBio
C1	Ogden constant, μ, within FEBio
k	Bulk modulus
W	Strain energy function

1   Introduction

1.1   Introduction

The use of cautery to achieve haemostasis dates as far back as prehistoric times, where hot stones were used to achieve haemostasis. Conductive heating of tissue became a well-used medical tool as early as the sixth century BC. In the early 1900's advances were made using electricity in medicine, with Bovie, largely credited with being the father of electrosurgical devices, constructing a diathermy unit which was first used in Boston in 1926. This unit produced high frequency current delivered by a cutting loop, used for cutting, coagulation and desiccation, and was used by surgeons on previously inoperable patients. Over the next century the technology surrounding electrosurgery made huge advances and as such the technology developed into an essential tool for surgeons for a number of different surgical procedures (Massarweh *et al.*, 2006).

As the use of electrosurgical devices in surgery expanded so did the range of devices that became available to the surgeon, for example the electrosurgical morcellator was developed for removing the uterus, argon plasma coagulators were developed for controlling bleeding in the gastrointestinal tract, and cutting loops were developed for tumour removal.   The focus of this study was on electrosurgical vessel sealing devices, with these devices designed to stop bleeding and achieve haemostasis. Electrosurgical vessel sealing devices have been produced in many different designs, with the different devices being used for both laparoscopic and open surgery procedures. Such devices are used for a number of surgical procedures including haemorrhoidectomy (haemorrhoid surgery), pulmonary resection (removal of all or part of a lung), gastric resection (removal of all or part of the stomach) and hysterectomy (removal of the uterus). The devices were designed to replace the more traditional methods of achieving haemostasis such as staples and sutures (Massarweh *et al.*, 2006).

Electrosurgical vessel sealing devices work by passing a high frequency alternating current (within the radio frequency range, 3kHz – 300GHz), through the tissue,

causing the temperature of the tissue to rise (Massarweh *et al.*, 2006). Subsequently this causes the collagen within the blood vessel wall to denature, and through the application of pressure the seal is formed (Presthus *et al.*, 2003). This method has many advantages over more conventional methods of achieving haemostasis including: not leaving foreign bodies in the patient, a reduction in patient blood loss, and a reduction in operative time (Van Kesteren, 2005). Although the benefits of such devices are widely reported, there is still a significant variation in the quality of the seals produced and an inconsistency in the performance of the devices.

1.2   Preliminary Study

Prior to the commencement of this research a preliminary study was carried out as part of an undergraduate research project at Cardiff University, *Investigation into the factors affecting the quality of blood vessel seals produced using radiofrequency energy, Rosie Richards, 2010*. The study investigated the effect of various parameters on the seal quality, including force, seal width and blood vessel diameter. The quality of the seal was assessed using an industry standard burst pressure test. The study found no correlation between the variables tested and the seal quality, and found that the most influential factor in regards to seal quality was the vessel morphology, with this parameter being investigated in terms of the position along the vessel. Furthermore the study investigated the behaviour of the porcine carotid artery, using uniaxial tensile tests to determine the material parameters for an Ogden model, with this data being used to model vessel behaviour in a finite element model (FEM).

The FEM produced as part of the study modelled vessel compression and inflation in FEBio, but was a model that required significant work to improve the accuracy and simulation of compression, sealing and inflation for an electrosurgical seal. The model did not account for residual stresses, or achieve complete lumen occlusion. Although the model did model the inflation test following an electrosurgical seal, the model did not remove the shims, and therefore was of limited use. However the FEM produced as part of the study did demonstrate how such a model would

be of great use in investigating electrosurgical vessel sealing, and the author suggested that a future aim of work regarding vessel sealing should be to develop an FEM with improved accuracy.

Furthermore the study also investigated the failure of the seal, with failure occurring at or close to the centre of the seal. The failures appeared to originate at a small 'pin' hole, but the author stated that the cause of the pin holes manifesting in the seal remains unknown. The study provided a valuable insight into electrosurgical vessel sealing and presented previously unreported information further advancing the knowledge surrounding the surgical technique. Although this study did improve the understanding of electrosurgical vessel sealing, there is still a large amount of research required to fully understand the process and improve the technology. The study conducted by Richards provided an excellent starting point for the research conducted as part of this project and also in developing the aims of the project.

1.3   Aims of the Study

Existing research within the literature has suggested that vessel parameters, such as size, device parameters, such as application force, and environmental factors all affect the seal quality. Whilst significant research has been conducted to improve understanding as to how various parameters affect the seal quality, there is still a lack of understanding as to why these parameters affect the seal quality and what can be done to improve device design. It is this lack of understanding and knowledge surrounding the vessel sealing process that provided the motivation for this study. The main focus of this study was to improve the understanding of the changes that occur during the vessel sealing process and to improve the seal quality produced by an electrosurgical vessel sealing device. The study aimed to investigate the effect of vessel properties and device properties on the electrosurgical sealing process through the assessment of seal quality. The study aimed to understand why the various parameters affected the seal quality and the changes occurring during the sealing process through the use of more advanced experimental techniques and FEM.

1.3.1   Objectives of the Study

In order to achieve the thesis aims a number of study objectives were determined:

1. Experimentally examine the effect of vessel size and morphology on electrosurgical vessel seal quality

2. Develop and design modifications to the existing device and experimentally assess the performance.

3. Use digital image correlation (DIC) to investigate the changes occurring during the sealing process and to understand why the various parameters affect the seal quality.

4. Develop an FEM to model the compression of the blood vessel, and use the FEM as a tool to assess device modifications and investigate the effect of vessel morphology on vessel compression.

5. Develop an FEM to model the electrical and thermal performance of the sealing process and use the FEM as a tool to assess device modifications.

1.4   Novelty Statement

The research presented in this study provided a number of novel techniques and findings in the area of electrosurgical vessel sealing. These novel aspects of the research are summarised below;

- The relationship of the vessel morphology and vessel outer diameter with the quality of the seal was explored, considering how this relationship changed along the length of the vessel. There were a number of significant correlations: with increasing outer diameter there was a reduction in seal quality, and with an increase in elastin content there was a reduction in seal quality. Progressing along the length of the vessel there was a reduction in vessel size and elastin content leading to an increase in seal quality. Furthermore there was a relationship between elastin content and vessel diameter making it difficult to attribute the effect on seal quality to one parameter alone.

- A peel test method was presented for quantifying the level of adhesion of the blood vessel to the surface of the shims. This was the first time the adhesion of the blood vessel had been quantified.

- A number of non-stick coatings were assessed to try to reduce the level of adhesion. Although none of the coatings tested provided an improvement when compared to the pre-existing shim design, this was the first reported study to compare a number of different coatings and quantify their adhesion level.

- A number of new shim designs were created, with varying groove characteristics on the surface to assess the effect of shim design on both the level of adhesion and the quality of the seal. No study has previously conducted such an extensive test on the surface structure of the shims, quantifying both the level of adhesion and also the effect on seal quality. The results from this assessment demonstrated that one of the shim structures tested significantly improved the quality of the seal and the performance of the device.

- DIC was used to capture the sealing process; this was the first time to the author's knowledge that this testing method had been applied. The results from this study provided vital information as to the changes that occur in the tissue during the surgical procedure, and also showed that there were changes in the way the device performed during the process.

- The vessel compression model was used to compare the performance of multiple shims; again this was the first time that such an extensive study comparing five different shim designs and exploring the effect of morphology had been conducted. Furthermore this was the first time the adhesion part of the vessel sealing process had been modelled.

- The multiphysics model was used to compare the performance of multiple shims; again this was the first time such an extensive study comparing seven shim designs had been conducted. The results from this analysis were used in conjunction with the experimental data and showed that the ideal vessel sealing device had a low temperature at the surface of the shims whilst still

creating a high tissue temperature, with these properties being indicative of the shims creating a good heat distribution.

1.5   Published Outcomes

- Wyatt H, Richards R, Evans S, Pullin R, Blain E, Yang J, Relationship of tissue composition on arterial adhesion strength, European Society for Biomaterials, Dublin, 4 – 9 September, 2011

- Wyatt H, Richards R, Evans S, Pullin R, Blain E, Yang J, The effect of arterial tissue properties on adhesion strength, 4th International Conference on Mechanics of Biomaterials and Tissues, Hawaii, 11-14 December, 2011

- Wyatt H, Pullin R, Yang J, Vivien L, Le Gall M, Evans S, Comparison of Electrosurgical Vessel Sealing Devices Using Digital Image Correlation, 9th International Conference on Advances in Experimental Mechanics, 3-5 September, 2013

- Wyatt H, Richards R, Pullin R, Yang J, Blain E, Evans S, Variation in electrosurgical vessel seal quality along the length of a porcine carotid artery, planned to submit to Cardiovascular Engineering and Technology

- Wyatt H, Pullin R, Yang J, Evans S, Using Digital Image Correlation to capture the electrosurgical vessel sealing process, planned to submit to Strain

- Wyatt H, Pullin R, Yang J, Evans S, A finite element model simulating vessel compression and adhesion for an electrosurgical seal, planned to submit to Computer Methods in Biomechanics and Biomedical Engineering.

1.6   Thesis Structure

Chapter 2 provides an overview of existing literature, reviewing sealing techniques, the current knowledge relating to electrosurgical vessel sealing devices and the relevant investigation techniques. Table 1-1 shows the thesis summary for all the experimental and modelling work conducted, Chapters 3 – 6. Finally the thesis will include a general discussion, overall conclusion and future work, chapters 7, 8 and 9 respectively.

Table 1-1 Thesis Summary

Chapter	Objective of Chapter
Chapter 3 Assessment of Seal Quality and Adhesion	• Effect of vessel properties on seal quality • Details of the device modifications • Assessment of the effect of device modifications on seal quality • Details of relevant test methods
Chapter 4 Analysis of Shim Performance using Digital Image Correlation	• Details of DIC methodology used • Investigation of the changes that occur to the tissue during the vessel sealing process • Investigation into how the device modifications and variation in vessel properties affect the seal quality.
Chapter 5 FE Modelling of Vessel Compression	• Produce and validate an FE Model using FEBio to be used as a tool in assessing the performance of different shim designs.
Chapter 6 Multiphysics Modelling of Vessel Sealing	• Produce and validate a multiphysics FE Model using AutoDesk Mulitphysics Simulation to be used as a tool in assessing the performance of different shim designs.

2 Literature Review

2.1 Chapter Overview

This section will detail the relevant literature for this thesis including the function of arteries and their mechanical behaviour. Additionally the literature review will discuss different methods of vessel sealing available including the more traditional method of sutures. The principles of electrosurgical devices will be outlined and the current knowledge on the process of electrosurgical vessel sealing discussed. Finally the different factors that can affect the quality of an electrosurgical seal will be explored and different test methods used throughout existing work will be examined, including the use of finite element modelling and digital image correlation.

2.2 Artery Structure and Function

Blood vessels are part of the circulatory system, which mediates the continuous movement of all bodily fluids, with the arterial system transporting oxygen and nutrients to the tissue and the venous system returning the blood to the heart. The blood vessels of the arterial system can be broadly split into three categories: elastic arteries, muscular arteries and arterioles. Elastic arteries include the carotid artery and are typically larger in diameter and closer to the heart compared to muscular arteries (Heath *et al*., 2000). Each type of vessel has a significant variation in vessel morphology, with elastic vessels having a higher amount of elastin compared to muscular vessels. The change in morphology is a gradual change and therefore varies along the length of the vessel, for example, the proximal end of a carotid artery contains significantly more elastin than the distal end, with little variation in collagen (García *et al.*, 2011).

Arteries are made up of three layers; the tunica intima, the tunica media and the tunica adventitia (Figure 2-1). The tunica adventitia is the outermost layer of the blood vessel and is surrounded by loose connective tissue; it is primarily made up of thick bundles of collagen fibres arranged in helical structures. The tunica media is the middle layer; it is separated from the tunica adventitia and tunica intima by the

external and internal lamina respectively. The tunica media is composed of smooth muscle cells, a network of elastic and collagen fibrils and elastic laminae which separate the media into a number of fibre reinforced layers. The tunica intima is the innermost layer of an artery. It consists of a single layer of endothelial cells that rest on a thick basal membrane and subendothelial layer. The thickness of the layers varies depending on the location of the vessel within the body (Holzapfel *et al*., 2002, Holzapfel *et al*., 2000).
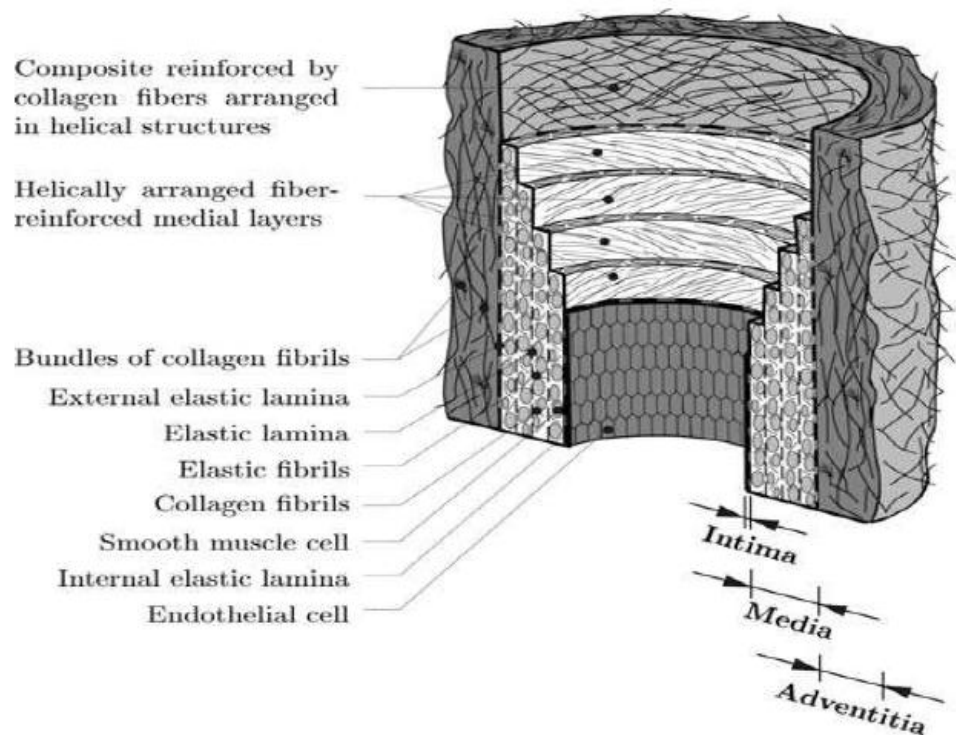
Figure 2-1 The structure of the healthy elastic artery wall, figure reproduced from Holzapfel (2000). The relative thickness of each layer is indicated (Holzapfel *et al*., 2000)

2.3 *Mechanical Characteristics of Blood Vessels*

Arteries are thick walled cylindrical tubes, which consist of three concentric layers. Each layer has specific histological features and mechanical properties, although all layers have a common general composition. The elastin fibres of each layer are arranged in an irregular matrix and display isotropic behaviour, however the collagen fibres have a highly ordered arrangement, which displays anisotropic behaviour. The overall response of arteries is highly anisotropic and non-linear, however for deformations occurring *in vivo* within the physiological range the behaviour is not vastly different to that of an isotropic material (Weizsacker, 1988).

This causes an overall anisotropic response of arteries (Holzapfel *et al.*, 2004, Gasser *et al.*, 2002). When considering the functions of the three arterial layers each have different mechanical properties. The tunica intima makes limited or no contribution to the mechanical properties; although with increasing age the tunica intima can thicken and stiffen resulting in a greater contribution to the mechanical properties. The tunica media plays the most significant role in determining the mechanical properties with the tunica adventitia becoming more important at higher pressure (Holzapfel *et al.*, 2002, Holzapfel *et al.*, 2000)

In the tunica media the orientation and close interconnection between the elastic and collagen fibrils, elastic laminae and smooth muscle cells form a continuous fibrous helix. The small pitch of the helix results in the fibrils being almost circumferentially orientated. This fibre arrangement results in the media having high strength and the ability to resist loads in both the longitudinal and circumferential direction (Holzapfel *et al.*, 2002, Holzapfel *et al.*, 2000).

In the tunica adventitia the wavy collagen fibrils are arranged in helical structures and serve to reinforce the vessel wall. The tunica adventitia is less stiff in the load free state and at low pressures compared to the tunica media layer. At higher pressures the tunica adventitia becomes stiff, preventing over stretch and rupture of the vessel. This is due to the straightening out of the collagen fibres (Holzapfel *et al.*, 2002, Holzapfel *et al.*, 2000).

2.3.1 Stress-Strain Curves

Healthy arteries are highly deformable composite structures and show a non-linear stress strain response with typical stiffening at higher pressures, with a typical stress-strain curve shown in Figure 2-2. The arterial wall expands during the systolic phase to accommodate an increase in blood volume, with the elastic lamellae dilating. The elastic lamellae are thought to dilate first due to their relatively lower stiffness when compared with collagen. In order to maintain the vessel wall shape as strain increases the collagen starts engaging, with the straightening of the wavy collagen fibrils causing the stiffening of the arterial wall. This results in the anisotropic mechanical behaviour of arteries. Loading the arterial wall beyond the physiological range often occurs during medical procedures and leads to a very

different response in terms of the mechanical properties, with the vessel typically becoming stiffer; this could in part be due to damage to the vessels (Holzapfel *et al.*, 2000, Holzapfel *et al.*, 2002, Danpinid *et al.*, 2010).
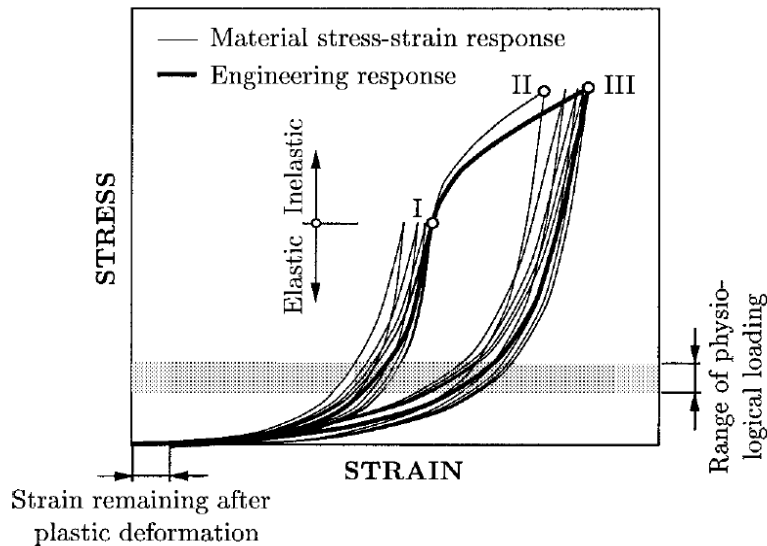
Figure 2-2 Schematic diagram of typical uniaxial stress-strain curves for circumferential arterial strips (from the media) in a passive condition: cyclic loading and unloading lead to a pre-conditioned material which behaves (perfectly) elastically or viscoelastically – point I. Loading beyond the viscoelastic domain up to point II leads to inelastic deformations. Additional loading and unloading cycles display stress softening until point III is reached. Then the material exhibits (perfectly) elastic or viscoelastic response. The thick solid line indicated the (approximate) engineering response of the material. Taken from (Holzapfel *et al.*, 2002, Holzapfel *et al.*, 2000).

2.3.2 Residual Strains and Stresses

When a ring segment is cut from an artery and a radial cut is made in the ring, the segment uncoils, demonstrating the existence of circumferential residual strains and stresses (Figure 2-3). To characterize the residual stresses the opening angle (OA) (Figure 2-3) is commonly used (Rachev *et al.*, 2003, Tain *et al.*, 2011), although this method provides an estimation of the residual stresses (Badel *et al.*, 2012).

A typical thickness to radius ratio for the porcine carotid artery is in the range 2.5 to 3, classifying the vessel as a thick walled cylinder. As such the Laplace equations are no longer valid when calculating the hoop stress and the Lamé equations must be used. When considering a thick walled cylinder the stresses vary significantly between the inner and outer wall and the shear stress can no longer be ignored as with thin walled cylinders.

(a)   (b)
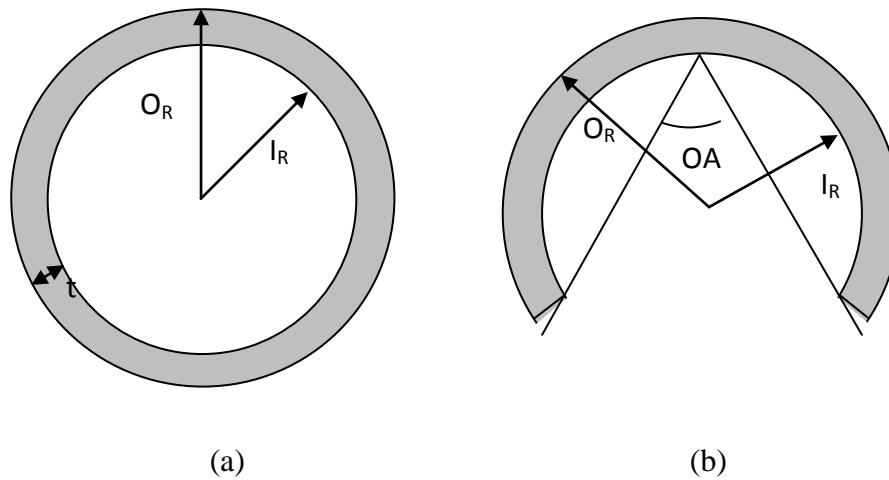
Figure 2-3 Schematic showing the load free and stress free configurations of an arterial ring segment. (a) Shows the load free configuration, the cross section is considered to be a circular ring in this state. (b) Shows the zero-stress state of an arterial ring segment once the radial cut has been made, with the residual stresses characterized by OA (Opening Angle). O_R is the outer vessel diameter, I_R is the inner vessel diameter and t is the vessel thickness.

In 1983 Fung proposed 'the principle of optimal operation'. The principle suggests that residual strains homogenise the circumferential stress distribution, ensuring the optimal performance of an artery as a load bearing thick walled structure (Fung, 1983) . A further study found that the residual strains decreased the magnitude of the stretch ratio at the inner vessel surface and increased it at the outer surface (Chuong *et al.*, 1986). In 2003 Rachev and Greenwald performed additional analysis on data collected by Fung and Chuong (1986), and discovered that residual strains increase the wall tension and mean circumferential stress. Findings agreed with the original principle proposed by Fung in that the circumferential stress distribution was homogenized, and expanded upon it further stating that the residual strains do not have a beneficial effect on the arterial function as far as blood flow was concerned, due to the residual stresses leading to a low shear stress at the vessel wall. This low shear stress encourages intimal hyperplasia (thickening of the tunica intima) which is not considered beneficial to the biomechanics of a blood vessel (Rachev *et al.*, 2003).

2.4 Vessel Sealing Techniques

There are a variety of techniques that can be used to seal blood vessels and achieve haemostasis. The use of different techniques during surgery can affect the procedure time, recovery time, blood loss and patient pain (Levy *et al*, 2003, Lee *et al*., 2003, Petrakis *et al*., 2004). Such techniques are also characterised by the burst pressure following sealing. The greater the burst pressure the greater the quality of the seal with a burst pressure of around 300mmHg being acceptable (Presthus *et al*., 2003). A number of modalities are summarised below;

2.4.1 Sutures

There are a wide variety of suturing techniques, but the underlying principle involves sealing the blood vessels using a thread liked material, and threading it through the vessel and knotting it to achieve haemostasis (Klingler *et al*., 2006). This technique can be seen in Figure 2-4. A disadvantage of this technique is the 'fiddliness' of the technique. An alternative method is endo-clips although these are prone to slipping off the vessel (Klingler *et al*., 2006) . An endo-clip is a metallic clip used to achieve haemostasis and is similar in structure to a cable tie.
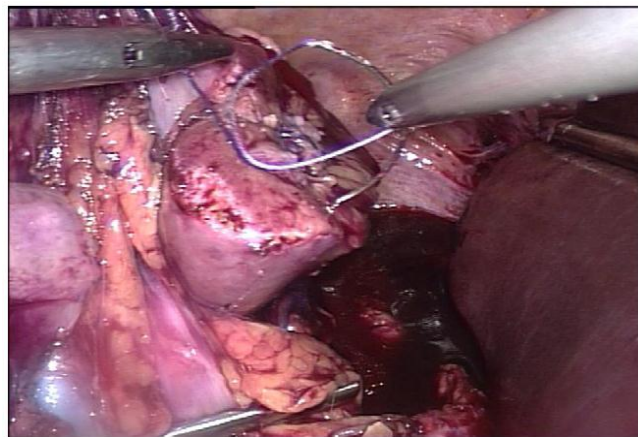
Figure 2-4 Suturing during a laparoscopic procedure. Image taken (Klingler et al., 2006)

2.4.2 Clipping / staples

Clipping or staples use a mechanical applicator to apply a clip or a staple to achieve haemostasis as seen in Figure 2-5. There are a variety of surgical clips and staples available in a range of different sizes. The main advantage of such devices is the simplicity of use, with the disadvantages of clips including the clips slipping off, and

the reloading time of the applicator. The advantages and disadvantages can be dependent upon the system used. Klinger *et al* (2006) reported titanium clips have a tendency to slip whereas the self-locking, polymer ligation system (Hem-o-lock clips) have a self-locking mechanism when applied correctly reducing the tendency to slip off. An additional advantage of clips is the ability to seal larger vessels compared with other modalities (Klingler *et al.*, 2006).

Staple systems require a large access port (12mm) due to the bulkiness of the stapler. Additionally typically more than one staple is required to achieve adequate haemostasis. Surgeons also require training to use systems as the main reason for malfunction is inappropriate use of the equipment. (Klingler *et al.*, 2006)

(a)   (b)
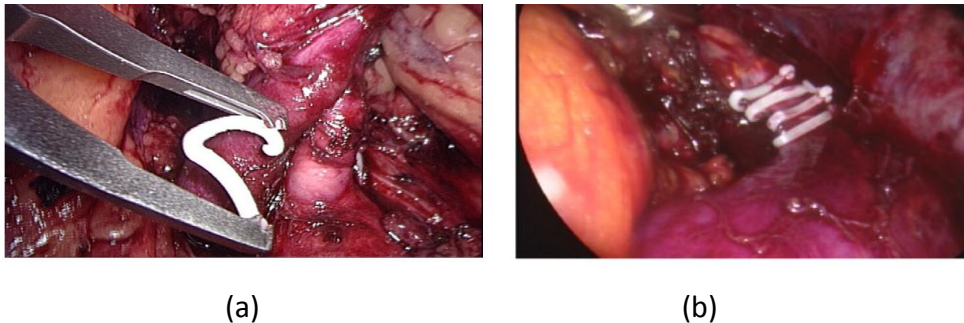
Figure 2-5 Use of clips to achieve haemostasis during laparoscopic surgery.(a) showing application of polymer ligation clips with the hook-like locking system clips and (b) showing polymer ligation clips in position. (Klingler *et al.*, 2006)

2.4.3   Ultrasonic Coagulation

Ultrasound coagulation is relatively new technology in comparison to some of the other modalities. Coagulation is achieved through the generation of frictional energy, which is transferred to the tissue as mechanical energy and heat. This results in the raising of the endothelial cells and the unveiling of the basal membrane, in addition to heating the blood. Each of these effects results in making coagulation easier to achieve. (Foschi *et al.*, 2002) There was also evidence that a certain amount of 'mixing' took place during the process of coagulation.

One issue with the use of ultrasound technology is the frequency and vibrating range. The settings typically used (Foschi *et al.*, 2002) was a frequency of 55.5 KHz and a vibrating range of 80 microns. When the frequency of the scalpel is set too high the necrosis of the wall is complete but it becomes impossible to anchor the

necrotic tissue because the method relies on the collagen retaining its fibrillar form, and the necrosis is too severe for this to be achieved. This results in the vessel being cut but not coagulated. One of the benefits of using ultrasound is that the technology can achieve a burst pressure of between 350 and 2200mmHg (Foschi *et al.*, 2002) .

2.4.4   Radiofrequency Devices

Radiofrequency (RF) devices consist of two main parts; the generator, and the device Figure 2-6. The method works by passing a high frequency electrical current through the tissue, with the voltage supplied by the generator and the current being delivered to the tissue through an electrode. Due to the resistance of the tissue, the tissue heats up causing a change in tissue structure. With an appropriate electrode, such as that seen in Figure 2-6, this system can be used to effectively seal blood vessels, with benefits including leaving no foreign bodies in the patient, saving time and money, and reduced blood loss. Although RF devices have their benefits, a major disadvantage is their ability to seal large vessels and the variation in the strength of the seal that is achieved. (Presthus *et al.*, 2003, Massarweh *et al.*, 2006) Both waveform characteristics and device characteristics affect seal quality, with the effect of these characteristics discussed in section 2.7.

(a)   (b)

Figure 2-6 The components of an RF vessel sealing system, showing (a) the system generator, and (b) the Gyrus Open Forceps, images reproduced with permission (Gyrus).

Each modality has its own benefits and limitations as summarised in Table 2-1. Further literature throughout this report will focus on radiofrequency devices, with this technology being the main subject of this thesis.
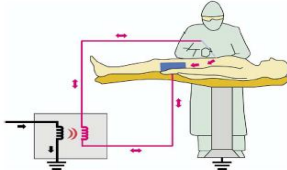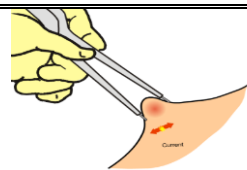
Table 2-1 A summary of the different modalities of vessel sealing. All burst pressure data taken from Harold (2003) and (Milsom *et al.*, 2012), with the remaining information taken from van Kesteren (2005) , Klingler (2006) and Pons (2009) .

Modality	Burst Pressure		Benefits	Limitations
	OD	BP (mmHg)		
RF – bipolar devices, burst pressure data for LigaSure device	2-3mm	822.6	• Shorter operative time • Overall lower operative cost • Reduced patient blood loss • Reduced post-operative pain	• Equipment can be expensive • Still a need for conventional methods • Limitations in the size of vessel capable of being sealed. • Thermal damage to vessels
	4-5mm	740.9		
	6-7mm	788.9		
Clipping / stapling (data displayed for plastic clips)	2-3mm	737	• Major vessels such as the renal vein or artery can be sealed safely • Variety of clip sizes available depending on vessel size	• Clipping can require the use to numerous clips due to slippage • Staples can require a large entry port • Foreign bodies are left in the patient • Reloading the instrument
	4-5mm	584		
	6-7mm	767		
Sutures	No data was found		• Variety of techniques available to suit skills and requirements of surgeon	• Can require specialist training • Need to sacrifice large amounts of healthy tissue • Slow
Ultrasound / harmonic scalpel	2-3mm	544.5	• Shorter operative time • Overall lower operative cost • Reduced patient blood loss • Reduced post-operative pain	• Possible problems with operating conditions due to high frequency of device • Still a need for conventional methods • Limited to vessels under 4mm in diameter. • Low burst pressure • High capital equipment cost
	4-5mm	950.8		
	6-7mm	436.5		

2.5   Basics of Electrosurgery Technology

As mentioned previously, electrosurgery works by passing a high- frequency alternating current through the tissue; this generates heat and a rise in temperature of the tissue. It was found by Morton in 1881 that passing an AC at a frequency of 100kHz through the human body would not result in pain, spasm, or burns to the patient (Massarweh *et al*., 2006). When the frequency of AC is relatively low the RF energy incites depolarization of the nerves and muscles and creates action potentials that result in muscle pain and spasm, this is known as the Faradic effect. However when higher frequency AC is applied, the pulse durations are too short for the cells to respond, and therefore there is no pain or muscle spasm (Munro, 2012). There are two main types of electrosurgery; monopolar and bipolar, with the differences between the two systems being summarised in Table 2-2.

Table 2-2 Summary of monopolar and bipolar technology (references Valleylab Website, (Massarweh *et al*., 2006, Farrugia *et al*., 2001)

	Monopolar	Bipolar
Technological Differences	The active electrode delivers the current to the treatment site. A return pad typically placed on the upper leg completes the circuit.	The electrode is both the active and return, meaning current only passes between the two surfaces of the electrode and no return pad is needed.
Advantages	• Simple in construction and low cost devices • Good haemostasis • Can coagulate tissue surface (fulguration), not available for bipolar devices	• Reduced thermal spread • Reduced risk of burns to the patient • Less chance of unintended dispersal of the current
Disadvantages	• Danger of burns to the patient due to the return pad • Electrical energy travels through the rest of the body to complete the circuit • Large thermal margin	• Complex device design both electrically and mechanically • More expensive device

Equipment for electrosurgery consists of a generator and electrode as shown in Figure 2-6 (page15). The generator controls the output waveform and thus controls the tissue effects. The tissue effect is directly related to the temperature used during the surgery, as shown in Table 2-3 the exact values vary greatly throughout the literature, but what can be widely agreed is that at a higher temperature the tissue effects are greater with cells being vaporized (cutting), and at a lower temperature the tissue effects are less extensive with tissue being desiccated (coagulation). This tissue effect can partly be controlled by the generator output (Farrugia *et al.*, 2001, Massarweh *et al.*, 2006). Figure 2-7 shows an example of the different output waveforms of a generator.
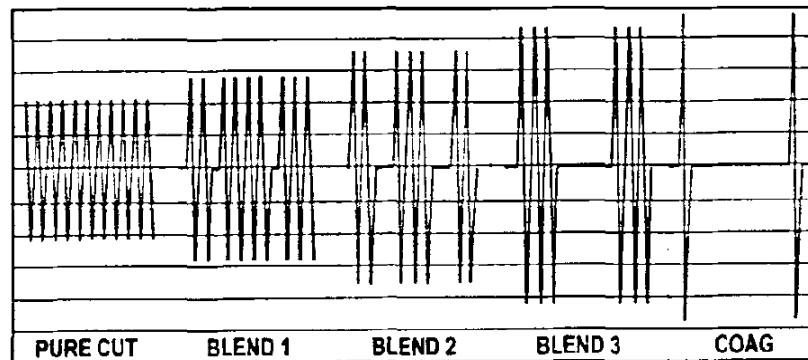
Figure 2-7 Non-modulated (cutting), blended and modulated (coagulation) current waveforms for conventional electrosurgery. Taken from (Farrugia *et al.*, 2001).

The cut waveform shown in Figure 2-7 is a non-modulated current and results in a high tissue temperature vaporising the tissue. In contrast the coagulation waveform shown is a modulated waveform, where bursts of current are separated by periods with no current flowing. This allows the heat to be dissipated in the tissue and an overall lower temperature is achieved, creating haemostasis. The three blend waveforms seen in Figure 2-7 are a combination of both the modulated and non-modulated (coagulation and cutting) waveforms, allowing greater amounts of heat dissipation and in theory, coagulation during the cutting process(Farrugia *et al.*, 2001).

This current is delivered to the tissue through an electrode, with the design of this electrode being affected by the surgical use and the desired tissue effects (Massarweh *et al.*, 2006). The size and shape of this electrode controls the current

density, a larger surface area means a lower current density; this can significantly change the tissue effects (Farrugia *et al*., 2001)**.** There are a number of different types of devices that can be used to seal vessels as seen in Figure 2-8 below. Each of these devices was designed to seal blood vessels in different applications, such as laparoscopic surgery, open surgery and different procedures within each group. Although the designs are very different the principles behind each piece of technology remain the same.

(a) Cutting forceps   (b) Halo PKS cutting forceps   (c) OMNI
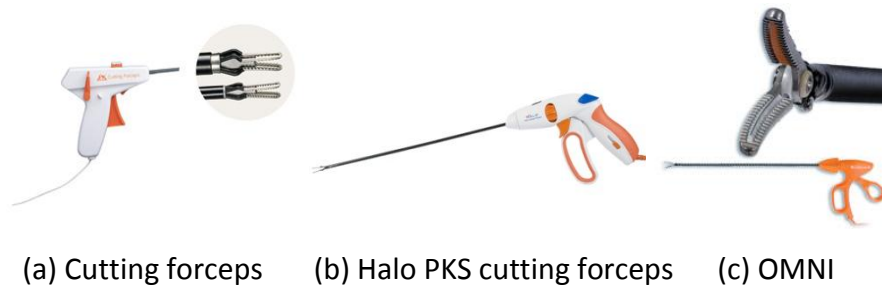
Figure 2-8 A variety of different vessel sealing devices, showing (a) the cutting forceps device, available for laparoscopy and open surgery, (b) the Halo cutting forceps for laparoscopic procedures and (c) showing OMNI used for laparoscopic procedures. All figures reproduced with permission (Gyrus)**.**

2.6 *Mechanism of Sealing and Tissue Fusion*

The mechanism for sealing blood vessels was hypothesised, with the process of denaturation being fundamental to the process (Sigel and Acevedo, 1963, Sigel *et al*, 1965, Winter *et al*., 2010). Denaturation is a process in which proteins lose the tertiary structure and secondary structure which is present in their native state, by application of some external stress of compound such as heat. A number of factors were found to influence denaturation, these include; level of hydration, mechanical loading and temperature (Wright and Humphrey, 2003). Although denaturation is affected by these factors, Wright and Humphrey report the following;

'A specific level of heating damage can be achieved via a multitude of combinations of temperature level, applied mechanical stress, and duration of heating as long as the scaled duration of heating remains the same. A potentially important clinical consequence of this equivalency is that it allows one to pick from multiple strategies that would achieve the same outcome via different paths.'

This statement is useful in suggesting that a different combination of parameters may result in the same tissue effects. The study focused on elements such as those described above, and it would be possible to expand upon this theory to improve the design of both the electrode and the generator waveform.

Winter reported that during tissue heating the triple helical structure of collagen type I monomers uncoil and transmutes to a random coiled mass of peptide chains. In compressing two tissue layers together, the peptide chains become a fused mass forming a coagulum (Winter *et al.*, 2010). This same phenomena can be described on a more basic level as the increase in heat causes the collagen and other cellular proteins to shrink and denature, and in the case of vessel sealing, it is suggested this forms a gel like substance acting as a glue between the vessel walls (Massarweh *et al.*, 2006, Presthus *et al.*, 2003). The clot was also found to take the shape of the electrode (Sigel *et al*, 1965).

Sigel *et al* (1965) found that at the site of the seal there was an alteration of the connective tissue, with a reduction in the number of cells seen and cell nucleii being fragmented (Sigel *et al*, 1965). Despite the noticeable difference the physical features of the connective tissue were retained along with the orientation of the fibres. If the vessel is subjected to more extensive coagulation the structural detail is then obliterated, resulting in a marked alteration of the elastic and collagen fibres. Sigel *et al* (1965) described this as the three stages of coagulation;

1. Produces connective tissue coagulation with preservation of fibre structure

2. amorphous coagulation

3. complete disintegration

2.7 *Factors Affecting the Quality of an Electrosurgical Seal*

Wright and Humphrey (2002) reported that the rate of denaturation can be affected by a number of factors including the level of hydration and the loading conditions of the tissue. As denaturation is thought to be a key process in the sealing of vessels it is plausible that the same conditions could directly affect the quality of the seal produced. Winter *et al* (2010) stated that the strength of the tissue connection depends on both tissue parameters and process parameters, with

protein content, and tissue thickness being classified as tissue parameters; and compressive pressure, temperature and sealing duration being classified as process parameters. These factors will be discussed further in this section.

2.7.1   Application force

Wallwiener *et al* (2008) reported that the application force the vessels are subjected to influences the overall quality of the seal. The application force of coagulating forceps is determined by both the shim gap (Figure 2-9), and also the geometry of the blood vessel. It is difficult to measure the application force directly on a device and therefore a number of studies, such as Wallwiener *et al* (2008) used a specially designed test rig, where a constant force can be applied to the vessel irrespective of vessel size.
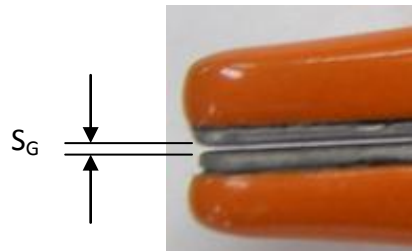
Figure 2-9 The shim gap (S_G) closed vessel sealing device

Wallwiener *et al*(2008) found an optimum force existed; if the compressive pressure was below or above this optimum force there would be a reduction in seal quality. This is difficult to achieve in reality due to current devices controlling the application force through the predetermined shim gap. Laine *et al* (1991, 2007) and Dilley *et al* (1995) stated that the optimal technique for electrocoagulation is to use the greatest force possible; with Laine *et al* (2007) reporting that increasing the application force increases the energy delivered, and also increases the coagulation depth. It should be noted that in these investigations the BICAP device was used, a probe used for achieving coagulation following complications of peptic ulceration and therefore the device was not a clamping device.

Additionally a study by Sigel *et al* (1965) suggested that if the seal is made up of excessively coagulated tissue, the seal quality is poor and it is more likely to fail. This suggestion in part supports both studies, with a greater force leading to too great a coagulation effect (Laine, 1991) and in turn a reduction in seal quality

(Wallwiener *et al.*, 2008). This concept could also be applied to a number of other properties including temperature and duration.

2.7.2 Surface Coatings and Structure

It is also thought that the shape of the shim and other surface characteristics, such as coatings and structure, can affect the quality of the seal. Novitsky *et al* (2005) reported on tissue sticking to the surface of the shims, suggesting that this could cause weakness in the seal and therefore inadvertently affect the quality of the seal. It is possible with a suitable non-stick coating that the risk of weakening the seal could be reduced, maintaining the initial strength of the seal providing the coating does not affect the electrical properties of the shims.

It may also be suggested that the shape of the seal can affect the quality of the seal produced. Sigel *et al* (1965) reported that at the site of the seal, the edges of the blood vessel take the shape of the shims, as does the clot formed. The extent to which this effects the quality of the seal is however unclear.

Additionally the structure of the shims, for example smooth or structured shims as shown in Figure 2-10, is thought to affect the quality of the seal. Richter *et al* (2006) studying the difference between devices with a structured and smooth surface found that seal failure rate was lower using clamps with a structured surface, although surface sticking was shown to increase. Dodde *et al* (2008) compared the temperature of grooved and smooth shims using a validated FE model and found a higher peak temperature for the smooth shim. This difference in temperature could account for the difference in failure rates found by Richter *et al* and highlights the importance of shim structure.

(a)	(b)
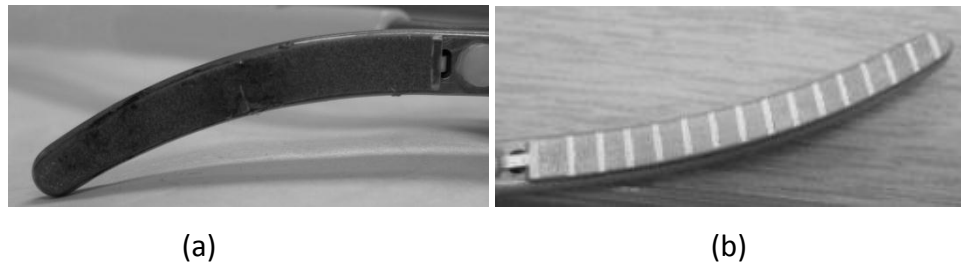
Figure 2-10 Two different shim surface showing, (a) a smooth surface and (b) a structured surface

2.7.3   Generator / Waveform Characteristics

The generator or waveform characteristics include parameters such as the duration of sealing, the current limit, the power supplied, and hence the tissue temperature. These settings are mainly controlled by the manufacturer, with the surgeon having limited control. Sigel *et al* (1965) stated that:

"Excessive heating leading to amorphous coagulation destroys the fibre arrangement of the connective tissue. One would suspect the bond not be strong because the strength of the union depends upon the integrity of the connective tissue fibres. If the bond has been comprised of excessively coagulated tissue, the vessel union has not held."

Sigel *et al* also reported that more excessive coagulation tended to be superficial on the outside blood vessel wall, meaning little or no heating effect on the inner layers of the blood vessel. The work by Sigel *et al* relates to work discussed previously by Wallweiner *et al* (2008) who suggested optimal parameters, specifically for force. It is thought that excessive coagulation, either due to excessive force, temperature, or duration would lead to a weakened seal and optimal parameters need to be determined. Additionally work by Wright and Humphrey (2003) suggested the same effect could be reached through a different route, for example reducing the temperature and increasing the duration, therefore all parameters should be considered as a collective not individually.

There have been various studies investigating the effect of duration on the quality of the seal, with each of these studies reporting that an increased duration leads to an improvement in seal strength (Laine, 1991, Laine *et al.*, 2007, Dilley *et al.*, 1995

and Harrison *et al.*, 1991). Laine *et al* (2007) reported the duration significantly influenced the depth of coagulation, and had a significant effect on the energy delivered and Harrison *et al* (1991) reported that increasing the duration of coagulation from 2 seconds to 20 seconds resulted in the seal strength approximately doubling. Although it should be noted a BICAP probe was used, not a clamping device.

Although no reports have been found to suggest it, it is hypothesized that if the duration of coagulation is excessively long it will lead to deterioration in seal strength. As discussed previously, work by Wallweiner *et al* (2008) and Sigel *et al* (1963, 1965) suggests optimal parameters exist.

Wallwiener *et al* (2008) stated that 'temperature is a key factor in thermal fusion as well as thermal damage'. This highlights the importance of temperature, again with optimal conditions being needed. Although it is known that temperature is a key component, it is unclear what the desired temperature is, with a wide range of values reported throughout literature (Table 2-3).

Table 2-3 Range of temperature values for different processes collected throughout literature (Sha *et al.*, 2001, Farrugia *et al.*, 2001, Kato *et al.*, 1998, Hayashi and Markel, 2001)

60°C	70°C	80°C	90°C	100°C	120°C	150°C	200°C	300°C	400°C
60°C	**Coagulation**			100°C		Carbonization 150°C		Smoke 300°C - 400°C	
	70°C Sticking 80°C						<200°C Cutting		
Reduced Sticking					<120°C				
	70°C Denature collagen 100°C								

Table 2-3 shows that temperature varies dependent on the desired tissue effect, with coagulation being achieved somewhere between 60-100°C and cutting being achieved at a temperature in excess of 200°C. Additionally the table also shows that sticking can be affected by the temperatures, which can possibly affect the quality of the seal.

Wallwiener *et al* (2008) suggested that there is an optimal temperature for bipolar coaptation, and that this optimal temperature appears to depend on the thermal capacity of the vessel, as determined by its wall thickness. Katoh *et al* (2010)

reported that adhesive strength increases with increased application temperature, and a minimum temperature of 70°C existed for complete adhesion.

In addition, work by Wallwiener *et al* (2010) quantifying thermal effects and damage, showed that after tissue desiccation had been completed the temperature of the tissue did not drop below 50°C for the following 20 seconds. Excessive temperature at sealing may result in a longer cooling down period, and tissue close to the desiccation site may be subjected to a hotter temperature, with the possibility of damage.

2.7.4   *Blood Vessel Characteristics*

Although it has been established that parameters that can be controlled such as application force and duration affect the quality of the seal, there are also factors that cannot be controlled that affect seal quality, these include blood vessel characteristics, most importantly vessel size and vessel morphology. Numerous studies investigating the seal quality have reported an inverse relationship between the size of the vessel and the strength of the seal (Dilley *et al*., 1995, Harrison *et al*., 1991, Carbonell *et al.,* 2003). Carbonell *et al* (2003) grouped vessels dependent on vessel size; 2-3mm, 4-5mm and finally 6-7mm and found that the seals became progressively weaker as the vessel became progressively larger for the 5mm laparoscopic PlasmaKinetics device (PK). Additionally Carbonell *et al* compared the performance of the PK device with the 5mm laparoscopic LigaSure device (LS), and found seal strength improved with increasing vessel diameter, the opposite of the PK device. This suggests although the vessel diameter can have an adverse effect this problem could be overcome with the correct device design.

However no correlation between vessel size and any other parameter has been reported, including burst pressure and elastin content (Sindram *et al.,* 2011). It should be noted that this investigation attempted to control vessel diameter by choosing vessels of approximately equal size. Additionally Sindram *et al (2011)* found the C/E ratio (collagen / elastin) to have the greatest correlation with burst pressure; those vessels with a high C/E ratio had the highest quality of seal. This suggests the vessel morphology can significantly influence the seal quality, a finding that supports work by Richter *et al* (2006) and Sigel *et al* (1965) who both found a

significant difference when sealing arteries and veins, with arteries producing the more successful seal. Richter *et al* suggested the difference in seal strength was due to the higher collagen and muscle content of arteries leading to an increased resistance to thermal spread. From values reported in existing literature it is unclear how much the thermal conductivity of different vessel types vary as data available for the canine femoral and carotid arteries show little variation, 0.404 and 0.449 W/mK respectively (Duck, 1990).

2.7.5   *Environmental Factors*

Additionally it is worth noting that the environment the seal is created in can affect the seal quality, with research showing that seals produced in the presence of saline are stronger than those produced in distilled water (Harrison and Morris, 1991). Although this does not directly influence electrosurgical seals, it is important as it could be used to lead to increased seal strength and it is important to be aware of when conducting *in vitro* experiments.

2.8   Variation in Vessel Sealing Methods

The process of electrosurgically sealing blood vessels is a standard surgical procedure with the major influence being the device and generator system used, with the control for the process coming from the generator. During bench testing however there can be significant variation in the method used, with both the conditions during sealing and the sealing process varying. This is important when considering the comparison of results from different studies.

Studies by Carbonell *et al* (2003) and Presthus *et al* (2003) used the vessel sealing system as provided by the manufacturer. The first of these two studies used a simple method where porcine arteries were harvested and skeletonised to remove the connective tissue. Following this the vessel diameter was measured and the seal performed (Carbonell *et al*, 2003). However in the second of these studies the vessel was pressurised to a resting pressure of 120mmHg prior to sealing(Presthus *et al.*, 2003).

Wallweiner *et al* (2008) chose to use a very different method where vessels were sealed in an incubator at 36°C and 90% humidity to mimic physiological conditions.

Additionally vessels were skeletonised similarly to other studies and warmed in a saline bath to 36°C prior to sealing Furthermore the study used specially designed jaws built into a pressure device capable of clamping the vessel with a defined vertical compressive pressure (Wallwiener *et al*., 2008).

A further variation of the vessel sealing process can be found in the study by Katoh *et al* (2010). The study used a specially designed test rig, capable of controlling compressive force, and investigating the effect of vibration on seal quality. Additionally the blood vessel tissue used was sectioned, using the test rig to seal two strips of arterial tissue together instead of sealing a blood vessel, as such the method for assessing seal quality also varied. The main advantage of using this method of tissue preparation is that the effect of vessel diameter on seal quality is eliminated, although the values recorded when assessing seal quality have no physiological meaning (Katoh *et al.*, 2010).

The methods used vary mainly in the use of a test rig to perform the electrosurgical seal, with the test rig allowing control over a number of properties that a device cannot. Although this is the case it is a device that would be required to be used in surgery and therefore using a device allows for performance similar to that during a surgical procedure.

2.9   *Assessment of Seal Quality*

Numerous studies (Presthus *et al.*, 2003, Sindram *et al.*, 2011, Wallwiener *et al.,* 2008, Carbonell, *et al* 2003) have used burst pressure testing as a method of assessing the quality of the seal produced. Burst pressure testing consists of attaching the sealed vessel to a syringe pump and infusing the vessel with a fluid, typically physiological saline, and measuring the pressure. The pressure is increased within the vessel up until the point of rupture where the maximum pressure achieved is recorded.

Presthus *et al* (2003) used burst pressure testing to assess the quality of the seal and also tested to see if the vessel could withstand a pressure of 300mmHg for 10 seconds. This criterion was chosen because it was substantially higher than physiologic human systolic pressure (120mmHg) and a time of 10 seconds was

chosen as the time it would take the vessel to refill and re-pressurise after treatment.

An alternative to using burst pressure testing is a shear tensile test (Katoh *et al.,* 2010). This method consisted of cutting strips of arterial tissue, with all samples being consistent in size, and sealing two strips together, with the two strips misaligned in the vertical direction to allow for a shear tensile test to be conducted. The strips were then fixed within a tensile test machine and the seal strength assessed. The use of mechanical testing to assess seal quality does have its limitations in that it is not physiologically relevant and the failure values recorded will not relate directly to something physiologically meaningful. However it does have benefits such as being able to exclude the effect of vessel outer diameter if the right methodology is used.

The method used by Kathoh *et al* (2010) used strips from vessels and as a result a standardised size would have been used for testing, irrespective of the outer diameter of the blood vessel. This would then isolate the effects of the thickness of the tissue and the effects of morphology. Although this is an advantage, it is possible that additional effects would become a consideration such as the strain rate of the test due to the viscoelastic nature of the tissue.

2.10 Assessing Level of Adhesion of the vessel to the instrument

There are limited studies exploring the effects of sticking during an electrosurgical procedure, with only two studies quantifying the level of adhesion. A number of studies used a qualitative method to quantify adhesion, with the user of the device assessing the level of adhesion using a numerical scale (Richter *et al.,* 2006b, Richter *et al.,* 2006a, Novitsky *et al.,* 2005). For example Richter *et al* (2006a) used a scale of 0-2, with 0 indicating no sticking, 1 indicating sticking without difficulties removing the instrument and 2 indicating sticking with difficulties removing the instrument. Although this method provides some indication of the level of adhesion, it does not quantify adhesion and therefore is subjective to the users' assessment of the level of sticking and as a result makes it difficult to compare results with similar studies or within the study itself.

Two methods for quantifying the level of adhesion following the use of an electrosurgical device were found in literature. The first of these methods was presented by Laine *et al* (1991); with sticking being quantified through the use of a balance scale and weights. The device was attached to the scale prior to testing, at 90° to the test specimen, in this case liver. The device was then activated and the procedure conducted. Following this weights were placed on the platform at the opposite end of the balance scale until the probe was pulled free from the liver surface, with the results presented in grams (Laine, 1991). The study controlled various parameters such as application force and duration and the effect this had on sticking and depth of coagulation. The study found the level of adhesion to parallel the depth of coagulation, increasing with application force and duration of application. The study did not assess the quality of an electrosurgical blood vessel seal and therefore provided no information on the effect sticking has on the quality of the seal.

The second of the two methods was presented by Hsu *et al* (2010) and involved weighing the electrode before and after sealing and thus the weight gain of the electrode. A greater gain in electrode weight indicated a greater level of adhesion following the procedure due to an increase in tissue adhered to the device. Although this method allowed for the comparison between different electrodes and their performance it did not provide data on the force required to remove the tissue from the device and therefore provided limited information on the effect of sticking on the quality of the electrosurgical seal.

Throughout the literature search no consistent method was found for quantifying the level of adhesion following an electrosurgical seal. As a result there was also very limited data available for comparison of results.

2.11 Digital Image Correlation (DIC)

Digital Image Correlation (DIC) is a non-contacting optical method used for measuring strain and displacement (Zhang and Arola, 2004). This method is commonly used for failure assessment in structures such as non-destructive testing of aircraft components (Worden *et al.*, 2010), crack growth in various materials including steel (Hamam *et al.*, 2007) and the velocity distribution in the

deformation zone of metal flow during rolling (Li *et al.*, 2003). This method also has many applications with biological tissues including; investigating the rupture of aortic aneurysms (Kim *et al.,* 2012, Kim *et al.*, 2011), monitoring the loosening in cemented total hip replacements (Zhang and Arola, 2004) and the mechanical properties of human skin (Evans and Holt, 2009). A summary of a number of key studies can be seen in Table 2-4. Due to a number of limitations with biological tissues including size, shape and the necessity of maintaining hydration, optical methods have many advantages due to being non-contact. Although there are a variety of optical methods available that are suitable for use with soft tissue, the measurement range is often small ($\leq$100 μm), limiting their application (Zhang and Arola, 2004).

Table 2-4 Summary of literature on biological applications of optical measurement systems

Paper	Application	High Contrast Pattern	Method Notes
Kim *et al* (2011)	To investigate the circumferential variations in mechanical properties of the porcine thoracic aorta	550μm microshperes were attached to the vessel wall	• Vessels were preconditioned and skeletonised • A two camera optical system was used
Zhang *et al* (2002)	Evaluate the potential to use DIC to study the mechanical behaviour of soft tissue at high strains using bovine aorta in uniaxial tension	Excess moisture on the surface of the vessel was removed and the high contrast speckle pattern was created using black enamel spray paint.	• Used flat sections of the aorta of uniform thickness • Results validated using rubber • Specimen subjected to uniaxial testing/loading • A one camera DIC system was used
Genovese (2009) and (Avril *et al.*, 2010)	Method to investigate at whole body motion of vascular segments	285 or 300 spherical beads affixed to vessel surface using cyanoacrylate glue	• Uses a one camera optical system with conical mirrors in order to investigate whole body motion of vascular segments
(Romo *et al.*, 2012)	Mechanical characterisation of the thoracic ascending aorta	Applied using spray paints	• Vessel was cut into square sections and split into individual layers • Speckle pattern was applied to the luminal surface
(Sutton *et al.*, 2008)	Make quantitative 3D displacement and strain measurements at the micro scale on mouse carotid arteries	High contrast pattern produced using white paint and toner powder	• Uses a two camera DIC system • Uses a stereomicroscope to image a small area

To capture 3D images a two camera DIC set-up is required, with the system using a pattern recognition technique to analyse images from the specimen. By acquiring images before the specimen is loaded and during the loading the software can

compare the images and produce displacement maps and thus allow strain to be computed (Zhang and Arola, 2004). One disadvantage of using DIC is that it only takes into account changes occurring on the surface of the specimen, not throughout the specimen.

In order for image acquisition to work and identify points on the specimen consistently in each image a unique pattern is required on the surface of the specimen. The ideal surface texture should be isotropic (no preferred orientation) and non-periodic. This leads to the use of random patterns such as speckle patterns. One of the key features of a good speckle pattern is high information content; information for pattern matching is available everywhere on the surface permitting the use of relatively small subsets for pattern matching(Sutton *et al*., 2009, Barton, 2012).

Following the acquisition of the images, the images are divided into subsets; these are sub-regions within the image, with their size being defined by the user. The pattern within each of these subsets is tracked to compare the displacements. This is achieved by applying a correlation function that searches for the centre points of the subsets by correlating corresponding subsets from two images until a matching intensity pattern is found. By recognition of the grey scale pattern from the non-deformed to the deformed condition information on the deformation of the specimen can be obtained (Sutton *et al*., 2009, Barton, 2012).

2.12 Finite Element Modelling

Finite element modelling (or analysis) (FEM/FEA) is a technique using computer software to simulate various scenarios and provide a detailed analysis of the mechanical behaviour. The method works by dividing the problem into non-overlapping components of simple geometry called elements, with the response of these for each element expressed in terms of a finite number of degrees of freedom. The response of the mathematical model is then considered to be an approximation of the model, obtained by connecting the collection of all the elements (Introduction to Finite Element Modelling, Berkeley). For medical applications FEM can be used to replicate procedures, compare medical devices and analyse implant performance. When considering the application to

electrosurgical vessel sealing devices, two types of FEM can be considered; mechanical analysis and multiphysics modelling. Mechanical analysis is concerned with the stresses and strains of the blood vessel during compression and the subsequent burst pressure tests and the multiphysics simulation is concerned with the electrical and thermal properties.

2.12.1 Mechanical Analysis

The mechanical analysis aspect of FEM consists of investigating the stresses and strains within the blood vessel wall. As discussed in section 2.2 and 2.3 the morphology of blood vessels varies greatly and has a significant effect on the mechanical behaviour. Through the use of FEM this effect can be eliminated, allowing for a direct comparison between devices.

2.12.1.1 Blood Vessel Models

One of the main areas of consideration for the mechanical analysis is the modelling of the blood vessel, including the geometry, number of layers and the material model. Many variations of blood vessel models exist throughout literature, with a number of these models summarised in Table 2-5.

Table 2-5 Summarising some of the various blood vessel models throughout literature

Study Primary Author (Ref)	Arterial Model Details
Perktold, *et al* 1995	• Used thin-shell structure theory to model vessel • Assumed sheel material was elastic, homogeneous and isotropic • Same approach used by Zhoa *et al* (2000)
Taylor, *et al* 1998	• Treated blood vessel as a rigid body (as a result of study type) • Focus was on modelling pulsatile blood flow
Lally, *et al* 2005	• Single layered blood vessel model • Uses a Mooney – Rivlin material model • Does not account for residual stresses
Gasser, *et al* 2007	• Models the adventitia and media layers of the blood vessel • Uses material model developed by Holzapfel and Gasser • Accounts for circumferential and axial residual stresses • Fails to achieve full lumen occlusions
Chen, *et al* 2009	• Single layered blood vessel model • Uses material model developed by Holzapfel and Gasser • Does not account for residual stresses
Famaey, *et al* 2012	• Single layered blood vessel model • Uses material model developed by Holzapfel and Gasser • Accounts for circumferential and axial residual stresses

As shown in Table 2-5 the way in which the blood vessel can be modelled varies greatly, depending on a number of factors including the function and purpose of the model. Famaey *et al* considered the vessel as a single layered structure, this was due to using rat abdominal aortas to determine the material properties, and therefore it was impossible to determine layer specific properties due to the difficulty of separating layers with a number of studies using a similar approach *(*Chen *et al.,* 2009*)(*Badel *et al.,* 2013*).* When considering the blood vessel as a single

layer model it fails to account for the different stress distributions through the layers with in the blood vessel wall, however it does result in a simpler model with a lower computational time. Gasser *et al* had a different approach and considered two layers of the vessel wall, the adventitia and media layers, stating that in a healthy artery the intimae has a limited effect on the ability of the vessel to withstand pressure (Gasser *et al.,* 2002). A two layer model provided a more realistic simulation, taking into account the different behaviour of each layer, whilst simplifying the approach by ignoring the intima layer.

2.12.1.2 Constitutive Models Summary

As discussed in the previous section, there are a number of variations in the way the blood vessel can be modelled, including the constitutive model used to model the material properties of the blood vessel wall. As discussed in Section 2.3, the mechanical behaviour of all biological soft tissues, including blood vessels, is anisotropic and displays a nonlinear stress strain relationship, with typical stiffening at higher pressures. Therefore any constitutive models to accurately represent the behaviour of soft tissues are complex. Biomechanical structural analysis should be able to provide predictions of deformation and stresses in healthy and diseased arteries to aid understanding and design of devices used with soft tissues (Simon *et al.,* 1993). A number of model examples are summarized in Table 2-6, including more recent models which take into account fibre direction and the resulting anisotropic properties, and the older models which are more representative of rubberlike materials, and provide a more simple solution to a complicated problem.

Table 2-6 Summarising a range of constitutive models used for modelling non-linear behavior

Model	Model Summary
Neo-Hookean, 1948	•Model provides a mathematically simple model for the non-linear deformation behaviour of rubberlike materials. •Single term strain energy function •Easy to treat mathematically •Poor fit to experimental data •Only applicable to low deformations
Mooney-Rivlin, 1952	• Model describes the isotropic behaviour of rubberlike materials • Uses a two term strain energy function •Gives a marginally better fit to experimental data than the Neo-Hookean model
Ogden, 1972	•Model represents the isotropic mechanical behaviour of rubberlike materials • Model is computationally simple • Uses a two or more term strain energy function • Good fit to experimental data
Weiss , 1996	• Models an incompressible, transversely isotropic, hyperelastic material • Developed for efficient finite element implementation • Includes a unit vector that describes the local fibre direction, and a strain energy function that depends on this vector • Assumes collagen fibres are responsible for the transversely isotropic behaviour •Uses a ground substance matrix, assumed this is isotropic
Holzapfel – Gasser , 2000	• Models each layer of the artery as a fibre-reinforced composite • Each layer uses the same strain energy function with different material parameters • Material parameters include parameters associated with the histological structure of arterial walls • Uses a ground substance matrix, assumed this is isotropic

The first three models shown in Table 2-6 are computationally simple and describe the behaviour of rubber like materials. The strain energy functions, *W*, for the neo-Hookean and Mooney-Rivlin models are shown in Equations 2.1 and 2.2 respectively. The neo-Hookean model has been shown not to reproduce experimental data accurately and only applies at low deformations (Holzapfel, 2000, Treloar, 1943), with the Mooney-Rivlin model only showing a marginal improvement to the neo-Hookean model (Ogden 1972). Although the neo-Hookean

model fails to reproduce experimental data it is regarded as a valid prototype for rubberlike materials and has the benefit of being computationally simple.

$$W = C_1(\lambda_1^2 + \lambda_2^2 + \lambda_3^2 - 3) = C_1(I_1 - 3)$$

Equation (2.1)

$$W = C_1(\lambda_1^2 + \lambda_2^2 + \lambda_3^2 - 3) + C_2(\lambda_1^{-2} + \lambda_2^{-2} + \lambda_3^{-2} - 3)$$

$$= C_1(I_1 - 3) + C_2(I_2 - 3)$$

Equation (2.2)

Where C_1 and C_2 are material constants and I_1 and I_2 are the first and second invariant respectively (Groves, 2012).

Out of the three models the Ogden model is the most accurate in representing the behaviour of rubberlike materials, this is due to the use of two or more terms in the strain energy functions. The Ogden model uses a strain energy function, *W*, (Equation 2.3) which is a linear combination of strain invariants (Equation 2.4). The principal stretches λ_1, λ_2, and λ_3 are used as independent variables subject to the incompressibility constraint $\lambda_1 \lambda_2 \lambda_3 = 1$. μ and α are material parameters (Ogden, 1972). For full model details and derivations please refer to (Ogden, 1972).

$$W = \mu_r W(\alpha_r)$$

Equation (2.3)

$$W(\alpha) = (\lambda_1^\alpha + \lambda_2^\alpha + \lambda_3^\alpha - 3)$$

Equation (2.4)

The final two models shown in Table 2-6 consider the material to be transversely isotropic. This means that the material is composed of a matrix material (ground substance), behaving in an isotropic manner, and one or more families of fibres. These materials have strong directional properties and account for the anisotropic behaviour of materials. The stiffness of this type of material in the fibre direction is typically much greater than in the directions orthogonal to the fibres (Holzapfel 2000) . These material models can be used to describe the behaviour of all layers of

the blood vessel, or be used to describe the behaviour of the vessel as a single layered structure (Famaey *et al.,* 2012, Gasser *et al.,* 2002). For these models to be applied to a layer specific blood vessel model, layer specific material parameters would be required including the parameters determined from the histological structure i.e. fibre orientation. The strain energy function for the Holzapfel-Gasser model is shown in Equation 2.5.

$$W = \frac{c}{2}(\bar{I_1} - 3) + \frac{k_1}{2k_2}\left\{exp\left[k_2(\bar{I_1} - 1)^2\right] - 1\right\} + \frac{k_1}{2k_2}\left\{exp\left[k_2(\bar{I_2} - 1)^2\right] - 1\right\}$$

Equation (2.5)

Where *c, k₁* and *k₂* are all material parameters.

2.12.1.3 Vessel Compression

The blood vessel models discussed previously have been used for a variety of FEM applications including arterial clamping of blood vessels. Studies investigating arterial clamping are concerned with the stresses through the blood vessel wall, and the effect of different clamp designs (Gasser *et al.,* 2002, Chen *et al.,* 2009, Famaey *et al.,* 2012, Famaey *et al.,* 2013). By examining the effect of different arterial clamps studies aim to find a clamp design that results in less damage to the arterial wall. Although these studies apply the clamping model purely to arterial clamps it is thought a similar approach can be taken in looking at the effect of different shim geometries for electrosurgical vessel sealing.

Each vessel compression model uses a number of loading steps to simulate different stages of the clamping process. The initial step accounts for the residual stress, this is through the application of prescribed constraints, taking into account residual stresses in both the axial and circumferential directions. The next step pressurises the vessel to a physiological pressure (100mmHg in and 120mmHg in) and the final step compressing the blood vessel (Gasser *et al.,* 2002).

One challenge associated with the modelling of arterial clamping is achieving complete lumen occlusion during the clamping process. Studies by both Gasser *et al* and Calvo *et al* failed to achieve complete occlusion, achieving 92% and 60% respectively, with both models failing to converge due to the high level of

deformation throughout the analysis. However more recent work, the studies by Chen *et al* and Famaey *et al* succeed in achieving complete lumen occlusion, with Famaey *et al* achieving this through the use of an explicit solver.

For nonlinear solid mechanics finite element equation solution methods are generally classed as either implicit or explicit solvers. Implicit solvers are unconditionally stable and use an iteration method to solve the problem, iterating the problem until a convergence criterion for each time step or increment. Explicit solvers reformulate equations so they can be solved directly to determine the solution at the end of the increment, without iteration. Explicit solvers however are not always stable, but if used correctly they can lead to a lower computational time (Becker, 2004, Harewood and McHugh, 2007).

2.12.2 Multiphysics Modelling

Multiphysics modelling couples multiple types of analyses together to replicate different situations, for example electrical and thermal analyses are coupled together for the simulation of electrosurgery techniques, typically with the results of the electrical analysis being used to compute temperature values in the thermal analysis. This technique has been used for a variety of applications relating to medical applications including researching shim geometry in electrosurgical vessel sealing (Dodde *at al.,* 2008), electrode design for cardiac ablation (Tungjitkusolmun *et al.,* 2000), and the effect of blood flow on tissue cooling (Jain *et al.,*2001*)*.

Multiphysics modelling can be used to optimise surgical procedures, both in the techniques and the devices used. For example Baraukas *et al* (2008) replicated the ablation process on liver tissue, this is a cancer treatment involving inserting a probe into the liver and applying RF energy to destroy tumours. The model was used to look at the size of the thermal heat destruction zone, allowing for more accurate insertion of the probe to ensure the entire tumour is within the zone . A further example of optimising a surgical procedure is work investigating electrode design during cardiac ablation. Cardiac ablation is a procedure used to treat faulty electrical pathways in hearts prone to developing cardiac arrhythmias. During the procedure it is important to get uniform heating and therefore a uniform current density of the electrode is required. Work by Tungjitkusolmun *et al* (2000) used

multiphysics modelling to optimise the design of the electrodes and demonstrated it was possible to produce such electrodes.

Multiphysics modelling can be a useful tool when investigating the design of electrosurgical vessel sealing devices. Dodde *et al* (2008) used the multiphysics modelling package, COMSOL, to compare the performance of two different shim designs, one structured and one smooth. The study focused on the thermal profiles of the different shims and validated the model through experimental work. The model found structured shims to be cooler than smooth ones with experimental data verifying the findings (Dodde *et al.,* 2008). This technique could be extended to compare a greater number of shim designs, and used in conjunction with experimental work to provide an insight into the difference in performance of shim designs, with structured shims already known to produce a lower seal failure rate when compared with smooth shims (Richter *et al.,* 2006a).

2.13 Chapter Summary

The reviewed literature has highlighted the importance of understanding and improving the performance of electrosurgical vessel sealing devices with the benefits of such devices over more conventional methods widely reported, although a large variation in seal quality remains. Existing research has focused on understanding the relationship between various parameters and seal quality, for example vessels with a larger diameter have been shown to lead to a lower seal quality, similarly vessels with a high collagen/elastin ratio lead to an improved seal quality (Carbonell *et al.,* 2003, Sindram *et al*., 2011). Whilst these studies aim to improve the understanding as to why there is a large variation in seal quality, they offer no way of improving technology to account for natural variation which cannot be eliminated. A number of studies examined the effect of device parameters on seal quality, such as application force and temperature. For both parameters optimal conditions exist; too low an application force or temperature and there will be insufficient pressure or heat to create a seal; too high an application force or temperature and damage occurs to the vessel (Wallwiener *et al.,* 2008). These optimal conditions go a long way in aiding device design and the understanding of the vessel sealing process.

A limited number of studies have considered the effect of shim surface features on seal quality, with existing studies comparing two shim designs, smooth and structured. The studies suggest that the structure of the surfaces affects the sealing temperature, seal quality, seal failure rate and the amount of adhesion when removing the vessel from the device (Richter *et al.,* 2006a, Dodde *et al.*, 2008). Existing studies show a promising avenue of research but are limited in the number of structured surfaces assessed and the way in which they are assessed. For example adhesion was assessed using a qualitative method, heavily reliant on the person conducting the test (Richeter *et al*., 2006a). The temperature assessment was conducted using a validated multiphysics finite element model, and therefore shows FE modeling can be a useful tool in aiding device design and can be beneficial for future research (Dodde *et al.,* 2008).

A number of test methods were reviewed, including the method for assessing the seal quality. Two methods have been discussed in the literature; a burst pressure test method and a shear tensile test. The shear tensile test had benefits including eliminating the effect of vessel geometry, however the data collected is difficult to relate to physiological data. Data collected from the burst pressure method relates directly to physiological pressures, and allows for an understanding as to how good the seal quality is; furthermore the burst pressure test is used as standard throughout industry making it the most appropriate test method (Katoh *et al.,* 2010, Presthus *et al.,* 2003). It is necessary to conduct more in-depth tests to improve understanding of the sealing process; a number of methods were reviewed including digital image correlation (DIC). This test method has a number of benefits including being non-contact and therefore would not affect the tests. Furthermore this technique has been demonstrated as being successful when used with other soft tissues, and it is hoped this technique could be used in capturing both the sealing and bursting of the blood vessel to improve understanding.

Additionally FEM was reviewed as a potentially useful technique. As discussed previously multiphysics FEM has already being demonstrated to be a useful tool in device design, allowing for a comparison in temperature performance of different shim designs (Dodde *et al.,* 2008). Existing studies have also considered arterial

clamping in terms of looking at the damage that occurs and assessing the performance of different clamp designs (Gasser *et al.,* 2006) (Famaey *et al.,* 2012). The FEM technique has many areas for consideration including arterial residual stresses, the material model used and the geometry of the blood vessel. There are many ways in which this FEM could be produced, and validation would be of exceptional importance, as with multiphysics modelling. By looking at arterial clamping in an FEM a greater understanding of the stresses and strains the vessel is subjected to would be gathered, and it would also be possible, in a similar manner to clamp design, that this could have significant implications for assessing the performance of shim surface structure.

3 Assessment of Seal Quality and Adhesion

3.1 Chapter Summary

This chapter explores the relationship between vessel characteristics and seal quality as well as investigating the effect of different shim designs on seal quality and the level of adhesion. Seal quality was assessed by measuring the burst pressure of the sealed porcine carotid artery and adhesion was quantified using a peel test method. This chapter includes details of the methods used and processing of the collected data including statistical analysis. The results demonstrate the effect of vessel characteristics on seal quality, with larger diameter vessels and vessels with a larger elastin content leading to a lower seal quality. Furthermore, results revealed the shim design to have a significant effect on both the seal quality and level of adhesion, with results indicating that groove orientation is the most influential factor in shim design for seal quality, and that with the optimum shim surface design adhesion could be reduced. Although results from this chapter demonstrate a significant difference in performance for the different shim designs, further experimental work and computer modelling is required to provide answers as to why these shim designs performed differently, with this work being presented in subsequent chapters.

3.2 Introduction

The benefits of electrosurgical vessel sealing devices have being widely reported in the literature as discussed in Chapter 2. Although the benefits are widely reported, there is significant variation in the quality of the seal achieved, with reported burst pressures varying between approximately 170mmHg- 1934mmHg (Richter *et al.,* 2006a, Sindram *et al*., 2011). Existing studies have explored different factors affecting the quality of the seal, including force and temperature. For both force and temperature a minimum and maximum threshold exists; below the minimum threshold a strong seal will not be created, whereas above the threshold excessive heat and force can cause damage and weaken the seal (Wallwiener *et al*., 2008).

A further aspect of the device design known to affect the performance is the surface structure of the shims. The shims are the part of the device contacting with the tissue and delivering the current. Existing work in this area is limited to comparing structured shims against smooth shims in terms of the number of seal failures and a qualitative assessment of seal sticking. When comparing the two types of shims, structured surfaces provided a lower seal failure rate but more pronounced adhesion (Richter *et al.*, 2006b). Furthermore smooth surfaces have being shown to have a higher peak temperature during sealing (Dodde *et al.,* 2008). A further area for investigation is the surface coatings of the shims with a number of coatings being available that change the tribological properties of the components to which they are applied, including changing the resistance to wear and friction coefficients (Holmberg *et al.*, 1994, Davis *et al.*, 2000). It is possible for the right coating to lower the level of adhesion for tissue sticking to the surface of the shims and as such to improve the performance of the device. The properties and application of the coatings depend on the composition, microstructure, porosity and homogeneity of the material (Ghosh, 2008), and there are a large number of coatings available. Due to the coatings being used for a medical application it is necessary for the coating to be biocompatible, significantly reducing the number of suitable coatings.

The properties of the vessel are also known to affect the seal quality, for example with increasing outer diameter there is a progressive reduction in the burst strength of the seal (Caronell *et al.*, 2003). More recently the effect of vessel morphology on seal quality has been investigated with the collagen/elastin ratio providing a good prediction of seal strength when considering vessels from different regions of the body (Sindram *et al.*, 2011). The effect of morphology on seal quality has been discussed in a number of studies as a possible explanation for the different behaviour of arteries and veins and highlights the importance of morphology in the sealing process (Richter *et al.,* 2006a, Wallwiener *et al.*, 2008). Morphology of the vessel varies depending on anatomical location, age, sex, species and vessel size. Furthermore the morphology of a vessel can vary significantly along its length. For example the proximal region of a porcine carotid artery has greater

elastin content than the distal region, with little change in the level of collagen and an increase in smooth muscle cells in the distal regions (Wallwiener *et al.*, 2008, García *et al.*, 2011, Shadwick, 1999).

The current chapter aims to examine the variation in electrosurgical seal quality along the length of a porcine carotid artery and explore the relationships between seal quality, vessel size and vessel morphology. A number of shim surface coatings were assessed with the aim of determining if coatings are available that can reduce the level of adhesion and improve the device performance. Furthermore the chapter aims to investigate the effect of shim surface structure in terms of seal quality, failure rate and the level of adhesion. Additionally the study aimed to look at the minimum safety threshold for successful seals and the influence on both vessel and device characteristics for meeting this requirement.

The work in this chapter was carried out as part of undergraduate research projects, with the author providing the necessary guidance and supervision and helping with the development of the projects, but with the undergraduate students conducting a significant proportion of the testing. The analysis of the results and the subsequent discussion were conducted solely by the author.

3.3 Methods

3.3.1 Tissue Preparation

Porcine carotid arteries, from pigs aged 4-6 months, were obtained from a local abattoir (within four hours of slaughter). Treatment of the vessels varied depending on the test being conducted as detailed in subsequent sections.

3.3.1.1 Morphology Analysis

Vessels were skeletonised, removing all connective tissue, and sectioned using a scalpel; a 2 mm sample was fixed in 10 % buffered formalin for histological analysis and a 20 mm section taken for sealing (Figure 3-1). The position from the bifurcation was measured, along with the outer vessel diameter and wall thickness. All measurements were carried out using digital Vernier callipers and were repeated three times.
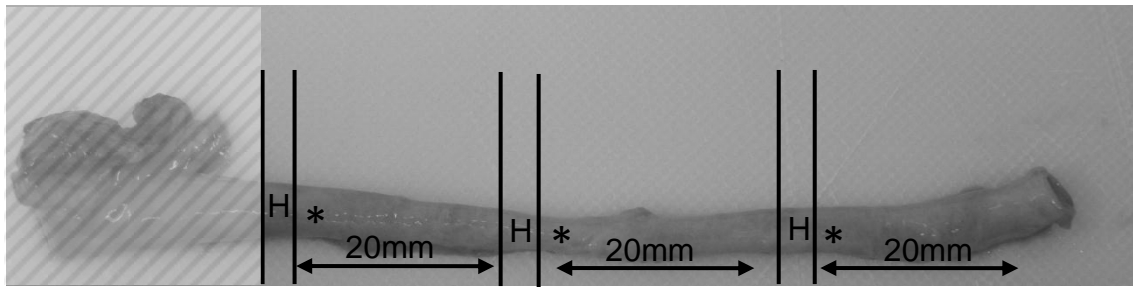
Figure 3-1 Schematic representation of the sectioning of a common carotid artery. * indicates the location of the electrosurgical seal and H shows the position of the 2mm ring sample taken for histology. The shaded region of the image indicates the area of the vessel not use, with tissue 6mm from the bifurcation omitted from the study.

3.3.1.2 Shim Assessment

Vessels were frozen on the day of slaughter and defrosted on the day of testing. Vessels were skeletonised and sectioned using surgical scissors. The position from the bifurcation was measured, along with the outer vessel diameter and wall thickness. All measurements were carried out using digital Vernier callipers and were repeated three times. The sectioning of the blood vessel varied for the testing of the shim surface features and for the shim coatings, with both methods being detailed subsequently. The variation in the methods was due to the progression in knowledge of vessel sealing throughout the course of the PhD, and the supervision of different project students and as such their impacts on the project.

Sectioning of blood vessel for shim surface coatings

The first 10mm of the vessel from the bifurcation was not used due to the largely elastic nature of this region, and the branching of the blood vessel. All sections were 30mm in length, with seals being positioned 25mm, 55mm, and 85mm from the bifurcation. The seal was performed at the centre of vessel sections prepared for sealing, allowing one side to be peel tested and the other to be burst pressure tested (Gunasekara 2011, Beddoes 2012).

Sectioning of blood vessel for shim surface features

The first 40mm of the vessel from the bifurcation was not used due to the variation in vessel morphology and size throughout this section. This eliminated the effect of

vessel morphology and diameter from the study. The seal was performed at the centre of subsequent sections, allowing one side to be peel tested and the other to be burst pressure tested (Figure 3-2) (Le Gall, 2013 and Vivien, 2013).
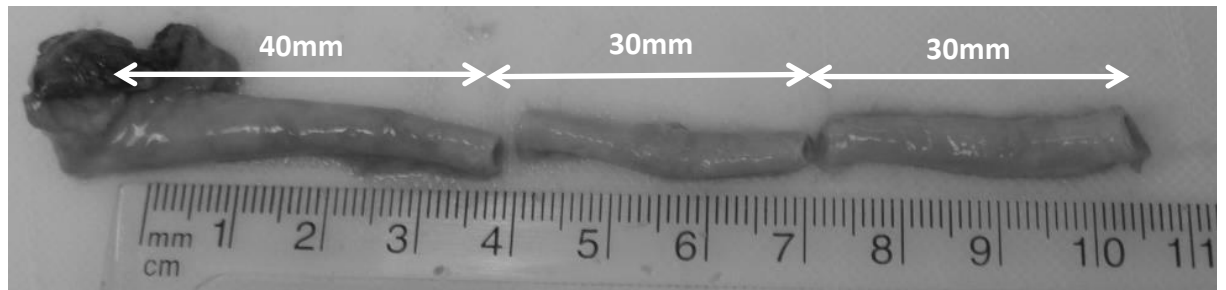
Figure 3-2 Image showing the sectioning of the blood vessel for shim performance assessment.

3.3.2 Vessel Sealing System

3.3.2.1 Equipment and Set-up

The vessel sealing system consists of two main parts; the generator and the device. For all experimental work the Gyrus G400 generator and PlasmaKinetic OpenSeal device (original and modified versions, with device modifications discussed in section 3.4) were used. A schematic set-up of the vessel sealing system can be seen in Figure 3-3, with the footswitch and power supply connected to the generator via ports located at the back, with the device connected to either of the two ports located at the front. On connecting the device the generator automatically recognises the device due to capacitors in the device cable, allowing the generator to use the default waveforms and power settings for each device. For work during this study the default settings of VP2 60 were used unless stated otherwise.
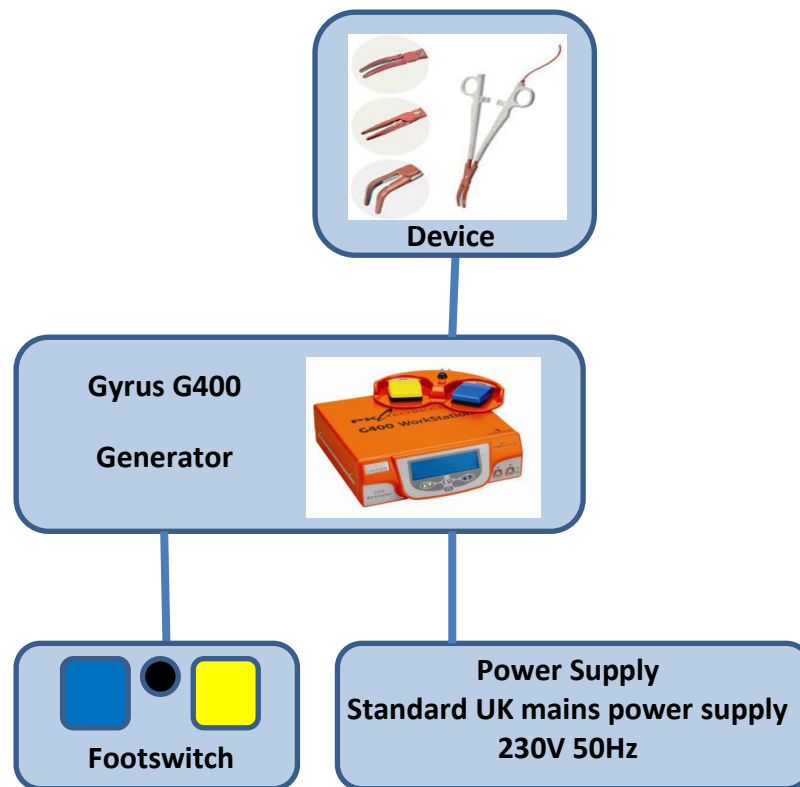
Figure 3-3 Schematic of the vessel sealing system set-up

3.3.2.2 Using the system

To perform an electrosurgical seal, the blood vessel was placed between the jaws of the device. The device was then clamped shut, using the ratchets located on the handles of the device, providing a consistent and repeatable user technique. Subsequently the device was activated using the blue pedal of the footswitch. Upon activation the generator begins to beep, allowing the user to know the device is activated. Once the vessel is sealed there will be a tone change in the generator, signalling for the user to remove their foot from the footswitch, thus deactivating the device. The duration and the applied current vary between the different seals, with the generator monitoring the tissue impedance to determine when the seal is complete. The waveform of the generator is adaptive meaning the waveform for each seal varies, with the applied waveform being dependent on vessel properties such as morphology and size. Although the applied waveform would vary for each seal, this is done to achieve consistency within the seals. The technique used would

be repeatable for the user, but would result in slight variation in energy delivery depending on the vessel properties.

3.3.3 Quantifying Adhesion

A number of previous studies have attempted to assess the level of adhesion following an electrosurgical procedure, as discussed in Chapter 2, with the majority of studies using a qualitative method. As no standard method of quantifying adhesion for this application was found, a methodology is proposed using a peel test to quantify adhesion.

3.3.3.1 Equipment and Set-up

To perform the peel test a set-up was developed using a hand held Mecmesin force gauge and a test rig. The test rig was designed for use with the force gauge, with the gauge attached securely at an angle of 90° to the base plate, through a dove-tail joint connector affixed to the back of the device. The hand held force gauge measured the peak peeling force and does not record load-extension curves throughout the test. To hold the device in place a rig was attached to the base plate. The set-up of the equipment can be seen in Figure 3-4**.**
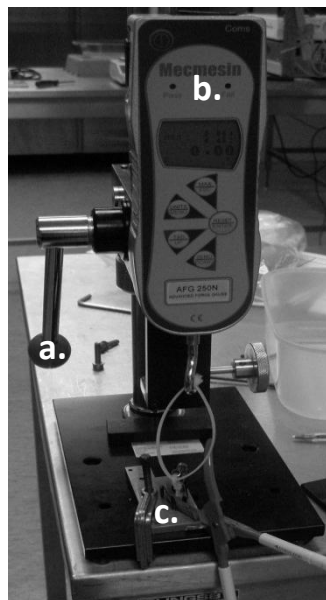
Figure 3-4 Diagrammatic representation of the test rig used for quantifying surface adhesion.

     a. The handle for displacement control;

     b. Hand held Mecmesin force gauge;

     c. Fixture for holding the vessel sealing device in place.

3.3.3.2 Testing Procedure

Following the electrosurgical sealing process the device was slowly opened, with the sealed vessel primarily adhering to one shim. The device was then loaded into the test rig (Figure 3-4) and the blood vessel connected using the crocodile clip. Subsequently the handle of the test rig was pulled, moving the force gauge up and peeling the blood vessel from the surface of the shim. The peak peeling force was recorded and the length and width of the seal were measured using digital Vernier callipers.

3.3.3.3 Data Processing

Following the testing method data was processed by applying Equation 3.1 to the data.

Peel Strength (N/mm) = *Peel Force* (N) / *Length of sealed area* (mm)　　– (3. 1)
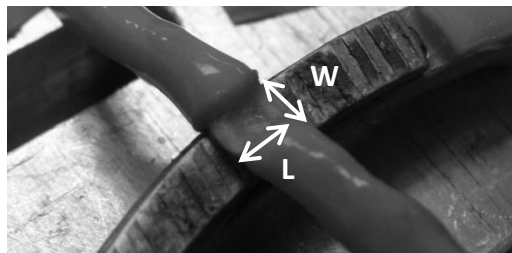
Figure 3-5 Image showing the definition of the length (L) and width (W) of a seal.

3.3.4 Assessing Seal Quality

As discussed in Chapter 2, industry typically uses burst pressure testing to assess the quality of an electrosurgical seal. Variations in the methodology exist although the principle remains the same throughout.

3.3.4.1 Equipment and Set-up

To perform a burst pressure test the sealed blood vessel was infused with physiological saline. The apparatus used to do this consisted of a syringe pump used to deliver saline and a Druck digital pressure indicator to measure the burst pressure. A syringe was fixed into the syringe pump and connected to a 3-point adaptor. The remaining two outlets of the adaptor were connected to the pressure

indicator and a blunt needle used for specimen attachment (Figure 3-6). Saline was infused through the circuit to ensure all air was removed.
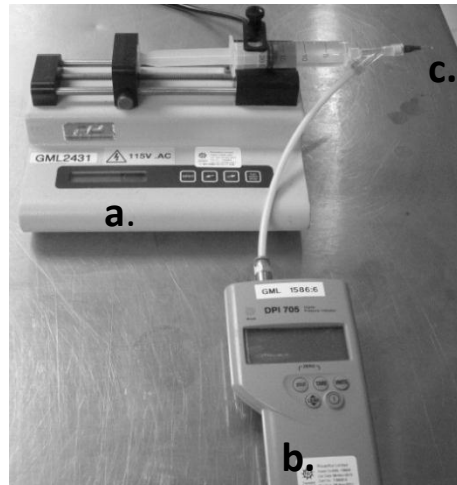
Figure 3-6 Diagrammatic representation of the perfusion circuit used for burst pressure testing of vessels
   a. Cole-Parmer syringe pump set at an infusion rate of 50 ml/hr
   b. Druck digital pressure indicator
   c. Blunt needle for the attachment of the blood vessel

3.3.4.2 Burst Pressure Testing Procedure

The sealed carotid was connected to the circuit using a haemostat and infused with physiological saline (10% w/v) at a rate of 50ml/hr. The burst pressure, defined as a sudden and rapid decrease in seal pressure, was recorded for each segment. A seal was considered successful if it withstood a pressure greater than 360 mmHg; this pressure was chosen in line with standards used by Gyrus Medical Ltd and accepted by medical device regulators such as the Food and Drug Administration (FDA).

3.3.5   Quantifying Vessel Morphology

In order to investigate the effect of vessel morphology and changes that occur during the sealing process at a microscopic level it was necessary to use histology techniques. This primarily consists of staining tissue to highlight the features of interest and looking at the results under a light microscope.

3.3.5.1 Tissue Preparation and Staining

Vessels were prepared and sectioned as described in Section 3.3.1.1 of this chapter. Sections were cut using a surgical scalpel, resulting in 2mm thick sections. Following

the sectioning each sample was placed in a vial and fixed in 10% buffered formalin. Tissue processing and histological slides were prepared by the University of Wales Histopathology department, with specimens being stained using Elastin van Gieson's (EVG) stain. This stained the elastin component of the samples black, and the collagen components stained red.

3.3.5.2 Image Capture and Processing

Images were collected using the Leica DMRB micrcoscope with a colour Moticam 2000 digital camera and basic image acquisition software (Motic Image Plus). Quantitative morphological analysis was carried out using a thresholding technique in Image J (DebRoy), with both collagen and elastin content quantified for each sample. The image was converted into an 8-bit greyscale image, with the thresholds for each image being adjusted manually using the sliding scale feature within Image J. The scale was adjusted until the black areas representing the elastin, or the grey areas (previously red) representing collagen, turned red within the software. The percentage area of the image that was now red was computed by the software, determining the material composition. Each measurement was repeated three times and an average value was taken for the media layer of the vessel. It should be noted that the results from the image processing can depend greatly on the staining process and slice preparation; to reduce this effect each image was analysed individually instead of using a batch processing technique.

3.3.5.3 Data Processing

Samples were grouped according to whether the segment was predominantly muscular or elastic (Figure 3-7), with muscular segments having an elastin content of less than 20% and a well-defined internal elastic lamina (IEL), and elastic segments having an elastin content of greater than or equal to 20% and no well-defined IEL.

(a)   (b)
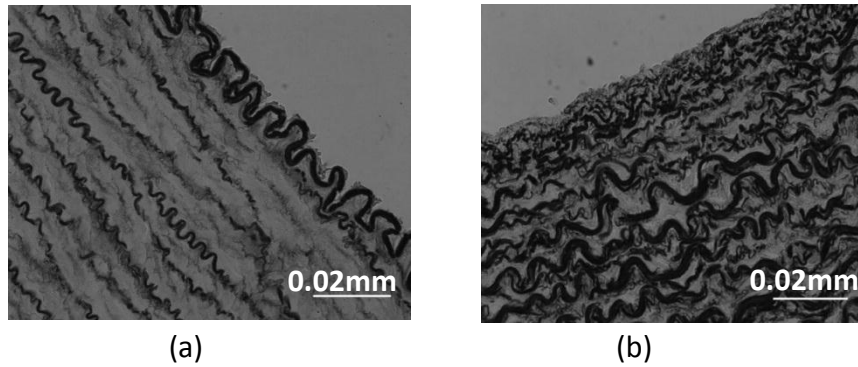
Figure 3-7 Representative sections depicting blood vessels stained with Elastin van Geison (elastin stains black). Depiction of (a) a predominantly muscular vessel containing < 20 % elastin and (b) a predominantly elastic vessel containing ≥ 20 % elastin (scale bar = 0.02mm).

3.3.6 Surface Roughness Measurement

Surface roughness was measured using a Talysurf (Form Talysurf Series 2, Taylor Hobson). The shims were mounted onto the machine using a mount, and the probe was moved within 1mm of the surface. The probe measures a roughness of up to 1mm, with an accuracy of 10nm. The surface roughness was measured using Ultra Software to control the probe over a length of 10mm for each shim, with each measurement repeated three times.

3.3.6.1 Data Processing

Data was exported to Microsoft Excel for processing. For shims with no grooves all data points were used, calculating the average R_{rms} and R_a values over the three measurements. For grooved shims data points for the peaks were used to calculate the roughness values, using all data points for each peak, and calculating the mean for each of the shims. The formula for calculating the R_{rms} and Ra values are shown below (Equations 3.2 and 3.3) (ASME, 2010).

$$R_a = \frac{1}{n} \sum_{i=1}^{n} |y_i| \qquad\qquad (3.2)$$

$$R_{rms} = \sqrt{\frac{1}{n} \sum_{i=1}^{n} y_i^2} \qquad\qquad (3.3)$$

The roughness profile contains n ordered, equally spaced points along the trace, and y_i is the vertical distance from the mean line to the ith data point. Height is assumed to be positive in the up direction, away from the bulk material.

3.3.7   Statistical Analysis

Data was tested for normality and equal variance using SPSS; as the data was not normally distributed, non-parametric tests were used All data was used to test for significant correlations between the different variables with the Spearman's rank correlation test used. A p-value of <0.05 rejected the null hypothesis that there was no correlation and indicated a significant relationship. An s value approaching -1 or +1 indicated a strong correlation with the sign indicating the direction (Berk, *et al* 2010).

Differences between two groups were tested using the Mann-Whitney test (2-tailed), with a p-value of <0.05 rejecting the null hypothesis that the medians of the two groups were equal and indicating a significant difference between the two groups (Berk, *et al* 2010). Where differences between three or more groups were tested the Kruskal-Wallis test (2-tailed) was used, with a p-value of <0.05 rejecting the null hypothesis and indicating a significant difference between the two groups. Following this a post hoc paired comparison was performed to test for differences between the individual groups .

3.4   Device Modifications

3.4.1   Shim coatings

Coatings can be applied to components to improve performance in terms of resistance to wear, corrosion resistance and adhesion, and are commonly used in medical applications for a variety of reasons including improving biocompatibility and tribological properties (Homberg *et al.,* 1994, Davis *et al.,* 2000). Tribology coatings are known as thin coatings, typically with a thickness range of 0.1μm - 10μm that play an important role in the components friction and wear performance (Holmberg *et al*., 1994). The properties and application of the coatings depends on the composition, microstructure, porosity and homogeneity of the material (Ghosh 2008).

A number of coatings and treatments were chosen for analysis, with Tecvac UK - heat treatment and hard coating service (Cambridge, UK) producing the Titanium Nitride (TiN), Chromium Nitride (CrN), and Diamond-like-Carbon (DLC) coatings, and

WS2 coating Ltd. (York, UK) producing the Tungsten Disulphide (WS$_2$) coating. The material properties of these coatings are summarised in Table 3-1. All chosen coatings were applied to the shims using a gaseous state process. It is also important to note that the original shims for the PlasmaKinetic OpenSeal device are coated in Nickel-Chromium (NiCr) coating.

Table 3-1 Summary of material properties for the chosen coatings, details provided by Tecvac UK and WS2 coatings Ltd, table modified from Gunasekara-Dimunge (2011) .

Material Property	Titanium Nitride (TiN)	Chromium Nitride (CrN)	Diamond-like-Carbon (DLC)	Tungsten Disulphide (WS$_2$)
Coating Thickness (µm)	$1-4$	$1-4$	$3-5$	0.5
Hardness (Hv)	2300	2000	4500	30Rc
Maximum operating temperature (°C)	500	600	400	Air 273 Vacuum 188
Friction Coefficient with itself	Static 0.08-0.25 Dynamic 0.05 -0.15		0.05	Static 0.070 Dynamic 0.030
Friction Coefficient with steel	$0.25-0.35$	Low firction against steels, values range from 0.05 - 0.90 with typical 0.4	0.1	
Application Process	Physical Vapour Deposition	Physical Vapour Deposition	Plasma – enhanced Chemical Vapour Deposition	Chemical Vapour Deposition

In addition to these coatings passivated shims were tested, with passivated stainless steel having been previously demonstrated to improve corrosion resistance (Maller 1998). The passivation process consists of mechanical cleaning, degreasing, inspection, passivation and rinsing, as such the initial step was to clean

the shims using an IPA (Isoproyl Alcohol) ultrasonic bath. Following the cleaning of the shims, they were immersed in a nitric acid solution (20% vol.) at 55°C for 30 minutes, and rinsed afterwards in water (Gunasekara 2011). .

In addition to the various shim coatings and treatments tested, Electrolube was also tested. Electrolube is a sticky, electrosurgery lubricant which is applied to the shims of the device before use and also during the surgical procedure, reducing the tissue adhesion to the shims and keeping the shims clean (Mectra Labs) . The Electrolube used for this analysis was made by Mectra Labs Inc. (Indiana, USA), and was applied to the shims before every seal when analysing its performance (Beddoes, 2012).

3.4.2 Shim Surface Features

The original shims for the PlasmaKinetic OpenSeal device were modified to create a number of shim sets to test the effect of different surface structures, Table 3-2. The original shim was modified using sand paper to remove the rough surface coating. The surface features were then applied using a milling machine by a qualified technician. Due to the curved profile of the original shim, and for ease of manufacture it was decided that grooves would be applied to the surface of the shim using the straight edge at the end of the shim as a datum (Figure 3-8).

Figure 3-8 Image showing a modified shim of the PlasmaKinetic OpenSeal device, with the straight edge used as a datum for producing the grooves indicated by **D.**

The shim designs were chosen to explore the effect of different groove designs, with the normal grooved shim being used as the standard design. The other shims were designed to allow for the effect of groove width, frequency and orientation to be investigated, comparing their performance to that of the standard grooved shim.

Table 3-2 Description and details of shim designs, including images of the different designs.

Shim No	Shim Name	Description	Details	Image
1_OR	Original	Unmodified original shim	N/A	
2_SM	Smooth	Rough surface coating removed	N/A	
3_GR	Normal Grooved	Smooth shim (2_SM) with transverse grooves	Groove Width =1mm Peak Width = 1mm Groove Depth = 0.1mm	
4_NA	Narrow Grooved	Smooth shim (2_SM) with transverse grooves applied with half the width and same frequency compared to 3_GR	Groove Width = 0.5mm Peak Width = 1.5mm Groove Depth = 0.1mm	
5_HF	HF Grooved	Smooth shim (2_SM) with transverse grooves applied with half the width and double the frequency compared to 3_GR	Groove Width = 0.5mm Peak Width = 0.5mm Groove Depth = 0.1mm	
6_LO	Longitudinal Grooved	Smooth shim (2_SM) with longitudinal grooves applied with same width and frequency as 3_GR	Groove Width = 1mm Peak Width = 1mm Groove Depth = 0.1mm	
7_45	45 ° Grooved	Smooth shim (2_SM) with 45° grooves applied with the same width and frequency as 3_GR	Groove Width = 1mm Peak Width = 1mm Groove Depth = 0.1mm	
8_CC	Combination	A combination of the longitudinal grooved (6_LO) and normal grooved (3_GR)		

3.4.3 Attachment to Device

Original shims were removed from the PlasmaKinetic OpenSeal device to allow for modified shims to be attached. An insulating strip was attached to the underside of the modified shim and the shim was then glued onto the device. The metal tab at the end of the shim (Figure 3-8) connected the shim to the device to allow the current to conduct.

3.4.3.1 Application Force Control

As the project progressed, the methodology evolved to include application force control, with this being implemented for the shim surface features analysis. When changing the shim the shim gap was controlled, ensuring the shim gap remained constant for each shim. The shim gap was measured for the original device and the appropriate nylon stopper was chosen for each device to create a consistent shim gap. Whilst every precaution was taken to ensure that the shim gap remained constant, variation in the shim gap would be present although limited as much as possible. Furthermore to control the application force a region was marked on the device (Figure 3-9) to show the user where to place the vessel during the sealing process, thus eliminating the variation in application force due to positioning of the vessel within the jaws of the device.

Figure 3-9 Image showing sealing region marked on the device to eliminate the variation in application force due to positioning of the vessel within the jaws of the device.

3.5 Results

The results section will be split into three main subsections; vessel properties, effect of shim coatings and the effect of shim surface features. Vessel properties

will present the effect of outer diameter and morphology on the seal quality, whilst the subsequent sections will explore the effect of shim coatings and design on seal quality and the level of adhesion.

3.5.1   Vessel Properties

Vessels were grouped based on position from the bifurcation and data was analysed for burst pressure, outer diameter, vessel thickness, elastin content, collagen content and failure rate (Table 3-3), with a seal failure being defined as a burst pressure <360mmHg.

Table 3-3 Data for vessels grouped according to position from the bifurcation. % composition quantified in conjunction with Image J software. All data is presented as mean ± SD.

	12mm	**38mm**	**64mm**	**90mm**
Burst Pressure (mmHg)	246.67 ± 193.00	963.22 ± 718.20	1076.11 ± 532.89	1243.38 ± 424.08
Outer Diameter (mm)	5.91 ± 0.46	4.51 ± 0.95	3.50 ± 0.55	3.46 ± 0.44
Thickness (mm)	1.04 ± 0.26	0.86 ± 0.17	0.95 ± 0.15	0.92 ± 0.16
% Elastin	35.28 ± 5.21	26.25 ± 11.52	14.99 ± 8.95	10.95 ± 4.70
% Collagen	20.64 ± 2.11	22.18 ± 2.62	22.50 ± 3.04	21.54 ± 2.76
Seal Failure Rate	77.8%	11.1%	0.0%	0.0%

A significant correlation was found between burst pressure with both outer diameter (p = <0.0001, s = -0.665) and % elastin (p = 0.001, s = -0.520), Figure 3-10. Furthermore, a correlation was also found between elastin and outer diameter (p = <0.0001, s = 0.559). The results were further analysed by grouping the vessels as either predominantly muscular or predominantly elastic based on criteria described

previously (Figure 3-7). When comparing the burst pressure of the two groups a significant difference was found (*p*=0.001, Figure 3-11).
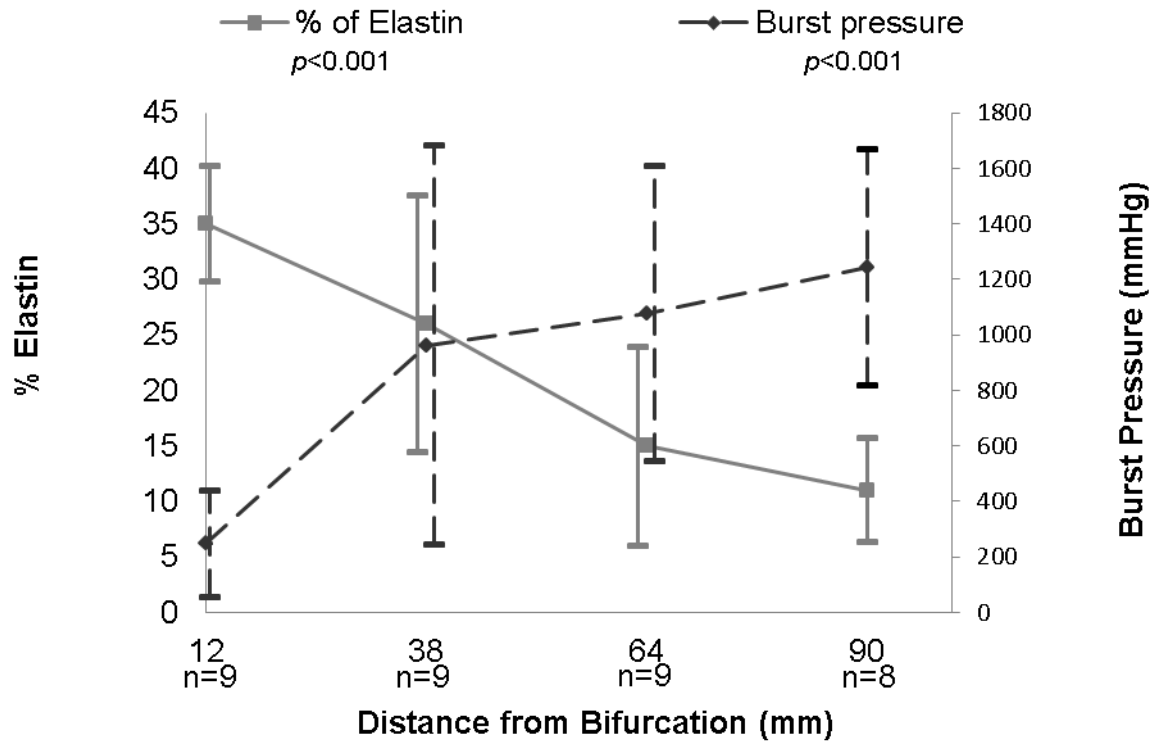
Figure 3-10. Variation in elastin content and burst pressure with position from bifurcation, % composition quantified in conjunction with Image J software. Data is presented as mean ± SD.
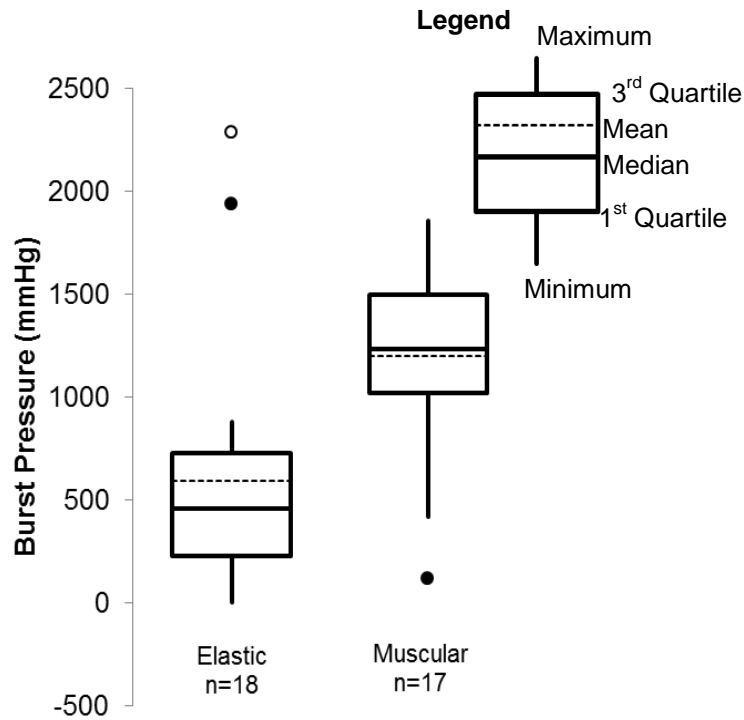
Figure 3-11. Box plot showing the difference in burst pressure with predominantly muscular and elastic vessels. The black circles show moderate outliers and white circles show extreme outliers.

Outliers were observed for the burst pressure measurements (Figure 3-11), which were either considered as moderate (black circles) or extreme (white circles). The outliers are values which are beyond a range calculated using the first and third quartile, with an outlier defined as any value more than 1.5 x inter quartile range (IQR) below the first quartile, or above the third quartile. It is possible to explain the outlier for the muscular group as this is the only muscular vessel with an outer diameter greater than 5mm, and as shown (Figure 3-12) vessels with a diameter of greater than 5mm are more likely to produce a weak seal. However vessel size does not account for the outliers of the elastic group, and at present there is no clear explanation for this.
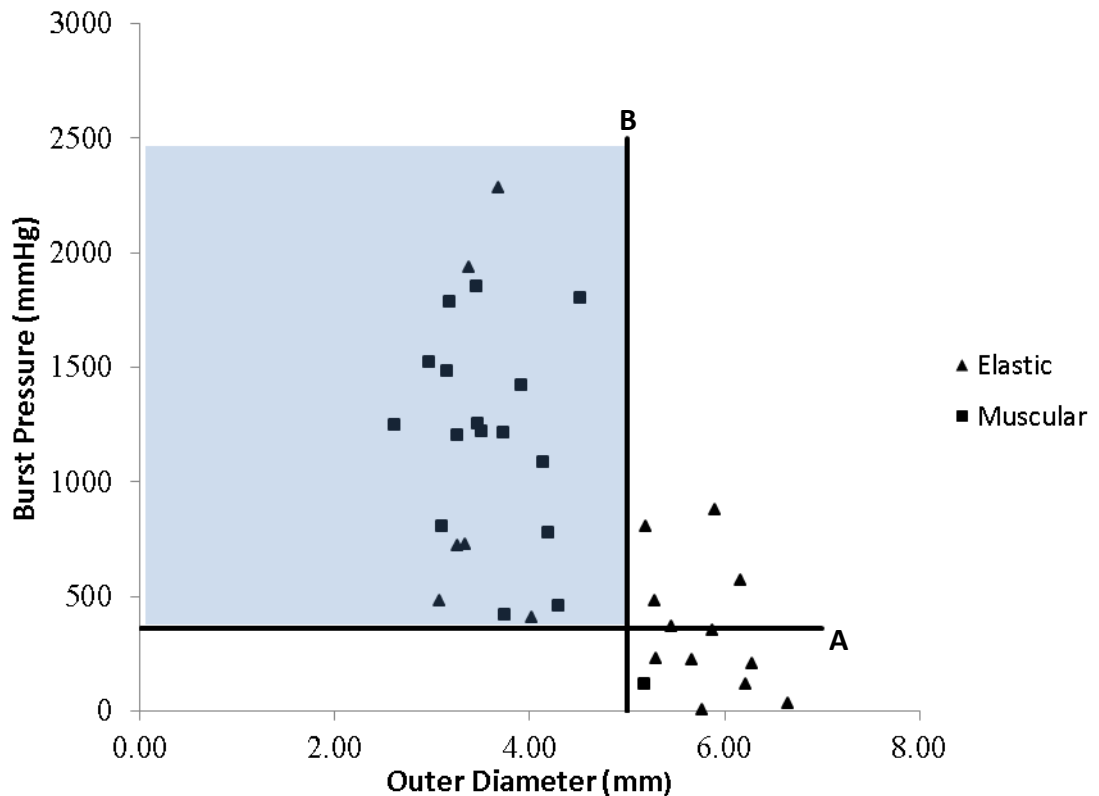
Figure 3-12. Scatter graph showing the relationship between vessel outer diameter and burst pressure (p=<0.0001, s=-0.665), with data grouped as predominantly muscular or elastic as based on the criteria described in Figure 3. Line A indicates the minimum standard for a sufficient seal, 360mmHg, and line B indicates the maximum threshold for vessel size, 5mm outer diameter.

The minimum threshold of a successful seal was observed, with a burst pressure of 360mmHg considered to be the minimum pressure (Figure 3-12), in line with standards used by Gyrus Medical Ltd, and other regulators. Using this as the minimum standard, it is possible to determine the maximum vessel size that led to a seal quality consistently meeting these standards. The vertical line B (Figure 3-12) shows that all vessels below 5mm in outer diameter produced a seal above the minimum standard, irrespective of the morphology of the vessel. Furthermore, a relationship exists between vessel outer diameter and seal strength (Figure 3-12), with a reduction in outer diameter resulting in an increase in seal strength as mentioned previously.

3.5.2 Shim Modifications

3.5.2.1 Effect of Shim Coatings

Data sets for each shim coating were analysed for burst pressure, seal failure rate and peel strength, with a summary of the data presented in Table 3-4.

Table 3-4 Summary of shim coating results, with a burst pressure <360mmHg considered a seal failure and data presented as mean ± SD

Shim Coating	Burst Pressure (mmHg)	Seal Failure Rate	Peel Strength (N/mm)
Original *n=39	679.95 ±368.80	17.9%	0.052 ±0.035
TiN n=22	706.70 ±477.64	33.3%	0.097 ±0.054
CrN n=21	1096.90 ±546.75	9.1%	0.104 ±0.085
DLC n=21	204.10 ±259.35	76.2%	0.275 ±0.120
WS$_2$ n=21	455.12 ±278.75	41.2%	0.141 ±0.072
Passivated n=20	340.91 ±139.31	63.6%	0.147 ±0.095
Electrolube n=19	749.68 ±415.82	9.1%	0.057 ±0.051

A significant difference was found between the peak peel strengths (Kruskal – Wallis, $p<0.001$) and peak peel forces (Kruskal – Wallis, $p<0.001$) of the different shim coatings. When the data was analysed further it was found that no shim performed statistically significantly differently to the original shim (Figure 3-13), with the difference between the group coming as a result of the difference in performance between the other groups.
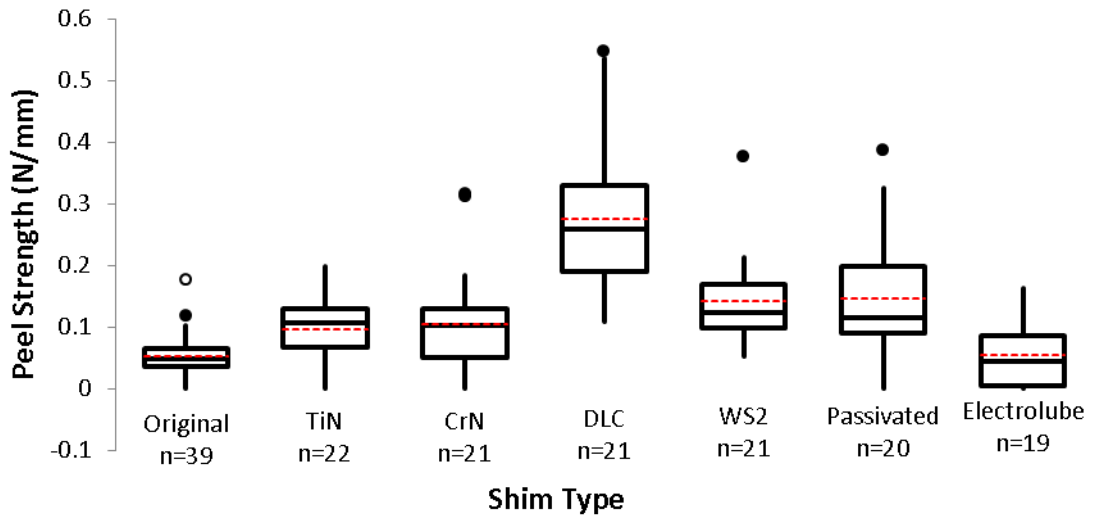
Figure 3-13 Box plot showing the difference in peel strength for each of the different shim coatings, n = number of samples (Kruskal − Wallis, *p*<0.001). The black circles show moderate outliers and white circles show extreme outliers.

A significant difference was found between the burst pressures (Kruskal − Wallis, *p*<0.001) of the different shim coatings. When the data was analysed further it was found that DLC (*p*<0.01), WS$_2$ (*p*<0.01) and passivated (*p*<0.01) shims performed significantly worse than the original shims (Figure 3-14), but no shim presented a statistically significant improvement for the seal quality.
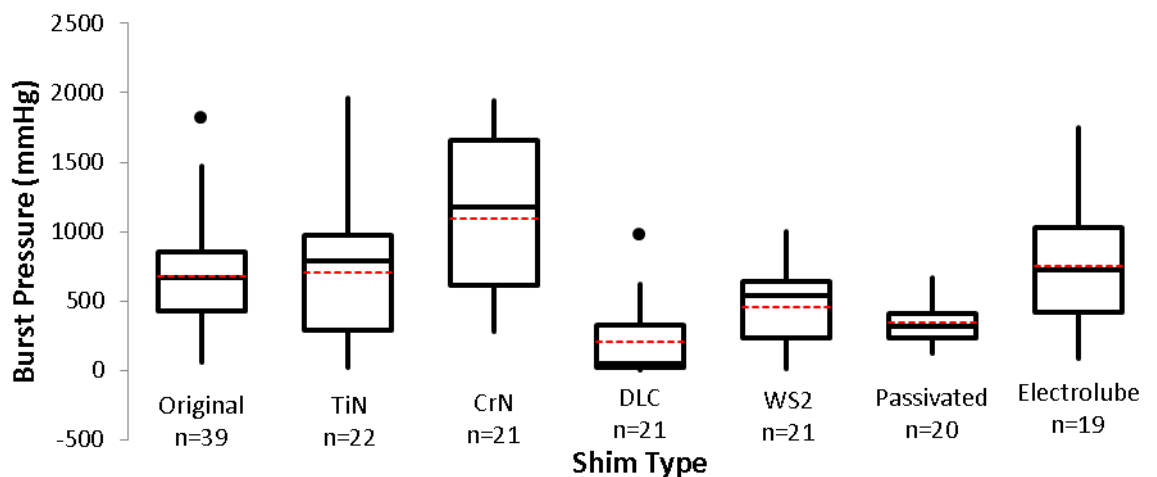
Figure 3-14 Box plot showing the difference in burst pressure for each of the different shim coatings, n = number of samples (Kruskal − Wallis, *p*<0.001). The black circles show moderate outliers and white circles show extreme outliers.

3.5.2.2 Effect of Shim Surface Features

Data sets for each shim surface structure were analysed for burst pressure, seal failure rate, peel strength and seal area, with a summary of the data presented in Table 3-5.

Table 3-5. Summary of shim results, with a burst pressure <360mmHg considered a seal failure and data presented as mean±SD.

Shim Name	Burst Pressure (mmHg)	Seal Failure Rate	Peel Strength (N/mm)	Seal Area (mm2)
Original (1_OR) *n=20	585.45 ±261.77	5.0%	0.088 ±0.037	18.35 ±2.51
Smooth (2_SM) n=22	468.77 ±192.80	27.3%	0.120 ±0.073	16.34 ±3.96
Normal Grooved (3_GR) n=21	547.05 ±266.24	14.3%	0.096 ±0.042	16.64 ±2.99
Narrow Grooved (4_NA) n=21	507.00 ±209.07	33.3%	0.074 ±0.039	14.79 ±3.37
HF Grooved (5_HF) n=21	606.33 ±238.74	14.3%	0.084 ±0.042	14.89 ±2.61
Long Grooved (6_LO) n=20	549.85 ±253.22	25.0%	0.164 ±0.053	14.62 ±4.78
45° Grooved (7_45) n=19	191.05 ±113.17	89.5%	0.063 ±0.038	16.07 ±3.32
Combination (8_CC) n=24	764.46 ±388.331	0.0%	0.111 ±0.070	12.80 ±3.26

*n= number of tests

A significant difference was found between the burst pressures of the different shim designs (Kruskal-Wallis, $p<0.001$). When the data was further analysed it was found the 45° grooved shim presented a statistically weaker seal when compared with all other shim designs ($p<0.05$, Figure 3-15).
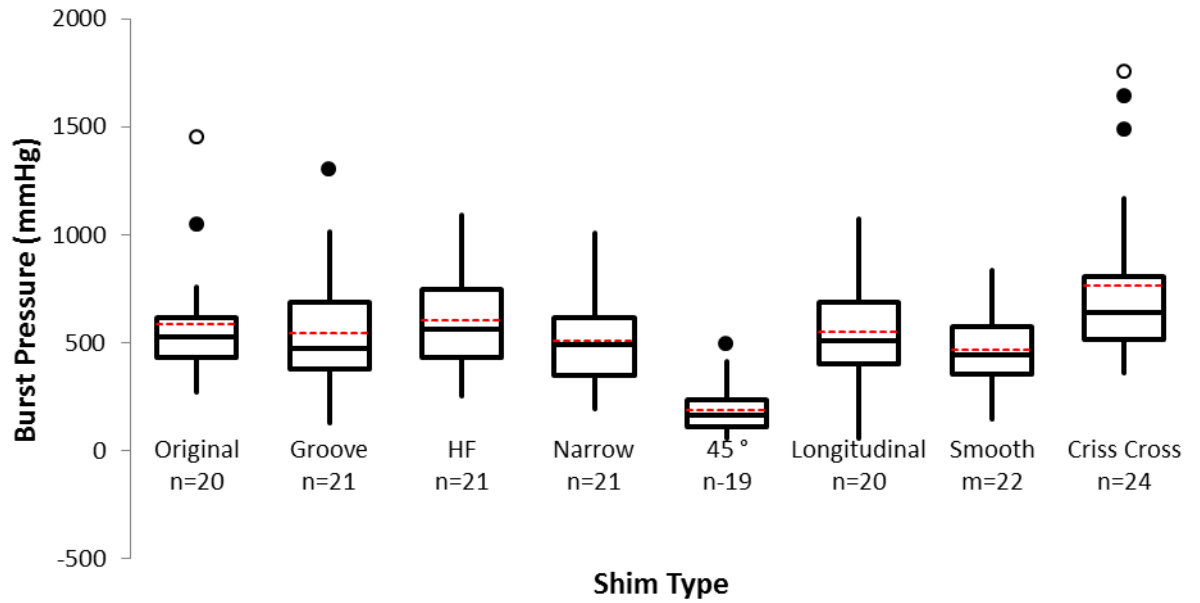
Figure 3-15. Box plot showing the difference in burst pressure for each of the different shim designs, n= number of tests. The black circles show moderate outliers and white circles show extreme outliers.

A significant difference was found between the peel strength of the different shim designs (Kruskal-Wallis, $p<0.001$, Figure 3-16). When the data was further analysed it was found the longitudinal grooved shim presented significantly worse sticking than the original, grooved, HF grooved, narrow grooved and 45° grooved shims ($p<0.05$).
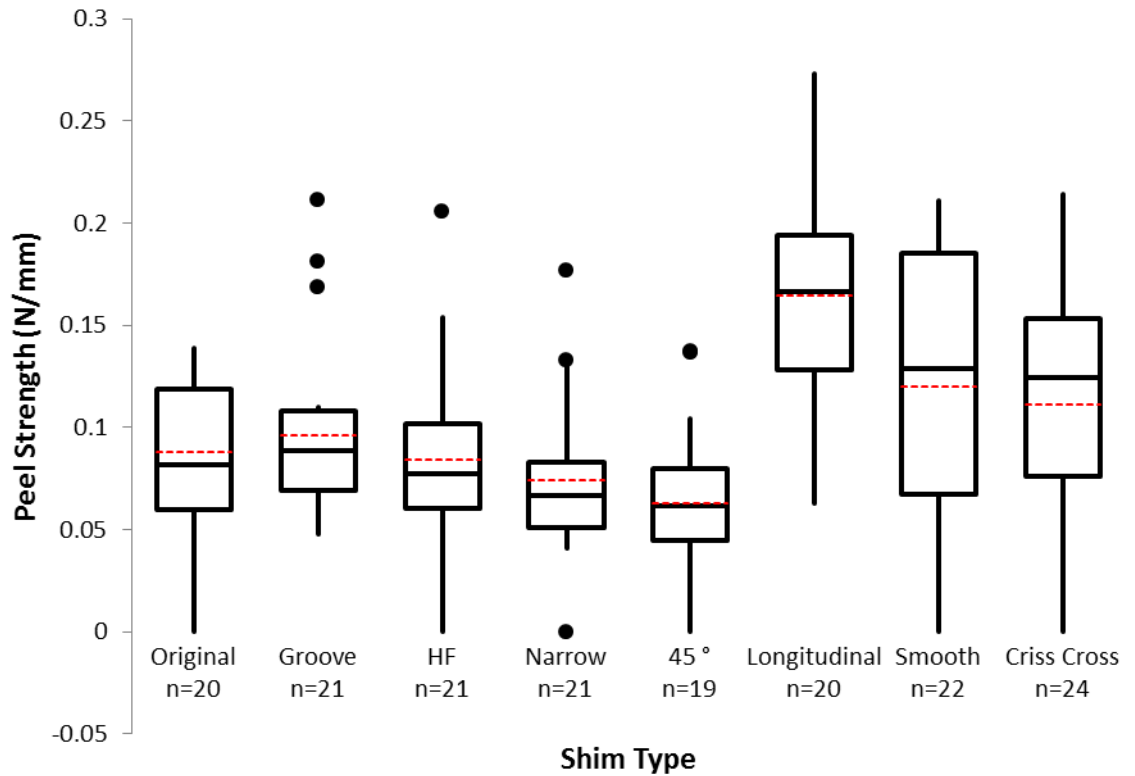
Figure 3-16 Box plot showing the difference in peel strength for each of the different shim designs, n= number of tests. The black circles show moderate outliers and white circles show extreme outliers.

A significant difference was found between the seal area of the different shim designs (Kruskal-Wallis, *p*<0.001, Figure 3-17). When the data was further analysed it was found the original shim produced a significantly larger seal compared to the HF grooved, narrow grooved, longitudinal grooved and combination shim (*p*<0.05).
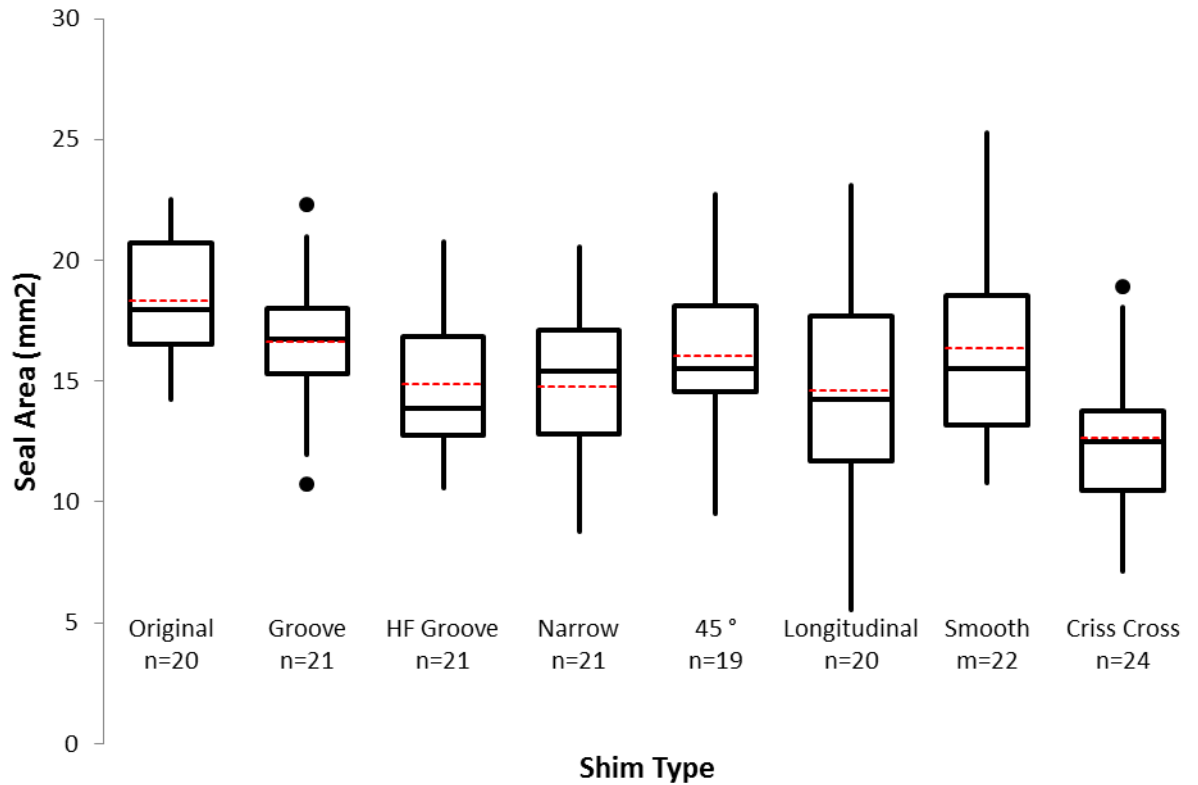
Figure 3-17. Box plot showing the different in seal size (area) for each of the different shim designs, n= number of tests.

Outliers were observed in all box plots (Figure 3-15, Figure 3-16 and Figure 3-17), which were either considered as moderate (black circles) or extreme (white circles). The outliers are values which are beyond a range calculated using the first and third quartile, with an outlier defined as any value more than 1.5 x IQR below the first quartile and above the third quartile (Berk, 2010).

Surface roughness values of the surfaces of each of the shims were measured, with the results presented as RMS values (Figure 3-18) and Ra values (Figure 3-19). Both Figure 3-18 and Figure 3-19 show a significantly higher roughness value for the original shims when compared with all other shim designs, with little difference between the roughness values for the other shim designs.
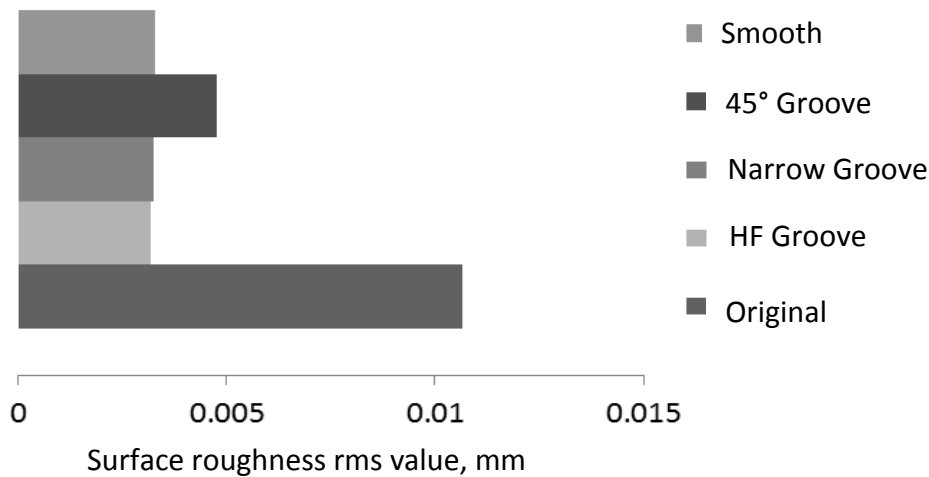
Figure 3-18. Bar chart showing the surface roughness, rms, value for each of the different shim designs.
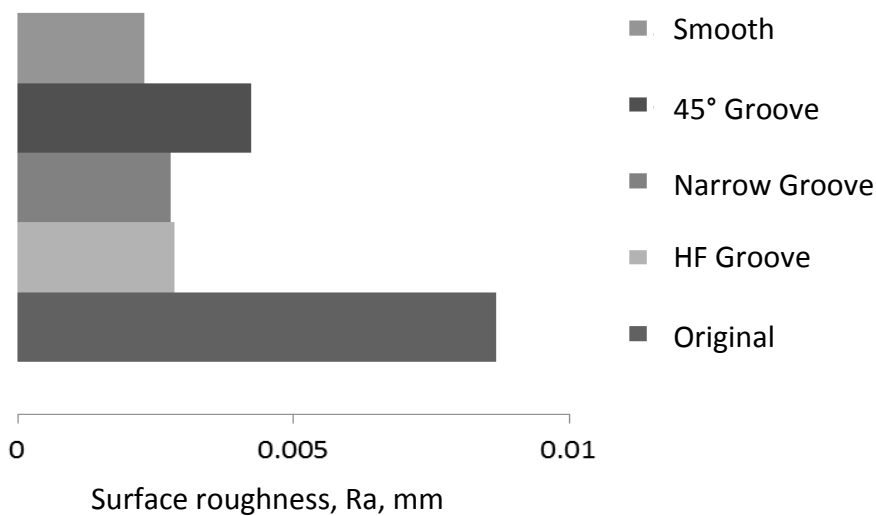
Figure 3-19. Bar chart showing the surface roughness value, Ra, for each of the different shim designs.

3.5.2.3 Significant Correlations

The data from both data sets, the shim coatings and surface structures were combined to test for significant correlations throughout the data set, totaling 327 samples. For normally distributed data the Pearson's correlation test was used and for non-parametric data the Spearman's Rank correlation test was used. Although the relationship between seal surface area and burst pressure was not clear, Figure

3-20, a significant correlation was found between burst pressure and seal area when using Spearman's Rank correlation test (p = 0.021, s = 0.119, Figure 3-20), with a reduction in seal surface area there was an increase in burst pressure.
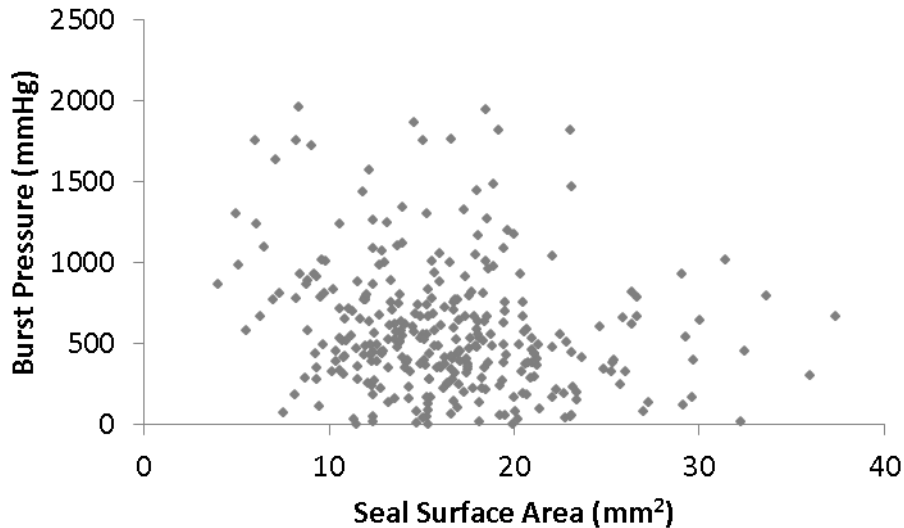
Figure 3-20 Scatter graph showing the relationship between burst pressure and seal area (p = 0.021, s = 0.119)

A significant correlation was found between burst pressure and peak peeling force (p = 0.027, s = -0.12, Figure 3-21). With an increase in peak peeling force there was a reduction in the burst pressure of the seal. A further correlation present within the data was a correlation between vessel wall thickness and peak peeling force (p= 0.012, s = 0.139), with an increase in vessel thickness resulting in an increase in peak peeling force, although there was substantial scatter present in the data, with trends difficult to see on the graph.
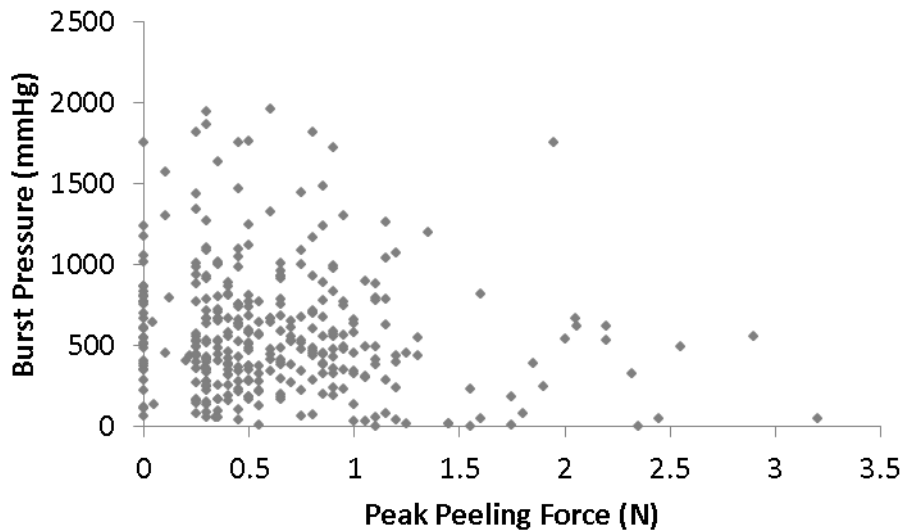
Figure 3-21 Scatter graph showing the relationship between burst pressure and peak peeling force ($p = 0.027$, $s = -0.12$).

3.6 Discussion

3.6.1 Vessel Properties

Electrosurgical seal strength has previously been shown to vary based on vessel outer diameter, the region of the body the vessel is from and whether it is an artery or vein (Carbonell, *et al* 2003, Richter *et al.*, 2006a, Sindram *et al.*, 2011, Wallwiener *et al.*, 2008). This study investigated the variation in seal strength along the length of a porcine carotid artery, where the strength was found to increase with increasing distance from the bifurcation. Additionally, with increasing distance from the bifurcation there was a reduction in elastin content and outer diameter of the vessel, indicating both of these factors influence the seal quality. At 12mm from the bifurcation the lowest seal strength (246.67 ± 193.00 mmHg) was recorded, with this position also recording the least variation in seal strength, and the highest seal failure rate (77.5%). This could be due to the region of the vessel having little variation in both outer diameter (5.91 ± 0.46 mm) and elastin content (35.28 ± 5.21 %). In the mid region of the vessels, at a distance of approximately 38mm from the bifurcation there was a large variation in seal strength (963.22 ± 718.20 mmHg), with this region having the highest variation in both elastin content (26.25 ± 11.52

%) and vessel outer diameter (4.51 ± 0.95 mm), and the second highest seal failure rate (11.1%)

With increasing distance from the bifurcation there was a reduction in the amount of elastin with little change in the collagen content, supporting existing research (García *et al.*, 2011). As a result no correlation was found between collagen and any other variable. However a significant correlation was found between seal strength and elastin content (*p*= 0.001, *s*= -0.520); with a reduction in elastin content there was an increase in seal strength. Due to the histological staining used it was not possible to quantify the smooth muscle content of the blood vessels, although an increase in smooth muscle cells with increasing distance from the bifurcation has been reported (García *et al.*, 2011). Previous studies highlighted the importance of morphology on the seal strength (Richter *et al.*, 2006a, Wallwiener *et al.*, 2008) and it is thought that a reduction in smooth muscle content in more elastic vessels results in less resistance to thermal damage, possibly leading to larger areas being excessively heated (Richter *et al.,* 2006a), with excessive heating thought to damage the seal and tissue adjacent to the seal leading to a reduction in seal quality. This study found a significant difference between the burst pressures of predominantly muscular and elastic vessels (*p*= 0.0001) suggesting that electrosurgical sealing will be more effective in the more muscular regions of the blood vessels.

With increasing distance from the bifurcation there was also a reduction in the outer diameter of the vessel, with this reduction in vessel size correlating with an increase in seal strength (*p*= <0.0001, *s*= -0.665).This relationship has previously been widely reported in literature (Carbonell, *et al* 2003, Dilley *et al.,* 1995) with one explanation for this relationship being the increased amount of material between the device jaws for larger vessels leading to a more superficial penetration of current (Sigel and Acevedo, 1963). This results in the greatest thermal effects being in the adventitia layer of the blood vessel wall (Sigel and Acevedo, 1963), although further work is required to explore this idea further. One suggestion to create a deeper penetration of current and a more even thermal spread through the vessel wall is the use of fine teeth on the contact surface of the jaws.

Additionally a larger diameter vessel will be subjected to higher stresses throughout the vessel wall when compared to a smaller vessel with the same wall thickness at the same pressure. This higher stress within the vessel wall may also provide an explanation as to why larger vessels fail at lower burst pressures.

A significant correlation existed between vessel outer diameter and % of elastin ($p=$ <0.0001, $s=$ 0.559); with a reduction in vessel outer diameter there was a reduction in % of elastin. This relationship makes it difficult to attribute the variation in seal strength to one factor alone, although it is thought that both vessel morphology and size do contribute significantly to seal strength. Although it is difficult to attribute an increase in seal strength to one factor, the data indicates that the size of the vessel is the more influential factor in determining the strength of a seal, with all vessels with an outer diameter of less than 5mm resulting in a seal quality of sufficient standard (BP$\geq$ 360mmHg), irrespective of whether the vessel was predominantly muscular or elastic. Additionally, the anomaly observed in the muscular group of the study can be explained by the fact that this was the only muscular sample with a vessel size greater than 5mm, further demonstrating the significance of vessel size. However, vessel size does not explain the anomalies in the elastic group.

As stated previously, the results demonstrated that a seal of sufficient strength will be produced for a vessel with an outer diameter less than 5mm. When looking at a porcine carotid artery, seals performed at a distance of greater than 64mm from the bifurcation also met the minimum safety threshold, with a seal failure rate of 0.0%. This is due to vessels of 5mm or less being found in this region. Additionally at this distance the vessel morphology is more muscular (lower percentage of elastin) which is thought to help achieve a good seal strength. Vessels sealed at 12mm from the bifurcation were too large and elastic to produce a successful seal consistently. In the mid region of the vessel, approximately 38mm from the bifurcation, there was large variation in the vessel diameter and vessel morphology, making it difficult to achieve a consistent seal quality in this region.

Although the trends do exist in the data there was still substantial scatter, a finding that appears throughout a number of other studies (Presthus *et al.*, 2003,

Carbonell, *et al* 2003, Sindram *et al.*, 2011, Wallwiener *et al.*, 2008). The change in vessel diameter and morphology do not appear to account for all the variation in the seal strength thus further work is required to gain a greater understanding of the sealing process. However the variation in seal strength can, in part, be attributed to varying vessel characteristics and as such technology needs to adapt to account for variation amongst vessels and provide more consistent results.

3.6.2 Shim Modifications

Tissue sticking is known to be a problem for surgeons during electrosurgical procedures and can affect the performance of devices. The level of adhesion has been investigated previously within literature, although the numbers of studies quantifying adhesion are limited, with the majority opting to use a qualitative method. Therefore the effect of adhesion on seal quality has not previously been thoroughly investigated. This chapter has demonstrated a significant relationship between the level of adhesion and the seal quality (p = 0.027, s = -0.120), with an increase in adhesion there is a reduction in the seal quality, indicating the seal was damaged during removal from the surface of the shims. To verify damage was occurring to the seal during removal from the device, the seal should be assessed using microscopic imaging and histology techniques to closer inspect the integrity of the seal. The correlation between burst pressure and adhesion highlights the importance of reducing adhesion during the electrosurgical sealing process.

Two areas were investigated in an attempt to reduce the level of adhesion during the sealing process; non-stick coatings and shim surface features, with both areas previously being investigated and being shown to effect the level of adhesion, although in the case of shim surface features only a simple comparison between structured versus smooth shims was conducted (Richter *et al.*, 2006a). The original shims were compared to five surface coatings, Electrolube, and seven surface feature designs.

When considering the performance of the different coatings and the Electrolube, no coating or treatment offered a statistically improved performance in terms of the level of adhesion. The original shims are coated in NiCr, and results from work conducted suggest that this is the best coating out of those tested. However, work

by Hsu *et al* (2010) found coatings that led to less adhesion, suggesting that if more coatings were tested it would be possible to improve the performance of the device in terms of the level of adhesion.

The level of adhesion was significantly affected by the surface features of the shims, with grooves in the longitudinal direction performing statistically worse in terms of peel strength than the other shims considered in the shim surface features analysis. Shims with grooves orientated at 45° to the datum point resulted in the lowest mean peel strength, although they were only statistically lower than the smooth shims. These results suggest that the groove orientation is one the most influential factors affecting the level of adhesion, with all shims with transverse grooves performing similarly. The HF grooved shims and the narrow grooved shims resulted in lower levels of adhesion when compared with the original grooved shims, indicating that narrower grooves result in less adhesion.

Previous studies have reported more pronounced adhesion when comparing structured shims to smooth shims, although the level of adhesion was not quantified and only compared with one structured surface. When comparing the smooth shims to shims with a transverse groove, all shims with a transverse groove performed better in terms of adhesion (mean peel strength), contradicting previous findings. However as discussed previously shims with grooves in a longitudinal direction result in a higher level of adhesion, this demonstrates that the optimum surface structure could lead to a lower level of adhesion, but if the wrong surface features are applied it could have a negative effect on the level of adhesion.

When considering the level of adhesion it is also important to consider the surface roughness of the shims, although it is important to note that this study did not aim to investigate this parameter, and therefore only two surface roughness's were compared. There was no statistical difference when comparing the peel strengths of the smooth and original shims, although there was a significant difference between the surface roughness of the two shim designs. Although there was no statistical difference in the performance of the shims when considering the peel strength, the effect of the roughness and coating was clearly demonstrated Figure 3-16, Table 3-5), with a lower mean peel strength and less variation in the original

shims with the coating and higher surface roughness, although it was not clear whether the coating or surface roughness led to the improvement in performance. When considering the adhesion a significant correlation was found between the vessel wall thickness and the peak peeling force (p = 0.012, s = 0.139). With an increase in vessel wall thickness there was an increase in adhesion. It is thought this is due to the increase in tissue between the shims resulting in a prolonged sealing time and excessive heating of the outside of the vessel wall, as discussed in section 3.6.1. With excessive heating there would be more charring and heating of the tissue on the outside of the vessel, leading to more pronounced adhesion.

Furthermore the burst pressures of the shims using different coatings and treatments were compared. A statistical difference was found between the burst pressures of the different coatings, although none performed statistically better than the original shims, but the DLC, WS_2 and the passivated shims lead to a reduction in seal quality compared to the original shims. This difference in performance could be due to the thickness of the coatings and the conductivity of the coatings, with DLC a known insulator and therefore expected to reduce the seal quality.

Shim surface structure has previously been shown to affect the seal quality although the extent of the effect of surface structure has not been investigated thoroughly with a simple comparison of structured versus smooth being provided (Richter *et al.,* 2006b). Work conducted throughout this chapter has demonstrated that the structure of the shim surface can both significantly affect the seal quality and the level of adhesion. When considering the effect of shim surface structure on burst pressure no shim performed statistically better than the original shims, although two shim designs, the HF grooved and combination, produced a higher mean burst pressure (Original = 585.45 ± 261.77mmHg, HF Grooved = 606.33 ± 238.74mmHg, and Combination = 764.46 ± 388.33mmHg). It should also be noted that the HF grooved shim had a lower standard deviation and thus less variation in burst pressure suggesting a more consistent performance. Although it appears to provide a more consistent performance it also had a higher seal failure rate when compared to the original shim, 14.3% and 5.0% respectively. The seal failure rate of

the combination shim was 0.0%, a further improvement compared with the original shim, although it did present more pronounced adhesion.

The 45° shims performed statistically worse when compared with all other shim designs and produced a significantly higher seal failure rate at 89.5%. Furthermore when a combination of different orientation grooved shims were used there was an improvement in the seal quality as discussed previously. When considering the variation in other surface structure properties there was no statistical difference found in seal quality, although it appears that having grooves and peaks of equal width led to better performance, enhanced further by making both the groove and peaks narrower.

Previous studies have suggested the shape of the electrode can affect the shape of the seal (Sigel and Acevedo, 1963), and this study demonstrated that this can be extended to include the structure of the surface of the shim (Figure 3-22). Figure 3-22 below shows the groove pattern of the shim is transferred to the sealed area, an observation that occurred repeatedly throughout the study but not consistently. It is unclear at this stage the effect this had on the quality of the seal although it is thought to affect the mechanism of seal failure. The orientation of the grooves on the shim will affect the orientation of the grooves on the seal thus affecting how the seal fails, and where stress concentrations occur in the seal. Additionally the thickness and frequency of the grooves would therefore also affect the seal quality, providing an explanation as to the difference in performance of the different shims. Further work in subsequent chapters will explore this hypothesis further. Additionally with a change of surface structure comes a change of surface area of the shim, with a structured surface there is an increase in surface area when compared to the smooth shims. It is therefore possible that this increase in surface area allows for a greater tissue effect because of the increase in contact area between the vessel and the shim.
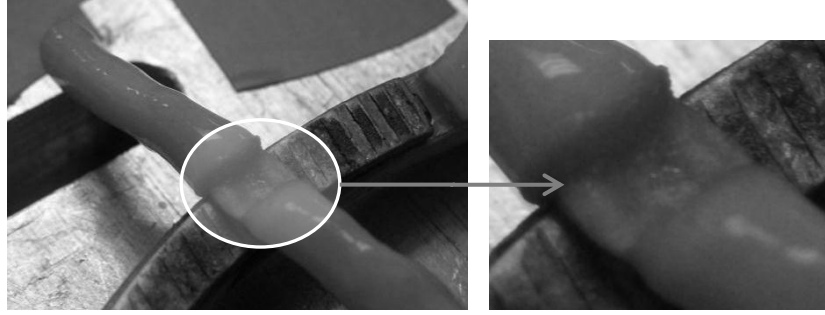
Figure 3-22. Image showing a sealed carotid artery using shims with a grooved surface structure. Image demonstrates how the grooved pattern is transferred to the sealed vessel.

There was no statistical difference between the original shims and the smooth shims when considering either burst pressure or adhesion levels, even though there was a significant difference between the surface roughness values of the two shim designs. As such this suggested that surface texture had a limited effect on the seal quality achieved, and that surface structure is the more influential factor, as all other shims have similar surface roughness values but present differences in both seal quality and adhesion levels.

There was a significant correlation found between the seal area and the quality of the seal (p= 0.021, s=0.119), with a smaller seal area resulting in a seal of greater quality. A smaller seal area suggests a greater level of contraction and a greater tissue effect. Furthermore it is also thought that the difference in seal size could be an indication of a different sealing process for each of the shims, although further experimental work is required to explore this idea further. There was a statistical difference in the seal area of the different shims, and in general shims with grooves produced a seal of smaller area than those without. Overall it was the combination shim set that created the smallest seal area, indicating that this device produced the greatest tissue effect, which could explain how the shim set achieved the greatest seal quality. This could be demonstrated further by the seal size for the 45° shims, which produced a larger seal when compared to the combination shim, but also a lower seal quality. Although the results of the original grooved shim and the original shim produced a large seal area, and suggest this trend is of limited effect.

The question remains as to why the grooves have such an effect on the vessel sealing performance. Previous studies have demonstrated a difference in

temperature profiles of shims with different surface features (Dodde *et al.*, 2008), and therefore further work is required to explore this idea further. As mentioned previously, the shape of the electrode, and the surface features, affects the shape of the seal (Sigel and Acevedo, 1963), and therefore further investigation is required to understand the influence of this shape on the quality of the seal and the failure mechanism during seal bursting.

3.7   Conclusion

With increasing distance from the bifurcation there was an increase in the strength of the seal, and a reduction in both vessel outer diameter and elastin content. A significant correlation was found between seal strength and both outer diameter and elastin content. However, there was also a correlation between outer diameter and elastin content making it difficult to attribute an improvement in seal strength to one factor alone. Although the vessel properties accounted for some of the variation in seal strength, substantial scatter was present in the data indicating a need for further investigation and study. When considering the minimum threshold for a successful seal, vessels of less than 5mm in outer diameter were shown to consistently produce a sufficient standard of seal irrespective of vessel morphology. At a distance of 64mm or greater from the bifurcation variation in both vessel size and vessel morphology reduced, and as a result all seals performed in this region met the threshold of a successful seal.

A significant correlation was found between peak peeling force and burst pressure, with an increase in peeling force leading to a reduction in seal quality, demonstrating a need to reduce the level of adhesion. The coatings and treatments tested offered no improvement to the performance of the original shims when considering tissue adhesion, although significant differences were found highlighting the importance of shim coatings. Furthermore the surface structure of the shims was shown to affect the level of tissue adhesion, with the orientation of the grooves being demonstrated to be the most influential factor, and results

suggesting if the optimum design was found it could lead to a reduction in tissue adhesion.

Shim surface structure was shown to have a significant effect on both seal quality and the level of adhesion. When considering the seal quality no shim performed statistically better than the original shim, although the 45° grooved shim performed statistically worse than all other shims. Whilst no shim performed statistically better, both the HF grooved shim and the combination shim resulted in a higher mean burst pressure with the combination shim also resulting in a lower seal failure rate. The orientation of the grooves appeared to be the most influential factor affecting burst pressure, thought to be due to the way the shape of the shim influences the shape of the seal, with the pattern of the grooves transferring to the seal. It is thought this influences the way in which the seal fails and its ability to withstand pressure although further work needs to be conducted to explore this idea further, with both further experimental work and computer modelling conducted in subsequent chapters to provide a greater insight.

4 Analysis of Shim Performance using Digital Image Correlation

4.1 Chapter Summary

This chapter expands upon the work from Chapter 3 by investigating the behaviour of the tissue during the sealing process. This was done through the use of digital image correlation (DIC), a non-contact optical method used to measure surface displacement and thus calculate strain. This technique was used to capture the sealing process and subsequently investigate the variation in sealing performance due to different vessel properties and different shim designs. This chapter includes details of the method used and the processing of the collected data. Results presented in this chapter provide a valuable insight into the changes that occur to both the vessel and the device during the sealing process, with the shim gap of the device shown to fluctuate throughout the sealing process and the vessel tissue to be pulled towards the device. Furthermore the results showed that no two seals were performed in the same way with a difference in displacement magnitude and the pattern of the displacement for both the displacement of the jaws and the tissue. To expand upon the work conducted within this chapter, subsequent chapters will describe the use of finite element modelling to improve the understanding of the variation in seal quality further.

4.2 Introduction

As discussed in the previous chapters there are many factors that can influence the quality of an electrosurgical seal including the morphology and size of the blood vessel and the surface structure of the shim. Work looking at the effect of these parameters is limited to understanding their relationship with seal quality with a limited understanding as to why these parameters affect sealing performance. The aims of the tests described in this chapter was to improve understanding as to the behaviour of the vessel during the sealing process and to establish why vessel parameters and shim designs have such a significant influence on seal quality.

Existing work in the literature has compared smooth and structured shims, with structured shims being shown to reduce the number of seal failures and lead to a lower sealing temperature. These results came from a simple comparison of just two shim designs and provided no understanding as to how different surface features would affect the sealing process (Richter *et al.,* 2006b). Work conducted in the previous chapter is the most comprehensive study to date in exploring the effect of surface structure on the sealing process, discussing the effect of surface structure on the quality of the seal, seal failure rate, adhesion and the size of the resulting seal (seal surface area). The design of the shim was shown to have a significant effect on each of these parameters and as such a further understanding as to how and why the shims performed differently was required.

To assess the performance of the different shims a non-contact method was required so it would not have any influence on the sealing process. As such it was decided to use digital image correlation (DIC). DIC is a non-contacting optical method used for measuring surface displacement and thus calculating strain(Zhang and Arola, 2004). The method has many applications with biological tissues including measuring the mechanical properties of the bovine artery, monitoring the loosening in cemented total hip replacements (Zhang and Arola, 2004) and the mechanical properties of human skin (Evans and Holt, 2009). Due to a number of limitations with biological tissues including size, shape, and the necessity of maintaining hydration, optical methods have many advantages due to being non-contact. There are a variety of optical methods available that are suitable for use with soft tissue. However their measurement range is often small (≤ 100 μm), limiting their application (Zhang and Arola, 2004).

The aim of the work in this chapter was to use DIC to capture the sealing process and use the results to provide a greater insight as to the changes occurring in the tissue during the sealing process. Furthermore the study aimed to investigate differences in the sealing process for the different vessels, considering the vessel morphology and the outer diameter of the blood vessel. Additionally the aim was to use DIC to investigate differences in the performance of the different shim designs

to understand why the different shim designs result in dissimilar sealing performances.

4.3 Methods

4.3.1 Digital Image Correlation

The theory behind DIC was discussed in Chapter 2, detailing how displacement and strain are computed by the software through the use of pattern recognition techniques. The subsequent sections will detail the DIC set-up used to conduct the experimental work and conduct the study.

4.3.1.1 Equipment

The DIC system used was the Q-400 (Dantec Dynamics), consisting of the necessary software, a HiLis light source and a data logging system to connect the cameras to the laptop. The HiLis light source is a high intensity LED illumination system which provides cool and homogeneous illumination. Two digital cameras were used with the system, along with the appropriate lenses. The specification of the cameras and lenses are displayed in Table 4-1.

Table 4-1 Manufactures specification for the cameras and the lenses used with the DIC system

Camera		
Number of Cameras	**Manufacturer**	**Resolution**
2	Limess	1600 x 1200 2/Megapixels
Lenses				

Manufacturer	Name	Magnification Range [1:]	Working Distance (mm)	Object to Image Distance (mm)
Schneider Kreuznach	XNP 2.0/28 Compact	>5.9	>174	>232

In order to position the cameras and light source a tripod stand was used with attachments so only one tripod stand was required. In addition to the DIC system the pressurisation apparatus used for the burst pressure testing was required for this study; with the equipment and set-up of this apparatus is detailed in Chapter 3.

4.3.1.2 Set up

The saline infusion apparatus was set up as described previously in Chapter 3. Once this was set up markers were placed on the testing surface (Figure 4-1) to ensure the equipment would remain in a consistent location throughout the analysis.

Markers for position of saline infusion apparatus
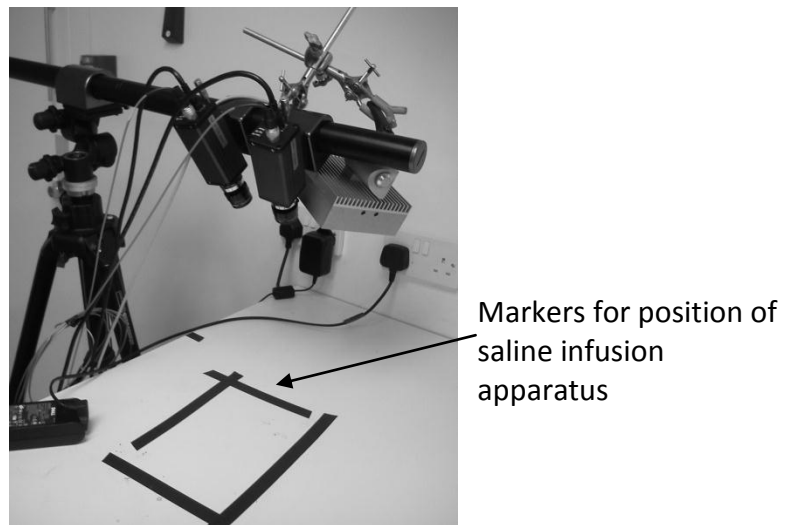
Figure 4-1 Image of the markers used to mark the position of the saline infusion circuit ensuring consistent location throughout the assessment

The two cameras were mounted onto a tripod with HiLis light source positioned between the two cameras. The cameras were positioned directly above the specimen to ensure no part of the blood vessel was obscured during the sealing process (Figure 4-2). The two cameras were connected to a data logging system, which in turn was connected to the laptop. Following this the aperture and focus of both cameras was adjusted, with cameras focusing on a rubber tube with a speckle pattern applied to simulate a blood vessel. This rubber tube was used throughout the system set-up. When adjusting the aperture and focus of the cameras it was necessary to ensure that both cameras had the same field of view and aperture, leading to an easier and better calibration.
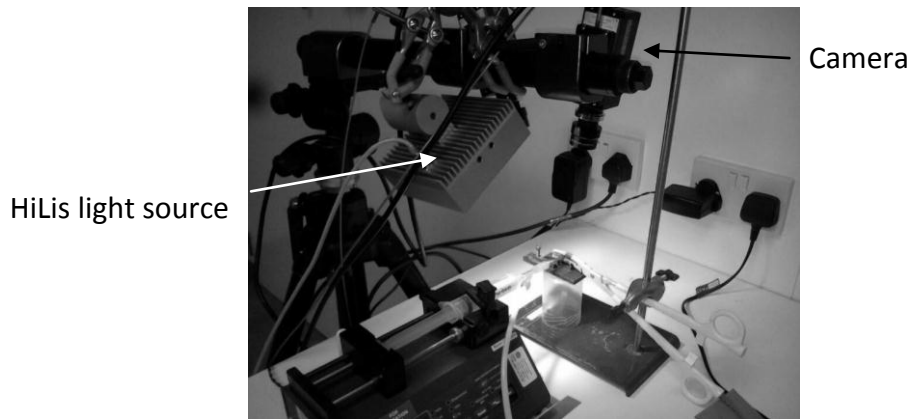
Figure 4-2 Image of the DIC system set up with the two cameras positioned above the specimen, along with the HiLis light source.

To ensure the vessel sealing device did not move during the analysis the device was mounted using a clamp and stand (Figure 4-3). The position of this clamp was also marked in the same way as the saline infusion apparatus to ensure the equipment remained in a consistent location during the analysis.
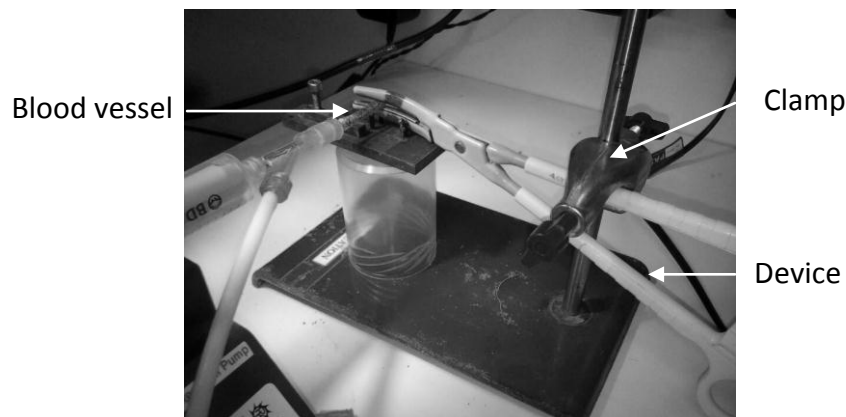
Figure 4-3 Image of the electrosurgical vessel sealing device held in position using the clamp and stand, ensuring the device did not move throughout the analysis.

4.3.1.3 System Calibration

Following the set-up of the DIC system it was necessary to calibrate the system. The calibration is necessary to determine the position and orientation of each of the cameras with respect to the surface of the specimen and relates to the pixel size of the object's image to the metric scale. In order to calibrate the system a series of eight calibration images were taken of a calibration target. The calibration target used for this study was a 9x9 grid, 40mm x 40mm (Dantec Dynamics). The target

was rotated and tilted for each image to allow the software to determine the required parameters. A calibration residuum of <0.1 was considered acceptable (Barton, 2012). The calibration residuum is the average uncertainty of the found markers in the unit of pixels.

4.3.1.4 Specimen Preparation

The blood vessels were prepared for testing in the same way as previously described in Chapter 3. Blood vessels were skeletonised using surgical scissors to remove all connective tissue and then split into sections. Blood vessels were split into 40mm sections with seals being located at 25mm and 65mm from the bifurcation.

4.3.1.5 Capturing the Sealing Process

Following the preparation of the specimen, the blood vessel was connected to the saline infusion circuit using a haemostat. The free end of the specimen was also clamped using a second haemostat to create a small amount of axial tension and to allow the vessel to be pressurised. The blood vessel was pressurised to approximately 60 mmHg and the speckle pattern was applied. The pattern was applied by first applying a layer of white face paint as a base layer, and subsequently using a make-up brush to sprinkle black powder over the surface of the specimen. In addition to applying the speckle pattern to the blood vessel, the pattern was applied in the same manner over the outer surface of the upper jaw. Once the speckle pattern was applied a trial run was conducted to ensure that the pattern was of sufficient standard to achieve good data collection. This consisted of capturing two shots using the DIC system, and processing the data through the software and checking for gaps within the resulting image. If there were no gaps the vessel was clamped using the device being tested. If there were gaps within the resulting image the speckle pattern was adjusted or reapplied and the trial process was repeated until the speckle pattern was of sufficient standard. The sealing process was then captured; the process was captured at a frame rate of 5Hz, with a 6 seconds period being captured. The sealing began 1.5 – 2 seconds after the DIC system began capturing the images.

4.3.1.6 Data Processing

Data was processed within the DIC software using the parameters displayed in Table 4-2. A mask was drawn covering both the surface of the jaws and the surface of the blood vessel, with these two areas being defined as the areas of interest. Two start points were defined for each sample, one located on the jaws and one on the vessel. The start point was a point which can be found within all captured images of the specimen to allow the software to conduct the necessary calculations and processing. For each sample the z displacement for the device jaws, the y displacement for the tissue, and the true principal strain for the tissue were considered. Instra 4D software was used to both capture and process the data.

Table 4-2 Parameters for the DIC testing

Technique Used	Digital Image Correlation
Calibration Residuum	<0.1 pixels
Speckle Pattern Size	0.06 - 0.28mm
Displacement Noise	0.0052 mm
Subset	17 pixels
Step Size	17 pixels
Total Number of Images	30 (5Hz)
Displacement	
Spatial Resolution	0.425mm
Strain	
Smoothing Method	None applied

When processing the z displacement of the jaws, a line was drawn along the length of the jaws and the data was exported as an ASCII file. This data was then imported into MATLAB (MathWorks, Massachusetts, USA) and a surface plot was created, showing how the mean z displacement varied along the length of the jaw throughout the duration of the analysis. The MATLAB commands and code used for this processing can be found in Appendix A. Additionally a line was drawn across the width of the jaws, 1.5-2 mm from the end of the jaws furthest from the handles of the device, with the mean z displacement exported to Excel. This allowed for the comparison of z displacement for all samples.

When processing the y displacement of the tissue it was more subjective as a number of samples lost significant detail in the area of the vessel adjacent to the jaws. When enough detail remained a line was drawn along the length of the vessel

and a surface plot showing how the mean y displacement varied along the length of the vessel for the duration of the seal was produced in the same way as described for the device jaws. Furthermore a line was drawn across the width of the vessel, 5.5 - 6 mm from the edge of the device jaws and the mean y displacement was exported to Excel. This allowed for the comparison of the mean y displacement amongst the different samples. The same was also done for the true principal strain, with the mean principal strain being considered.

4.3.2   Shims and Device Modification

The shims assessed in this chapter were the same as discussed in the previous Chapter 3, with the device being modified in the same way. A brief summary of these designs and previous results is presented in Table 4-3.

Table 4-3 Summary of shim designs including results from work in Chapter 3. Burst pressure is presented as the mean ± SD

Shim Number	Shim Name	Surface Features				Previous Results	
		Groove Width /mm	Groove Depth /mm	Peak Width /mm	Groove Orientation	Mean Burst Pressure /mmHg	Seal Failure Rate
1_OR	Original	No Surface Features				585.45 ± 261.77	5.0%
2_SM	Smooth	No Surface Features				468.77 ± 192.80	27.3%
3_GR	Grooved	1	0.1	1	Transverse	547.05 ± 266.24	14.3%
4_NA	Narrow Grooved	0.5	0.1	1.5	Transverse	507.00 ± 209.07	33.3%
5_HF	HF Grooved	1	0.1	1	Transverse	606.33 ± 238.74	14.3%
6_LO	Longitudinal Grooved	1	0.1	1	Longitudinal	549.85 ± 253.22	25.0%
7_45	45° Grooved	0.5	0.1	0.5	45 Degrees	191.05 ± 113.17	89.5%
8_CC	Combination	Combination of the grooved (3_GR) and longitudinal (6_LO) shims				764.46 ± 388.331	0.0%

4.4   Results

The number of samples captured for each shim was kept consistent at 6 samples per shim, with this number being chosen to give a sufficient number of samples for this study. The sample size reported for each shim varies however based on the quality of the data captured and the number of samples with useable data, where sufficient detail remained throughout the analysis.

4.4.1   Device Displacement

During the capturing of the sealing process using DIC the movement of the jaws was monitored. The displacement of the jaws in the z direction (Figure 4-4) was of interest.
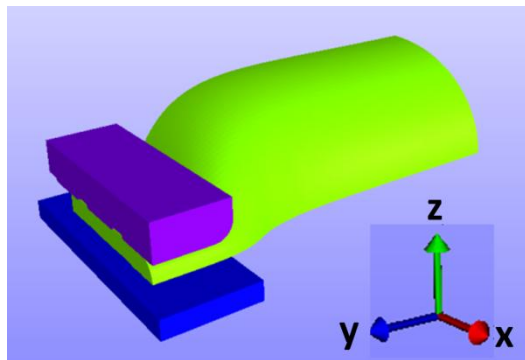
Figure 4-4 Definition of the axes for the processing of DIC data.

The displacement of the jaws for a total of 17 seals was analysed, with the results for the combination, narrow and original shim displayed in Figure 4-5, Figure 4-6 and Figure 4-7 respectively. Results for the remaining shims can be found in Appendix B. Figure 4-5, Figure 4-6 and Figure 4-7 show pulsing of the device jaws occurring throughout the sealing process, with this pulsing resulting in a fluctuation in the shim gap, with a maximum variation of shim gap ≈15%.
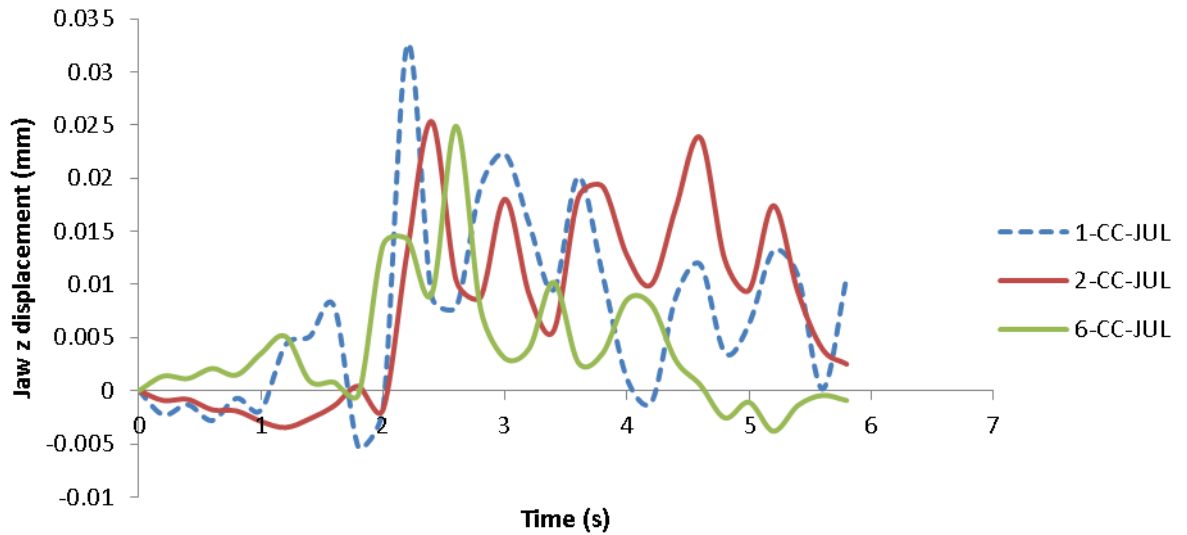
Figure 4-5 The z displacement of the jaws during the sealing process using the combination shim. A positive change in displacement indicates an increase in the shim gap. The different coloured lines refer to different seals performed, with dotted lines referring to specimens sealed at 25mm from the bifurcation and solid lines showing seals performed at 65mm from the bifurcation.
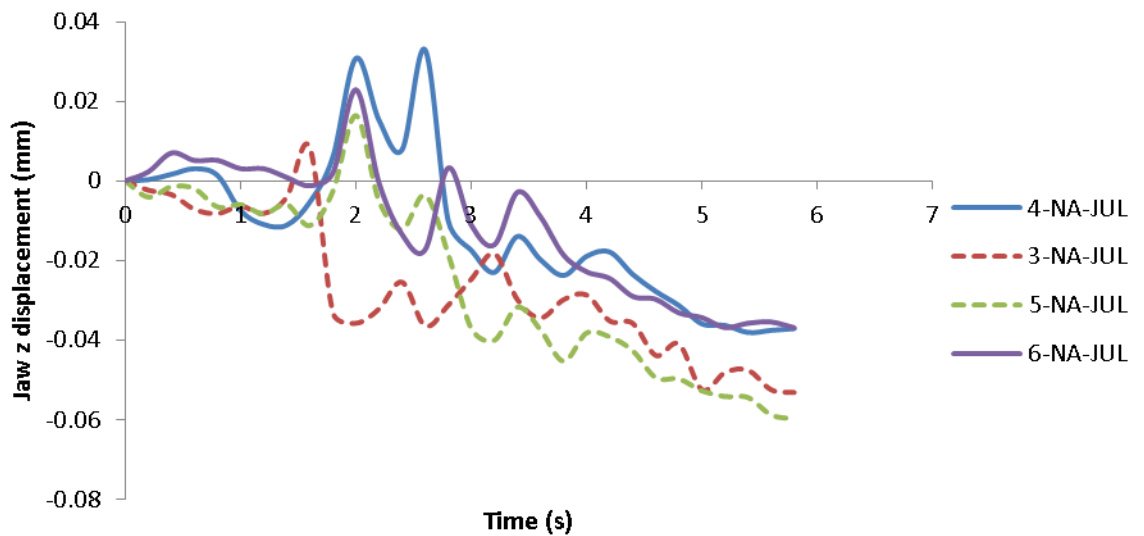
Figure 4-6 The z displacement of the jaws during the sealing process using the narrow grooved shim. A positive change in displacement indicates an increase in the shim gap. The different coloured lines refer to different seals performed, with dotted lines referring to specimens sealed at 25mm from the bifurcation and solid lines showing seals performed at 65mm from the bifurcation.
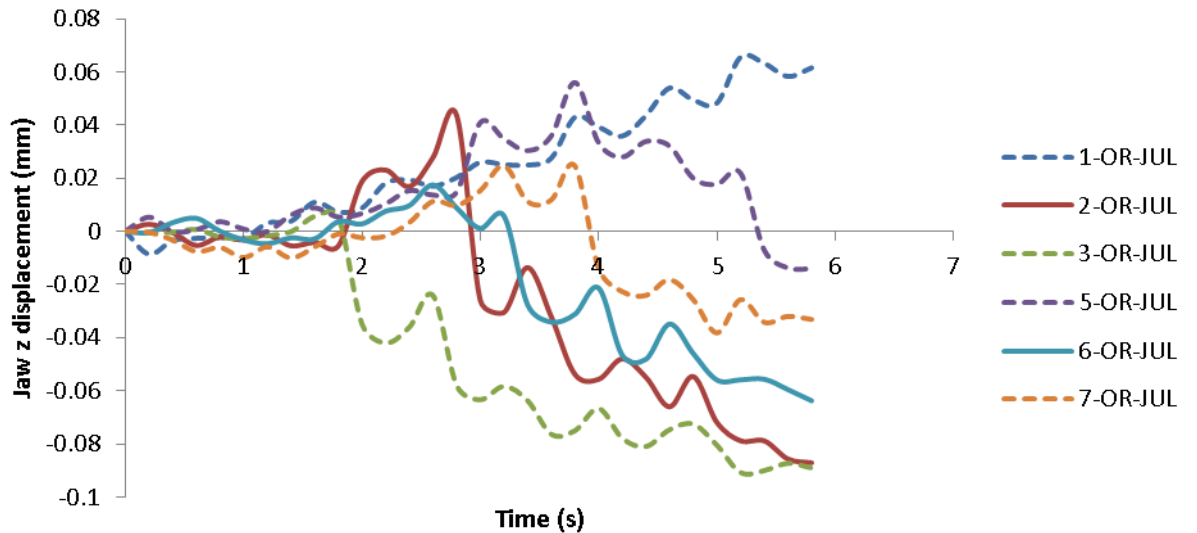
Figure 4-7 The z displacement of the jaws during the sealing process using the original shim. A positive change in displacement indicates an increase in the shim gap. The different coloured lines refer to different seals performed, with dotted lines referring to specimens sealed at 25mm from the bifurcation and solid lines showing seals performed at 65mm from the bifurcation.

Furthermore a surface plot for the displacement of the shims in the z direction was considered. Two examples of this can be seen in Figure 4-8 and Figure 4-9. With Figure 4-8 showing a surface plot for the z displacement of the jaw for a seal performed using a 45° grooved shim, and Figure 4-9 showing the same for an original shim. All other surface plots can be found in Appendix B. The surface plots also show the pulsing of the jaws and show that the change of displacement is greatest at the tip of the device, with the pulsing having a limited effect closer to the handles.
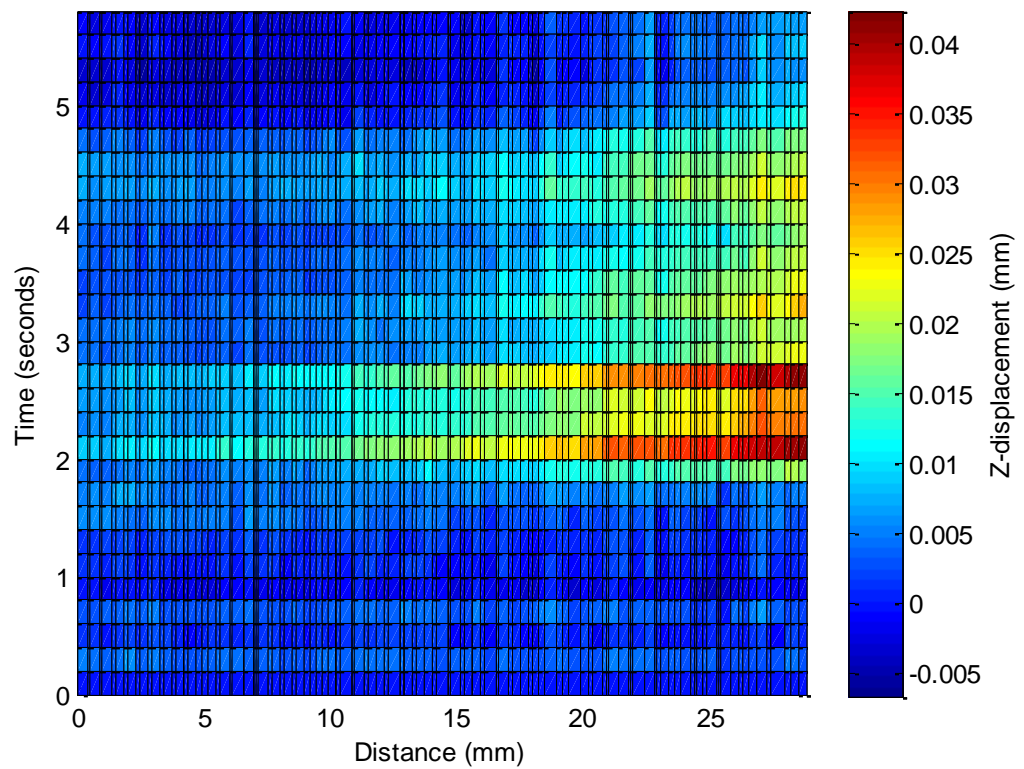
Figure 4-8 A surface plot showing the variation in z displacement along the length of the jaw for the sealing process. Distance refers to the position along the length of the jaw, with 0 indicating the position closest to the handles of the device. The example shown was sealed using the 45° grooved shims, sample number 7-45-JUL.
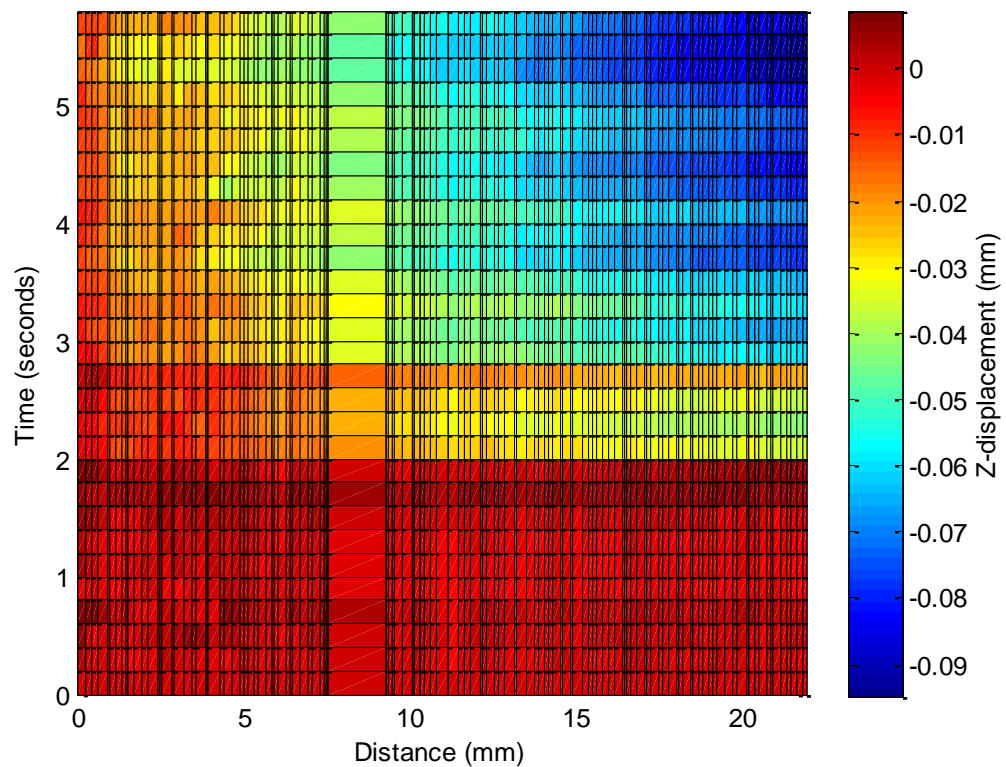
Figure 4-9 A surface plot showing the variation in z displacement along the length of the jaw for the sealing process. Distance refers to the position along the length of the jaw, with 0 indicating the position closest to the handles of the device. The example shown was sealed using the original shims, sample number 3-OR-JUL.

The displacement of the jaws for all samples analysed can be seen in Figure 4-10. The colours on the chart indicate the different shim types used, with the dashed lines indicating seals performed at 25mm from the bifurcation, and solid lines referring to seals performed at 65mm from the bifurcation. As seen in Figure 4-10, each of the seals resulted in a different magnitude of pulsing of the jaws, and each type of shim displayed a different pattern for the pulsating of the jaws, with no trends or patterns seen based on the shim type or the position of the seal.
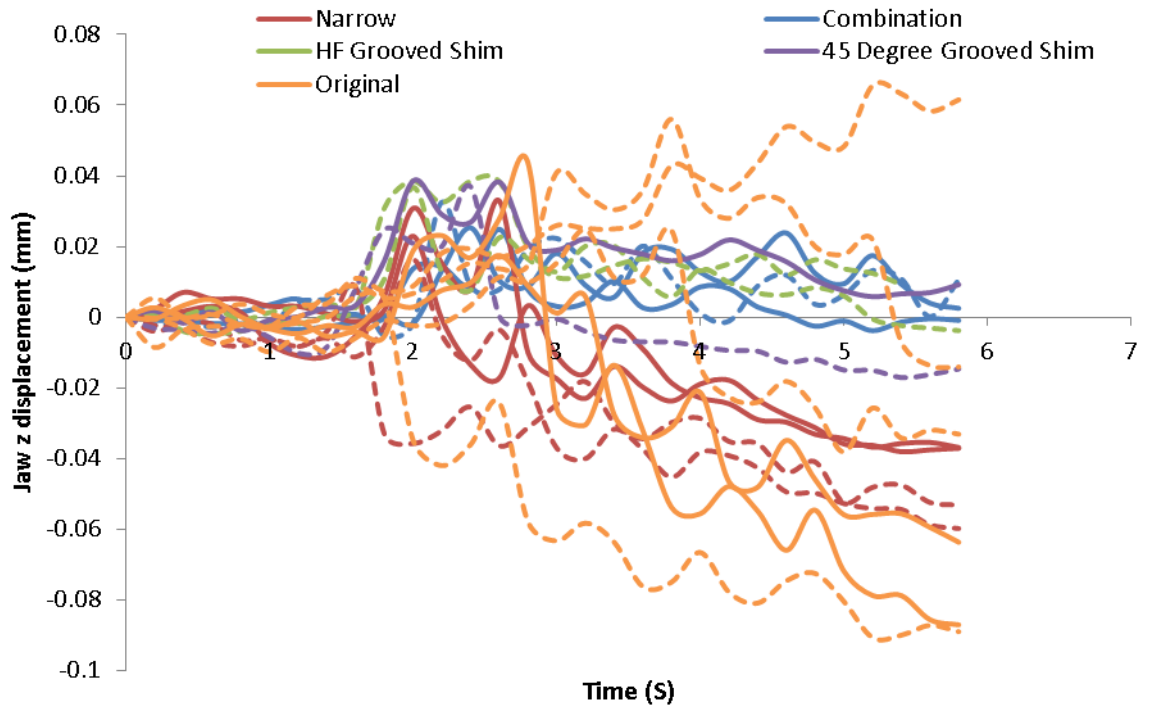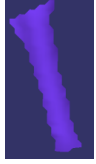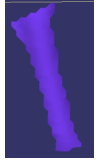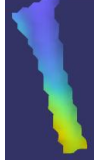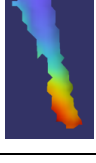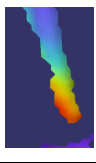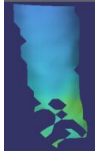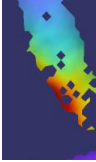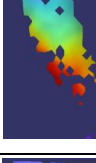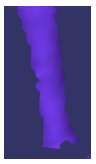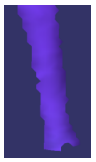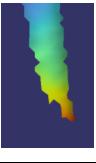
Figure 4-10 The z displacement of the jaws during the sealing process for various shims. A positive change in displacement indicates an increase in the shim gap. The different coloured lines refer to different shims tested, with dotted lines referring to specimens sealed at 25mm from the bifurcation and solid lines showing seals performed at 65mm from the bifurcation.

4.4.2   Tissue Displacement

The displacement of the tissue was analysed for a total of 15 samples, with the displacement in the y direction (Figure 4-4) being of significant interest. Displacement maps at various points throughout the sealing process for a number of seals can be seen in Table 4-4. As can be seen from the images in Table 4-4 there was a significant difference in the displacement between the different samples, with some seals resulting in more displacement in the y direction than others. The difference in the displacement was in both the distribution across the surface of the blood vessel, and the magnitude of this displacement.

Table 4-4 Variation in y displacement of various vessels throughout the sealing process, with seals performed using different shims.

When enough detail remained in the vessel wall throughout the analysis a surface plot of the y displacement along the length of the blood vessel was produced. Two examples of these plots can be seen in Figure 4-11 and Figure 4-12, with these two samples being sealed by the original shim, more samples are presented in Appendix C. As can be seen in the two surface plots show the area close to the shim is subjected to large amounts of displacement compared to the area of the vessel further away from the device. Furthermore Figure 4-12 demonstrated pulsing of the tissue along the length of the vessel. Both surface plots presented show a significant difference in the displacement of the tissue, with both different magnitudes and different patterns presented.
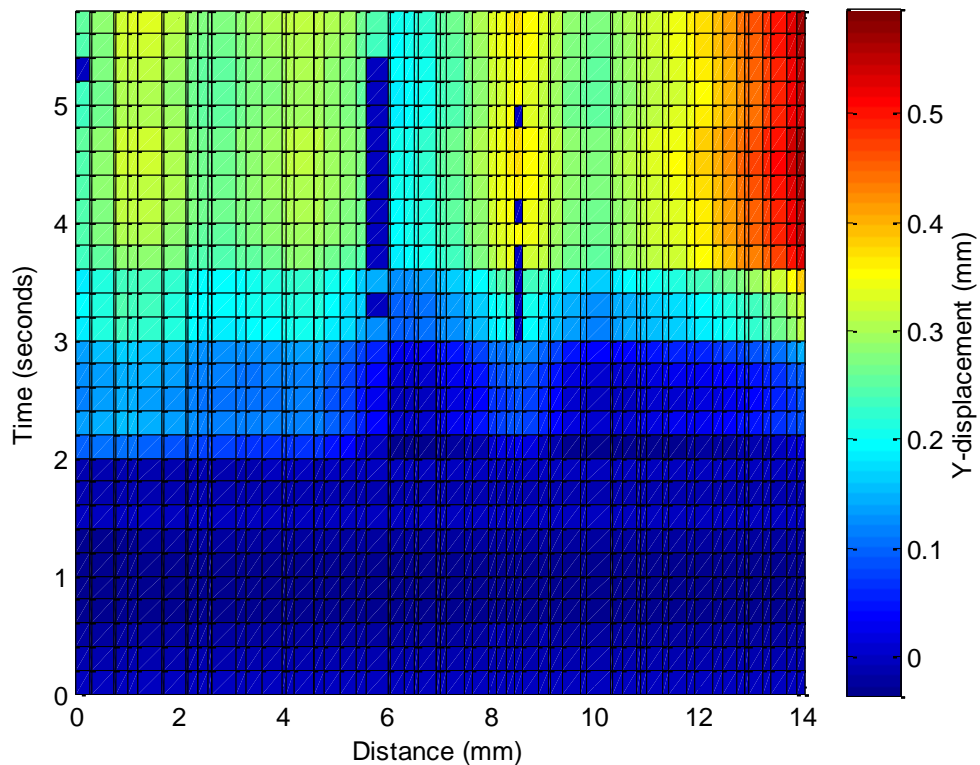
Figure 4-11 Surface plots showing the variation in y displacement along the length of the vessel for the sealing process. Distance refers to the position along the length of the vessel, with 0 indicating the position furthest from the device. Example shown was sealed using the original shims, sample number 2-OR-JUL.
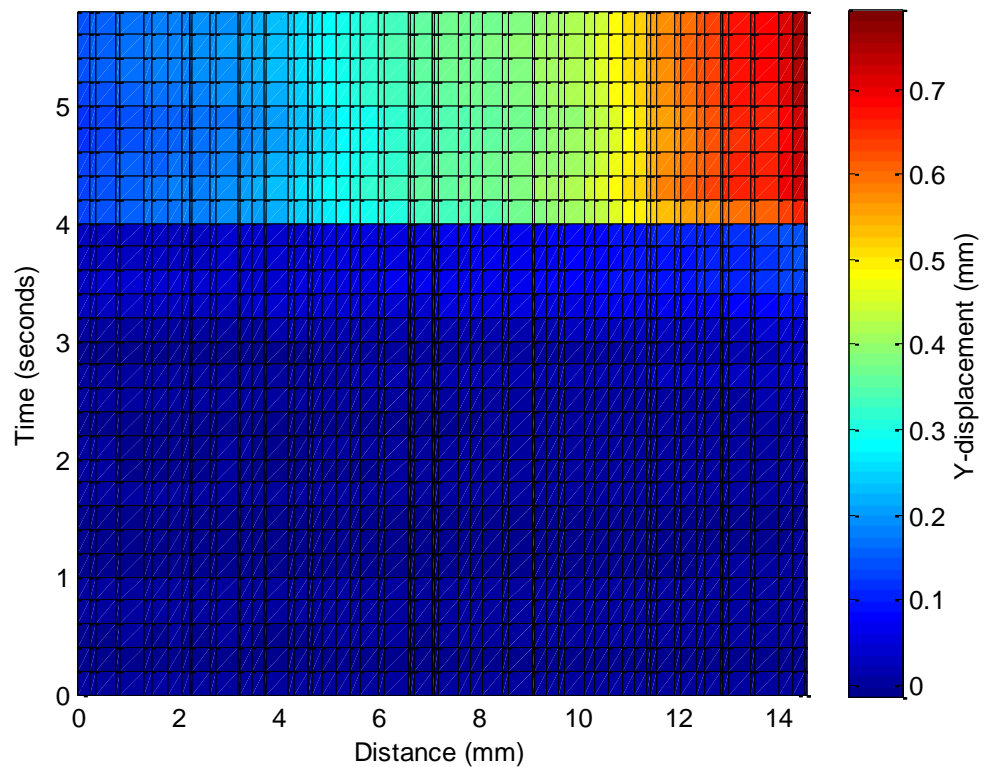
Figure 4-12 Surface plots showing the variation in y displacement along the length of the vessel for the sealing process. Distance refers to the position along the length of the vessel, with 0 indicating the position furthest from the device. Example shown was sealed using the original shims, sample number 7-OR-JUL.

Furthermore the displacement of the tissue was analysed midway along the length of the vessel (5.5 – 6 mm away from the jaw edge). Figure 4-13 shows one example for the HF grooved shims, with the remaining data for each shim set displayed in Appendix C. The Figure shows pulsing of the tissue in the y direction, with periods of sudden and rapid contraction, and periods where the tissue relaxed. Figure 4-14 shows the y displacement of all tissue samples analysed; each seal displayed a different amount of tissue contraction and different patterns of contraction and relaxation. When all data was considered, no trends or patterns were seen in the data, based on both the position and the shim being used to perform the seal.
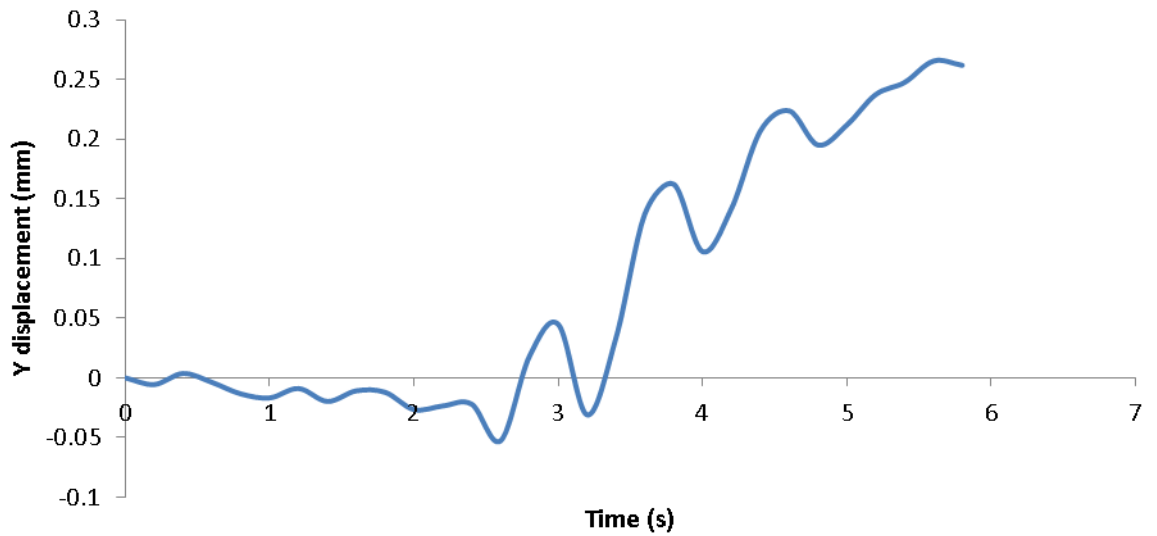
Figure 4-13 The y displacement of the tissue during the sealing process for the HF grooved shims. A positive change in displacement indicates the tissue moving closer to the device.
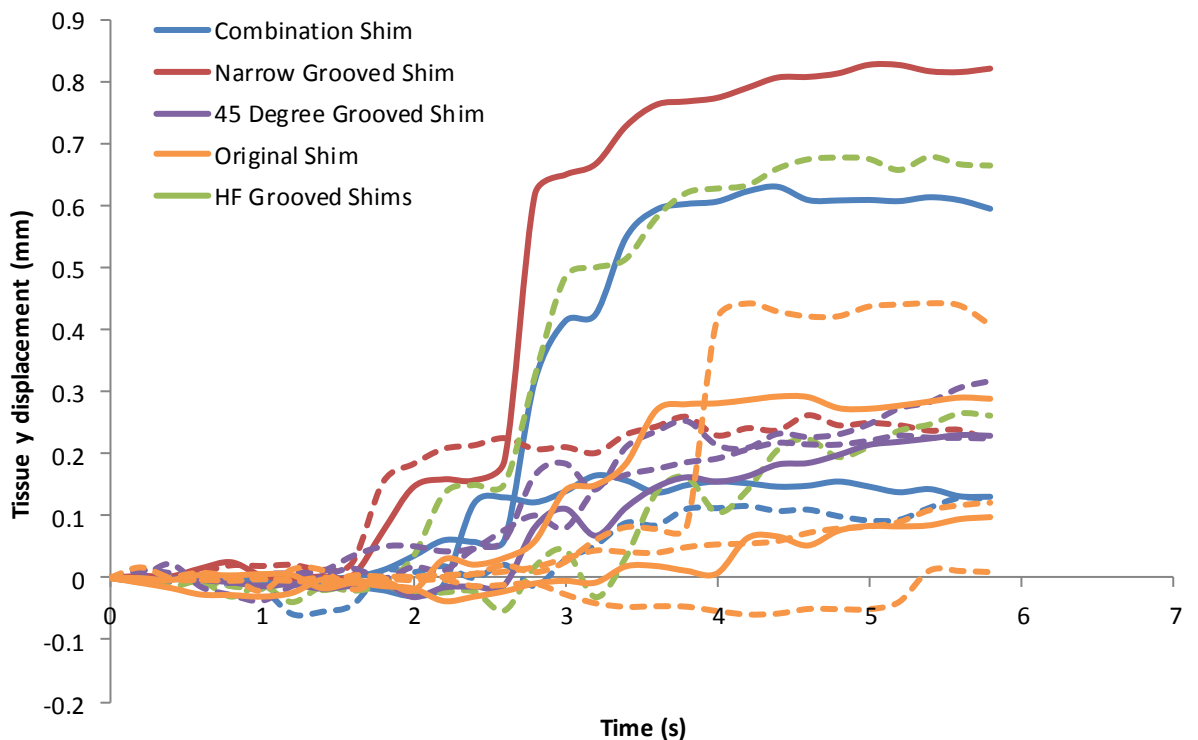
Figure 4-14 The y displacement of the tissue during the sealing process for various shims. A positive change in displacement indicates the tissue moving closer to the device. The different coloured lines refer to different shims tested, with dotted lines referring to specimens sealed at 25mm from the bifurcation and solid lines showing seals performed at 65mm from the bifurcation.

4.4.3   Tissue and Jaw Displacement

Following the analysis of the jaw and tissue displacement separately, the two displacements were considered together. Figure 4-15 – Figure 4-17 are examples of the comparison of the jaw and tissue displacement, with a full data set being available in Appendix D. In each Figure (Figure 4-15 - Figure 4-17), the pulses of the tissue and the jaw can be seen to coincide with one another.
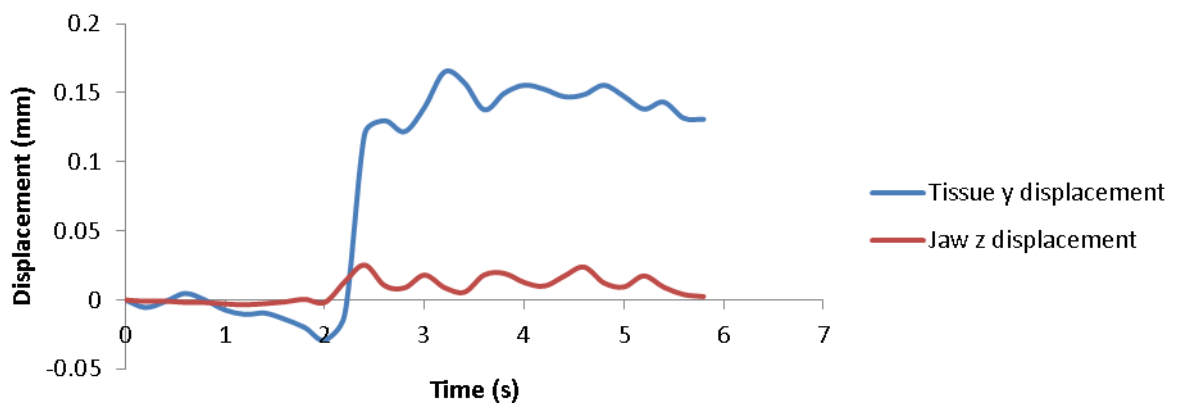
Figure 4-15 The y displacement of the tissue and the z displacement of the jaws during the sealing process for the combination shim, sample 2-CC-JUL. A positive change in tissue displacement indicates the tissue moving closer to the device, and a positive change in jaw displacement indicates an increase in shim gap.
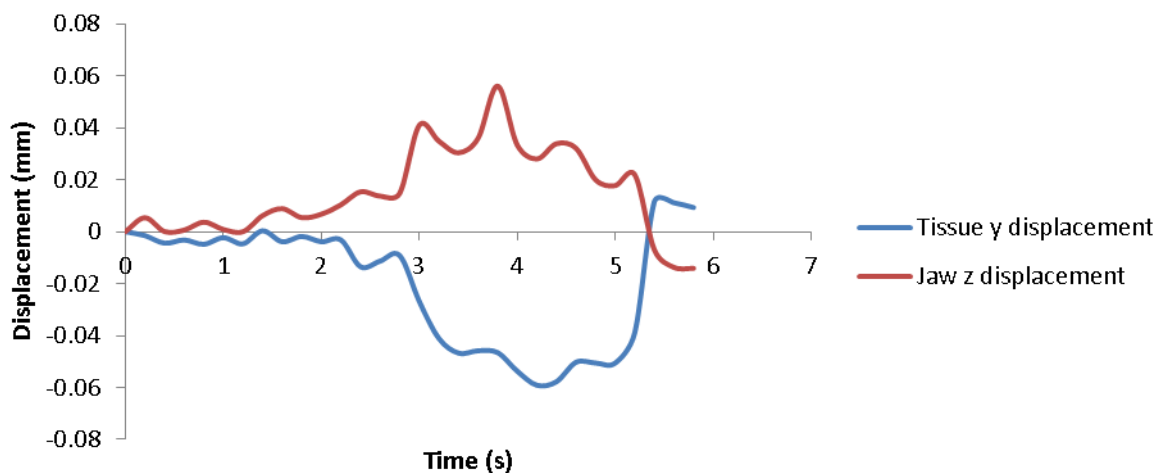
Figure 4-16 The y displacement of the tissue and the z displacement of the jaws during the sealing process for the original shim, sample 5-OR-JUL. A positive change in tissue displacement indicates the tissue moving closer to the device, and a positive change in jaw displacement indicates an increase in shim gap.
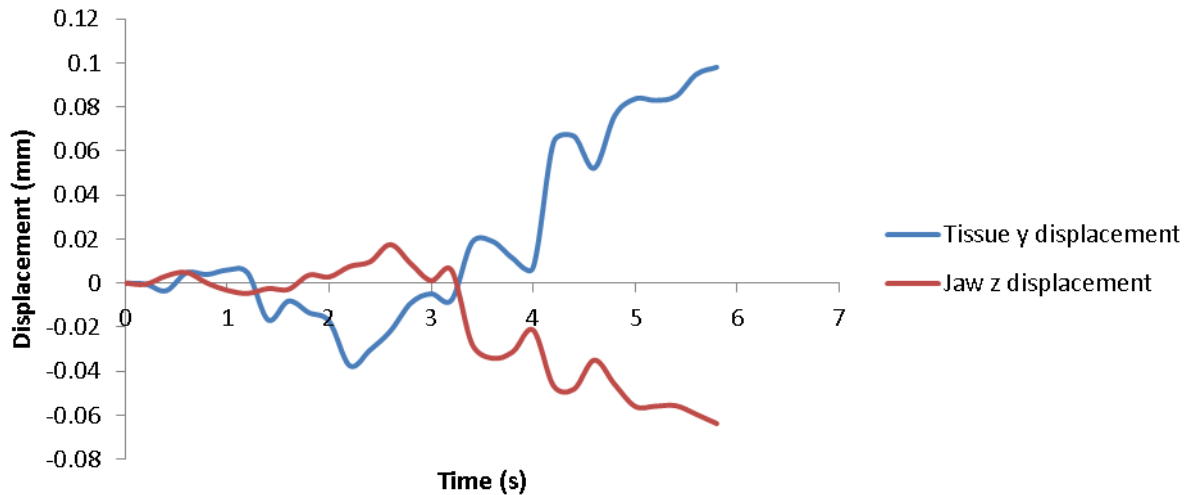
Figure 4-17 The y displacement of the tissue and the z displacement of the jaws during the sealing process for the original shim, sample 6-OR-JUL. A positive change in tissue displacement indicates the tissue moving closer to the device, and a positive change in jaw displacement indicates an increase in shim gap.

4.4.4   Tissue Strain

When analysing the strain the vessel was subjected to during the sealing process a number of interesting findings were discovered. Firstly the area of the vessel adjacent to the device jaws had a principal direction of strain in the x direction (refer to Figure 4-4 for axis definition) in the early stages of the sealing process (Figure 4-18). This was seen in all seals that were captured, irrespective of the vessel morphology or the shim design used to perform the sealing. Within Figure 4-18 high levels of strain can be seen on the surface of the device jaw, this was an artefact within the data due to an error within the software with subsets at the edge of the mask causing confusion within the software.
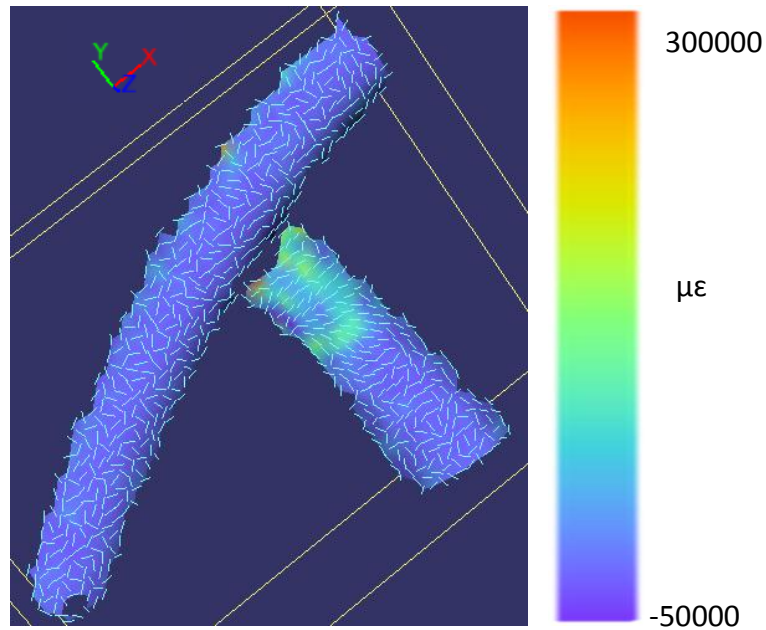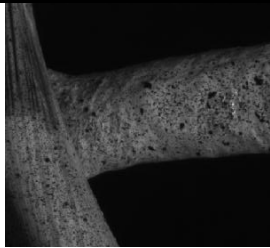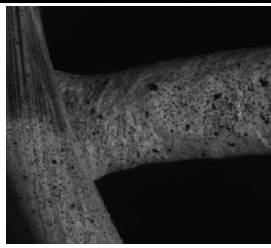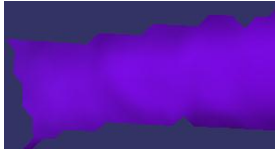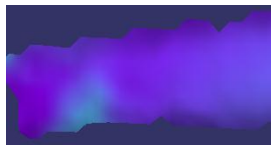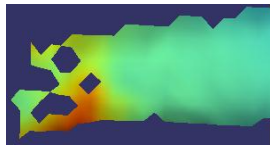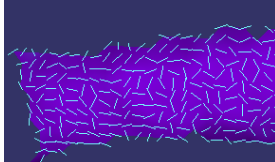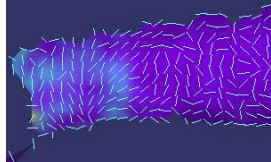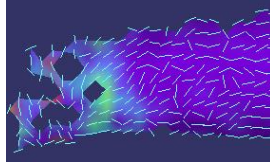
Figure 4-18 Image for sample 3-NA-JUL showing the surface strain distribution (true principal strain) for the blood vessel sealed using the narrow grooved shims. Images taken at 1.6s into the DIC recording. The region of the blood vessel adjacent to the device jaws shows the principle strain to be in the x direction.

Upon further investigation of the x direction strain, using the images captured during DIC with no processing, the vessel could be seen to extend in the x direction adjacent to the device jaws (Table 4-5). Unfortunately due the large amount of detail that was lost for a significant proportion of the samples it was not possible to quantify the tissue movement in the x direction. The displacement in the x direction occurred simultaneously with the displacement in the y direction (Table 4-5).

Table 4-5 Images captured during DIC, y displacement and true principal strain during the analysis showing the expansion of the blood vessel in the x direction in the region close to the blood vessel. The vessel was sealed using the narrow grooved shims, sample 3-NA-JUL. All images of the blood vessel are orientated with the shim on the left hand side of the image.

Additionally when considering the true principal strain, the direction gradually changed throughout the sealing process. Initially the principal strain was in the x direction adjacent to the seal, with the strain in the rest of the vessel being randomly orientated due to the low level of strain recorded. As the sealing process progressed the strain gradually changed orientation to be principally in the y direction, perpendicular to the device jaws. The sequential change in direction of

the principal strain can be seen in Figure 4-19. This gradual change was typical for all specimens, although the magnitude of strain and the general strain distribution varied for all samples in a similar way to the tissue y displacement.
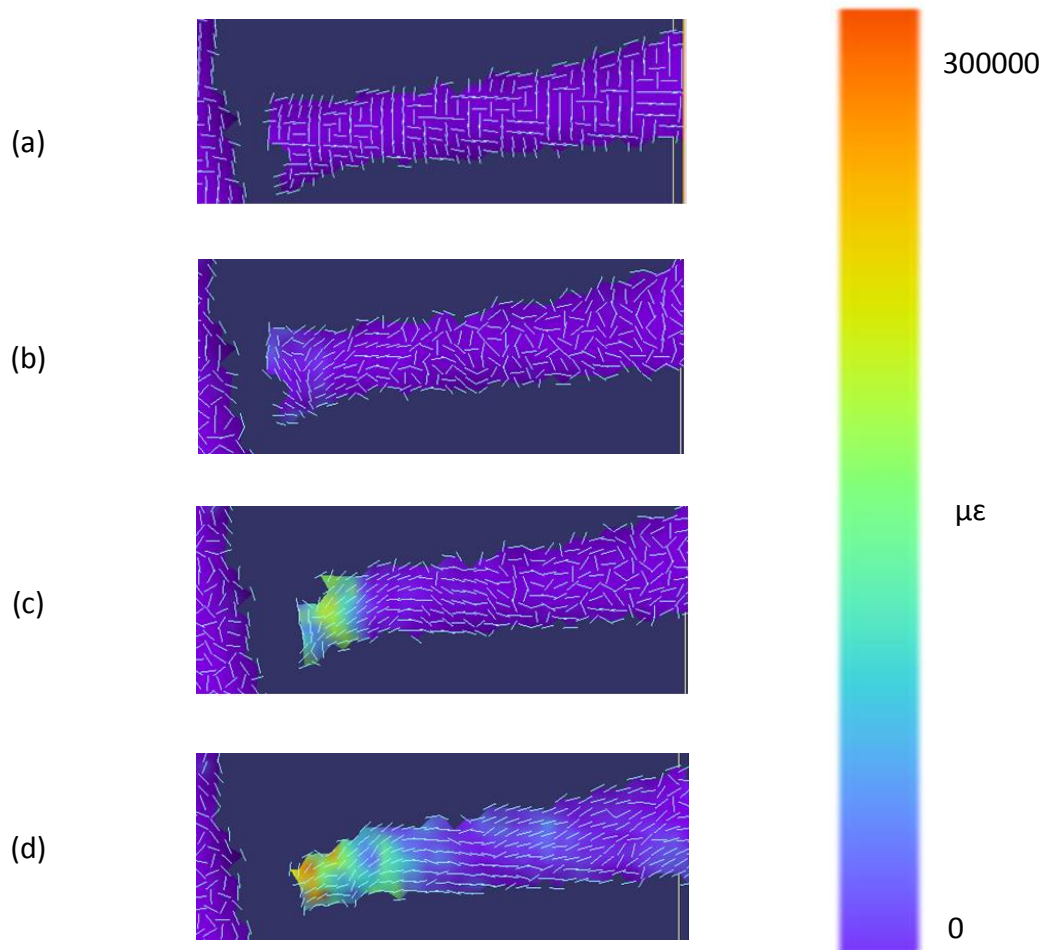
Figure 4-19 Images showing sequential stages of the sealing process, with the blood vessel orientated with the shim on the left hand side. Image (a) was taken at 0s, image (b) at 2.4s, image (c) at 3.6s and image (d) at 4s. Images show the strain map for the true principal strain, with all images using the same scale bar indicated on the right hand side. Vessel was sealed using the original shims, sample 6-OR-JUL.

Furthermore when analysing the strain the vessel was subjected to, an uneven strain distribution was observed across the surface of the blood vessel, with this being observed in a number of vessel samples, as seen in Table 4-5 and Figure 4-18, Figure 4-19. The uneven strain distribution was investigated further using the images captured during DIC with no processing. When examining a number of the seals it became apparent that during the sealing process the effect was not the same across the width of the vessel, with a number of samples appearing to have

one side that was favoured during the sealing process, with an increased level of contraction down one side of the vessel. Table 4-6 shows the images for one sample (6-45-JUL), where the contraction was favoured down one side of the vessel. Images for both the strain and the y displacement show an increase in displacement along one side, highlighting the effect of the increased level of contraction along the one side. This effect was seen in 50% of samples.

Graphs showing the comparison of the different levels and trends in the strain midway along the vessel can be found in the Appendix E. Trends shown in these graphs are similar to those seen in the tissue y displacement chart (Figure 4-14) with no groupings based on shim type or vessel position.

Table 4-6 Images for vessel sealed using the 45° grooved shims, sample 6-45-JUL, showing the camera image, y displacement and true principal strain for part of the sealing process. All images of the blood vessel are orientated with the shim on the left hand side of the image.

4.5 Discussion

From the use of DIC a valuable insight into the electrosurgical vessel sealing process has been gained, with a number of novel findings being presented. To the authors knowledge this is the first time such a technique has been used to capture the sealing process and as such a number of issues with the methodology were discovered. Each sample started with a speckle pattern that achieved good results, but throughout the sealing process this detail was lost in the area of the tissue adjacent to the seal. This loss of detail did not occur within all samples, and the loss of detail appeared to be random and unpredictable. The loss of detail was mainly due to the sudden and rapid contraction of the tissue, and problems with steam are thought to have made the loss of detail worse. It is thought that using a DIC system with a higher frame rate has the potential to reduce some of this detail loss.

The complex geometry of the vessel meant that the vessel orientation did not line up entirely with the defined co-ordinate system but the misalignment was minimal. The alignment of the vessel and device within the field of view was controlled with careful set-up of the equipment. Due to the variation in vessel geometry for each vessel the effect of misalignment would have varied for each sample, and therefore it was not practical to quantify the effect. The effect of misalignment would have been greatest in the z-direction for only the tissue; this was partially due to the curvature of the vessel surface. The misalignment would have a very minimal effect for the device jaws and the tissue in other directions.

As part of the DIC analysis the displacement of the jaws was considered in the z direction (please refer to Figure 4-4 for axis definition). Figure 4-5– Figure 4-7 show that the jaw moved in this direction throughout the sealing process, pulsing with the pulsating of the tissue, and causing a maximum variation in shim gap of ≈15%. The shim gap of the device is of great importance as it controls the application force. A fluctuation in the shim gap suggests a variation in the application force, although it is important to note that due to the changes in the tissue throughout sealing a constant application force would not be achieved irrelevant of the fluctuations in shim gap. With a displacement controlled application force, the force applied to each vessel is dependent on morphology and geometry and therefore an

ideal shim gap is difficult to establish. It is important to note that investigating the effect of shim gap and force was outside the scope of the study.

Additionally the change of shim gap would also mean that temperature fluctuations occur during the sealing process, with both force and temperature known to affect the seal quality (Wallwiener *et al.*, 2008) . Furthermore this variation in shim gap throughout the sealing process raises questions about the study performed by Wallweiner *et al* (2008) exploring the relationship between compressive pressure and seal quality. The study implies that a constant pressure was achieved throughout the sealing process, but does not specify if or how the shim gap altered to achieve this.

As part of the analysis the displacement of the device along the length of the jaws was analysed, with these results being presented in surface plots (Figure 4-8 and Figure 4-9). These results demonstrated increased displacement at the end of the jaws furthest from the device handles, and showed pulsing along the length of the jaws. The results from this analysis highlight the importance of the positioning of the vessel along the length of the jaws when performing a seal, not only due to the application force, but also due to the consistency of the shim gap throughout the seal. It is important for users of the device to be aware of this fluctuation and that such differences can have a significant effect on the seal quality.

It was chosen to analyse the y displacement (please refer to Figure 4-4 for axis definition) of the tissue due to observations made in previous experimental work, with significant contraction of the vessel observed in this direction. The decision to focus on the y displacement of the tissue was further justified when considering the direction of the principal strain, with the principal strain primarily being in the y direction. When considering the y displacement of the tissue, differences in distribution and magnitude were observed (Table 4-4) for each sample. This difference was considered in further detail by looking at how the displacement varied along the length of the vessel throughout the captured seal, with this data being presented in a surface plot (Figure 4-11, Figure 4-12). This data demonstrated that the tissue closest to the device jaws was subjected to the largest level of displacement in the y direction, which was to be expected. Furthermore the results

showed that, similar to the device jaws, the tissue pulsed in the y direction throughout the analysis.

Although the surface plots were suitable for a number of samples, due to the loss of detail in the majority of samples only five surface plots for the tissue could be created. As a result it was decided to analyse the displacement of the tissue midway along the length of the vessel, ensuring the same distance from the edge of the jaws was considered each time. All samples were compared against one another (Figure 4-14), with this demonstrating no trends based on the shim used or the position of the seal.

Furthermore each seal demonstrated both contraction and relaxation in the y direction, with this result being demonstrated more clearly in Figure 4-13. The vessels show pulsing in the y displacement, with this pulsing thought to be caused by the pulsing of the generator waveform and the resulting temperature of the tissue. When the tissue reaches the required temperature (≈70°C), created during one of the on periods of the generator waveform, the collagen within the vessel wall between the device jaws denatures. This denaturing of the collagen causes the tissue between the device jaws to shrink, thus resulting in the surrounding tissue being pulled toward the device jaws, causing the contraction seen throughout each seal. During the off period of the generator waveform, the tissue is allowed to cool slightly as no current is being applied. During this period the tissue relaxes (a reduction in y displacement) with this relaxation thought to be due to the collagen that was not denatured returning back to its original wavy state.

When comparing the pulsing of the device jaws and the tissue, the pulses appear to coincide with one another (Figure 4-15– Figure 4-17). This demonstrates that the pulsing of the devices jaws was caused by the pulsing of the tissue between the two shims. This pulsing of the device jaws was thought to be due to the expansion of water within the vessel wall, increasing the pressure between the jaws and forcing the shim gap to widen; explaining the positive displacement of the device jaws (an increase of up to 15% of the original shim gap). Once the water reached a sufficient pressure and temperature, the water was released from within the vessel wall as steam, leading to a reduction in pressure between the jaws and allowing for a

reduction in the shim gap, explaining the negative displacement of the device jaws. When considering the overall displacement of the jaws there was an increase at the start of the seal followed by a gradual reduction, indicative that overall there was a reduction in the volume of the tissue between the jaws.

The pulsing of the jaws and the tissue occurs simultaneously due to the behaviour of the tissue, with this pulsing being due to the pulsed waveform of the generator. Although the pulses of the jaws and the tissue were caused by different phenomena they coincide with one another due to the relationship with the generator pulses and the tissue temperature. The temperature of the tissue was responsible for both the expansion of the water and the denaturation of the collagen within the vessel wall.

When analysing the principal strain of the tissue it became apparent that for a number of samples the principal strain was in the x direction, parallel to the device jaws, during the early stages of the sealing process for the area of the tissue closest to the device jaws (Figure 4-18). This was investigated further and for all seals it was observed that the vessel initially stretches in the x direction, increasing the width of the vessel, but only in the area of the tissue adjacent to the jaws (Table 4-5). Unfortunately due to a loss of detail within this region it was not possible to quantify the x displacement throughout the sealing process. This initial increase in the width of the vessel wall was unexpected, and suggests further complexities to the vessel sealing process, with one possible explanation of this expansion being due to the production of steam within the vessel wall.

When considering the true principal strain throughout the analysis it became apparent that the orientation of the direction of the principle strain varied throughout the analysis (Figure 4-19). Initially the orientation was quite random due to the low level of strains recorded. As the sealing progressed, the tissue adjacent to the jaws had the principal strain in the x direction, and further away from the jaws the strain started to orientate itself in the y direction. As the sealing entered its final stages the strain was orientated in the y direction adjacent to the device jaws and this y direction orientation had progressed along the length of the vessel. The strain initially being principally in the x direction was thought to be due

to the circumferential bending of the vessel due to the compression and squeezing during the clamping of the vessel. The principal strain changes direction due to axial contraction due to the shrinking and denaturing of collagen. This strain orientation verifies considering the y displacement when analysing the movement of the tissue, and demonstrates that the most significant effect during the sealing process was the tissue contraction pulling the tissue towards the device jaws.

Furthermore when considering the strain distribution throughout the sealing process, vessels displayed an uneven strain distribution across the surface of the vessel. This warranted further investigation and upon reviewing the samples it was observed that 50% of the seals demonstrated an unequal sealing effect across the width of the seal. The example seen in Table 4-6 shows that the sample had greatest contraction on one side of the blood vessel wall. This resulted in a greater y displacement on this side and a higher level of strain. As the sealing progressed the displacement gradually spread across the width of the vessel and the sealing became more even. The unequal sealing is thought to be caused by a variation in tissue properties across the width of the vessel, most likely the tissue thickness which would allow the current to take the path of least resistance when completing the circuit, resulting in greater contraction in the region of the vessel with the smaller wall thickness. When the tissue is heated and the collagen is denatured the resistance of the tissue increases and therefore the thicker areas of the tissue would become the path of least resistance, resulting in the heating of the tissue across the width of the vessel. This effect shows that the sealing process varies within each seal, and that to achieve consistency from one seal to the next is a very complex challenge. The variation in z-displacement across the length of the jaws was considered as an explanation as to the uneven strain distribution seen within the tissue. Due to the strain distribution varying in terms of which side of the vessel was favoured, this seems an unlikely explanation as to this variation.

When considering the performance of all shims in terms of jaw z displacement, tissue y displacement, and principal strain there were no groupings or trends based on shim type, vessel type, or the resultant seal quality. Each seal was unique in terms of displacement and strain magnitude and distribution, with no two seals

performing in the same way. The different in performance was in part due to the variation in vessel properties, the size and the vessel morphology. Irrespective of this the data does provide a great insight into the vessel sealing process. The lack of explanation as to how the various parameters affect seal quality is in part attributable to the relatively small sample size used for testing. Data presented in Chapter 3 shows large variation within the individual groups i.e. elastic vessels or seals grouped based on shims and therefore variation is to be expected when capturing the seals using DIC. Significantly the data does show that no two seals behaved in the same way, there was always a difference in displacement magnitude or general behaviour, and as such provides evidence that the differences in seal quality are due to the difference in the sealing process, not due solely to the way in which the vessel morphology influences the ability of the vessel to withstand pressure.

4.6 Conclusion

Using DIC to capture the sealing process provided a valuable insight into the changes that are occurring during the sealing process, with pulses in the device jaws and the tissue being observed. These pulses were created by the pulses of the generator waveform and the resulting temperature of the tissue. The pulsing of the device jaws resulted in a variation in shim gap by as much as ≈15%, with the change of shim gap resulting in a variation in application force and a fluctuation in temperature throughout the sealing process.

By analysing the displacement of both the tissue and the device jaws throughout the sealing process it has been shown that no two seals are produced in the same way, with differences being shown in both the magnitude and pattern of the displacement for both the tissue and the jaws. The large variation in displacement was to be expected based on the larger variation that occurs in seal quality. Furthermore the difference in displacement occurs irrespective of the position of the seal along the length of the vessel, and the shim used to perform the seal, with a larger sample size being required to establish any trends within the data.

5   FE Modelling of Vessel Compression

5.1   Chapter Summary

This chapter details the creation of an FE model used to compare the performance of the different shim surface structures and vessel morphology in terms of the mechanical aspects. The FE model was created in the open source software package FEBio and was modelled as quarter blood vessels, taking advantage of the symmetry of the problem, and using an Ogden model to model the behaviour of the blood vessel wall. A total of five shim designs were compared using the model, comparing their performance in terms of force, maximum stress and strain. Two sets of material parameters were used allowing for the comparison of predominantly elastic and muscular vessels. Results demonstrated a significant difference in the performance of the two material types, with the difference between the two material models suggesting areas of weakness within the elastic model that would result in a lower burst pressure. Additionally the comparison of the shim designs showed that the application of transverse grooves resulted in a lower application force to compress the blood vessel, and lower stresses within the blood vessel wall. Furthermore the model was validated using digital image correlation (DIC), with both data showing areas of high strain at the edge of the vessel and areas of low strain at the centre of the vessel. The work in the chapter demonstrates how the FE model can be used to aid device design and improve understanding surrounding the electrosurgical vessel sealing process.

5.2   Introduction

Previous chapters have described the effect of varying shim surface structure on seal quality, with results demonstrating that the structure of the shim surface affects the device performance in terms of seal quality, adhesion and seal size (surface area), with two of the designs improving the mean burst pressure of the seals. Further experimental work used DIC to capture the vessel sealing process for the different shim designs, but this work failed to provide an insight into how the

different shims perform differently due to the small sample size used and highlighted the complexities of the vessel sealing process.

The experimental work has provided a great insight into how the surface structure of the shims affects device performance. To expand upon this knowledge further FE modelling was used. The application of FEA in biomechanics research and design has increased exponentially over the last 30 years with more specialist software becoming available. FEA in biomechanics is already a standard methodology, often used when experimental investigation is difficult or impossible . When considering electrosurgery most computer simulations use a multiphysics approach, considering the electrical and thermal effects of the procedure, with limited consideration given to the mechanical effects of the electrode design. Included in this thesis are computer simulations considering the multiphysics and mechanical aspects independently of one another. This Chapter will focus on the mechanical aspects, with Chapter 6 focusing on the multiphysics approach.

When considering the mechanical aspects of electrode design the most relevant work existing in the literature is FEA related to arterial clamping and the damage assessment of various clamp designs. A number of arterial blood vessel models and constitutive models were reviewed in Chapter 2, with the most relevant FEM's summarised in Table 5-1. Work by Famaey *et al* (2012) compared two clamp designs, one smooth and one grooved, with the grooved sample leading to more pronounced stress concentrations . Chen *et al* (2009) compared two clamp designs, one flat and one cylindrical, and found much larger stresses occurred in the cylindrical clamp . Both of these studies were concerned with the design and safety of arterial clamps and demonstrate the ability of FE modelling to aid surgical device design.

Table 5-1 Summary of the key studies relating to FE modelling of arterial clamping

Study Primary Author (Ref)	Year of Publication	Study Summary
Gasser *et al*	2002	•Modelled two layers of the blood vessel (adventitia and media) •Used material model developed by Holzapfel and Gasser •Main focus was damage occurring during arterial clamping •Failed to achieve complete lumen occlusion
Chen *et al*	2009	•Single layered blood vessel model •Used material model developed by Holzapfel and Gasser •Main focus was on the fluid interactions during clamping •Comparison of two clamp designs, finding higher stresses with the cylindrical clamp compared to the flat clamp. •Model achieved complete lumen occlusion
Famaey *et al*	2012	•Single layered blood vessel model •Used material model developed by Holzapfel and Gasser •Main focus was on damage occurring during clamping •Comparison of two clamp designs found more pronounced stress concentrations with the grooved clamp compared to the smooth clamp •Achieved complete lumen occlusion

Throughout all the experimental work there was constant variation in the properties of the blood vessel, within the vessel morphology, vessel wall thickness and the outer diameter of the vessel, as discussed in Chapter 3. Each of these parameters has been shown to significantly affect the performance of the device. Through the use of FEA the variation in these parameters can be eliminated, allowing for different shim designs to be compared against one another consistently. Furthermore the effect of these vessel parameters on the clamping process can be investigated in a controlled manner, comparing the difference in

performance between predominantly elastic and muscular vessels, and vessels of different outer diameters. Furthermore if the FEM produced results comparable with experimental data it could be used as a tool aiding device design, providing a cheaper, more accessible and more consistent alternative to tissue.

This chapter aims to produce an FEM replicating the clamping, sealing and bursting process of electrosurgical vessel sealing. Additionally through the use of FEA the performance of different shim designs shall be analysed, investigating the effect of clamp design on clamping force, and the maximum stresses and strains within the blood vessel wall. Furthermore the work in this chapter aims to produce different blood vessel models to investigate the effect of different vessel parameters on the sealing process to improve understanding of how and why these parameters affect the device performance.

5.3   FEBio

The model was produced using open source FEBio software developed by the University of Utah. The software consists of three parts; PreView, FEBio and PostView. PreView is a finite element pre-processor that offers a graphical user interface that facilitates the process of defining finite element models, including the ability to import models. Files are exported from PreView to be used in FEBio. FEBio is a non-linear implicit finite element framework designed specifically for analysis in computational solid biomechanics. As the file is exported from PreView there is an opportunity to modify the coding in the .feb file, to apply additional options that are unable to be applied within PreView. Finally the results can be viewed and analysed in PostView, a finite element post-processor. FEBio has been verified by the creators, through comparing results from a number of analyses to analytical solutions and verified FE codes, such as ABAQUS and NIKE3D. The results from FEBio demonstrated very good to excellent agreement with other solutions, with small discrepancies being attributed to the differences in numerical algorithms between different software packages .

5.4 The FE Model

The FE model simulates the compression of a blood vessel followed by the inflation test; as such the model was split into a number of stages as detailed in the loading step section. Due to the symmetry of the blood model, an eight of the blood vessel was modelled, along with one shim for compressing the blood vessel. In addition a displacement control object, mimicking the second shim was required; this prevented the blood vessel wall from going past complete lumen occlusion and allowed for slight compression within the vessel wall. This displacement control object was modelled as a simple cuboid, with the same material model and parameters as the shim, as detailed in Section 5.4.2. A number of assumptions and approximations were made producing the FEM including using the Ogden model to model vessel behaviour, simplification of the clamping method and simplification of the sealing process. These assumptions and their effects are discussed in greater detail in Section 5.8.1 of this Chapter.

5.4.1 The Blood Vessel

5.4.1.1 Blood Vessel Geometry

The blood vessel model was based on data presented by Gassser *et al* (2002), and had an inner diameter of 3.3mm, with a thickness of 0.8mm, with a 10mm vessel length prior to the residual stresses being applied to the vessel. These dimensions do vary slightly from those identified by Gasser *et al* (2002) due to a different approach taken in modelling the blood vessel (Gasser *et al.*, 2002). For this study a simplification to the model was applied, modelling the vessel wall as a single layered structure with the parameters for the model displayed in Table 5-2.

Table 5-2 Displaying the vessel parameters for the vessel geometry, with data based on data presented by (Gasser *et al.,* 2002)

Model	Vessel Wall Thickness	Outer Diameter	Inner Diameter	Vessel Length	Opening Angle
Gasser Geometry	0.8mm	4.1mm	3.3mm	10mm	34.5°

To account for the residual stresses the blood vessel was shaped as seen in Figure 5-1, with an opening angle of 140° used, this equated to an angle of 35° for the symmetry model. Once the residual stresses were applied to the model, the blood vessel formed a quarter circle, with the x and y distance from the origin equal (Figure 5-1). Residual stresses were discussed in greater detail in Chapter 2, and the will be discussed further in Section 5.5.2.
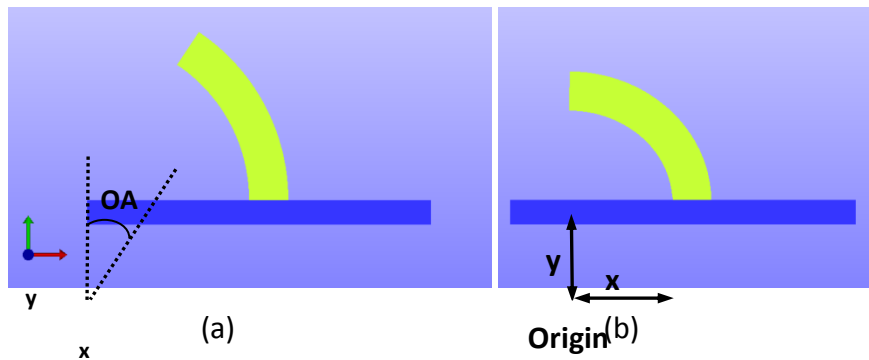
Figure 5-1 (a).The unloaded stress – free blood vessel, with OA showing the opening angle, 35°. (b) The unloaded but stressed blood vessel configuration, with x = y.

5.4.1.2 Material Model and Parameters

The Ogden model was applied to the blood vessel wall, this constitutive model was discussed in further detail in Chapter 2. This model was used because of its good fit to experimental data (Richards, 2010), its ease of convergence and because data was available to allow the comparison of different vessel morphologies. The model assumes the material is isotropic, incompressible and strain rate independent. The material parameters for this model were determined based on experimental work by Richards (2010), with material parameters being defined for two materials, a predominantly elastic artery and a predominantly muscular artery. Material properties defined by Richards were the instantaneous shear modulus, G, and the dimensionless Ogden constant, Equation 5.1 was used to calculate the Ogden constant μ (Persson *et al.*, 2010).

$$\mu = \frac{2G}{\alpha}$$

Equation (5.1)

The Ogden constant, α, is referred to as M1 in FEBio, and the Ogden constant, μ, is referred to as C1. The bulk modulus, k, used In FEBio is approximately 1000 times

larger than the value of C1. Both the experimental parameters and model parameters are displayed in Table 5-3.

Table 5-3 Displaying the experimental and model parameters for both the predominantly muscular and elastic material models (Richards, 2010).

Model	Experimental Parameters		FEBio Model Parameters		
Type	G, kPa	α	k , N/mm^2	C1 N/mm^2	M1
Muscular	100	19	10	0.01053	19
Elastic	25	22	1	0.00227	22

5.4.1.3 Mesh

A mesh convergence study was performed to determine an acceptable mesh that would produce accurate results in the minimum computing time for the blood vessel. The study examined a number of meshes, with the initial mesh coarser with a lower number of nodes and elements, and the meshing parameters being varied to gradually increase the number of elements and nodes. The original shim was used during the study and the vessel was modelled as a predominantly muscular vessel, using an 8-node trilinear hexahedral element. The opening angle varied based on the meshing parameters with the angle remaining as close to 35° as possible. Details on the meshing parameters and opening angles can be found in Table 5-4. The same step parameters as described in section 5.5 were applied to the model, with the adhesion and bursting step omitted from this analysis.

Table 5-4 Mesh convergence study summary including details of the mesh settings and the results summary for each mesh

Model	Mesh Details		Opening Angle
	Elements	Nodes	
Mesh 1	4160	5166	33.2°
Mesh 2	9120	10980	34.1°
Mesh 3	16000	18954	34.5°
Mesh 4	27280	31968	34.2°
Mesh 5	29920	34695	34.5°
Mesh 6	32640	38115	34.5°

Figure 5-2 and Figure 5-3 show the results from the mesh convergence study, showing the reaction force in the y direction (refer to Figure 5-4 for axis definition) and the maximum Von Mises stress respectively. As seen in Figure 5-2, meshes 4, 5 and 6 all converged, with a variation of ≈ 1 %, however in Figure 5-3 it was only meshes 5 and 6 that converged, with a variation of ≈ 1 %. Based on this mesh 5 was used for all subsequent analyses.
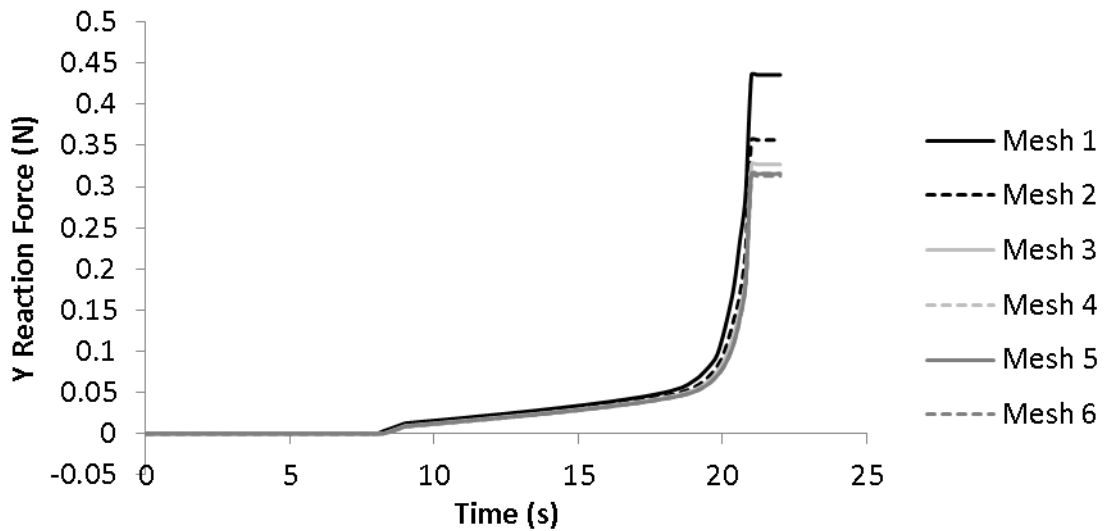
Figure 5-2. Graph showing the shim reaction force in the y direction for the various meshes
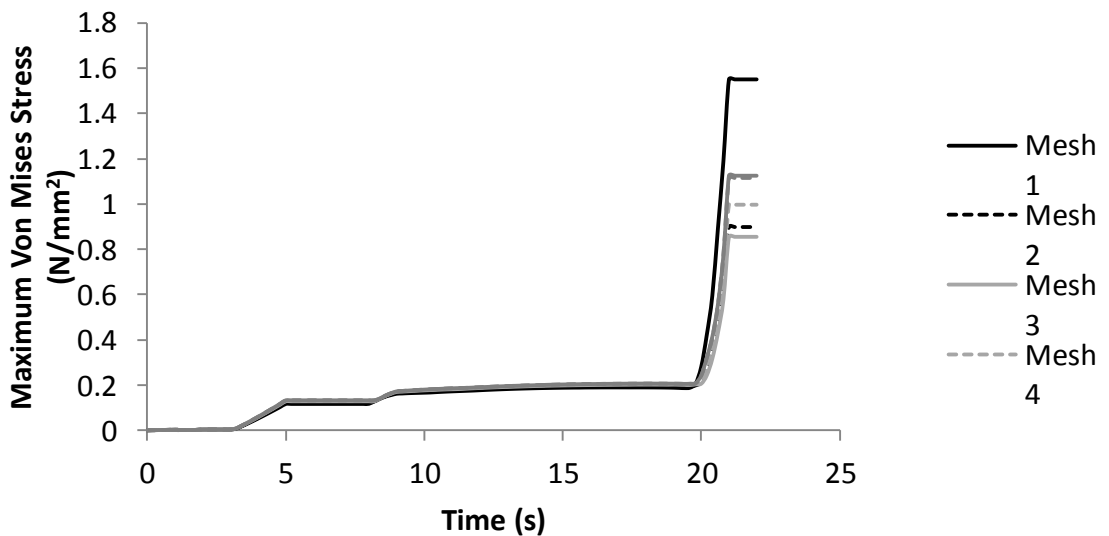
Figure 5-3. Graph showing the maximum Von Mises stress for the blood vessel for the various meshes.

5.4.2 Shim Models

The shims modelled for the analyses were based on those designed in Chapter 3, with these designs being summarised in Table 5-5. The shims designed previously were curved to allow for use with the OpenSeal device, to simplify the modelling problem the shims were modelled as straight shims with a smooth surface. Shims were originally created in SolidWorks (Massachusetts, USA) and then converted to a ASCII STL file before being imported into FEBio. A total of five shim designs were analysed, with the combination shim, 8_CC (Table 3-2), being omitted due to the use of symmetry, with a quarter blood vessel model being necessary to model this shim design. The 45° grooved shim 7_45 was not analysed due to issues importing the model into FEBio. Each shim was meshed using the tet generation function in PreView, with the same settings being used for each of the shim models. All shims were modelled as a rigid body, as the deformation of the shims is negligible compared to that of the blood vessel. For the purpose of the contact stiffness, the material of the shims was modelled as medical grade steel, with a Young's modulus of 190 GPa and a Poisson's ratio of 0.31.

Table 5-5 Details of shim designs, including images of the CAD models and actual shims for each shim design.

| Shim Number | Shim Name | Surface Features | | | | Number of Elements in Mesh |
		Groove Width (mm)	Groove Depth (mm)	Peak Width (mm)	Groove Orientation	
1_OR / 2_SM	Original / Smooth	No Surface Features				61477
3_GR	Grooved	1	0.1	1	Transverse	209341
4_NA	Narrow Grooved	0.5	0.1	1.5	Transverse	194421
5_HF	HF Grooved	1	0.1	1	Longitudinal	413624
6_LO	Longitudinal Grooved	1	0.1	1	45°	62369

Although the same settings were used to produce the mesh for each shim, the number of elements varied due to the radius of the curve on the edge of the grooves and the number of grooves on the shim.

5.4.3   Contacts

The contact between the shim and the blood vessel was defined as a sliding contact. This allowed for the two surfaces to separate and slide across one another but not to penetrate one another . The augmented Lagrangian method was used for the sliding contact, with the penalty used varying depending on the material parameters and the shim model used (Table 5-6). The same approach was used to model the contact between the blood vessel and the DCO, with the penalty factor used displayed in Table 5-6. The augmented Lagrangian method was chosen was this analysis over the penalty method, due to its improved stability for high level compression problems, and recommendations made in literature (Maas, *et al* 2013). Both the augmented Lagrangian and penalty methods are algorithms used for solving constrained optimization problems, such as the contact problem.

Table 5-6 Penalty Factors for the sliding contact between the shim and the blood vessel

Shim Analysis	Penalty Factor for Compression Shim		Penalty Factor for DCO
	Material Type		
	Predominantly Elastic	Predominantly Muscular	
Original Shim	50	70	10
Grooved Shim	50	NA	10
Longitudinal Grooved Shim	50	NA	10
Narrow Grooved Shim	70	NA	10
HF Grooved Shim	70	NA	10

5.4.4   Boundary Conditions

The constraints of the blood vessel were applied along the lines of symmetry, with fixed constraints applied in the y and z direction on the respective surfaces (Figure 5-4). A prescribed z constraint was applied across the surface of the free end of the blood vessel, with this constraint initially acting as a fixed constraint with a zero scale factor applied, and then creating the axial residual stress, applying a stretch $\lambda_z=1.1$, and then acting as fixed constraint throughout the remainder of the analysis. A rigid constraint was applied to the DCO, constraining all six degrees of freedom. The shim was also constrained using a rigid constraint, with all degrees of freedom fixed apart from the y displacement. The y displacement was controlled

throughout the analysis, and was used to move the shim in the negative y direction to compress the blood vessel.
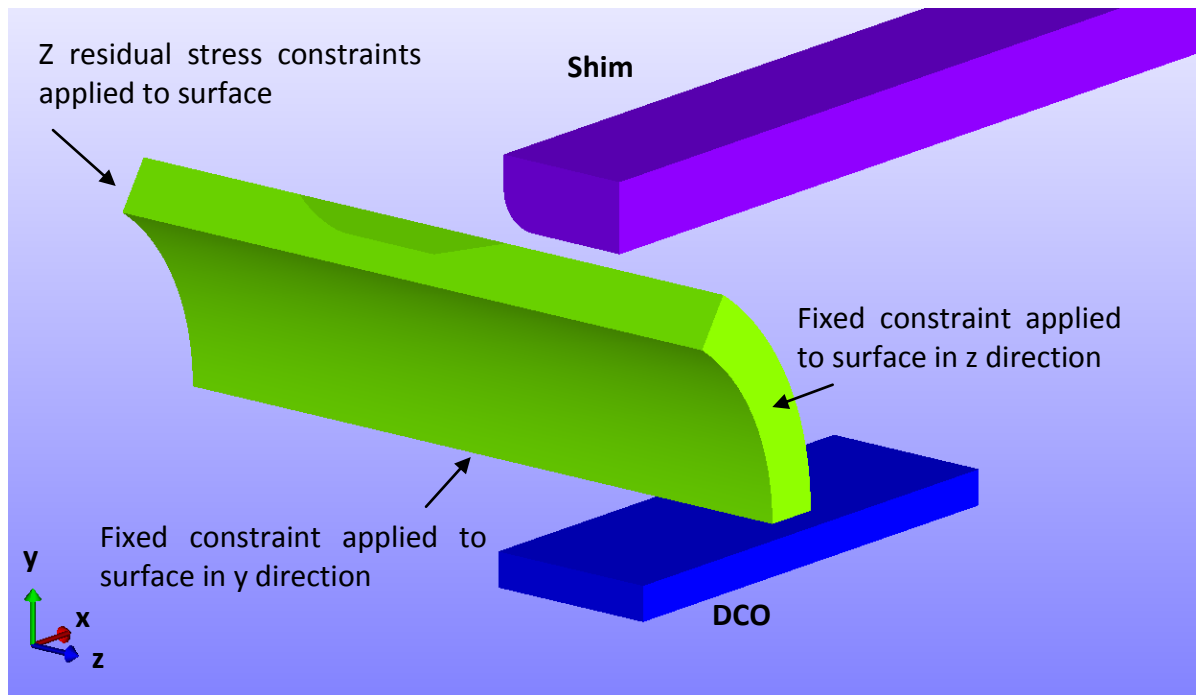
Figure 5-4 Showing the boundary conditions applied to the blood vessel in the initial step of the analysis. The displacement control object (DCO) and the compressive shim are also labeled.

5.5 *Loading Steps*

To control the constraints and loading of the model a multiple step analysis was used, allowing constraints to be active or inactive as required. A total of five steps were used for this analysis, with the initial step being used to apply constraints and loads that would be active throughout the analysis. The subsequent four steps were used to conduct the analysis; the first step creating the residual stresses in the circumferential direction; the second step changing the y constraints used to create the residual stresses to the x constraints required for the remainder of the analysis; the third step used to account for the z residual stresses, pressurise the vessel and compress the vessel; and the final step for modelling the adhesion and the following pressurisation. A summary of each step can be found in Table 5-7, along with the time step settings used for each step, with details of the boundary conditions and constraints applied provided in subsequent sections. The loading

stages of the analysis are in line with those carried out in studies by both Gasser *et al* (2002) and Famaey *et al* (2012).

Table 5-7 Summary of loading steps throughout the FE analysis.

Step Name	Description	Step Parameters	
Initial Step	Boundary conditions, loads and contacts applied in this step remain active throughout the analysis.	N/A	
Residual Stress	This step uses prescribed motion to create the residual stresses in the circumferential direction.	Number of time steps	1000
		Step Size	0.001
		Max Retries	100
		Cutback	Aggressive
Changing y to x	Y constraints used to create residual stresses are removed and x constraints applied as required for symmetry.	Number of time steps	100
		Step Size	0.001
		Max Retries	100
		Cut Back	Aggressive
Removing x constraint	The x constraint applied to allow residual stresses to be applied is removed from the model	Number of time steps	100
		Step Size	0.001
		Max Retries	100
		Cut Back	Aggressive
Pressurisation and Compression	Axial residual stresses are created. A pressure load is applied, pressurising the vessel to approximately 90mmHg, and the vessel is compressed.	Number of time steps	20800
		Step Size	0.001
		Max Retries	100
		Cutback	Aggressive
Adhesion and Inflation Test	The inner surface of the blood vessel wall is constrained in the y direction to recreate adhesion and the vessel is further pressurised.	Number of time steps	23000
		Step Size	0.001
		Max Retries	100
		Cutback	Aggressive

5.5.1 Initial Step

All constraints, loads, and contacts set during the initial step remained active throughout the analysis. Prescribed constraints and loads were then controlled through the use of graphs, whilst fixed constraints and contacts then remained unchanged throughout the analysis. The boundary conditions, as detailed in Section 5.4.4, and contacts, as detailed in Section 5.4.3, were applied in the initial step. A pressure load was applied to the inner surface of the blood vessel wall, and controlled through the use of graphs in a similar manner to the displacement of the shim.

5.5.2 *Residual Stresses Step*

Excised arteries are associated with complex residual stresses as discussed in Chapter 2, with arterial rings springing open when cut in the radial direction. As a result of the arterial ring springing open, different opening angles are measured depending on the residual stresses within that sample. An opening angle of 140° was applied to the blood vessel, equating to an angle of 35° due to symmetry (Figure 5-1). The edge of the vessel, highlighted in Figure 5-5, was prescribed to move in the negative y direction to create the 90° wedge, with the x and y distance from the origin being equal to one another. Additionally it was necessary for a fixed x constraint to be applied for this analysis step, with this applied to the node highlighted in Figure 5-5.
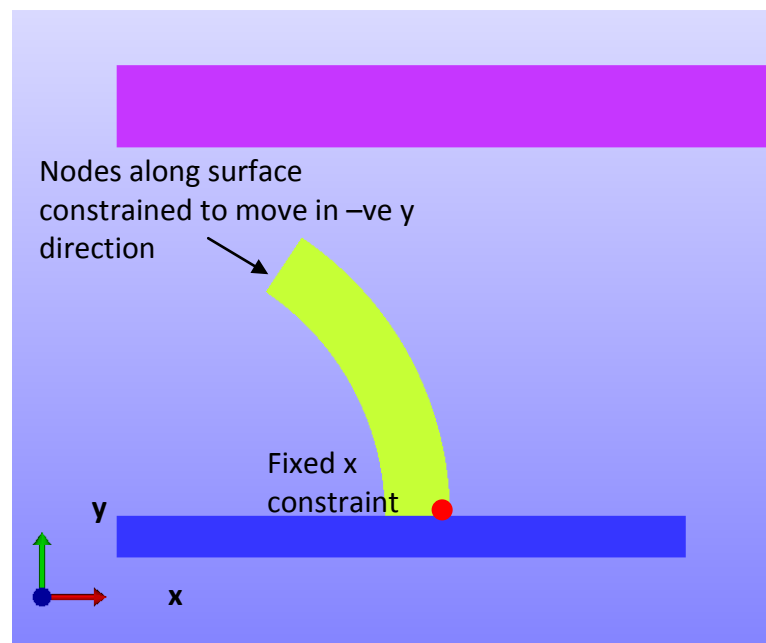
Figure 5-5 Showing the constraints applied to create the circumferential residual stresses during the residual stress step.

5.5.3 *Changing prescribed y constraints to x constraints*

Following the application of the circumferential residual stresses, it was necessary for the y prescribed constraints to be replaced with x constraints for the remainder of the analysis. As such the y prescribed constraints remain inactive from this point forward, and the x constraint acts as fixed constraints accounting for the model symmetry. Furthermore the x constraint applied in the residual stress remained

active for this step (Figure 5-5), but was then inactive for all subsequent steps, being removed in the following step. This step was used to remove the constraint as it made it easier for the model to converge in the subsequent steps.

5.5.4 Pressurisation and Compression Step

The first stage of this step applied an axial residual stress, $\lambda_z = 1.1$, with a prescribed constraint applied to the free end of the vessel wall, stretching the vessel in the negative z direction. Following the application of the axial residual stress the prescribed z constraint acts as a fixed constraint. The pressure load applied in the initial step was then activated through the use of load curves. A scale factor of 0.012 was applied to the pressure loads, resulting in a pressure of 90mmHg once the load curve reached 1 in the positive y direction. The scale factor was applied to the analysis to control the pressure level, with the value chosen based on the units used throughout the analysis and the desired pressure. The pressure remained fixed at 90mmHg throughout the remainder of this analysis step.

The vessel was then compressed; this was achieved by applying a prescribed motion to the shim in the negative y direction. The movement of the shim was set in the initial step with a load curve used to control the shim displacement. The load curve remained constant at zero displacement during the pressurisation of the vessel, and then gradually moved in the negative y direction over a period of 13 seconds until complete compression of the vessel was achieved, the total displacement of the shim resulted in a 0.5mm shim gap. The compression of the vessel was achieved over a period of 13 s, significantly longer than in reality, but necessary due to the high level of deformation occurring. During this step the DCO becomes active, preventing the vessel wall going past complete lumen occlusion, and allowing for slight compression of the vessel wall.

5.5.5 Adhesion and Inflation Test

The initial stage of this analysis step was to model the adhesion. This was achieved by applying a fixed y constraint to the inner surface of the blood vessel wall to those nodes beneath the shims (Figure 5-6). This prevented the nodes from moving in the y direction but allowed movement in all other directions, replicating the adhesion taking place during the sealing process. Following the adhesion the shims

were removed, initially at a very slow rate, with the movement of the shims being controlled through the load curve. Once the shim was removed the vessel was pressurised further to replicate the inflation test that takes place following sealing to assess the quality of the seal. During this step the vessel was pressurised to approximately 360mmHg, the pressure that is considered a minimum pressure for a successful seal (Chapter 3).

(a)   (b)
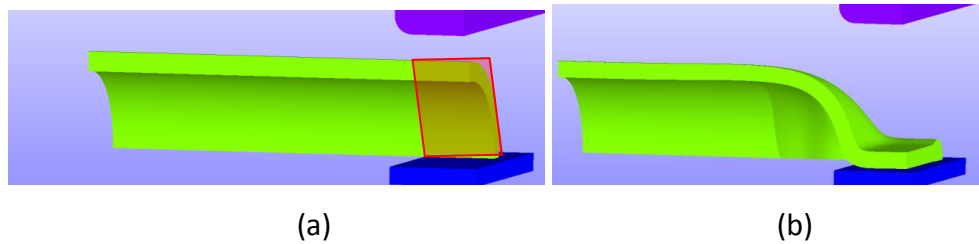
Figure 5-6 (a) Showing the area of the blood vessel wall constrained to recreate the adhesion following the electrosurgical vessel sealing process. Nodes on the inner surface of the vessel wall within this region have fixed constraints applied in the y direction. (b) Showing the vessel following the simulation of adhesion and the removal of the shim.

5.6   Experimental Validation

As with all FE models it was necessary to validate the model to ensure the accuracy of the results. To validate the model DIC was used to capture the clamping process, and these results compared to those of the FE model, for the original shims of the device.

5.6.1   Validation Method

The DIC method detailed in Chapter 4 forms the basis of the method used to validate the model, with the reader referred back to this section for the equipment set-up and the theory behind DIC. Details of the testing procedure used to capture the sealing process will be described in this section.

5.6.1.1 Capturing the clamping process

Tissue was prepared in a similar manner as described previously in Section 3.3.1.1 of Chapter 3, with 40mm sections being used instead of the 20mm sections used previously. The longer specimen size was necessary due to the change in testing procedure. Once the vessel sample had been prepared the specimen was

connected to the saline infusion equipment using a haemostat. The free end of the specimen was also clamped using a haemostat to create a small amount of axial tension. The vessel was then pressurised to approximately 60mmHg and the speckle pattern was applied. The speckle pattern was applied using a sponge to apply white face paint as a base layer, and then using a make-up brush to sprinkle black powder over the surface. Once the speckle pattern was applied a trial run was conducted to ensure that the pattern was of sufficient standard to achieve good results. This consisted of capturing two shots using the DIC system, and processing the data through the software and checking for gaps within the resulting image. If there were gaps within the resulting image, the speckle pattern was adjusted and the trial process repeated until the speckle pattern was of sufficient standard. The clamping process was then captured; this was achieved at a frame rate of 5Hz, over a period of 10 seconds. The device was held in a clamp and the handle manually closed at a slow rate during the capturing process.

5.6.2 Results Processing/ Analysis

Data was processed within the DIC software; a new evaluation was created and the procedure for processing stated by the software providers (Dantec Dynamics) was followed. This involved identifying the start point, a point which can be found in all images to allow for the software to conduct the necessary calculations and processing, and drawing a mask to identify the area of interest. For this analysis the blood vessel area between the device and the saline infusion equipment was selected as the area of interest. The data was then processed with the software computing the displacement and strain. The engineering principal strain was of interest for the purpose of model validation.

5.7 Results

5.7.1 Validation of FE Model

The principal strain collected using the DIC data was compared to the principal strain resulting from the FEBio model. The comparison of three blood vessels to the two different material types can be seen in Figure 5-7, with all images showing the distribution of the principal strain at the point of complete lumen occlusion.
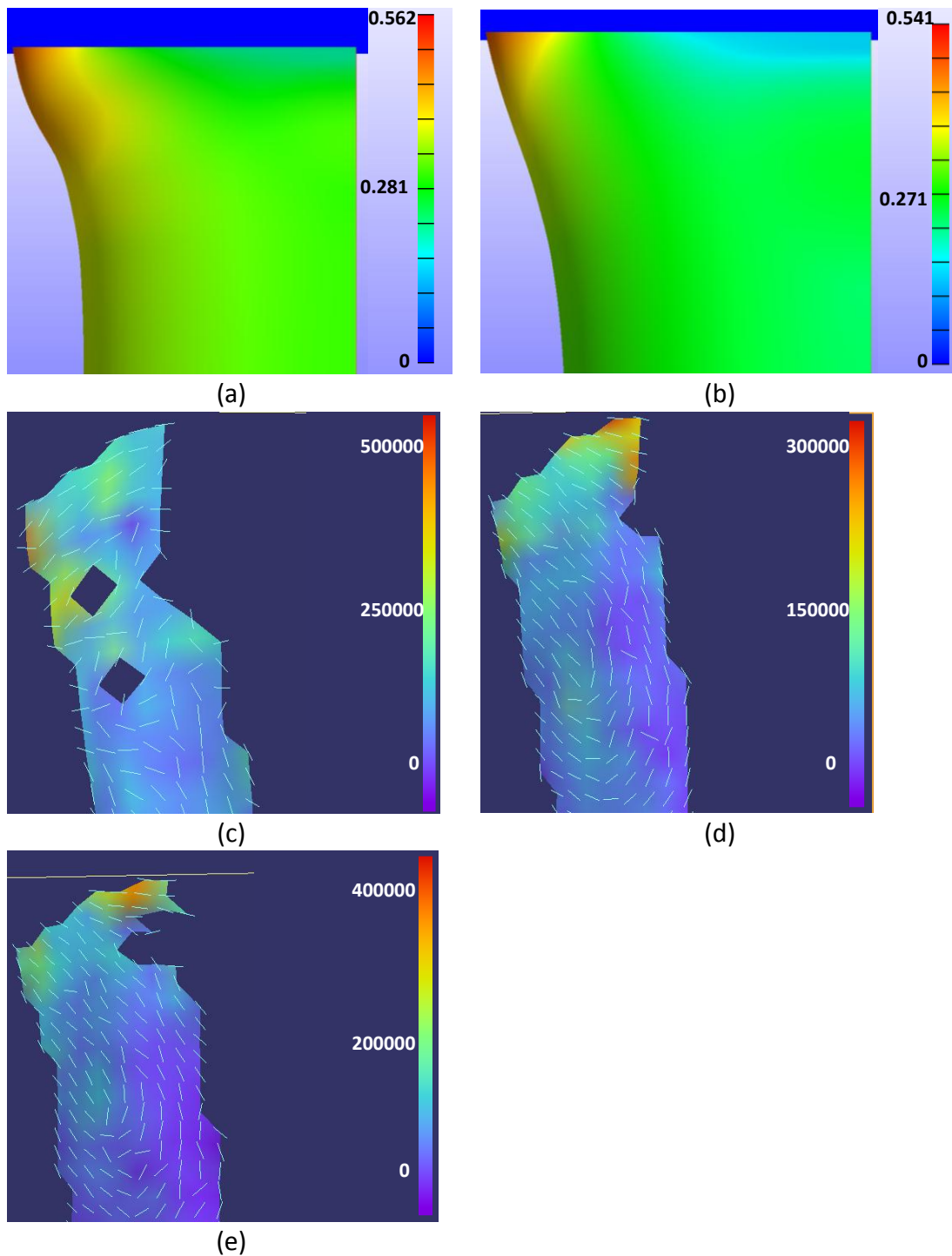
Figure 5-7 Comparison of principal strain between the FE model and DIC data, with (a) showing the strain across the surface of half the width of the vessel for the elastic FEM, (b) showing the strain across the surface of half of the width of the vessel for the muscular FEM, Figures (c), (d) and (e) showing three samples captured using DIC, with strain displayed across the full width of the vessel. Note for all images the shim is positioned at the top of the image.

When comparing the DIC data with the results from the FEM, a higher level of strain at the edge of the vessel wall and a lower level of strain at the centre of the vessel wall was seen in both data sets (Figure 5-7). The images for the DIC show the strain distribution across the full width of the vessel, where the images for the FEM show strain distribution for half the width of the vessel. The maximum magnitude of the principal strain measured using DIC varied (350000 – 540000 µε), with DIC samples 1 and 3 showing strain of a similar magnitude to the FEM.

Whilst the method presented allowed a comparison of the strain on the surface of the vessel it does not validate the behaviour through the vessel wall. Additionally the compressive force should be captured to further validate fully the results similar to Famaey (2012). The Ogden model has previously been shown to be a good fit with experimental data for blood vessels (Richards 2010). The similarity in performance between the Ogden model and the experimental values suggests the effect of anisotropy is limited during clamping in terms of overall values. It is thought that the effect of anisotropy would be more influential during the inflation stage at pressures beyond the physiological range.
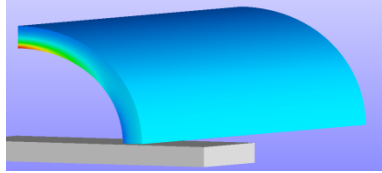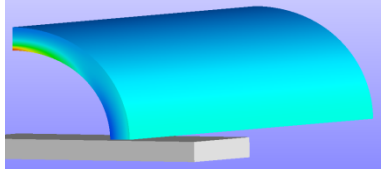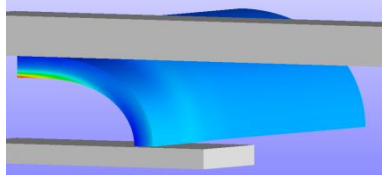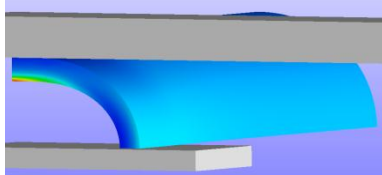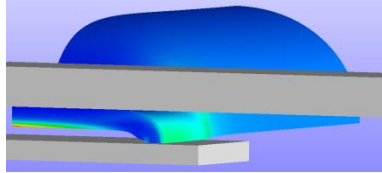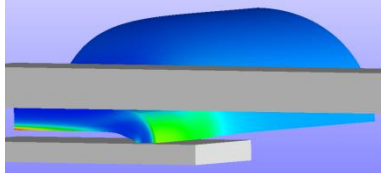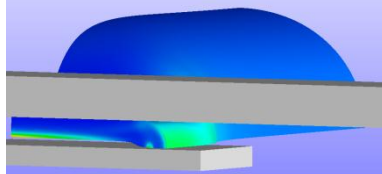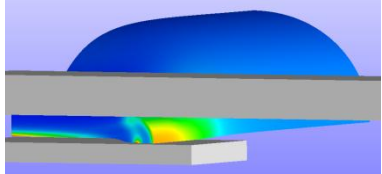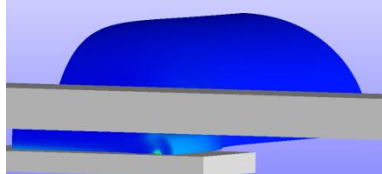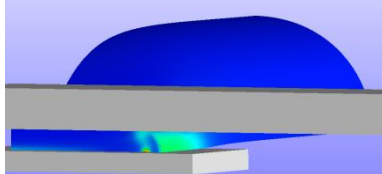
5.7.2   Comparison of Elastic and Muscular Blood Vessel Models

Two different vessel models were compared, predominantly elastic and predominantly muscular, with the results presented for vessel compression and the inflation test.

5.7.2.1 Vessel Compression

Ideally the hoop stress throughout the vessel wall would have been considered, but due to software limitations this was not possible and as such the Von Mises stress was considered throughout. This was chosen to give a general indication of the stress throughout the vessel wall, although it should be noted that using the hoop, radial and axial stress would provide greater detail and a greater insight into the behaviour of the blood vessel. Table 5-8 shows the difference between the two vessel models throughout this stage. The images shown within Table 5-8 show that both models had a similar pattern for the stress distribution, but the stress was of different magnitudes for the two different models, with the muscular model showing higher levels of stress.

Table 5-8 Images of the blood vessel wall at different stages throughout the blood vessel compression stage. Images show the Von Mises stress through the vessel wall, with a varying scale used for each step displayed.

Time	Elastic	Muscular	Stress / (N/mm^2)
5.4s			0.14 0
10s			0.19 0
19s			0.21 0
20s			0.24 0
21s			1.1 0

The difference in stress magnitudes was considered further (Figure 5-8) with the stress on the inside of the vessel wall, and the outside of the vessel wall, within the region of highest stress, points 1 and 2 in Figure 5-9 being considered. This Figure shows that the higher stress occurred at the inner wall of the vessel, and a lower stress on the outside for both material types.
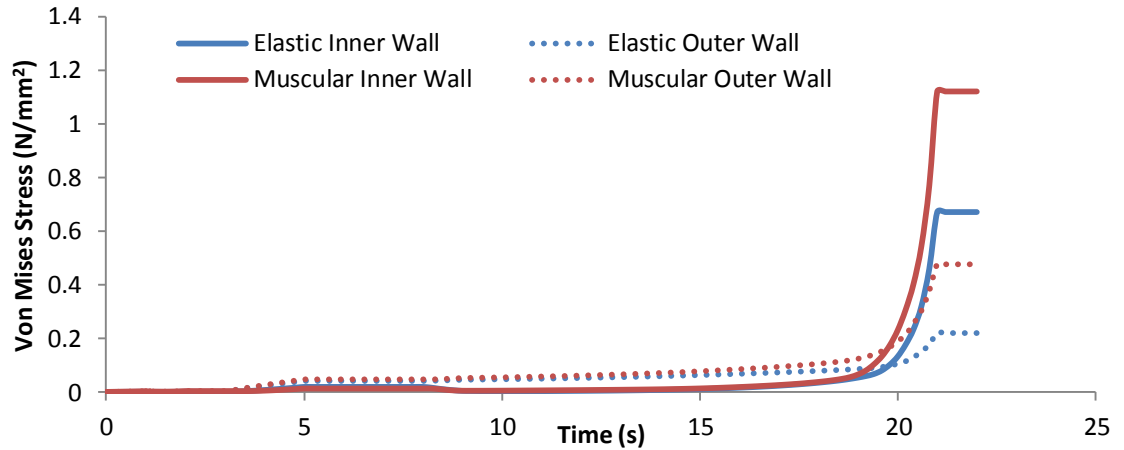
Figure 5-8 The Von Mises stress at the inner and outer wall of the blood vessel wall throughout the vessel compression. The different coloured lines represent the different material types.
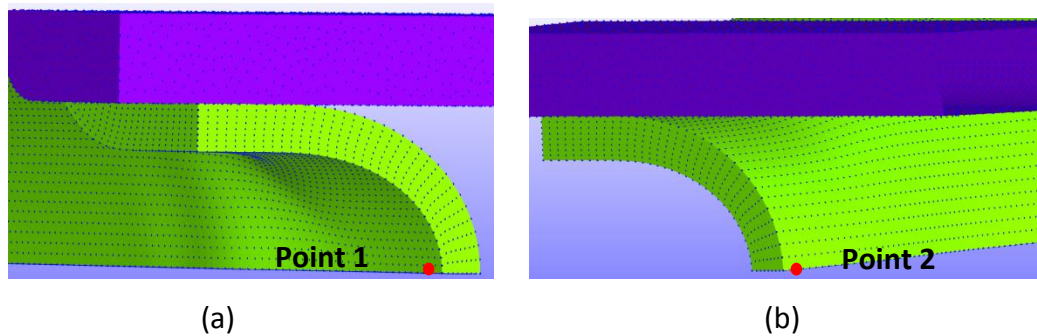
Figure 5-9 Image showing the points of interest (POI) for the different analyses. (a) Point 1 shows the POI on the inner wall of the vessel, (b) Point 2 shows the POI on the outer wall of the vessel. The area of interest considered for the surface plot was the line joining point 1 and point 2.

Due to Figure 5-8 showing a difference in the behaviour of the stress distributions throughout the vessel wall, a surface plot of how the stress varied for both models was produced (Figure 5-10). These surface plots show that again both models have the same stress distribution throughout the wall at this point, but the stress is of different magnitudes.
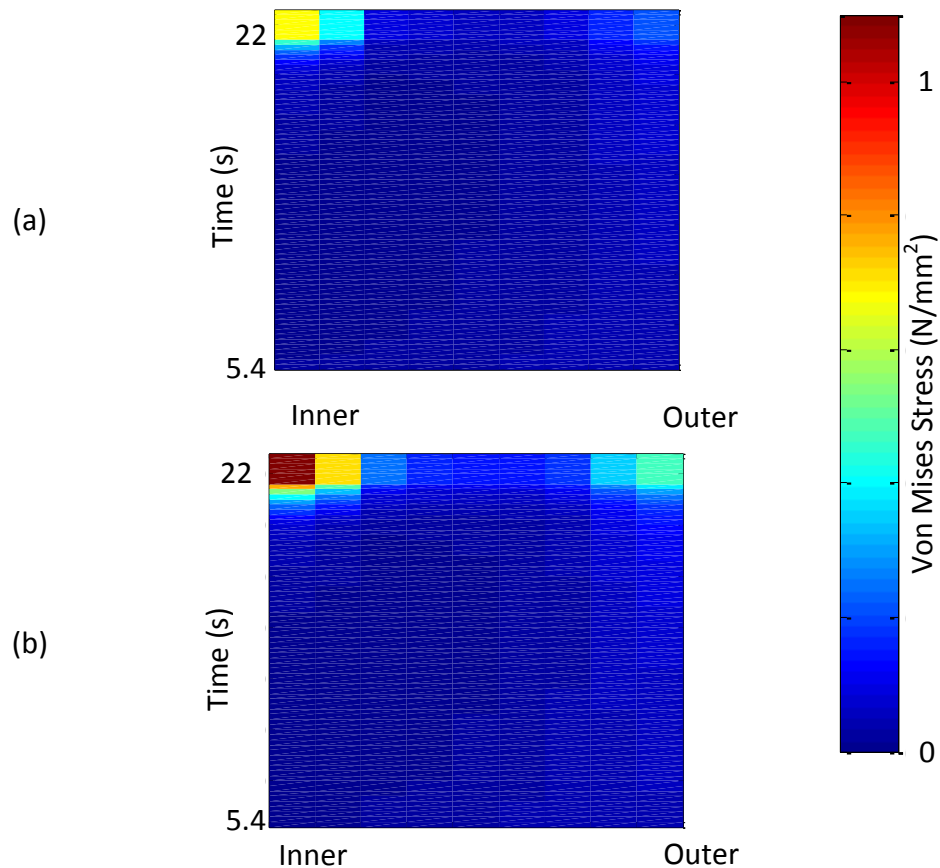
Figure 5-10 Surface plots for the two material types showing the Von Mises stress distribution through the wall of the vessel during the compression stage of the analysis. (a) Showing the elastic material type and (b) showing the muscular material type.

The effective strain throughout the compression stage of the analysis was considered. Table 5-9 shows the difference between the two vessel models throughout this stage. The images shown in Table 5-9 show that both models had a similar strain distribution, but the strain was of different magnitudes for the two different models, with the elastic vessel showing higher levels of strain.

Table 5-9 Images of the blood vessel wall at different stages throughout the blood vessel compression stage. Images show the effective strain through the vessel wall, with a varying scale used for each step displayed.

Time	Elastic	Muscular	Strain, ε
5.4s			0.66 – 0
10s			0.76 – 0
19s			0.84 – 0
20s			0.85 – 0
21s			0.86 – 0
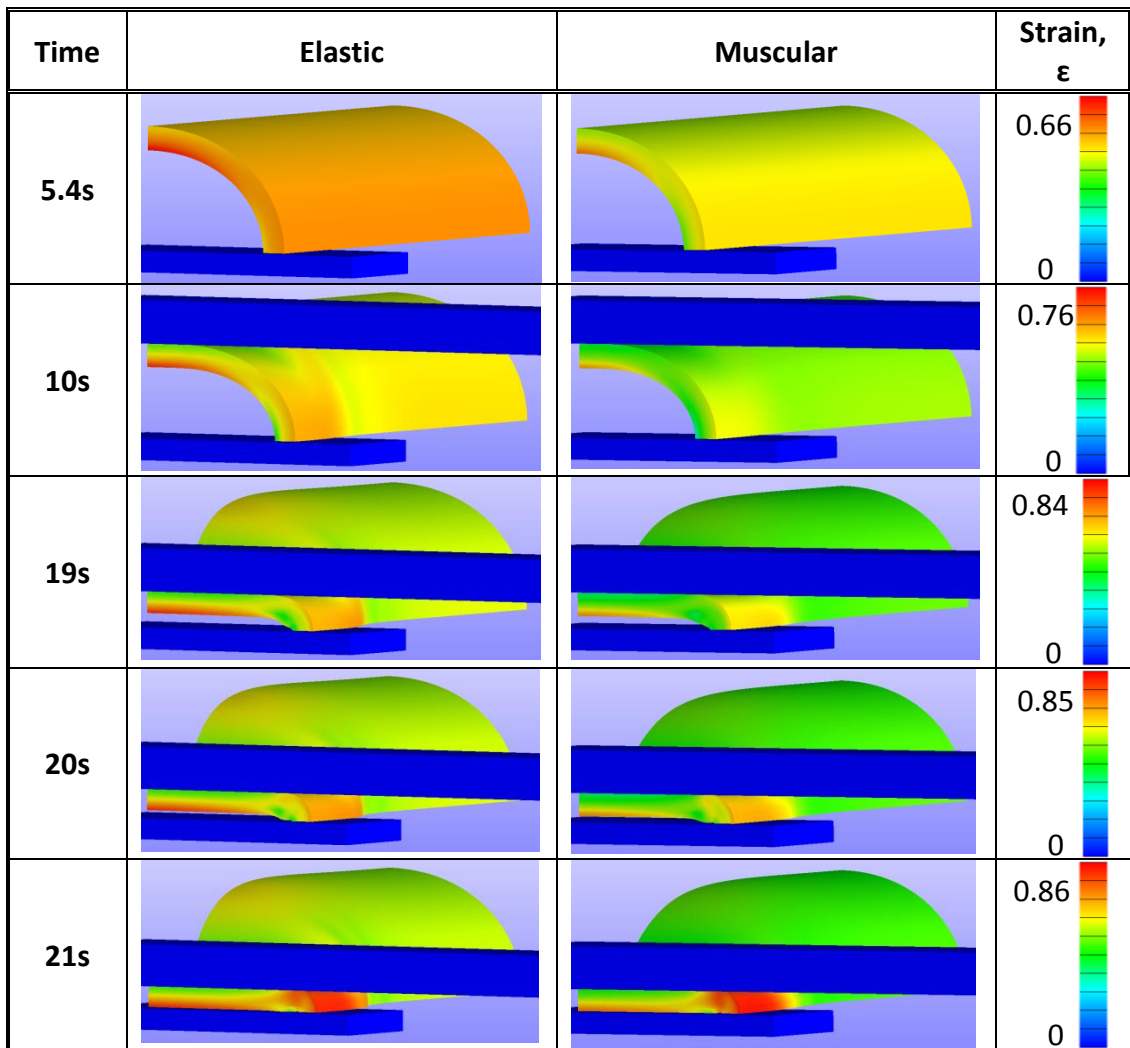
The difference in strain magnitudes was considered further (Figure 5-11) with the strain on the inside of the vessel wall, and the outside of the vessel wall, within the region of highest strain (Figure 5-9) being considered. This Figure shows the highest strain occurring on the outside of the vessel wall, with the strain on the inside being significantly lower. Furthermore the results suggest that at this point within the vessel wall the muscular vessel was actually subjected to greater strains than the elastic vessel at the point of complete compression.
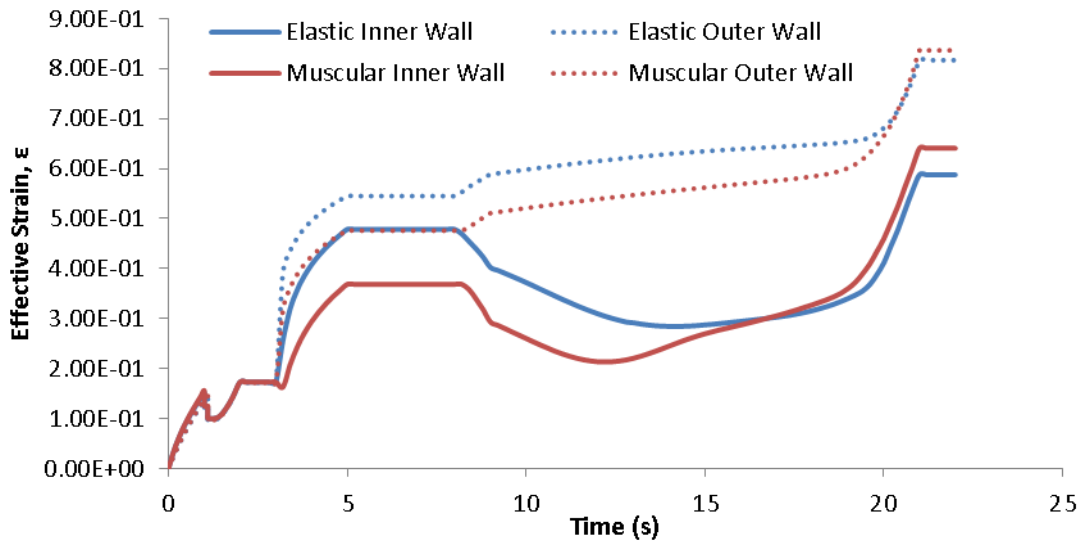
Figure 5-11 The effective strain at the inner and outer wall of the blood vessel wall throughout the vessel compression. The different coloured lines represent the different material types.

Due to Figure 5-11 showing a difference in the behaviours of the strain distributions throughout the vessel wall, a surface plot of how the strain varied for both models was produced (Figure 5-12). These surface plots show the same pattern of strain distribution throughout the wall at this point, but the strain is of different magnitudes.
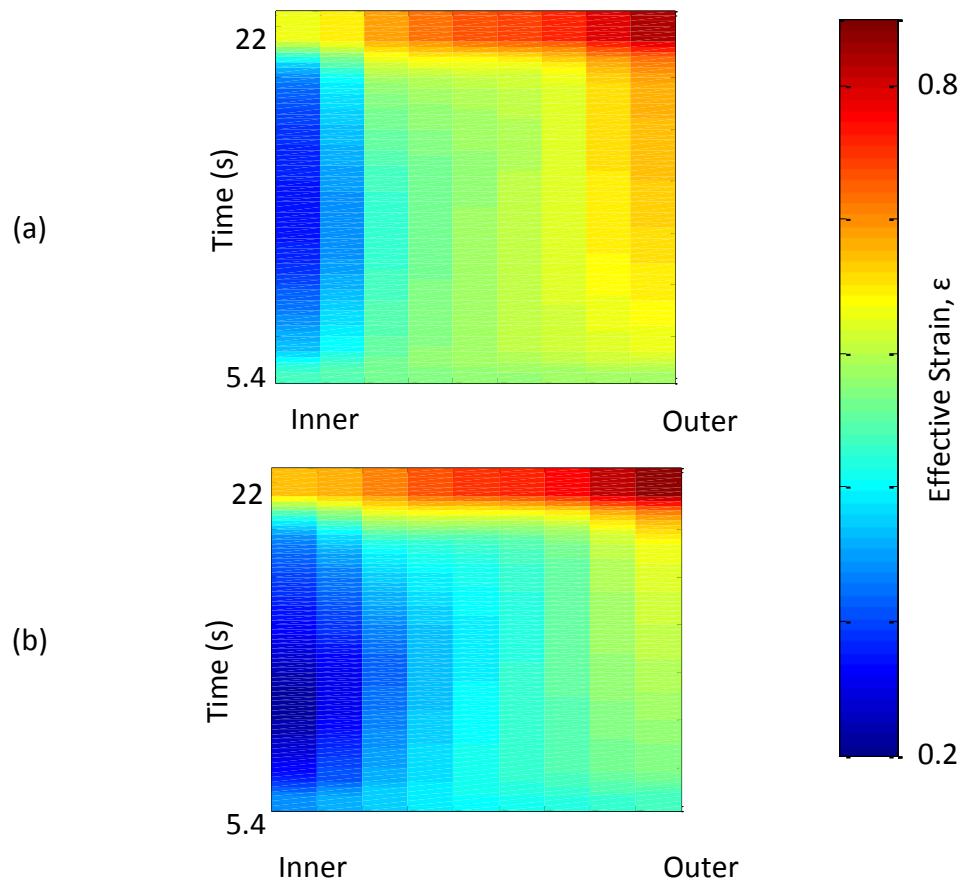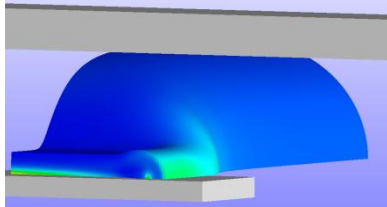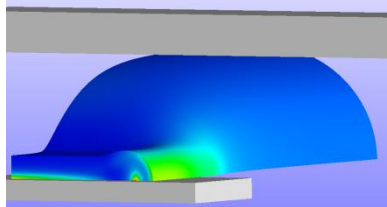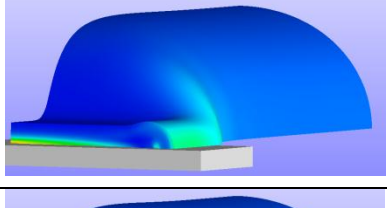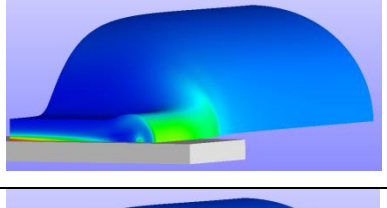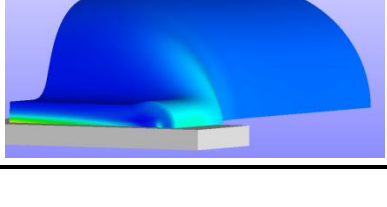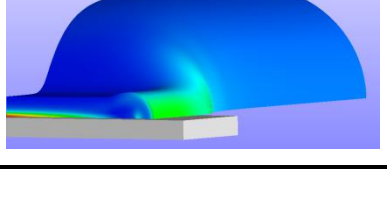
Figure 5-12 Surface plots for the two material types showing the effective strain distribution through the wall of the vessel during the compression stage of the analysis. (a) Showing the elastic material type and (b) showing the muscular material type.

5.7.2.2 Adhesion and Inflation

The Von Mises stress throughout the adhesion and inflation stage of the analysis was considered. Table 5-10 shows the difference between the two vessel models throughout this stage. The images shown within Table 5-10 show that both models have a similar pattern for the stress distribution, but the stress is of different magnitudes for the two different models, with the muscular model showing higher levels of stress.

Table 5-10 Images of the blood vessel wall at different stages throughout the inflation stage following the vessel compression and adhesion. Images show the Von Mises stress through the vessel wall, with a varying scale used for each step displayed.

Time	Elastic	Muscular	Stress / (N/mm^2)
33.8s			0.28 0
39.8s			0.54 0
45s			0.84 0

The difference in stress magnitudes was considered further (Figure 5-13) with the stress on the inside of the vessel wall, and the outside of the vessel wall, within the region of highest stress, points 1 and 2 in Figure 5-9 being considered. This figure shows a difference in stress distributions between the two vessel models with the higher stress occurring on the outside of the muscular vessel wall, but on the inside of the elastic vessel wall.
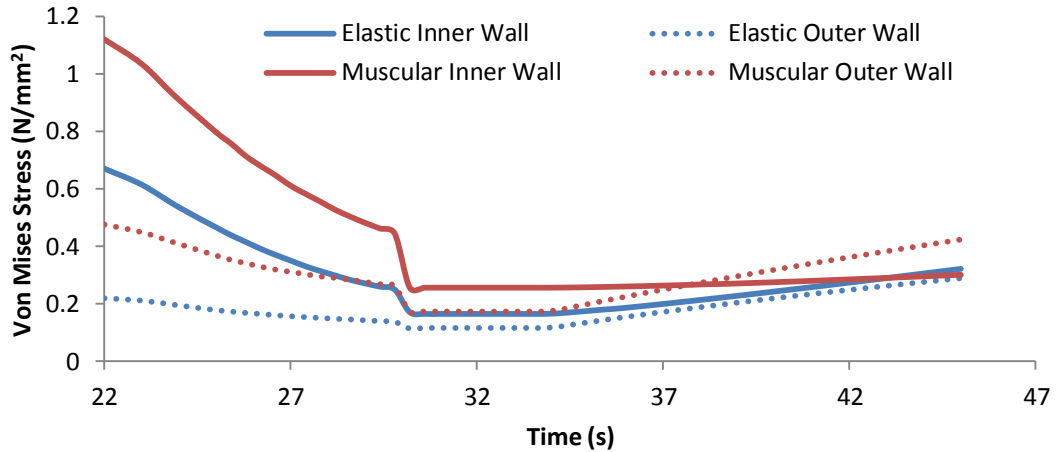
Figure 5-13 The Von Mises stress at the inner and outer wall of the blood vessel wall throughout the vessel inflation stage of the analysis. The different coloured lines represent the different material types.

Due to Figure 5-13 showing a difference in the behaviours of the stress distributions throughout the vessel wall, a surface plot of how the stress varies for both models was produced (Figure 5-14). These surface plots show a difference in the stress distributions between the two material models, with the elastic model having a higher stress on the inside of the vessel wall, and a lower stress on the outside of the vessel wall, whereas the muscular vessel shows the higher stress initially occurring on the inside of the vessel wall and then gradually transitioning to the outer wall having the higher stress.

Current research being conducted by Famaey *et al* (2013) was working towards damage models for the clamping of blood vessels. As such the current limitations as to the stresses the vessels can withstand before damage occurs are not fully known. When considering the stress limitations during bursting, testing conducted by Kim *et al* (2012) found vessels ruptured at between 0.34-1.05 MPa, when testing human thoracic aortas. There is significant variation in the stress the vessel can withstand, and the data available is for thoracic ascending aorta for aneurysmal tissue. Further testing would be required to understand the stress limitations for sealed carotid arteries before rupture occurs.
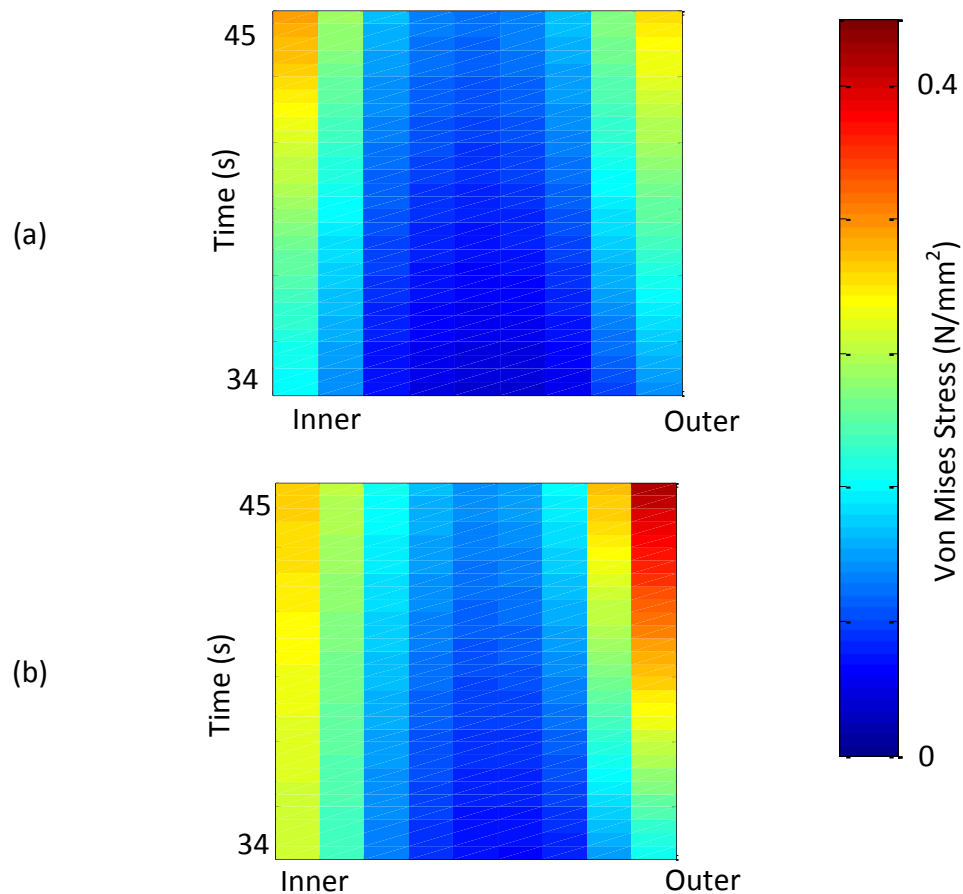
Figure 5-14 Surface plots for the two material types showing the Von Mises stress distribution through the wall of the vessel during the inflation stage of the analysis. (a) Showing the elastic material type and (b) showing the muscular material type.

The effective strain throughout the adhesion and inflation stage of the analysis was considered. Table 5-11 shows the difference between the two vessel models throughout this stage. The images shown within Table 5-11 show that both models have a similar pattern for the strain distribution, but the strain is of different magnitudes for the two different models, with the elastic model showing higher levels of strain, this was due to the higher elastin content within the predominantly elastic vessel which allows the vessel to meet physiological requirements by being highly deformable.

Table 5-11 Images of the blood vessel wall at different stages throughout the inflation stage following the vessel compression and adhesion. Images show the effective strain through the vessel wall, with a varying scale used for each step displayed.

Time	Elastic	Muscular	Strain, ε
33.8s			0.83 — 0
39.8s			1 — 0
45s			1.1 — 0
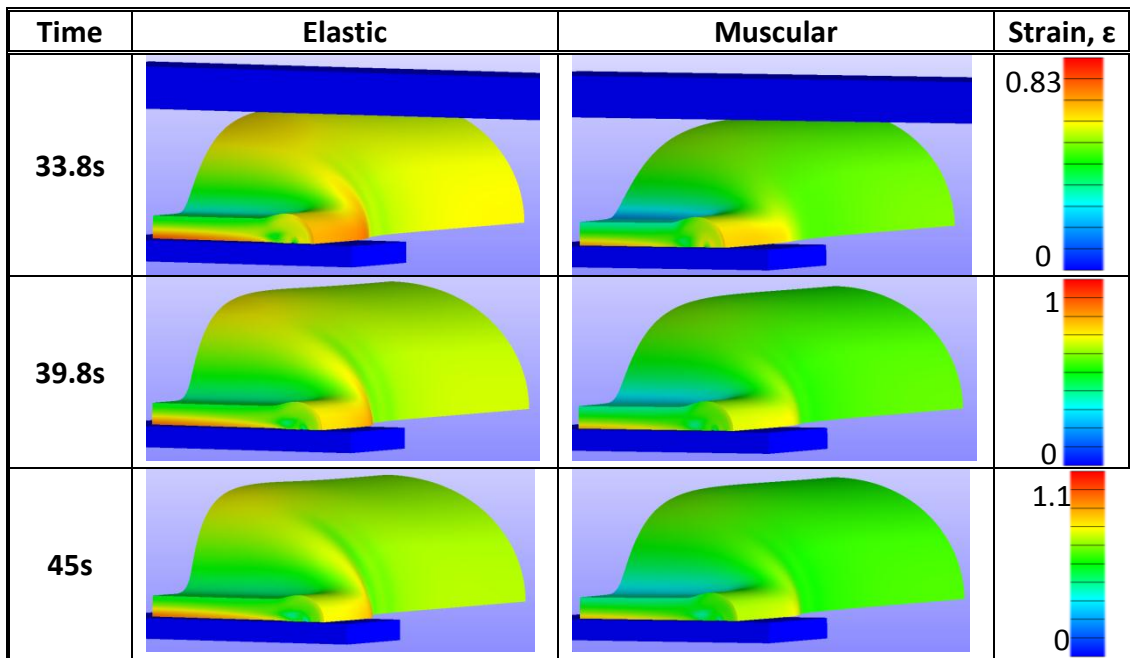
The difference in strain magnitudes was considered further (Figure 5-15) with the strain on the inside of the vessel wall, and the outside of the vessel wall, within the region of highest strain, points 1 and 2 in Figure 5-9 being considered. This figure shows the same strain distributions for the different material types, with the strain being of different magnitudes. Although the two material types show the same strain distributions Figure 5-15 shows a difference in the two material types in their ability to distribute strain throughout the vessel wall, with the muscular vessel having the highest strain at the inside of the vessel wall, and the elastic vessel having the highest strain at the outside of the vessel wall.
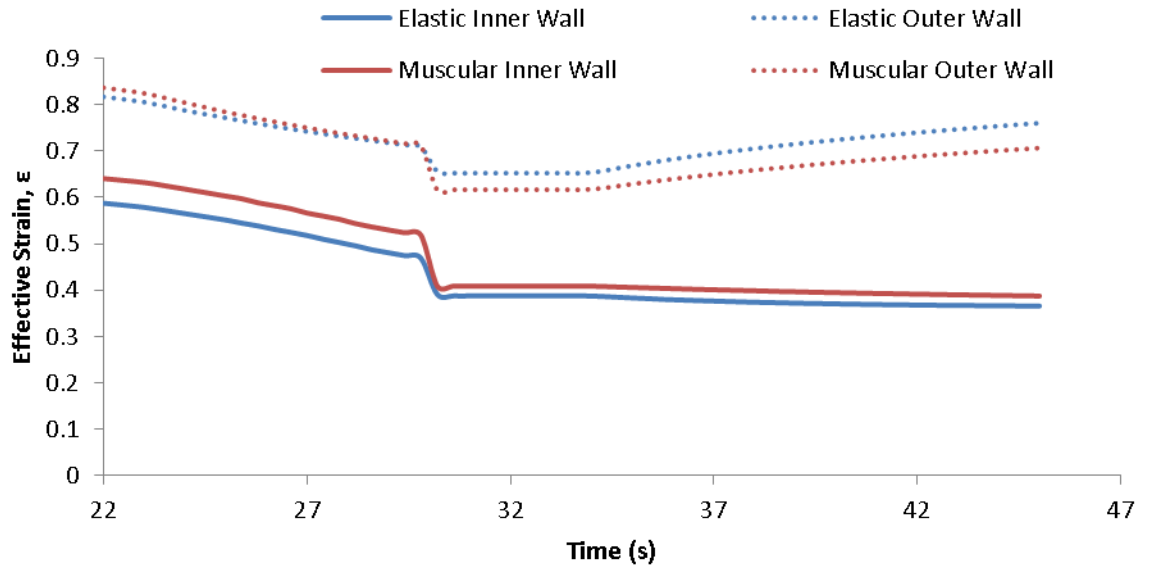
Figure 5-15 The effective strain at the inner and outer wall of the blood vessel wall throughout the vessel inflation analysis stage. The different coloured lines represent the different material types.

Due to Figure 5-15 showing a difference in the behaviours of the strain distributions throughout the vessel wall, a surface plot of how the strain varied for both models was produced (Figure 5-16). These surface plots show the same pattern of strain distribution throughout the wall at this point, but the strain was of different magnitudes.
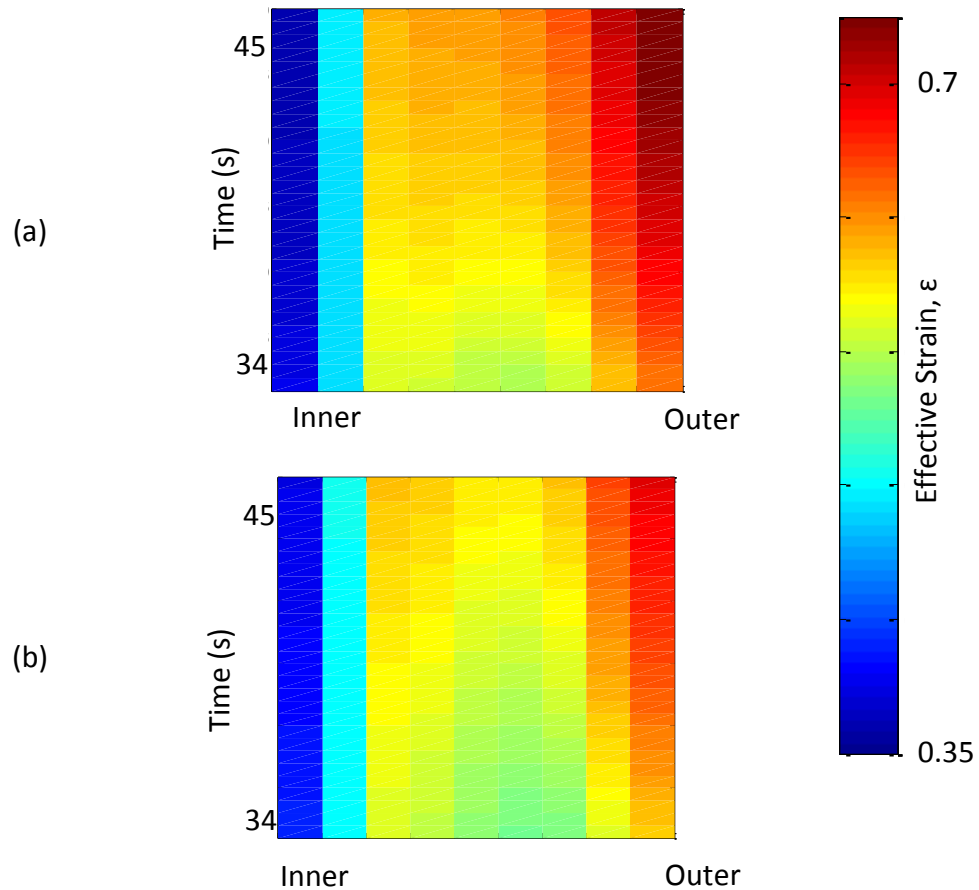
Figure 5-16 Surface plots for the two material types showing the effective strain distribution through the wall of the vessel during the inflation stage of the analysis. (a) Showing the elastic material type and (b) showing the muscular material type.

5.7.3   Comparison of Shim Geometry
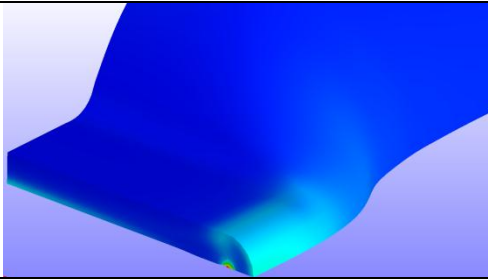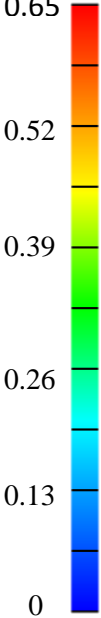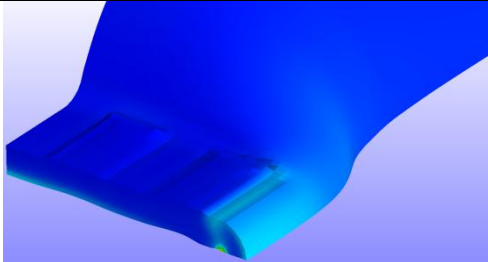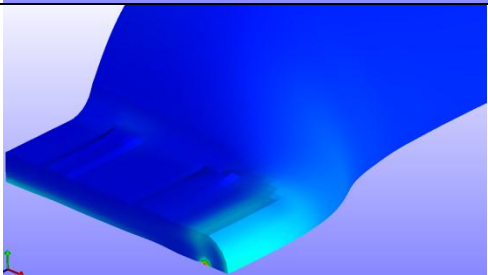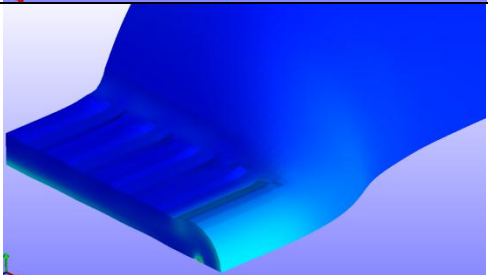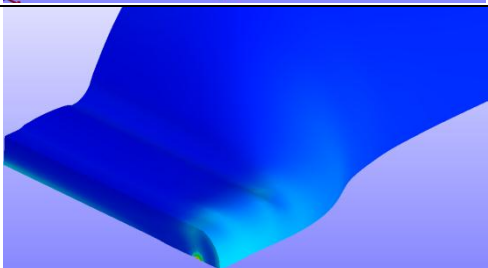
Five different shim designs were modelled for assessment using the FEM. These models all achieved complete compression during the compression stage of the model, but only three models managed to converge for the adhesion and inflation stage of the analysis.

5.7.3.1 Vessel Compression

The Von Mises stress throughout the compression stage was considered for the different shim designs, with the stress distributions at complete compression displayed in Table 5-12. The images within this table show the area of high stress occurred in the same place on each vessel irrespective of the shim design. Furthermore the images demonstrate how the tissue follows the shape of the shims surface features.

Table 5-12 Images of the blood vessel wall at full compression with images showing the Von Mises stress through the vessel wall for the different shim designs assessed.

Shim Type	Von Mises Stress t=22s	Scale Bar / (N/mm²)
Original Shim		0.65 0.52 0.39 0.26 0.13 0
Grooved Shim		
Narrow Grooved Shim		
HF Grooved Shim		
Longitudinal Grooved Shim		

The magnitude of the Von Mises stress was considered for the different shims at two POI's (as defined in (Figure 5-9), with the results showing a difference in magnitude of the different shims at both the inner and outer wall (Figure 5-17). The results show that when grooves were added to the surface of the shims there was a
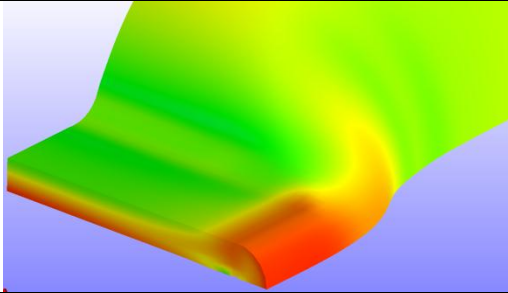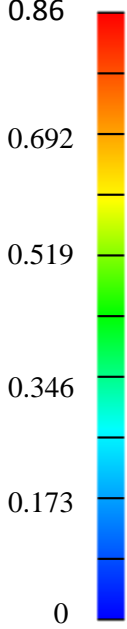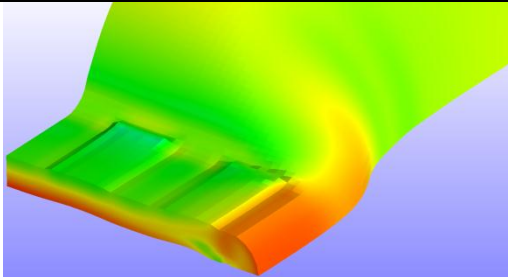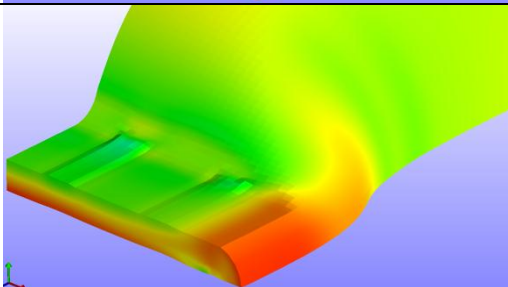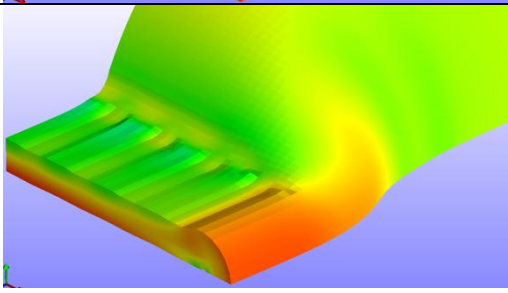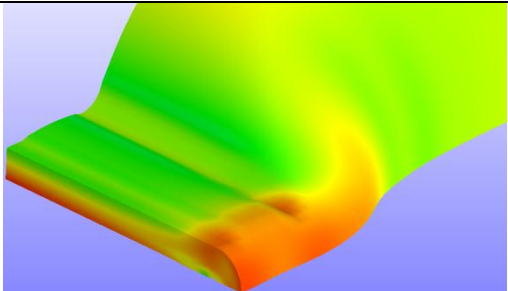
reduction in the stress throughout the vessel wall due to less overall compression of the vessel wall.
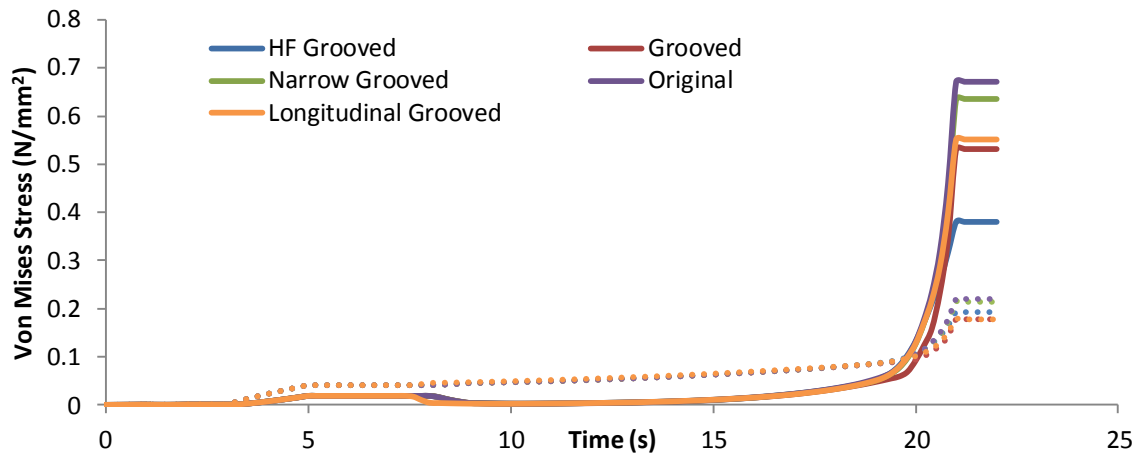
Figure 5-17 The Von Mises stress at the inner and outer wall of the blood vessel wall throughout the vessel compression. The different coloured lines represent the different shim designs assessed, with the solid lines showing the stress at the inner wall and the dashed lines showing the stress at the outer wall.

The effective strain throughout the compression stage was also analysed for the different shim designs, with the strain distrubutions once complete compression was achieved displayed in Table 5-13. The images within this table show a variation in the strain distribution through the vessel wall, along the axis of symmetry for the different shim designs. All models displayed a high area of strain at the edge of the vessel wall beneath the compressive shim.

Table 5-13 Images of the blood vessel wall at full compression with images showing the effective strain through the vessel wall for the different shim designs assessed.

Shim Type	Effective Strain t=22s	Scale Bar, ε
Original Shim		0.86
Grooved Shim		0.692
Narrow Grooved Shim		0.519
HF Grooved Shim		0.346
Longitudinal Grooved Shim		0.173
		0

The magnitude of the effective strain was considered for the different shims at two points of interest (as defined in Figure 5-9), with the results showing little difference in the strain at these points for the different shim designs (Figure 5-18).
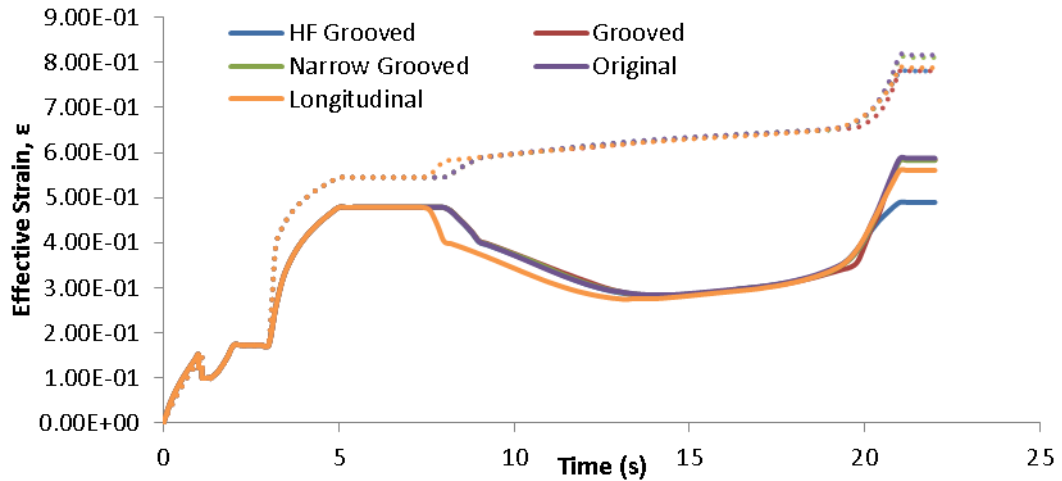
Figure 5-18 The effective strain at the inner and outer wall of the blood vessel wall throughout the vessel compression. The different coloured lines represent the different shim designs assessed, with the solid lines showing the strain at the inner wall and the dashed lines showing the strain at the outer wall.

Additionally the compressive force of the shim throughout the compressive stage of the analysis was considered, (Figure 5-19) with the results showing that the addition of grooves resulted in a lower application force being required to achieve complete compression.
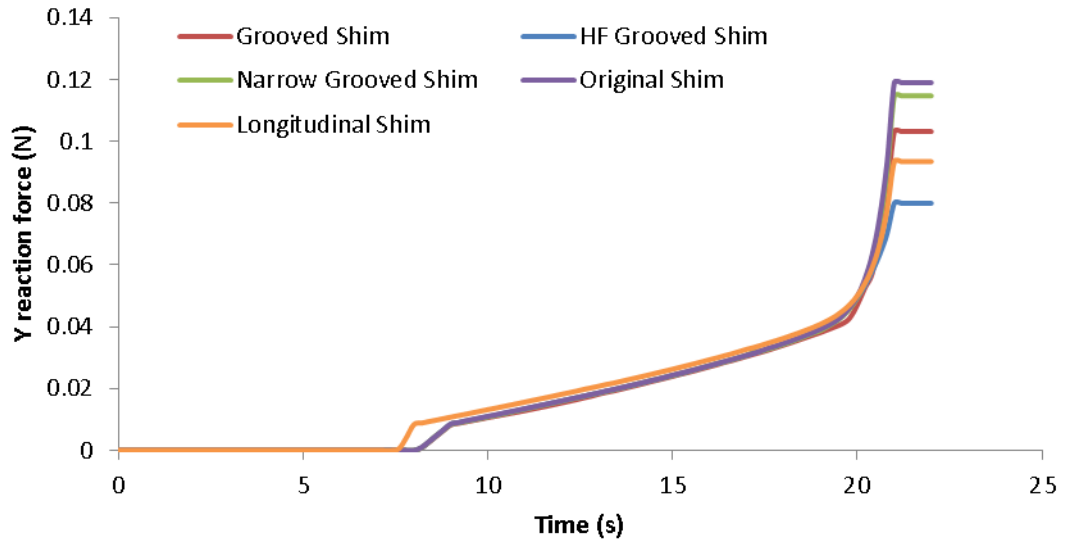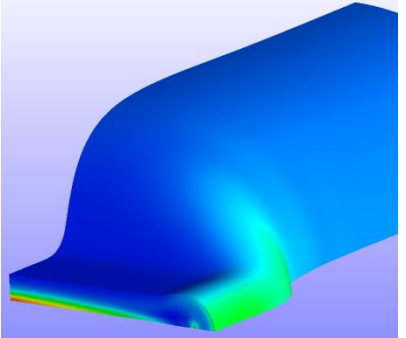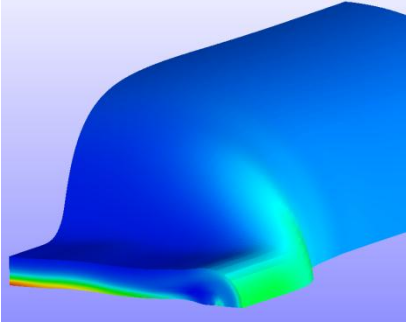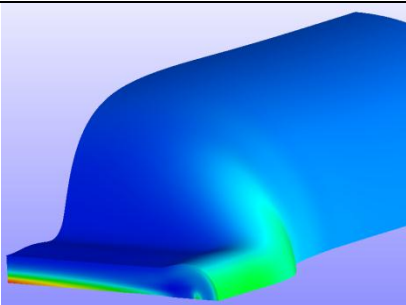
Figure 5-19 The reaction force acting on the shim in the y direction. The different coloured lines represent the different shim designs assessed.

5.7.3.2 Adhesion and Bursting

The Von Mises stress throughout the adhesion and bursting process was analysed for the three shim designs where adhesion and inflation were successfully modelled (Table 5-14). Images presented in Table 5-14 show no noticeable difference in the stress distribution during the inflation stage of the analysis, with similar magnitudes being presented for all shims.

Table 5-14 Images of the blood vessel wall at the final step within the adhesion and inflation step with images showing the Von Mises stress through the vessel wall for different shim designs.

Shim Type	Von Mises Stress t=22s	Scale Bar / (N/mm²)
Original Shim		0.62 0.496 0.372
Grooved Shim		0.248 0.124 0
Longitudinal Grooved Shim		
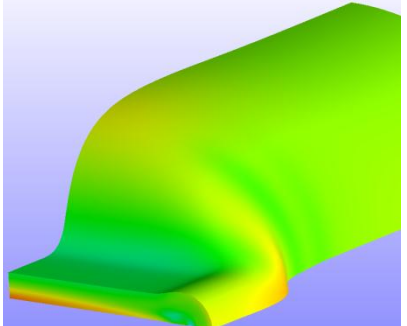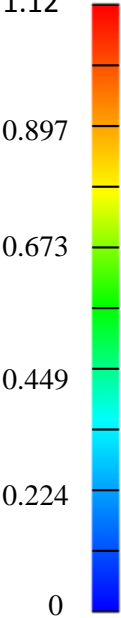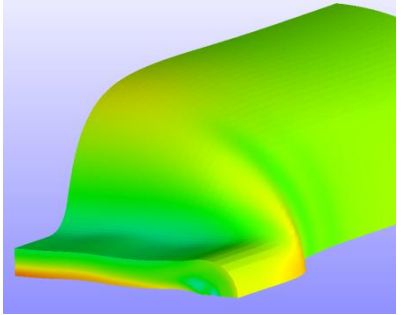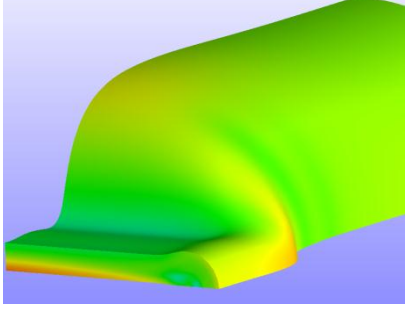
The magnitude of the Von Mises stress was analysed for the different shims at two points of interest (as defined in Figure 5-9) in greater detail, with the results again showing little difference between the two shim designs. The grooved shims did result in a slightly lower stress during vessel inflation at the inner vessel wall (Figure 5-20).
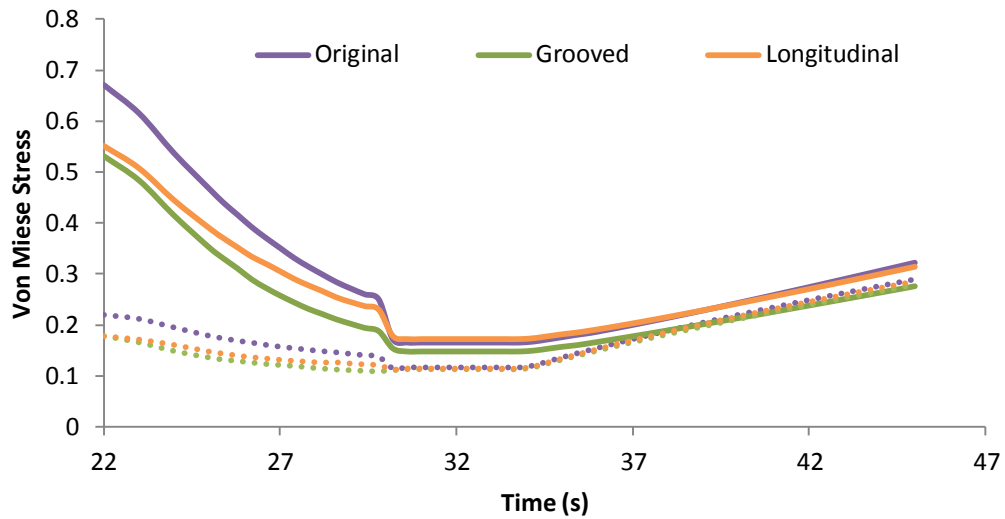
Figure 5-20 The Von Mises stress at the inner and outer wall of the blood vessel wall throughout the adhesion and inflation analysis stage. The different coloured lines represent the different shim designs assessed, with the solid lines showing the stress at the inner wall and the dashed lines showing the stress at the outer wall.

The effective strain throughout the adhesion and bursting process was analysed for the three shim designs where adhesion and inflation were successfully modelled (Table 5-15). Images presented in Table 5-15 show no noticeable difference in the strain distributions during the inflation stage of the analysis, with similar magnitudes being presented for all shims.

Table 5-15 Images of the blood vessel wall at the final step within the adhesion and inflation step with images showing the effective strain through the vessel wall for different shim designs.

Shim Type	Effective Strain t=45s	Scale Bar, ε
Original Shim		1.12
		0.897
Grooved Shim		0.673
		0.449
		0.224
Longitudinal Grooved Shim		0

The magnitude of the effective strain was analysed for the different shims at two points of interest (as defined in Figure 5-9) in greater detail, with the results again showing little difference between the two shim designs (Figure 5-21).
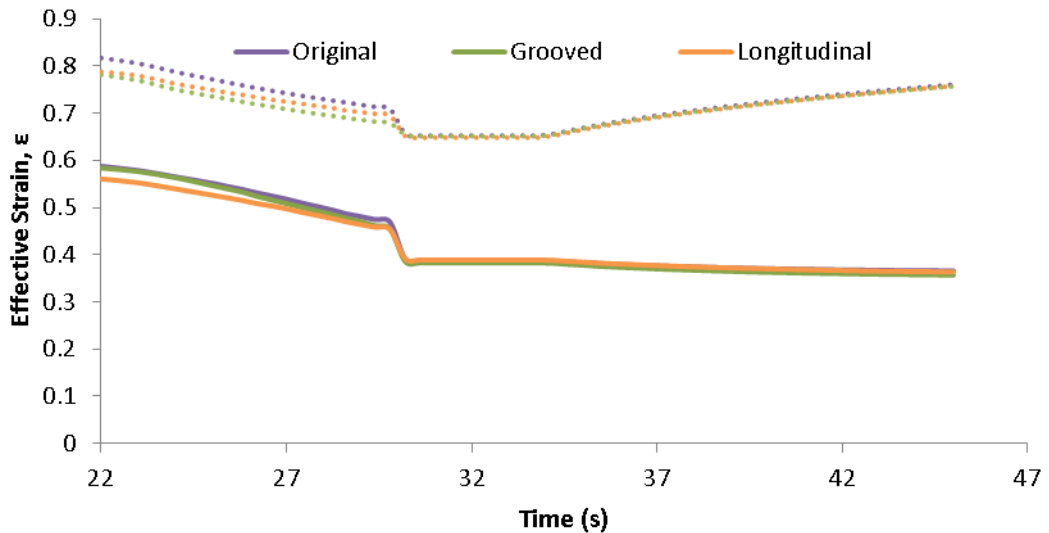
Figure 5-21 The effective strain at the inner and outer wall of the blood vessel wall throughout the adhesion and inflation analysis stage. The different coloured lines represent the different shim designs assessed, with the solid lines showing the strain at the inner wall and the dashed lines showing the strain at the outer wall.

5.8 Discussion

5.8.1 The FE Model

The FE model described in this Chapter was produced to assess the mechanical aspects of the vessel clamping and as such the stress and strain distributions throughout the vessel wall were considered. As with all FE models there were a number of assumptions that were made within the model. Firstly the shim gap considered for this analysis was significantly larger than that of the actual device. During clamping of the tissue with the actual device the process is more complex, with the movement of water within the vessel wall and the compressibility of the tissue needing to be considered. Due to the software being used and a lack of information available on this subject this was not modelled within the FEM, and as such the shim gap was larger than desired.

Furthermore the actual compression method was simplified, being modelled as two parallel plates. In reality the compression the vessel is achieved with the jaws moving in a similar way to scissors due to the pivot in the device handle. This means that the compression modelled here is even across the width of the vessel instead

of being greater towards one side. This simplification allowed for symmetry to be used to the full extent within the model. This difference in compression method could alter the stress and strain distributions seen across the vessel wall, but is unlikely to affect the results from the comparison of the different models. This simplification in clamping has also been implemented in other models throughout literature, justifying its use within the model (Famaey *et al.*, 2012, Famaey *et al.,* 2010, Famaey *et al.*, 2013, Gasser *et al.*, 2002, Chen *et al.*, 2009).

The model used to simulate the behaviour of the tissue was the Ogden model, which was not an ideal choice, although the does replicate the behaviour of the blood vessel wall well when comparing the strain distribution achieved experimentally with that of the FEM (Figure 5-7). Furthermore the Ogden model has previously been demonstrated within the literature to be a good fit to experimental data for the behaviour of blood vessels (Ogden, 1972). The model was also used due to the good convergence achieved with the model. Ideally the Holzapfel – Gasser model would have been used to replicate the behaviour of the tissue, taking into account the orientation of the fibres and the different layers of the blood vessel wall (Gasser *et al.*, 2002). Furthermore when considering the modelling of the adhesion, no change in material properties was considered for the region beneath the shim. The material within this region has a significant change in material properties, although this change has not being quantified. Furthermore the region of the vessel that the change in material properties applies is not known, with the change in material properties thought to progress along the length of the vessel for a small distance, even though this region is not directly affected by heat, and is minimal in size in comparison to the length of the vessel.

The stress in the model presented in this chapter shows areas of high stress in the same regions of the vessel wall as were found by Famaey *et al* for the smooth shims (Famaey *et al.*, 2012). Although this is the case due to differences within both models and the difference in software used it was neither possible nor beneficial to compare the magnitude of this stress. It was not possible to compare the magnitudes of stress due to Famaey *et al* using a hoop stress, which was not possible to analyse using the FEBio software suite. Furthermore the principal strain

from the FEM was compared to data collected using DIC to capture the vessel compression. Images show a similar strain distribution, with high levels of strain being captured at the same part of each vessel. Although this is the case the strain distributions did vary, and were not uniform across the surface of the vessel. This uneven distribution was seen throughout the data collected in Chapter 4, and was attributed to a difference in thickness throughout the wall of the vessel, which was observed in the arteries used throughout the experimental work. This was not accounted for within the FEM. The data captured using DIC also showed different magnitudes of strain, with the differences attributed to a variation in vessel properties, such as thickness, outer diameter and vessel morphology. Although these values varied, the magnitude of strain from samples 1 and 3 was comparable with the magnitudes of strain in the FEM. Additionally there was a slight variation in the shape of the shims used between the different analyses, with the shims used in DIC being curved and the shims used in the FEM being straight. This could account for the slight differences in the strain distribution and be a contributing factor to the differences in magnitude.

When considering the inflation stage of the analysis a high level of stress was observed on the inside of the vessel wall for the sealed region, near the centre line of the vessel. This high level of stress indicates a likely point of failure during the burst testing of the seal, and is in line with results reported by Richards, 2010, where the position of seal failure was observed as being at the centre or close to the centre of the seal. This high level of stress at this point provides an explanation at the why the seal failure occurs at the centre of the vessel.

5.8.2   *Comparison of Material Types*

Two material types were analysed, with each of the models using the same boundary conditions and loads. As seen in Sections 5.7.2.1 and 5.7.2.2 there were significant differences in the performance of the elastic and muscular vessels during both the compression and inflation stages. At the points of interest (Figure 5-9) the muscular vessel had the highest levels of stress and strain during the compression stage of the analysis, although both material models had similar distribution patterns. More notable differences were observed during the inflation stage of the

analysis where there was a significant difference in the way stress and strain was distributed through the vessel walls.

Considering the compression of the stage of the analysis the muscular vessel had the highest level of stress at both the inside and the outside of the vessel wall (Figure 5-8 and Figure 5-10), this was to be expected due to the increase in stiffness of the muscular vessel compared to the elastic vessel. Although there was a difference between the two material types in terms of stress magnitude, both models demonstrated a similar stress distribution through the wall of the vessel (Figure 5-10). Furthermore both the elastic and muscular vessels showed a high stress concentration on the inside and outside of the vessel wall in the tissue being clamped, which is again expected due to the high level of deformation occurring at this point. This high level of stress is also indicative that this is an area of the vessel that could be damaged during the clamping process, possibly leading to a weakness within this area of the blood vessel wall which influences the ability of the vessel to withstand pressure during the inflation test.

The strain analysis during the compression stage showed that the elastic vessel had higher levels of strains throughout the vessel wall (Table 5-9), although the muscular vessel had the highest level of strain at the POI's (Figure 5-11). This suggests that the deformation as a result from the compression and the subsequent effects were more localised within the wall of the muscular vessel (Table 5-9 and Figure 5-12). With the elastic vessel the compression appears to affect a larger area of the blood vessel, and could be indicative of why the two material types perform so differently during the inflation tests, with the elastic vessel bursting at a lower pressure (refer to chapter 3 for results).

Moving on to consider the inflation stage of the analysis the results suggest a difference between the material types in their ability to withstand the pressure. When analysing the stress the elastic vessel had the higher stress at the inside wall, but the muscular vessel had the highest stress at the outside of the vessel wall (Figure 5-13 and Figure 5-14). This provides a possible explanation as to why the two vessels performed differently during the inflation test, with the vessels

demonstrating a difference in their effectiveness in distributing stress throughout the vessel wall.

Considering the strain of the vessel during the inflation stage of the analysis the elastic vessel had a higher level of strain on the outer wall of the vessel suggesting a higher level of deformation. The high levels of strain occurred at the point between the seal and the unaffected part of the vessel, where there is a large difference in dimensions in the y direction (Table 5-11). This high level of strain was more noticeable for the elastic vessel and affected a larger region of the vessel wall. This suggests that the elastic vessels failed at lower pressures because of the high strain occurring within this region, presenting a weakness within the vessel wall.

5.8.3   Comparison of Shim Geometry

A total of five different shim models were assessed using the elastic vessel model. Each model was modelled using the same boundary conditions and loads. The original aim of the modelling work was to compare six different shim designs, but due to problems importing the 45° grooved shim only five shim designs were compared. Shims with grooves resulted in lower stresses through the vessel wall, and required a lower application force when compared to the original shim during the compression stage. When considering the inflation stage there was little difference in the behaviour of the vessel wall for the three shim designs analysed.

When considering the Von Mises stress throughout the vessel wall during the compression stage there was a significant difference between the smooth shim and those with grooves (Table 5-12 and Figure 5-17). The addition of grooves to the surface of the shims resulted in lower stresses at the points of interest (Figure 5-17), with the most effective reduction of stress occurring when the grooves were equal in width to the peaks, with the stress reduction improved further with higher frequency grooves. Results from Chapter 3 show that the HF Grooved shims resulted in a higher mean burst pressure when compared to the other tested shim designs, suggesting that a significant reduction in stress results in a higher mean burst pressure.

The reduction in stress due to the addition of grooves was to be expected due to less overall compression of the tissue. Tissue that fills the grooves of the shims

during the compression is subjected to less displacement in the y direction than if the surface of the shims was smooth, resulting in a reduction in compression and therefore stress. However these findings are inconsistent with those presented by Famaey *et al* (2012) who reported an increase in stress when comparing a mosquito clamp (grooved) against a smooth clamp (Famaey *et al.,* 2012). This difference in results can be attributed to a number of differences between the two models. A difference in clamp design, for example the width of the grooves, depth of the grooves, and a radius of curvature applied to the grooves, would make a significant difference to the level of stress recorded within the vessel wall. Furthermore the alignment of the grooves could have a significant effect, with Famaey *et al* modelling the clamp assuming a groove is opposite a peak, whereas this study assumed the grooves were aligned. This suggests the alignment of the surface features of the shims should be investigated to understand the effect on stresses within the vessel wall.

When considering the strain distribution during clamping there was a noticeable difference between the different shim designs (Table 5-13), with all shim designs with grooves presenting a higher strain at the seal – vessel interface suggesting the addition of grooves leads to a higher level of deformation. Based on the results from Chapter 3 this does not appear to have a negative effect on the burst pressure. The only shim design to show a lower level of strain at the points of interest was the HF grooved shim (Figure 5-18), suggesting a lower level of deformation at the point of weakness within the sealed area. This suggests that increased deformation at this point of the vessel wall will lead to a reduction in the seal quality due to damage occurring to the vessel wall.

The adhesion and inflation was investigated for three shim designs. For the other models convergence was not achieved when modelling the adhesion of the vessel. Future work should consider improving the model and analyse the adhesion and inflation of more shim designs. The three shim designs that were analysed presented little difference in either the stress or the strain throughout the vessel wall throughout this analysis stage (Table 5-14, Table 5-15, Figure 5-20 and Figure 5-21). This suggests that the amount of damage (the level of stress and strain)

throughout the compression stage is the more influential factor in determining the quality of the resultant seal. Improvements can be made when modelling the adhesion, taking into account the change in material properties and modelling fluid surface interaction to make the model more realistic.

Furthermore it is important to note how the tissue takes the shape of the surface features of the shims. This was seen within the experiment as discussed in Chapter 4. This suggests that the tissue takes the shape of the features of the shim due to the way in which the tissue deforms and squashes between the device jaws and as the tissue heats up and the collagen denatures the tissue remains in this shape once the jaws are removed, acting as a sort of mould for the shape of the seal. Although results presented in this chapter suggest this has a limited factor on seal quality, it is an area that should be given considerable thought during the device design process as a different seal shape may lead to an improvement in seal quality.

5.9 Conclusion

The FE model described in this Chapter recreated the vessel sealing process, with the model taking into account the residual stresses within the blood vessel, and being used to compare different vessel types and different shim designs. When considering the comparison of the vessel types the analysis of the data suggested a difference in the ability of the different vessel types to withstand pressure. Furthermore the strain and stress distribution of the elastic vessel suggested that the effect of clamping had a greater effect over a larger area of the blood vessel and suggested that the elastic vessel was unable to withstand high pressures during bursting due to higher strain occurring in the region between the vessel seal and the unaffected area of the vessel wall.

Analysis of the different shim designs found significant differences in the performance of the different shims, with the addition of grooves resulting in a lower application force being required and lower stresses throughout the vessel wall. Additionally the HF grooved shim resulted in lower strains throughout the vessel wall, indicating that the correct shim design can also lower the strains the vessel is subjected to and reduce the damage occurring to the wall of vessel. These

results suggest that the surface features of the shims can lead to an improvement in the device performance due to less damage occurring within the vessel wall, and a stronger seal being produced as a result.

6   Multiphysics Modelling of Vessel Sealing

6.1   Chapter Summary

This chapter details the creation of an FE model used to compare the performance of the different shim surface structures in terms of the electrical and thermal aspects. The FE model was created in AutoDesk Multiphysics simulation, with the model making use of symmetry and modelling a quarter of the tissue and shim geometry. A total of seven shim pairs were compared using the model, comparing their performance by looking at the temperature throughout the analyses. The results demonstrated that the best shims were those that had a lower temperature at the surface of the shims whilst still producing good heat distribution throughout the tissue. Furthermore the results suggest that the orientation of the grooves affects the seal quality due to the imprint of the groove pattern onto the seal thus affecting the ability of the seal to withstand pressure, and not because of poor temperature performance. The work in the chapter demonstrates how the FE model can be used to aid device design and improve the understanding surrounding the electrosurgical vessel sealing process.

6.2   Introduction

Previous chapters have described the effect of varying shim surface structure on seal quality, with results demonstrating that the structure of the shim surface affects the device performance in terms of seal quality and adhesion. Further investigation into the vessel sealing process and the performance of the different shims using DIC provided a valuable insight into the changes that occur during the sealing process. However the results from this testing did not provide an explanation as to why each shim performed differently, as each seal produced was unique in terms of both tissue displacement and fluctuations in shim gap throughout the sealing process.

Work in the previous chapter used FEM to explore the effect of shim surface structure on the mechanical aspects of vessel clamping and the electrosurgical sealing process. The results demonstrated that the surface structure had a significant effect on the clamping force and the stress throughout the vessel wall, but did not affect the maximum stress within the vessel wall during the inflation test. The work described within this chapter expands upon previous work by creating a multiphysics FE model to investigate the effect of shim surface structure on temperature and heat distribution.

Multiphysics modelling has been used extensively for the simulation of electrosurgery procedures, with the technique being used to model RF ablation in liver tissue , cardiac ablation , and electrosurgical vessel sealing . Work by Dodde *et al* (2008) modelled the process of electrosurgical vessel sealing, using spleen for the tissue model. The work was validated through experimental work using microthermistors, with the FE model being used to compare two shim designs, one smooth and one with grooves. Results from the analysis showed a higher temperature for the smooth shim compared with the grooved shim, highlighting the difference in shim performance and how FEM can be used to aid device design. Multiphysics modelling is a powerful tool for this application, providing vital information on the electrical and thermal behaviour at a low cost, and facilitating the assessment of the feasibility of new electrode geometries .

The aim of this chapter was to create a multiphysics FE model to compare the performance of the shims designed in Chapter 3. A total of seven shim sets were assessed, in terms of overall temperature and heat distribution during the analysis. An additional aim was to explore the effect of the alignment of the shim surface features. Furthermore the model was validated using experimental data, and the results from the analyses were used in conjunction with those from previous chapters to improve understanding of the effect of shim design on the performance of electrosurgical vessel sealing devices.

6.3 Modelling the sealing process

There are various commercial software packages available with the capability to conduct multiphysics analysis. ANSYS and COMSOL provide all the necessary elements to build the model, to solve the problem, and post-process the results, with both of these software packages capable of performing an electric – thermal coupled field analysis with temperature dependent properties . An alternative to these software packages is Autodesk Simulation Multiphysics, with this software being capable of conducting various multiphysics analyses, including electrical and thermal analyses. When using this software, it was necessary for the analysis to be spilt into two stages; an electrostatic analysis, and a transient heat analysis. The results from the electrostatic analysis were used to generate the heat in the transient heat analysis, through Joule effect heating. This process differs to that used by COMSOL, where there is the capability for constant feedback between the electrostatic and transient heat analyses, running the two stages simultaneously. The method used by COMSOL would provide more accurate results, but models produced using Autodesk Simulation allow for comparisons to be made, and it has the advantage of the software being available on a student licence.

To model the process of electrosurgical vessel sealing, it was necessary to simplify the geometry. The model produced takes advantage of the axes of symmetry (Figure 6-1), and only considers the most significant tissue, in this case the blood vessel wall, which is standard practice for modelling RF procedures . Furthermore the electrical input for the model was simplified by converting the ac voltage into a dc voltage by calculating its root mean square (rms) (Berjano, 2006).The subsequent sections will detail the creation of the FE model and the input parameters and boundary conditions for the model.
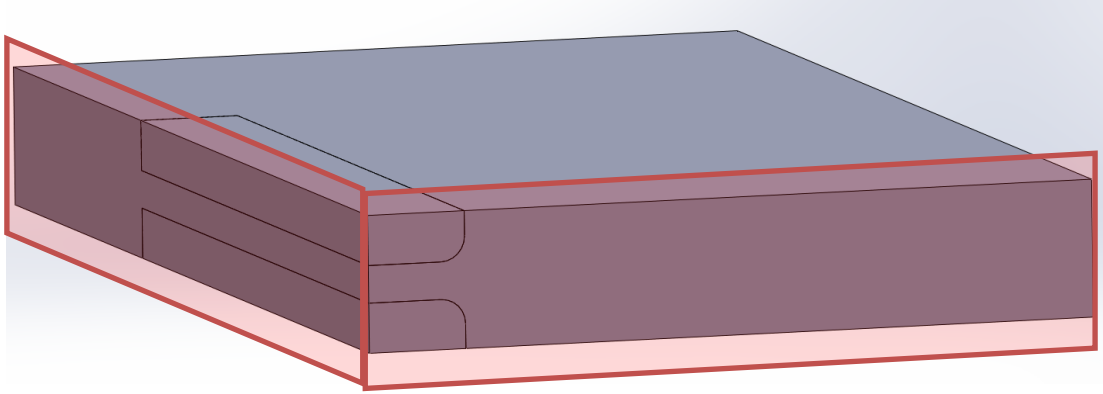
Figure 6-1 Schematic showing the plans of symmetry for the model, with the highlighted surfaces showing the symmetry planes for the model.

6.3.1   Tissue Model

6.3.1.1 Tissue Geometry

The tissue was created in SolidWorks (Massachusetts, USA), with cavities being created for the shims. Dimensions for the tissue were based on those used by Dodde *et al* (2008) (Figure 6-2), with the shims embedded into a 25mm x 15mm x 2.75mm region that simulates the tissue the forceps act upon. The model for the tissue was slightly larger than required to ensure that the entirety of the heat affected zone was modelled. The geometry used results in a shim gap of 0.75mm, significantly less than that modelled by Dodde *et al*, but more representative of the actual device shim gap. A second tissue geometry was created replicating that used by Dodde *et al* (a shim gap of 2mm) to allow for comparison between the two models.
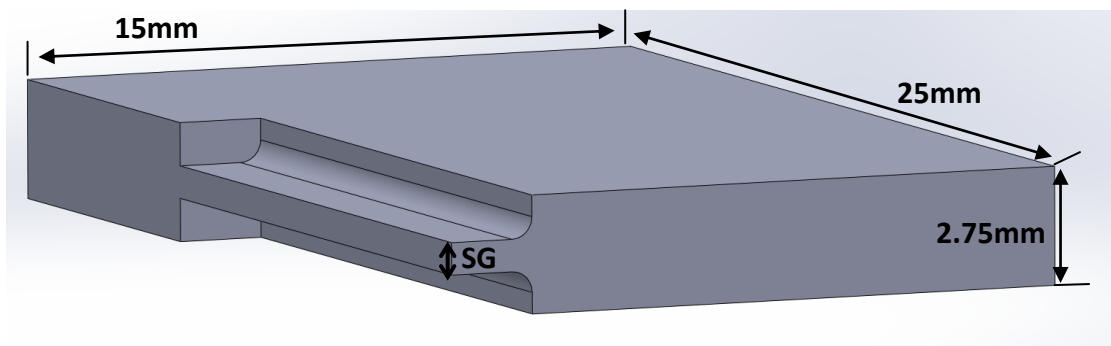
Figure 6-2 Schematic showing the tissue geometry with the cavity formed for the shims, (image shows cavity for original shim, 1_OR). **SG** showing the shim gap, equal to 0.75mm.

6.3.1.2 Material Properties

The tissue for the analysis was modelled as human spleen. This allowed for the results from the model to be compared with those produced by Dodde *et al* (2008). The material parameters used for this model are displayed in Table 6-1. The material modelled throughout this analysis was the spleen, due to the availability of data. Data for a carotid artery was expected to be minimally different to that of the spleen; with available data for thermal conductivity being compared (blood vessel and spleen) varying by approximately 0.07 J/s.m.°C . Additionally the material properties would not affect the outcome of the comparative study being performed.
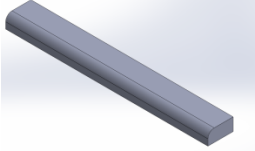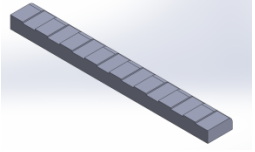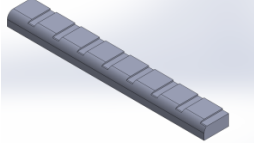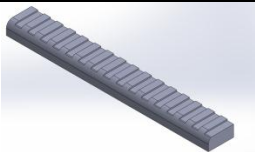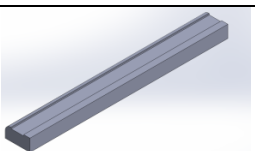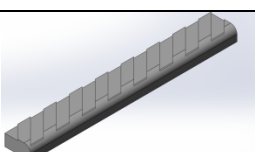
Table 6-1 Showing the material properties for the spleen. Values with the superscript [1] were taken from Druck (1990), and values with the superscript [2] were taken from (Dodde *et al.*, 2008).

Spleen material properties	
Mass Density[1]	1054 (kg/m^3)
Thermal Conductivity [1]	0.539 (J/s.m.°C)
Specific Heat Capacity [1]	3720 (J/kg.°C)
Electrical Conductivity [2]	0.33 (A/v.m)

6.3.2   Shim Model

The shims modelled for the analyses were based on those designed in Chapter 3, with the designs summarised in Table 6-2. The shim models were simplified for the analysis, with the shims being modelled as simple straight smooth shims, as opposed to curved shims with a rough surface. The shims were originally created in SolidWorks (Massachusetts, USA) and were combined with the tissue geometry model as described in Section 6.3.1.1. A total of seven shim pairs were analysed. The material of the shims was modelled as medical grade stainless steel, with the following material parameters; Mass density 8000 (kg/m^3), thermal conductivity 16.5 (J/s.m.°C), specific heat 500 (J/kg.°C) and electrical conductivity 1,388,889 (A/v.m); material properties were provided by Gyrus Medical Ltd.

Table 6-2 Summary of shim designs, note all grooves are 0.1mm deep

Shim	Shim Surface Design Features			CAD Model
	Groove Width	Peak Width	Design Orientation	
Original Shim **1_OR**	No surface features			
Grooved Shim **3_GR**	1mm	1mm	Transverse	
Narrow Grooved Shim **4_NA**	0.5mm	1.5mm	Transverse	
HF Grooved Shim **5_HF**	0.5mm	0.5mm	Transverse	
Longitudinal Grooved Shim **6_LO**	1mm	1mm	Longitudinal	
45° Grooved Shim **7_45**	1mm	1mm	45°	
Combination Shim Set **8_CC**	Combination of the grooved shim (3_GR) and the longitudinal grooved shim (6_LO)			

In addition to comparing the performance of the different shims, two alignments of shims were tested; one where the surface features were aligned, and one where they were not (Figure 6-3). This investigation was conducted to assess the effect of shim alignment on the temperature and also the heat distribution and to see how

important this parameter could be when designing and manufacturing future devices.

a.   b.
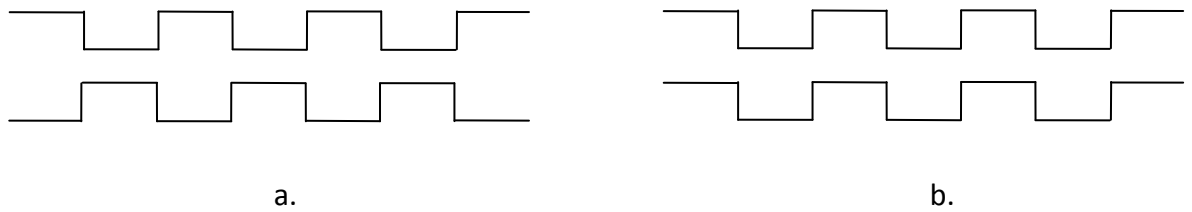
Figure 6-3 Schematic drawing showing a. the shims where the surface features are aligned, and b. the shims where the surface features are not aligned. Drawing is representative of the grooved (3_GR) shims.

6.3.3 Electrostatic Analysis

The electrostatic analysis was performed to establish the necessary inputs for the transient heat analysis. The outputs from this analysis include the voltage at the nodes, current flux density (vectors) at the element centroids, and current flow through edges of faces (AutoDesk). The outputs were used to generate heat in the transient heat analysis based on the Joule heating effect.

6.3.3.1 Boundary Conditions and Loads

For this step of the analysis the boundary conditions and loads that needed to be applied were minimal, and consisted of two applied voltage loads that were applied to the surface of the shims. The surface applied voltage applies a nodal voltage to each node on the surface, and was used to fix a node to a certain voltage throughout the analysis. The voltage is transferred from one node to another through an element with a conductance stiffness specified. A high stiffness value will cause the node on the model to be very close to the magnitude of the applied voltage, and a low stiffness value means that the voltage of the node on the model could be significantly lower that the magnitude of the applied voltage. The stiffness value assigned was left at the default value of 10^7, with a high stiffness being required to maintain the node at the same value as the applied voltage.

One shim in the analysis was modelled as an active electrode, with the 75 V applied to the surface. The other shim was modelled as the return electrode and had a surface applied voltage of 0V applied. The surfaces highlighted in Figure 6-4 shows

the surfaces of the shim to which the applied voltage constraint was applied, with the same surfaces being selected on both the active and return shim.
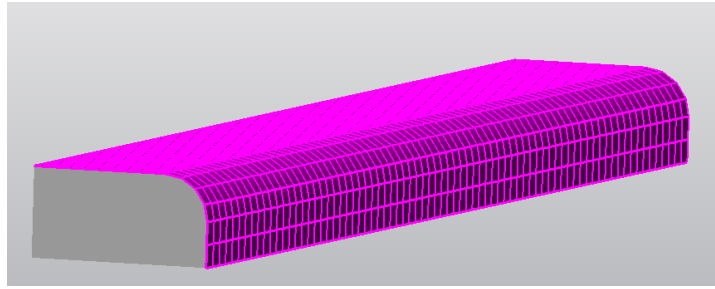
Figure 6-4 CAD model showing the surfaces of the shim with the applied voltage constraints applied.

6.3.4 Transient Heat Analysis

The transient heat analysis was conducted to determine the temperature distribution and heat flow within the tissue. Loads applied for this analysis include convection, and applied nodal temperature, with these loads remaining constant throughout the analysis. Additionally an internal heat generation load was applied to the tissue, with this load being pulsed to replicate the pulsing waveform of the generator. The input for the internal heat generation object was the result from the electrostatic analysis (AutoDesk).

6.3.4.1 Boundary Conditions and Loads

The loads and boundary conditions applied to the transient heat analysis step are more complex than those applied in the electrostatic analysis step. Surfaces that are symmetry planes have a Neumann boundary condition applied (null thermal heat flux), these are the surfaces labelled ABDC and AECG in Figure 6-5. The upper and lower surfaces of the tissue (ABFE and CDHG, Figure 6-5), were constrained as surface convection objects, with the ambient temperature set as 25°C. The remaining two surfaces of the tissue (surfaces BDHF and EFHG, Figure 6-5) were set as controlled temperature objects, with the temperature being set as 22°C, and the stiffness value, similar to the stiffness parameter described for the electrostatic analysis, set high at a value of 10^{10}. Furthermore an initial nodal temperature of 22°C was applied to the model. For the model comparison with Dodde *et al* (2008) the surfaces constrained as controlled temperature objects, were set at a temperature of 31°C, and an initial nodal temperature of 31°C was applied. The

heat was generated within the FEM by modelling the tissue as a heat generation object.
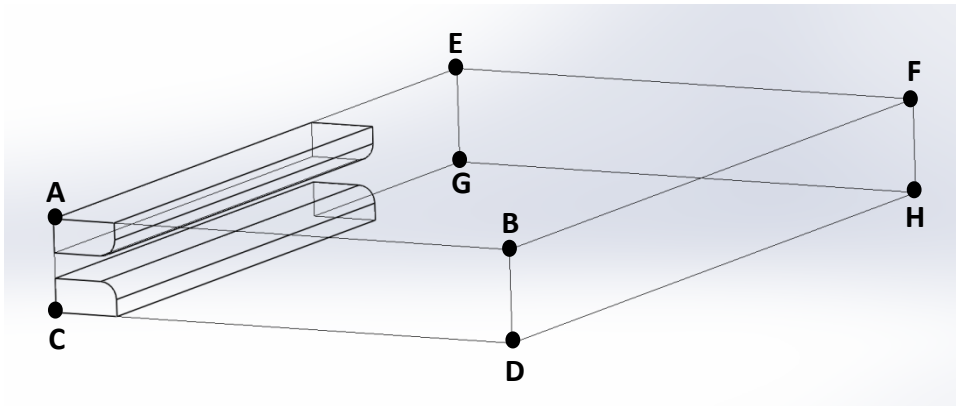
Figure 6-5 Schematic showing the surfaces of the model for the transient heat analysis boundary conditions. Surfaces ABCD and AECG have Neumann boundary conditions applied, surfaces ABFE and CDHG are modeled as surface convection objects and surfaces BDHF and EFHG are controlled temperature surfaces.

The results from the electrostatic analysis were input into the model by defining the tissue as a heat generation object; this resulted in different thermal inputs for the different shim designs. This simulated the heating of the tissue through Joule heating and used the results for electrical current that were output from the electrostatic analysis. The pulsing of the generator waveform was recreated through a load curve, switching the load on using a value of 1, and turning it off using a value of 0, Figure 6-6. Five pulses were defined with a pulse on mode of 0.22s and an off model of 0.53s, parameters defined by Dodde *et al* (2008).
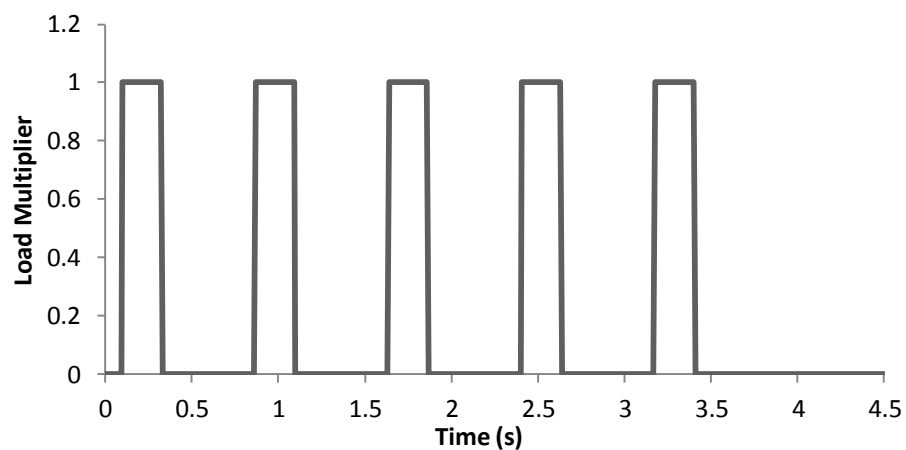
Figure 6-6 Chart showing the load multiplier factor against time for controlling the pulses of the heat generation object to simulate the pulsed input of the generator.

6.3.4.2 Step Parameters

The analysis period for the transient heat analysis was set at a total time of 4.5s, covering the duration of the sealing process and a short period after the sealing was complete. A total of 90 times steps were used for the analysis.

6.3.5 Model Mesh

The model was meshed in AutoDesk Multiphysics Simulation, using the meshing capabilities within the software. The model was meshed as a whole model, with the software differentiating the different parts of the assembly and automatically refining the mesh to focus on corners, curved faces and the borders between the shim and the tissue.

6.3.5.1 Mesh Refinement Analysis

As part of the study a mesh refinement analysis was performed to determine the most suitable mesh to be used for the model. The parameters for the different meshes assessed are displayed in .
Table 6-3.

Table 6-3 Presenting the mesh study details, with the mesh study number relating to Figure 6-7, the percentage mesh referring to the parameter used in AutoDesk Multiphysics Simulation to create the 3D mesh, and the resulting number of elements and nodes.

Mesh Study Number	Percentage Mesh	Number of Elements	Number of Nodes
1	100	7767	5648
2	90	10887	7177
3	80	12662	9601
4	70	23204	15916
5	60	30748	23497
6	50	45832	35050
7	40	94325	70391

The boundary conditions and loading conditions previously described were used for the mesh convergence study. The maximum temperature resulting from each mesh was recorded and compared (Figure 6-7). From mesh study number 3 onwards convergence with the model was achieved, and therefore any of these meshes would be suitable for use for the model. It was chosen to use mesh study number 6 for the analysis, as this mesh showed good convergence, and did not take excessive computational time. Furthermore this mesh was more fine than mesh 3,4, or 5 and therefore was expected to be slightly more accurate.
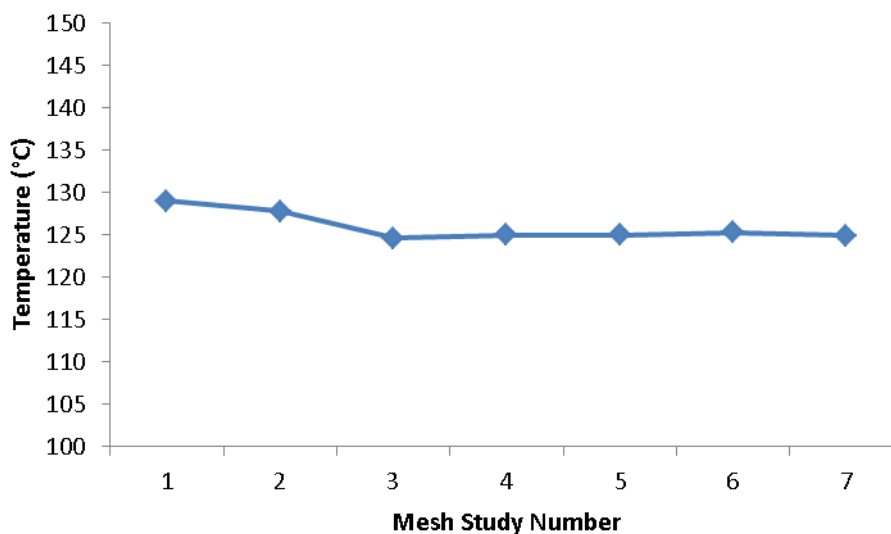
Figure 6-7 Showing the results from the mesh convergence study, with the y axis showing the maximum temperature resulting from each model, and the mesh study number referring to the parameters detailed in .

Table 6-3.

6.4 Results

6.4.1 Validation of FE Model

Results from the replication of the Dodde *et al* (2008) model were compared with data from the Dodde *et al* (2008) study, Figure 6-8. The results used from the Dodde *et al* study were for a constant thermal conductivity, temperature dependent electrical conductivity for a compression independent simulation. The temperatures 1mm and 3mm from the edge of the shims on the outer surface of the tissue were compared; there was a difference of ≈5% at 1mm and ≈4% at 3mm

from the edge of the shims when comparing the FEM data. The differences between the two models can be attributed to a slight difference in the shim geometry between the shims in the models and also by the difference in algorithms used by the different software packages. Although there was a slight difference in the temperature produced by the two models, this difference was deemed to be acceptable due to the data following the same trends with the pulsing at 1mm from the shims, and the smooth line at 3mm, and the similarity between data values.
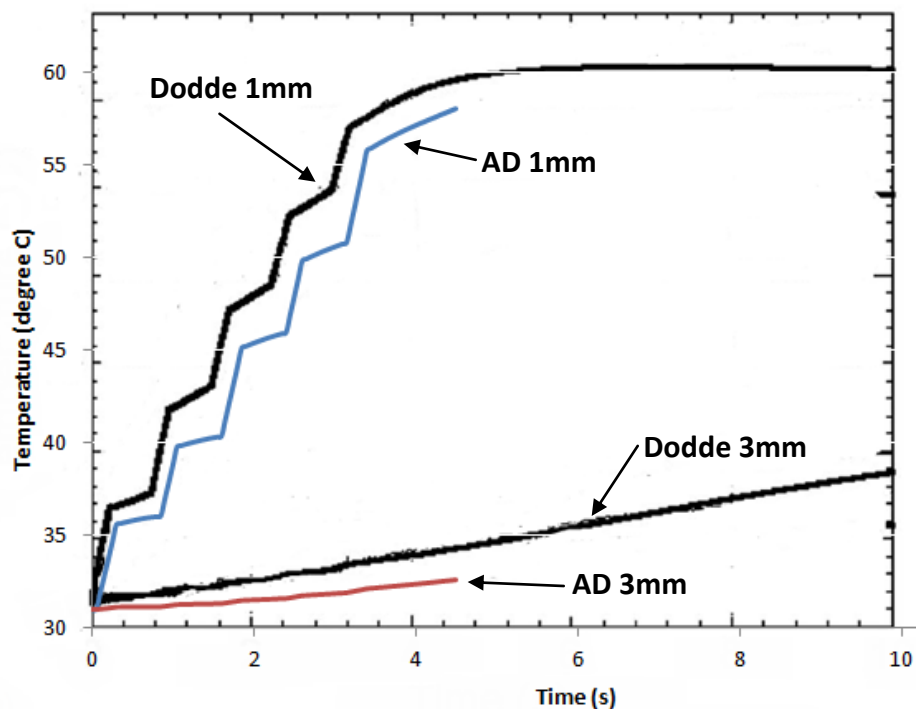
Figure 6-8 Showing the comparison of the Dodde *et al* (2008) FE model results with those replicating the model using AutoDesk Multiphysics Simulation. Lines labeled with the initial **AD** show the results from AutoDesk Multipjhycsi simulation, and those labelled Dodde show the results presented by Dodde *et al* (2008). The distances refer to the distance from the edge of the shim on the outer surface of the tissue.

6.4.2 Comparison of Shim Geometry

6.4.2.1 Alignment of Shims

The temperature at the distances of 1mm and 3mm from the edge of the shim on the outer surface of the tissue were compared for all shim sets where alignment was a consideration. The grooved, narrow grooved, HF grooved, and 45° grooved

shims (Figure 6-9, Figure 6-10, Figure 6-11, and Figure 6-12 respectively) were assessed.
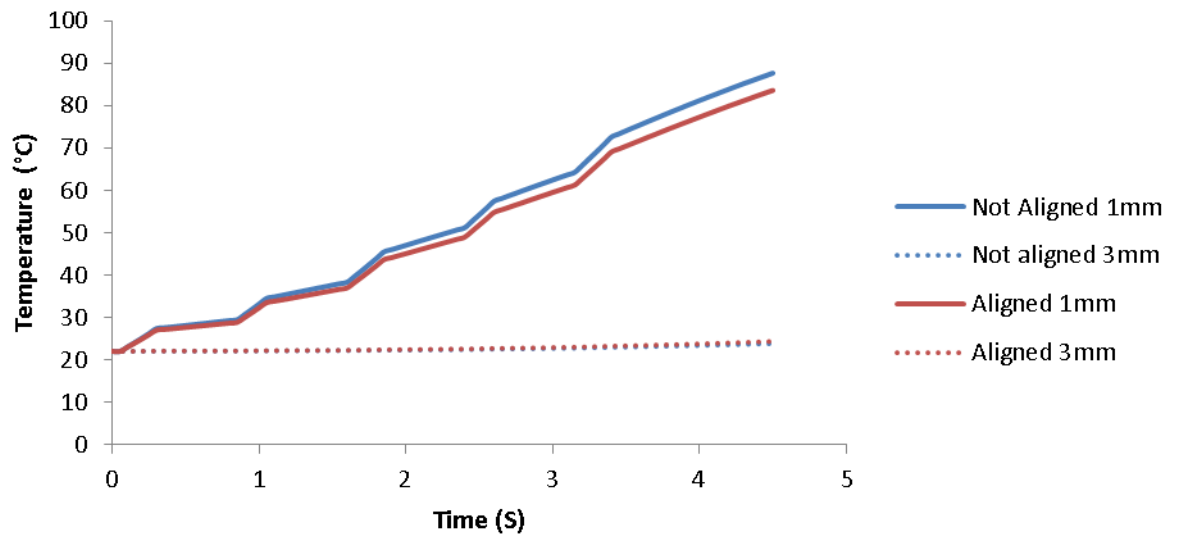
Figure 6-9 Showing the comparison between the grooved (3_GR) shims with the surface features aligned and with the surface features not aligned. Solid lines represent the temperature 1mm from the edge of the shim on the outer surface of the tissue, and the dotted lines represent the temperature 3mm from the edge of the shim on the outer surface of the tissue.
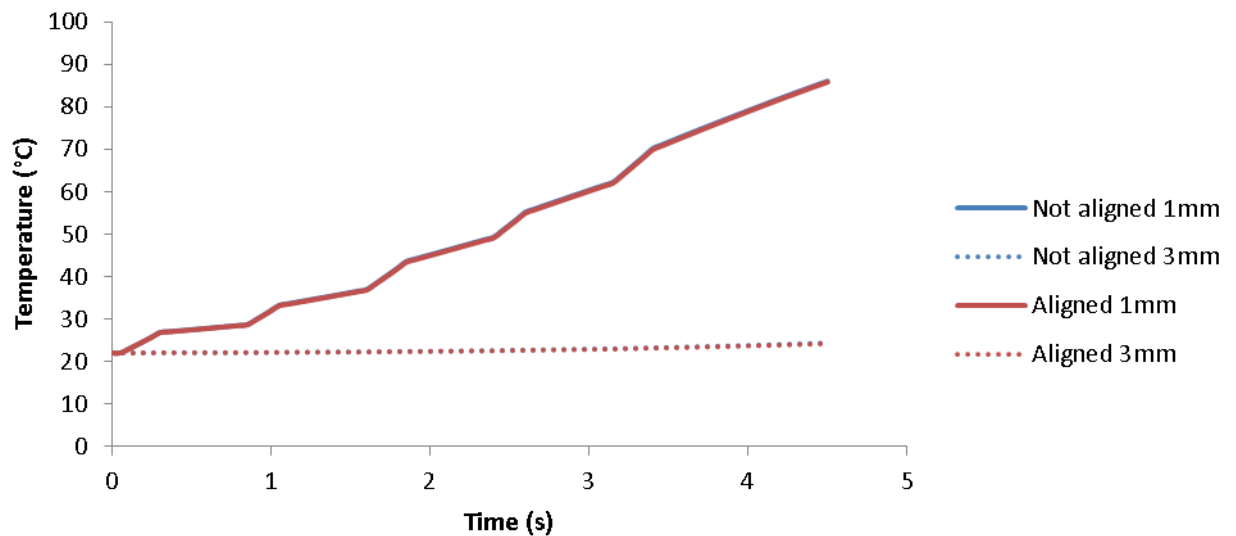
Figure 6-10 Showing the comparison between the narrow grooved (4_NA) shims with the surface features aligned and with the surface features not aligned. Solid lines represent the temperature 1mm from the edge of the shim on the outer surface of the tissue, and the dotted lines represent

the temperature 3mm from the edge of the shim on the outer surface of the tissue. Please note the blue lines are present on the figure, but are very similar in value to the red lines and therefore difficult to view.
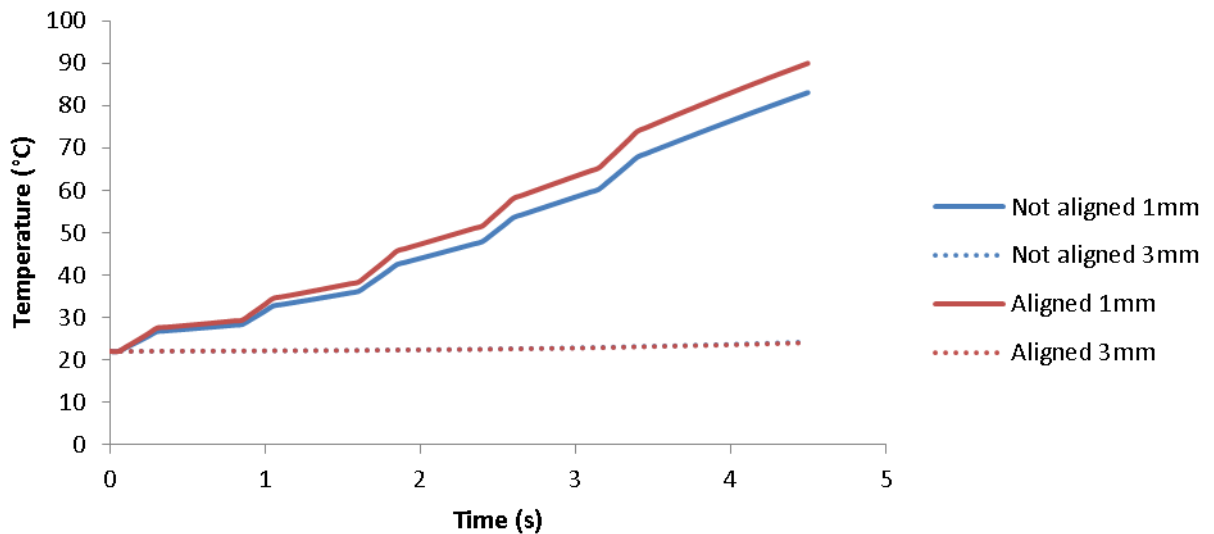
Figure 6-11 Showing the comparison between the HF grooved (5_HF) shims with the surface features aligned and with the surface features not aligned. Solid lines represent the temperature 1mm from the edge of the shim on the outer surface of the tissue, and the dotted lines represent the temperature 3mm from the edge of the shim on the outer surface of the tissue.
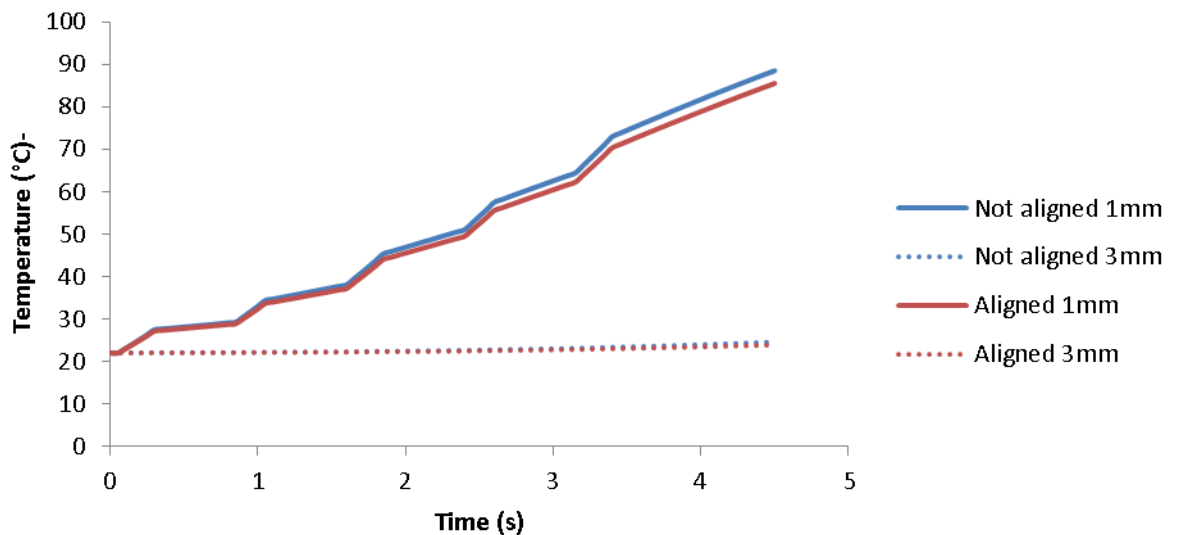
Figure 6-12 Showing the comparison between the 45° grooved (7_45) shims with the surface features aligned and with the surface features not aligned. Solid lines represent the temperature 1mm from the edge of the shim on the outer surface of the tissue, and the dotted lines represent the temperature 3mm from the edge of the shim on the outer surface of the tissue.

In addition to the temperature comparison, the heat distribution of the different shim alignments was considered. Table 6-4 shows the different heat distributions for the shims assessed for both alignment cases considered.

Table 6-4 Showing the comparison of the heat distributions for the different shims with the surface features aligned and the surface features not aligned. Images were taken at time step 10, 0.45s into the analysis.

Model	Surface features not aligned	Surface features aligned	
Grooved **3_GR**			220 / 200.2 / 180.4 / 160.6
Narrow Grooved **4_NA**			140.8 / 121 / 101.2
HF Grooved **5_HF**			81.4 / 61.6 / 41.8
45° Grooved **7_45**			22 / Temp (°C)
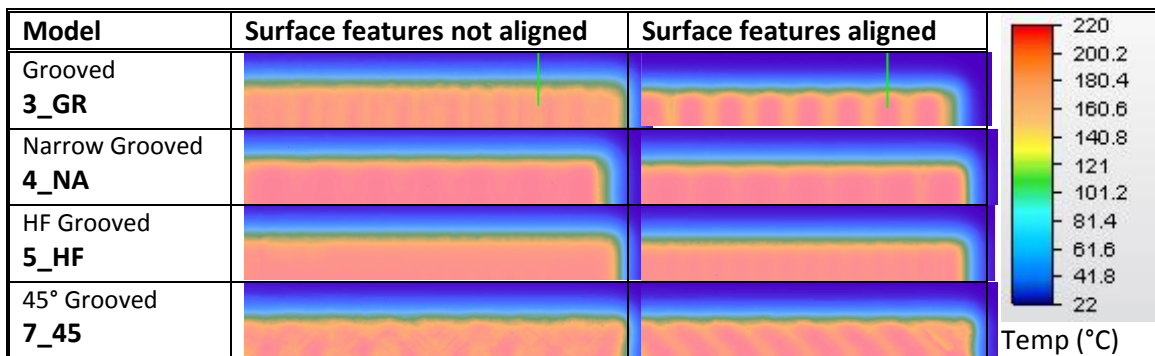
6.4.2.2 Combination Shim

Two different combination shim models were assessed, one with the longitudinal shim set as the active shim, and one with the grooved shim set as the active shim to ensure there were no differences between the models. No differences were found between the two models as expected.

6.4.2.3 Shim Type

When comparing the different shim designs, the models with the surface features aligned were used. The temperature of the tissue at 1mm and 3mm away from the edge of the shims was compared (Figure 6-13 and Figure 6-14 respectively).
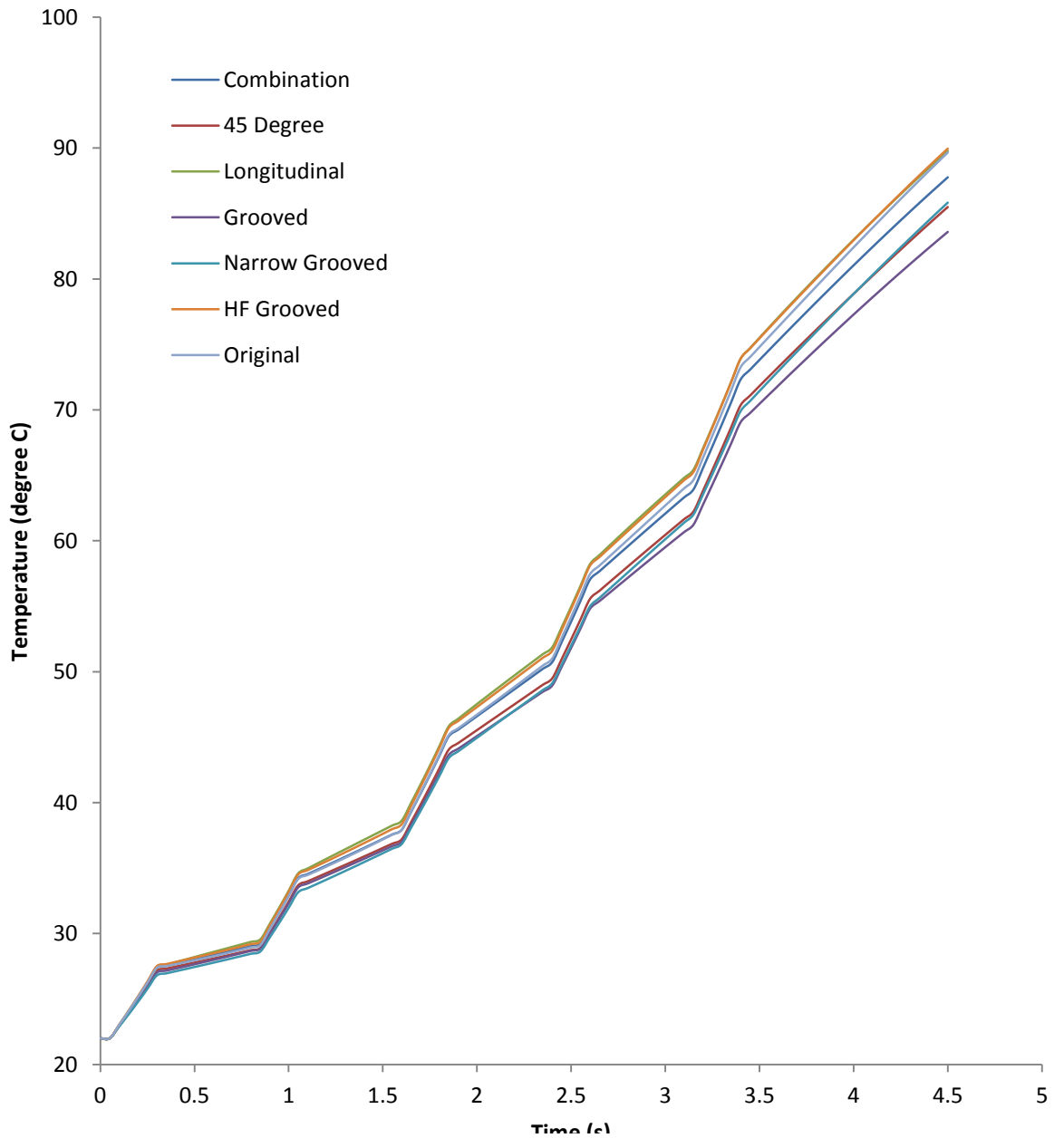
Figure 6-13 Chart showing the temperature for the various shim designs, with the surface features aligned. Temperature was taken 1mm away from the edge of the shims at the surface of the tissue.
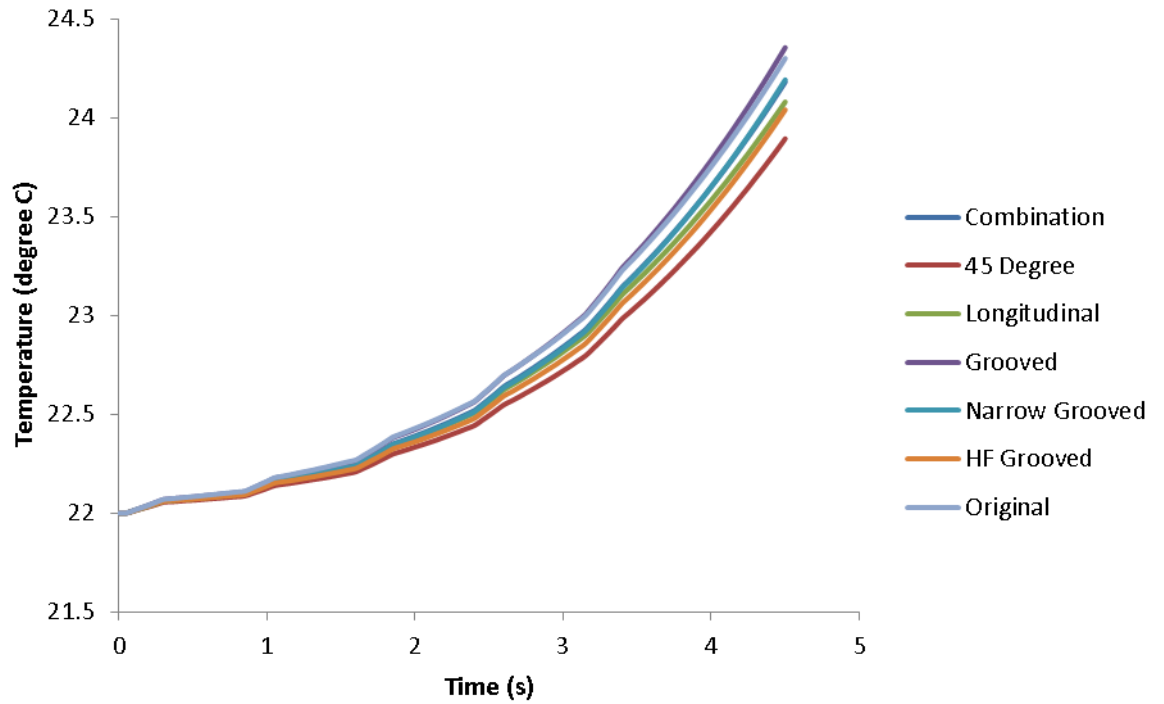
Figure 6-14 Chart showing the temperature for the various shim designs, with the surface features aligned. Temperature was taken 3mm away from the edge of the shims at the surface of the tissue.

Furthermore the maximum temperature at the surface of the shims was compared (Figure 6-15). The point was identified using a maximum temperature point identification feature within AutoDesk Multiphysics Simulation.
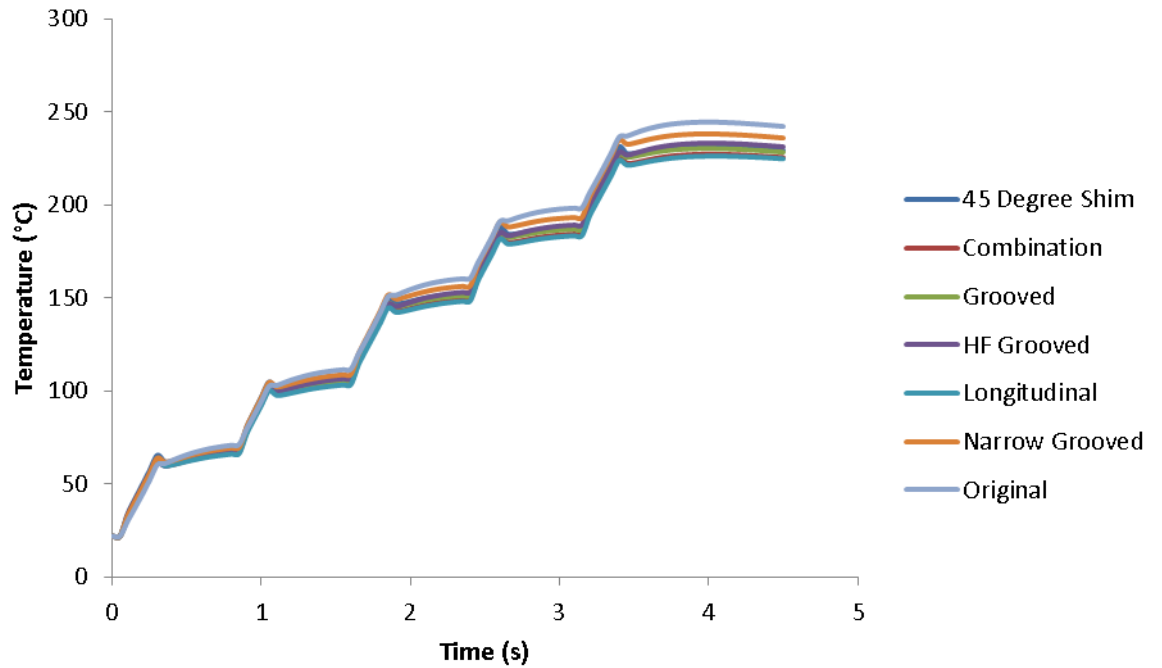
Figure 6-15 Chart showing the temperature of the various shim designs, with the surface features aligned. Temperature was the maximum temperature recorded at the surface of the shims.

In addition the heat distribution pattern for the shims was compared (Table 6-5). Images were taken at an early time step in the analysis, 0.45s to allow for the heat distribution to be presented more clearly. View 1 within Table 6-5 shows the temperature distribution on the surface of the shims; however it is important to note that the heat distribution was the same for the tissue between the two shims as on the shim surface. View 2 within Table 6-5 shows an end view of the heat distribution between the two shims; with the hot areas showing the temperature of the tissue between the two shims.

Table 6-5 Showing the temperature distribution across the surface of the shims for the various shim designs. Two views are presented, view 1 is a plan view of the shims, and view 2 is an end view of the shims.

Model	Time Step 10, 0.45s		
	View 1	View 2	
Original Shim **1_OR**			
Grooved Shim **3_GR**			
Narrow Grooved Shim **4_NA**			
HF Grooved Shim **5_HF**			
Longitudinal Grooved Shim **6_LO**			Temp (°C)
45° Grooved Shim **7_45**			
Combination **8_CC**			

6.5   Discussion

6.5.1   The FE Model

The model presented in this study provided a simplification of the electrosurgical process, and as such applied numerous assumptions. The most significant assumption within this model was the simplification of the tissue model, with tissue properties being modelled not accounting for how the properties change with temperature, tissue compression, and the directionality of the tissue properties (Berjano, 2006). It has previously been demonstrated in the literature that these assumptions can affect the performance of the FEM (Dodde *et al,* 2008), although this is the case these assumptions do not affect the capabilities of the model when comparing multiple shim designs as done in this study. This is because the same assumptions were made within all of the models and therefore allow for direct comparisons between the models.

Whilst the assumptions made in this model create inaccuracies with the simulation the results produced are comparable with other simulations. Data from the study was compared with data from Dodde *et al* (2008) (Figure 6-8), with results from this study being comparable with those of Dodde *et al*, with a variation of ≈5% at 1mm from the shim, and a variation of ≈4% at 3mm from the shim. This difference in temperature could be attributed to a number of factors including the difference in geometry of the shims being tested, and the algorithms used by the different modelling packages. Although the Autodesk Multiphysics simulation software is a less sophisticated compared with the capabilities of COMSOL, it still produced results in line with those of COMSOL, verifying the software as a viable package for modelling electrosurgical procedures.

6.5.2   Comparison of Shim Geometry

The alignment of the shims was shown to have a significant effect on both the temperature of the tissue and the heat distribution. In general when the surface features of the shims were not aligned there appeared to be a more even heat distribution with less distinctive features (Table 6-4). When considering the heat distribution the difference was most noticeable for the 45° shims, when the

grooves were aligned the features from the 45° shim were more obvious, with the heat distribution forming the same pattern as that seen on the surface of the shims. When the surface features were not aligned the heat distribution was more even and the features from the surface of the shims were less distinguishable. Although the 45° shims presented the most noticeable difference in heat distributions when comparing alignments, there was only a small difference in the temperature of the two scenarios (Figure 6-12) throughout the analysis at both 1mm and 3mm from the shim edge. The effect of alignment was minimal with the narrow grooved shims, as seen in Figure 6-10. There was little temperature difference at both 1mm and 3mm from the edge of the shim. No temperature difference was expected at 3mm as little difference was found at this distance between all shim designs (Figure 6-13). The similarity between the two different shim alignments is thought to be due to the small width of the grooves compared with the width of the peaks.

When considering the grooved shims there was a clear difference in performance between the two alignment models; when the surface features of the shim were not aligned a higher tissue temperature was recorded compared with the model where surface features were aligned (Figure 6-9). This difference in performance was due to the difference in heat distributions between the two models. When the grooves were aligned there were areas where there was a larger distance between the shims and as a result the tissue within these gaps remained cooler resulting in a lower overall temperature. However when the grooves were no longer aligned these gaps no longer existed, resulting in a higher overall temperature and the more even heat distribution seen in Table 6-4.

When considering the HF grooved shims there was again a difference in performance for the two models comparing the alignment of the surface features; when the surface features of the shim were not aligned the model predicted in a lower tissue temperature compared with the model where the surface features were aligned (Figure 6-11). This differs from the performance of the grooved shims where the model with the surface features aligned resulted in a lower tissue temperature, with this difference in performance between the two shim designs being attributable to the difference in the width of the grooves. When the surface

features of the HF grooves were aligned the same heat distribution as with the grooved shims was produced. However when the HF grooved surface features were not aligned the heat passed only between the peaks due to the small groove width, creating large cool spots within the tissue, thus explaining the lower tissue temperature compared to the aligned shim. Results suggest that the alignment of the HF grooved shims would have the most significant effect on seal quality compared to the effect of alignment on the other shim designs. When the HF grooves were aligned a higher seal quality would be expected compared to those where the surface features were not aligned.

The results from the FEM demonstrate a significant difference in the performance of the different shim designs, in terms of shim temperature, tissue temperature and heat distribution. In general the addition of surface features to the shim resulted in a lower temperature in both the tissue and the shim (the exception being the HF grooved shims (5_HF)). These results were in line with those presented by Dodde *et al* (2008), who reported a reduction in tissue temperature for grooved shims compared to shims with no surface features.

When considering the heat distribution of the different shim designs Table 6-5 demonstrates a significant variation in the heat distributions of the different shims. In general the heat distribution follows the surface features of the shims, for example the grooved shims (3_GR) had a heat distribution with hotter temperatures at the grooves, and cooler temperatures at the peaks. Similarly both the longitudinal (6_LO) and the 45° (7_45) shims follow the same pattern, but the orientation reflects the orientation of the grooves. Furthermore when considering the two shims with the more narrow grooves (4_NA and 5_HF), a more uniform temperature distribution was achieved, with this more even heat distribution being created due to the narrow width of the grooves.

The results from the FEM were considered alongside the experimental work conducted in Chapter 3. As part of the experimental work it was observed that the surface features of the shims were reproduced on the sealed region of the blood vessel (Figure 6-16). This was the same pattern that the heat distribution of the various shim designs follows (Table 6-5). These results suggest that the 45° shim

resulted in the lowest quality of seal due to the orientation of the grooves and how they affect the ability of the seal to with stand pressure, and is not due to the ability of the shim to distribute heat. This is also true of the longitudinal grooved shims, but the effect of the groove orientation was less severe.
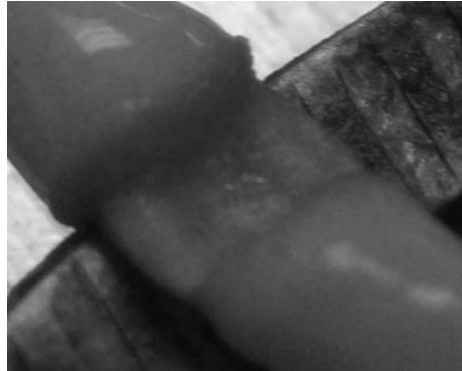
Figure 6-16 Image showing the seal for a grooved shim (3_GR), with the pattern of the shims been reproduced on the sealed region of the blood vessel.

Knowing that the surface features were reproduced on the surface of the sealed vessels, it was important to give further consideration to the difference in the model performance of the 45° shims based on the alignment of the surface features. For the 45° shim with the surface features aligned a weaker seal was produced due to the orientation of the grooves and how the orientation affected the ability of the seal to withstand pressure. However when considering the 45° shims with the surface features not aligned, a very different heat distribution was created, and with this different heat distribution a different pattern would be expected to be produced on the surface of the seal. As such a different quality of seal would be expected to be produced, and based on the results it would be expected for this burst pressure to be significantly higher than that of the aligned shims.

When considering the temperature for the different shims it was important to consider both the maximum temperature at the surface of the shims (Figure 6-15) and the temperature of the tissue simultaneously (Figure 6-13). The narrow grooved shims (4_NA) had a high maximum temperature at the surface of the shim, and a relatively low tissue temperature. This suggests that there was poor heat distribution created by the shims, and this was reflected by the relatively poor seal quality achieved by the shim during the experimental testing. In contrast the

combination shim (8_CC) had a low maximum temperature at the surface of the shims, and a medium tissue temperature, suggesting good heat distribution which was again reflected by the results from the experimental data presented in Chapter 3, with this shim producing a higher burst pressure and a lower seal failure rate.

The original shim had both a high maximum temperature at the surface of the shim, and a high tissue temperature. The high temperature at the surface of the shim is a possible explanation as to why it performed worse that the combination shim and the HF shim in terms of mean burst pressure. The high temperature at the surface of the shim may have resulted in excessive heating of the outer layers of the blood vessel wall, resulting in tissue damage and having a negative effect on the quality of the seal.

The results from the multiphysics analysis suggest that the having a high temperature at the surface of the shim has a negative effect on the quality of the seal, but having a good heat distribution can counteract this negative effect. The ideal shim design would have a low temperature at the surface of the shim, whilst still resulting in good heat distribution and a relatively high tissue temperature. Furthermore those shims that have surface features that are not perpendicular to the length of the blood vessel, produce a weakness within the vessel wall due to the directionality of the surface features of the shims and the pattern of the shims being reproduced on the surface of the seal and affecting the ability of the seal to withstand pressure. Results also suggest that if grooves of higher frequency were used on both the grooved shim and the longitudinal shim an even better seal quality would be achieved for the combination shim, with the HF grooved shims resulting in a higher tissue temperature.

6.6 Conclusion

Results produced by the FE model are in line with those in the literature for a similar FE model (Dodde *et al,* 2008), with the FE model presented in the literature being validated through experimental work. The model was used to compare the alignment of the shims and the performance of the different shims. Results demonstrated that both the heat distribution and the temperature were

significantly affected by the alignment of the shims. The narrow grooved shims were the shims least affected by the alignment of the surface features, with the 45° shims presenting the most drastic difference in heat distributions. Furthermore when the surface features of the shims were not aligned a more even heat distribution was produced.

When considering the different shim designs alongside the experimental data collected in Chapter 3, the surface features were shown to affect the tissue temperature and the heat distribution. The narrow grooved shim performed worse in terms of seal quality, with results from this chapter suggesting this was because of a high temperature at the surface of the shim, and poor heat distribution resulting in a lower tissue temperature. Furthermore the results suggested that the ideal shim would have a low temperature at the surface of the shim and a good heat distribution, characterised by a high tissue temperature 1mm from the edge of the shims, as demonstrated by the combination shim set.

7 General Discussion

The discussion will be split into four main sections. The first section will review all methods used throughout the thesis, the second section will discuss the effect of vessel properties on the seal quality, the third section will discuss the device modifications and the final section will discuss the changes occurring during the vessel sealing process. This chapter brings together all previous chapters of the thesis.

7.1 Methods Review

Throughout the testing conducted as part of this thesis it was necessary to use tissue as no other material would provide a suitable alternative. For this research porcine carotid arteries were used, these were chosen as previous work by Gyrus Medical Ltd had found these arteries were easy to harvest and also performed in a similar manner to the human carotid. It is important to state that no animal was killed specifically for this study, with all tissue provided from a local abattoir. Due to the way in which the tissue was collected there was no control over the animals, for example the age of the pig or its diet. These factors are known to affect the tissue properties and could therefore influence the quality of the seal. Without changing the way in which tissue was collected for the study this was an unavoidable problem. A limitation of the study could be the use of this tissue, and the consideration of only one artery type being used, if different arteries were used the effect of morphology and vessel size could be investigated further (García *et al.*, 2011).

For this study the tissue was skeletonised, removing all connective tissue from the vessel. This allowed for consistency amongst the different samples. In surgery however this would not be the case, with the connective tissue remaining when the vessel is sealed. This difference in procedure will affect the application of current to the blood vessels and will therefore affect the quality of the seal. Additionally during surgery the blood vessel would be in tension, with blood flowing through and the tissue would be at a different temperature. There is therefore a significant

difference between the *in vitro* and *in vivo* testing, and it would be necessary for *in vivo* testing to be conducted to assess the performance of the shims to confirm an improvement in device performance.

A number of methods were used throughout the course of the thesis. The most commonly used method when assessing the performance of a vessel sealing device is to measure the burst pressure of the seal. This is an industry standard test, with the only variable being the pressure used to define a seal failure, with this value varying between 300-360mmHg. Although this method is an industry standard method, a peel testing method would be a viable alternative. This method would involve cutting strips of tissue from the blood vessel wall to a consistent size in terms of width and length, sealing the two sections together and then peeling them apart, using peel strength to compare the seal quality. The major drawback of this method would be the difficulty in relating to the peel strength to a physiological meaningful value. Using such a test would allow for the effect of vessel size to be eliminated from the study and therefore allow for the effect of vessel morphology and vessel thickness to be assessed. Furthermore it would eliminate the variable when comparing the performance of device modifications. Although this method would have many benefits the tissue would have to be prepared in a uniform manner (Katoh *et al.*, 2010), without damaging the tissue, making it a difficult test procedure.

Prior to this study being conducted no study had quantified the force required to remove the vessel from the surface of the shims. Therefore there was no established method and no bench mark for testing. This method provided an excellent insight into the forces required to remove tissue from the surface of the shims, and allowed for an accurate comparison of the modifications to the device. The method was kept consistent throughout the analyses, with the tissue being removed at a slow rate. This does not replicate the conditions during surgery where it may not always be possible for the surgeon to take time to remove the vessel. Additionally due to the viscoelasticity of the tissue, and the strain rate dependence of the material properties, this rate of removal could have a significant effect and is therefore an area that requires further investigation.

This was also the first time that digital image correlation was used to capture the sealing process. The method provided a valuable insight into the vessel sealing process, and provided essential detail in the understanding of the device behaviour and the tissue behaviour. Unfortunately the method did not show any trends when comparing the different shim designs and the different vessel properties. Due to the huge variation in seal quality of the electrosurgical seals this was to be expected, and due to the relatively small sample size used it is not possible to ascertain for certain if trends do or do not exist within the data. Furthermore the use of DIC highlighted a number of problems within the method, with the most significant of these problems being the loss of detail around the area of the shim, making it impossible to quantify the displacement of the tissue within this region. This loss of detail could be reduced by using a high speed DIC system, although because of the production of smoke and the rapid contraction of the tissue resulting in the blurring of the speckle pattern, it is unlikely that any changes to the method would yield a significant improvement.

Although it was not reported in the thesis, a number of experiments were conducted in an attempt to capture the bursting of the electrosurgical seal in an attempt to understand the failure mechanism of the seal. Unfortunately it was not possible to develop a methodology that worked in capturing the seal bursting due to a number of reasons. Again there was large deformation within the vessel wall, which led to a large amount of distortion of the speckle pattern, and as a result of the bursting small amounts of saline was released across the surface of the tissue, destroying the speckle pattern. Furthermore it was not possible to constrain the movement of the vessel during the bursting test, with a large amount of out of plane motion occurring, which resulted in a loss of focus of the speckle pattern. All of these factors meant it was not possible to capture the seal bursting using digital image correlation. Additionally the initial stages of the inflation test were not captured as it was the failing of the seal that was of great interest for this research. Additional work could focus on capturing this initial stage during the inflation tests to provide an insight into how the seal modifies the behaviour of the vessel.

Finite element modelling formed a significant part of this thesis, with two FE models being produced to explore the electrosurgical vessel sealing process in great depth. Both models created had a number of limitations, for example the multiphysics FEM used a very simplistic tissue model, failing to account for the temperature dependent properties of the blood vessel. Although this was the case the model still compared well to a similar study, with only a small difference in results. Although the model had its limitations the results provided a great insight into the performance of the different shim designs and proved to be an invaluable tool in understanding the difference in the seal quality produced by the different shims.

The second model was produced in FEBio, and focused on the mechanical aspects of the vessel compression process, investigating the compressive force and the stresses and strains within the vessel wall. An Ogden model was used to model the behaviour of the vessel wall. This was not the ideal model to use, with one aim of the research to produce a model using the Holzapfel – Gasser model, with this model accounting for the directional properties of the blood vessel by modelling the fibres of the blood vessel (Gasser *et al.*, 2002). Unfortunately due to time constraints and problems with getting the model to converge this aim was not achieved, but this remains a future target for the area of research. Although the Ogden model has its disadvantages, it also had many benefits, such as achieving good convergence, and having data available to allow for the comparison of different vessel morphologies.

Although this model used a simpler material model than desired, it was a huge achievement in getting the blood vessel to achieve complete lumen occlusion, with only two previous FE models achieving this. Furthermore this was the only FE model to model the adhesion of the blood vessel following the electrosurgical seal and the subsequent adhesion. The method for modelling adhesion was simplistic and does require further improvement to account for the change in vessel properties that occur as a result of the electrosurgical seal. The model was validated for vessel compression, through the use of DIC to capture the clamping process. The results from both sets of data showed areas of high strain occurring at the edge of the

vessel wall and lower strain occurring at the centre of the vessel. Furthermore the magnitudes of the strain were comparable between the different data sets. Additionally the results from the FEM were comparable with data from the literature, with the areas of high stress occurring in the same region of the blood vessel (Famaey *et al* 2012).

7.2 Effect of Vessel Properties

The investigation into the effect of vessel properties on the quality of the electrosurgical seal considered a number of properties including the outer diameter of the vessel, the thickness of the vessel wall, and the morphology of the vessel wall. The investigation into these parameters found a number of significant relationships; there was an increase in seal quality with both a reduction in elastin content and reduction in vessel size. Although both of these parameters were shown to affect the quality of the seal, there was also a significant relationship between vessel size and morphology; with a decrease in vessel diameter there was a decrease in elastin content, with this relationship reported in the literature (Carbonell, *et al* 2003, Garcia *et al.*, 2011). This relationship made it difficult to attribute the improvement in seal quality to one factor alone. It should also be noted that the amount of collagen had a limited effect on seal quality.

The relationships presented were already reported within existing literature (Carbonell, *et al* 2003, Garcia *et al.*, 2011, Sindram *et al.*, 2011), but this study expanded upon the existing knowledge by assessing the vessel parameters in unison with one another. Furthermore the study explored how these parameters changed along the length of the porcine carotid artery, finding that with increasing distance from the bifurcation there was a reduction in vessel size and elastin content, but little change in collagen content. These results suggest that surgeons should perform seals in the smaller more muscular regions of the blood vessels where possible. Furthermore although the relationships do exist, there is still a large variation in the quality of the seals that is not accounted for, this highlights the complexity of the vessel sealing process and also demonstrates the need for more extensive research within this area.

To investigate the effect of the various vessel properties on seal quality further, the results from the DIC testing were considered. These results were analysed taking into account the position of the seal and its location from the bifurcation of the vessel. No groupings or trends were seen within the data, with no distinctive characteristics of the different seals based upon the vessel diameter, thickness, or position. The data was normalised based on both vessel diameter and vessel thickness, but these results showed no different trends when compared to data that was not normalised and was therefore omitted from the thesis. Although no trends were noted this was partially due to the small sample size that was considered for the DIC testing and it was difficult to say for certain that no trends were present and a larger data set should be considered for future work.

Although no trends consisted in the data set as a whole one shim set, the narrow grooved shim, presented a trend, with the grouping of seals based on the distance from the bifurcation. The more muscular vessels showed less tissue compression and less reduction in the shim gap during the sealing process when compared to the more elastic vessel. This suggests that the elastic vessel was heated more extensively during the sealing process, potentially damaging the seal, although this was only suggested for the narrow grooved shim. This suggests that trends would exist in the data if a larger data set was considered, but also that the effect of vessel morphology is also dependent on the technology as to how influential this effect would be. This would therefore require a larger data set to be established for all shim sets tested to investigate this hypothesis further.

Furthermore two different vessel morphologies were considered in the FEBio model looking at the mechanical aspects of vessel compression. The results from this analysis showed that there was a significant difference in performance between the elastic and muscular vessel during both the compression and inflation stages. During the compression the muscular vessel was subjected to greater stress throughout the wall, which was to be expected due to the increase in stiffness. The elastic vessel was subjected to higher levels of strain, spread throughout the entire vessel wall. This suggests the effect of the compression was more localised within the more muscular vessel, with the compression of the more elastic vessel causing

a larger amount of deformation through the vessel wall. When considering the differences between the two models during the inflation stage results suggest a difference in the ability of the vessel types to withstand pressure, with a difference in the stress distributions through the sealed region of the vessel. Furthermore the elastic vessel has higher levels of strain at the vessel – seal interface, where there is a large difference in the dimensions in the y direction. This suggests that the elastic vessel fails at lower pressures because of the high strain occurring between the seal and the vessel wall, presenting a weakness within the vessel wall. Ideally the work using this FEM would be expanded further to look at the effect of vessel size to understand the effect of vessel properties further.

7.3   Shim Design

Two different aspects of shim design were considered during the research, with non-stick coating and shim surface features investigated. These factors were chosen for investigation as they were believed to be able to improve the device performance during the sealing process.

7.3.1   Non-Stick Coatings

Five coatings were assessed, in addition to the original shims, and the use of electrolube. The coatings that were chosen were chosen because they were known to be conductive, thus not affecting the conduction of current to the blood vessel significantly, because they were demonstrated to have good non-stick properties and because they were biocompatible. Electrolube is commonly used for electrosurgical procedures to reduce adhesion of the device to the tissue, although results from this study found that the use of electrolube offered no improvement on the level of adhesion of the tissue to the surface of the shims.

The performance of the non-stick coatings were assessed in terms of both seal quality and the level of adhesion. The seal quality was assessed in order to ensure that the coating on the shim did not have a detrimental effect on the quality of the seal, through a change in the conductional properties of the shims. The results for seal quality demonstrated that the DLC coating produced a worse quality of seal when compared with the original shim, with this thought to be due to a

combination of poor conductional properties of the shim and also a higher level of adhesion. Furthermore the passivated shim also had a detrimental effect on the quality of the seal, with this again thought to be due to the higher level of adhesion. Considering the results of the peel test for the different shim, no shim offered an improvement when compared with the existing shim used with the device, suggesting this is the best shim in terms of adhesion.
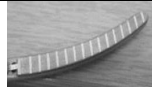
When considering the results from the analysis a number of relationships were discovered. The level of adhesion was related to the thickness of the blood vessel wall, with a thicker blood vessel resulting in a greater level of adhesion. These results appear to occur because thicker blood vessels require more current to be delivered to seal the blood vessel, which leads to more excessive heating on the outer walls of the blood vessel leading to a greater level of adhesion of the tissue to the surface of the shims. Furthermore there is a relationship between the seal quality and the level of adhesion with a higher level of adhesion resulting in a reduction in the quality of the seal. This relationship is to be expected as the seal can be damaged when removing the vessel from the surface of the shims. This result highlights the need to reduce the level of adhesion during the vessel sealing process.

7.3.2   Shim Surface Features

As a result of the literature review it became apparent that one avenue of research that could lead to an improvement in the performance of the device was the surface features of the shims. As a result a number of designs were developed that explored the relationship between different grooves, exploring the effect of varying groove orientations, widths and frequencies. Shims were designed with the coating removed to allow for comparison with one another. This was the main limitation of the design with the shims needing to be reassessed with the coating of the original shims applied; it is thought that with the coating applied there would be a reduction in the level of adhesion for each of the shims and a small improvement in the burst pressure for each shim. This hypothesis was based on the results comparing the original shim to the smooth shim, with the smooth shim presenting higher levels of adhesion and lower burst pressures compared to the original shim.

When testing the different shim designs there was a difference in performance in terms of seal quality, level of adhesion and size of the seal for the different shim designs. The shims with the 45° grooves resulted in the lowest burst pressure of all shims, and the combination shims resulted in the highest burst pressure of all shims. This difference in shim performance was also found for other parameters, such as peel strength and seal size. The difference in seal size of the different shims suggested that the different shim designs caused different levels of tissue contraction, which suggested a difference in heat distributions for the different shim designs. Table 7.1 summarises the findings for the different shim designs for the different investigations conducted throughout this study, including the use of DIC, FEBio and multiphysics modelling.

Table 7-1 Summary of the investigation of the different shim designs, including the main findings from the different test methods used.

Original	Grooved Shim	Narrow Grooved Shim	HF Grooved Shim	Longitudinal Grooved Shim	45° Grooved Shim	Combination Shim
						Combination of Longitudinal and 45° grooved
Chapter 3 Investigation of burst pressures and peel strength						
Mean Burst Pressure (±SD) / mmHg						
585.45 ± 261.77	547.05 ± 266.24	507.00 ± 209.07	606.33 ± 238.74	549.85 ± 253.22	191.05 ± 113.17	764.46 ± 388.331
Seal Failure Rate						
5.0%	14.3%	33.3%	14.3%	25.0%	89.5%	0.0%
Peel Strength (±SD) / Nmm⁻¹						
0.088 ± 0.037	0.096 ± 0.042	0.074 ± 0.039	0.084 ± 0.042	0.164 ± 0.053	0.06 3± 0.038	0.111 ± 0.070
Seal Size (surface area) (±SD) / mm²						
18.35 ± 2.51	16.64 ± 2.99	14.79 ± 3.37	14.89 ± 2.61	14.62 ± 4.78	16.07 ± 3.32	12.80 ± 3.26
•Statistical difference between groups (Kruskal-Wallis, *p*<0.001) •Significant difference found to be due to the poor performance of the 45° grooved shim • A seal failure was defined as a burst pressure < 360mmHg, with this criteria being used to determine the seal failure rate • The combination shim lead to an improvement in seal quality (increase in mean burst pressure and a 0.0% failure rate)						
Chapter 4 Investigation of the sealing process using DIC						
• DIC data provided no explanation as to why the different shim designs performed differently in terms of seal quality						
Chapter 5 Investigation of the sealing process using FEBio						
• Shims with grooves resulted in lower stresses through the vessel wall during the compression stage of the analysis. • The HF grooved shims resulted in a higher mean burst pressure when compared to other shims investigated using FEBio, with this shim design also resulting in the lowest strains during compression. • This suggests a significant reduction in strain during vessel compression results in an improvement in seal quality due to less damage occurring in the vessel wall. • There was little difference between seals during the inflation stage of the analysis for all shim designs assessed using the FEM.					• Not tested within this chapter due to problems importing the shim model	• Not tested within this chapter due to the use of symmetry to create FEM
Chapter 6 Investigation of the sealing process using Multiphysics Modelling						
• High temperature at the surface of the shims and high tissue temperature.	• The grooved and narrow grooved shims had a high temperature at the surface of the shims and a relatively low tissue temperature, suggesting poor heat distribution. • In contrast the HF grooved and the narrow grooved shims had a higher tissue temperature when compared to the temperature of the shims suggesting a good heat distribution. • These findings reflect the burst pressures achieved.				• Relatively low tissue temperature compared to a relatively high shim surface temperature	• Relatively high tissue temperature compared to a relatively low shim surface temperature

The summary of the main findings highlights how the combination shim set resulted in an improvement in seal quality. When considering the analysis from the multiphysics FEM there was a relatively high tissue temperature in comparison to the temperature at the surface of the shims suggesting the design achieved good heat distribution and penetration. Additionally the lower temperature found at the surface of the shims is likely to result in less heating occurring at the outer layers of the blood vessel wall, and therefore reducing the likelihood of thermal damage occurring at these outer layers. Excessive heating of the outer layers of the blood vessels was stated by Sigel (1965) to have a negative effect on the quality of the electrosurgical seal. When comparing this to the temperature of the original shims, there was a high temperature at the surface of the shims, suggesting that a greater amount of heating would occur to the outer layer of the blood vessel wall, and therefore this shim design is more likely to induce thermal damage to the wall of the vessel.

Furthermore the results from the FEBio FEM were considered whilst investigating the performance of the different shim designs. Although the combination shim was not modelled due to the use of symmetry within the model, the results from the analysis demonstrated that the inclusion of grooves within the other shims resulted in less stress throughout the wall of the vessel. Additionally when analysing the HF grooved shims lower strains were found indicating less damage occurring in the vessel wall, resulting in an improvement in device performance. It is therefore thought that the combination shim would also lead to a reduction in stress and strain providing an explanation in the higher seal quality and improvement in device design achieved when using this shim. It can be concluded that the increase in seal quality and the improvement in device performance produced can in part be attributed to less damage occurring at the vessel wall due to a reduction in strain and application force.

The main focus of the study was to improve the seal quality, which was achieved through the combination shim, but an interesting finding whilst investigating the performance of the shim designs was the negative performance of the 45° grooved shims. When considering these shims within the multiphysics FEM the design was

found to have a relatively high temperature at the surface of the shims, compared with a relatively low tissue temperature. This was indicative of poor heat distribution and penetration. This poor heat distribution contributes to the poor performance of the shim when considering the seal quality but does not entirely explain why the shims perform so much worse than the other designs. It should also be taken into consideration that the 45° grooved shims had the lowest peel strength of all designs tested, which whilst it could be considered a positive result, it could also be a further indication of the poor heat distribution with a lack of heating causing a lack of tissue adhesion.

Unfortunately due to problems importing the CAD model into FEBio it was not possible to analyse the 45° grooved shims to investigate the effect of shim design on the stresses through the wall of the vessel during the compression and inflation stage of the analysis. It is thought that this analysis would contribute knowledge and understanding as to why this design performed worse than other shims. The orientation of grooves on the surface of the shims was imprinted onto the seal, and it is therefore probable that the surface features of the shim influenced the structure of the seal and thus the failure mechanism. Analysing the model within the FEBio FEM would allow for this theory to be explored further and for a greater understanding as to the effects of groove orientation to be achieved.

Additionally the different levels of contraction were investigated using DIC, comparing the results for the different shim designs investigated. The results from the DIC testing demonstrated a different level of tissue contraction and jaw displacement for each seal performed. These results indicated that each seal resulted in a different level of contraction, which was indicated by the different sizes of seal produced in Chapter 3 when investigating the burst pressure. However the results from the DIC did not display any grouping based on the different shim designs, with each seal being produced in a unique way. Although no groupings were presented within the DIC data, this could be attributed to the small sample size of seals captured. Therefore to expand upon this work further a larger sample size is required to ascertain for certain if trends exist based on the different shim designs, and if vessel morphology is more influential for different shim designs.

The results from the FEBio FEM demonstrated that with the addition of grooves to the surface of the shims, there was a reduction in stress throughout the vessel wall and a reduction in the compressive force. The addition of the grooves to the shims demonstrates that it would be possible to use the shim design to aid the device in controlling the application force the vessel is subjected too. The application force has been demonstrated within literature to be an important factor in determining seal strength, with Wallwiener et al (2008) finding that too low or too high a compressive pressure would have a detrimental effect on the seal quality. The reduction in stress through the vessel wall suggests that less damage occurs through the wall of the vessel. A reduction in the damage occurring to the vessel during the compressive process is thought to be a contributing factor in the quality of the seal, with the HF grooved shim resulting in the lowest wall strain and the highest mean burst pressure of the shims assessed using FEBio. When considering the multiphysics model for the HF grooved shims, a good heat distribution and penetration was found. These results suggest that HF grooves were more effective than simple grooved shims in improving the device performance and that the combination shim design could be further improved by using higher frequency grooves.

The electrosurgical vessel sealing process is a complex process, with the quality of the resulting seal influenced by a number of factors including; vessel properties, device design and the generator used to supply the required energy. Results from the analysis of the different shim designs demonstrated that the surface features of the shims have a significant effect on the device performance, influencing the seal quality and the level of adhesion. This difference in performance is thought to be due to a combination of factors, including different heat distributions through the tissue and also different stress and strain levels through the vessel wall during compression, with the stress levels being indicative of damage occurring. Shims that lower the level of strain within the vessel wall and have a good heat distribution are the ideal shims, with a good heat distribution being defined by a lower temperature at the shim surface and a higher tissue temperature. It is important to further emphasize that an improvement in device performance was achieved through the

combination shim, with this shim resulting in a 0.0% failure rate, a significant improvement. The results found from the investigation conducted aimed to understand why the different shim designs performed differently, and have provided an explanation as to why they do so. Although this is the case the investigation has also raised numerous questions regarding the sealing process and why such devices perform differently and therefore further work is required to fully understand why the device modifications do affect the performance as they do. Future work is discussed in greater detail in Chapter 9.

7.4 Changes occurring during the vessel sealing process

As part of the research conducted using DIC the changes occurring during the vessel sealing process were considered in terms of displacement and strains. The displacement of the device jaws, and the displacement and strain of the vessel wall were analysed. The displacement of the device jaws showed pulsing of the device jaws which resulted in a change of shim gap and as such a change in the application force. This change in shim gap was thought to occur due to water expansion within the blood vessel wall and also the release of steam. These fluctuations in the device shim gap need to be given serious consideration when designing the device to understand their full effect and whether they have a negative or positive effect on the quality of the seal. The fluctuations in shim gap could be a necessary part of the device design, allowing for the steam to be released in a way that does not cause significant damage to the vessel. If a more rigid design was used this could force the steam to be released from a different point of the seal, causing a weaker seal to be produced. However, having a stiffer, more rigid jaw, would achieve a more consistent application force throughout the sealing process, possibly improving the quality of the seal.

When considering the displacement of the tissue throughout the sealing process, the tissue was pulled towards the jaws of the device, a significant contraction in the y direction. This y contraction was found in all seals, and occurred in pulses in the same way as the pulses of the device jaws. The magnitude of the displacement was different for all seals, indicative that all seals are performed in a slightly different

way, accounting for the variation seen with both the seal quality and the size of the seal. The tissue contracts in pulses due to the pulsing of the waveform delivered by the generator. The generator waveform affects the temperature of the tissue, once the tissue reaches a temperature sufficient to denature the collagen (approximately 70°C) the contraction within the tissue occurs, pulling the tissue towards the jaws of the device.

The strain within the vessel wall during the vessel sealing process was also analysed with the results demonstrating further complexities of the vessel sealing process. There was an initial expansion of the width of the blood vessels in the region close to the device jaws which was present in all seals. This caused the maximum principal strain to be parallel to the edge of the device jaws within the region of the blood vessel wall close to the device jaws. There was a gradual change in the orientation in the maximum principal strain, with the strain gradually becoming aligned to be perpendicular to the device jaws, with the maximum principal strain having the same orientation along the length of the vessel. Unfortunately due to the loss of detail when capturing the sealing process it was not possible to quantify the expansion in the width of the blood vessel and therefore the effect of this on the sealing process cannot be quantified. This is an area that warrants further investigation as this expansion could explain the difference in seal qualities amongst the different seals.

Furthermore the strain and the displacement showed an uneven distribution across the surface of the blood vessel, with around 50% of samples showing an uneven heating effect with contraction occurring at different rates across the width of the vessel. This is thought to be due to the varying thickness of the blood vessel wall, with thinner areas of the wall being heated first and at a faster rate followed by the thicker areas of the vessel wall. This suggests that the seal is performed in an inconsistent manner across the width of the vessel, and demonstrates how challenging it would be to get the device to perform in a consistent manner for all seals. This finding suggests that manufacturers should focus on improving the mean burst pressure and reduce seal failure rates, and not focus on achieving a consistent seal quality.

8 Conclusions

Relationships between vessel parameters and seal quality were investigated and a number of important relationships were found. With an increase in vessel diameter there was a reduction in the seal quality (p<0.0001) and with a reduction in elastin content there was an increase in seal quality (p=0.001). Furthermore there was a significant relationship between the amount of elastin and the size of the vessel; with a reduction in vessel size there was a reduction in elastin content (p<0.0001), making it difficult to attribute an improvement in seal quality to one factor alone. Additionally with increased peel strength there was a reduction in seal quality (p=0.027), highlighting the importance of tissue adhesion to the surface of the shims.

A number of modifications were made to the device, investigating a selection of non-stick coatings and a number of surface features for the shims. None of the non-stick coatings tested reduced the tissue adhesion to the surface of the shims when compared to the existing device. During the testing a significant relationship was highlighted, with vessels with a thicker wall requiring a greater force to remove the vessel from the surface of the shims (p=0.012). When investigating the different surface structures for the shims they were shown to affect the seal quality, level of adhesion and the size of the resultant seal. A number of shim designs had a negative effect on the seal quality, when compared to the original shim design, with groove orientation appearing to be the most influential factor. Two shim designs demonstrated an improvement in the quality of the seal in terms of mean burst pressure, with one of these designs, a combination of a transverse grooved shim and a longitudinal grooved shim, resulting in a 0.0% failure rate in addition to the increased mean burst pressure.

To investigate the effect of shim design and vessel properties further on the sealing process DIC was used to capture the sealing process. Results from this testing found no groupings based on tissue contraction or displacement of the jaws for the shim type or the vessel properties. Although this was the case the results presented some interesting findings, with the shim gap not remaining constant throughout the

sealing process, with fluctuations of up to ≈15%. This fluctuation in shim gap meant that the application force did not remain constant throughout the sealing process. Furthermore when analysing the contraction of the tissue it was shown that the tissue was pulled towards the device throughout the sealing process, with each seal produced having different levels of contraction. The changing in shim gap and the contraction of the tissue occurred in pulses which coincided with the pulses of the generator.

The different shim designs were further analysed using FEBio to model the compression and the adhesion stages of the vessel sealing process and investigate the stresses and strains throughout the vessel wall. Results from this analysis showed that the addition of grooves to the surface of the shim resulted in lower stresses through the vessel wall during compression. Additionally for the HF grooved shims there was a reduction in strain suggesting there would be less damage occurring to the vessel wall. Although there were significant differences during the compression stage of the analysis, there was little difference between the stress and strain of the blood vessel for the different shims during the inflation stage. This suggests the damage occurring during the compression stage was the more influential factor affecting the quality of the seal. Furthermore two different vessel types, predominantly elastic and muscular, were analysed during both the compression and inflation stage, with notable differences between the two models at both stages. The strain and stress distribution of the elastic vessel suggested that the effect of clamping had a greater effect over a larger area of the blood vessel and suggested that the elastic vessel was unable to withstand high pressures during bursting due to high strain occurring between and the seal and the vessel wall.

The different shim designs were also analysed using a multiphysics model to investigate the performance of the designs in terms of thermal and electrical performance. The results from the analysis demonstrated that the surface features of the shim affected the temperature of the sealing process and the heat distribution. The results from the analysis were considered along with the experimental data collected, and from this it was determined that the most effective shim design was found to have a lower temperature at the surface of the

shims, and a higher temperature for the tissue. This was indicative of an improved heat distribution for the different shim, allowing for a greater current penetration and heating effect throughout the wall of the vessel, thus improving seal quality. The combination shim set, which resulted in a 0.0% failure rate, created a lower temperature at the surface of the shims, whilst still creating a great enough temperature throughout the tissue, thus explaining why these shims led to an improvement in seal quality.

The results presented in this thesis demonstrate the complexities of the vessel sealing process and how various factors affect the seal quality. Although the vessel properties cannot be controlled, the device design can be modified to improve the device performance, with surface features of the shims been shown to be an effective way to do so. Furthermore the use of FEM has being demonstrated to be a useful tool in improving understanding surrounding the sealing process and should be used as a tool to aid device design.

9   Future Work

Although a significant amount of research was conducted as part of this thesis there is still a significant amount of work that is required to achieve a greater understanding of the vessel sealing process and the way in which the various parameters affect the seal quality. This chapter details the work that would be conducted to expand upon the existing research and continue to improve the knowledge surrounding the research of electrosurgical vessel sealing. This chapter will be split into three main sections; the first section detailing the future work associated with the experimental testing, the second detailing the future work associated with the FEBio modelling, and the final section detailing the future work associated with the multiphysics model.

9.1   Experimental Testing

As part of the experimental work conducted into the investigation of the adhesion of the tissue to the surface of the device shims, a peel test method was used. This was the first time such a method had been applied to measuring the adhesion of the tissue and as such there are a number of areas that require further investigation, including more specifically, the rate at which the tissue was peeled from the surface of the shims. Due to the viscoelastic and strain rate dependent properties of the blood vessel tissue, the rate at which the blood vessel was peeled from the surface of the shim could significantly affect both the recorded peel strength and also affect the damage that occurs to the seal upon removal.

As part of the research DIC was used to capture the vessel sealing process; this method provided a great deal of information on the changes that occur throughout the sealing process. As such applying the method to capturing the seal bursting would provide valuable information on the way in which the seal fails and also provide further information on the way in which the various parameters such as the shims and the vessel morphology influence the way in which the seal fails. Additionally when considering the use of DIC the sample size for the testing conducted as part of this thesis needs to be increased to ascertain whether there

were any trends amongst the data and any possible explanations as to the difference in performance of the different shims and the effect of vessel properties on the seal quality. Furthermore an increase in sample size would continue to provide valuable information into the changes that occur during the vessel sealing process and improve understanding. Additionally this work could further improve understanding as to why the variation is vessel morphology influences the seal quality.

When considering the testing conducted assessing the performance of the different shim designs, research conducted suggested a number of areas for further investigation. The effect of the alignment of the shim features were investigated using the multiphysics model, but no experimental work was conducted to investigate the effect of alignment on seal quality. Additionally a larger sample size would be preferred when assessing the performance of the different shims when considering the quality of the seal. A larger sample size would allow for the effect of the vessel properties to be considered, for example examining if the vessel morphology was of a greater influence for different shim designs as indicated by the results from the DIC testing.

9.2   FEBio Modelling

To improve the model created in FEBio a more advanced material model should be used, such as the Holzapfel-Gasser material model, which would allow for a fibre reinforced material model, with layer specific material properties. This would allow for a greater level of accuracy within the model. The material model could be advanced further to account for the change in material properties and shrinkage that occur as a result of the denaturing of collagen. This would require experimental work to be conducted to determine the material parameters and characterise the material properties.

Furthermore the work using the model should be expanded upon to fully explore the effect of the vessel properties. More vessel models need to be produced, one using the dimensions and geometry of a small vessel, and a one with the dimensions and geometry of a large blood vessel. Furthermore two versions of each

of the models are required, one as a predominantly elastic vessel, and one as a predominantly muscular vessel.

9.3 Multiphysics Modelling

Future work associated with the multiphysics model should consider a more advanced material model. The material model should account for the temperature dependent properties of the blood vessel, and should also account for the directional properties of the tissue in a similar manner to the fibre reinforced model used for the FEBio model. Additionally, material properties need to be examined, with material properties required specifically for blood vessels and ideally for a range of different vessel morphologies to allow for a greater analysis of the effect of vessel morphology and also to improve the accuracy of the FEM. Furthermore further experimental work should be conducted to establish shim specific properties for the electrical input; this would also provide a more in-depth analysis of the difference in the performance of each of the shim designs.

9.4 Improving Seal Quality

Furthermore future work should continue to explore various parameters that would result in an improvement in the quality of an electrosurgical seal. This could include investigating the ideal shim gap and application force to understand fully their effects on seal quality. In addition the generator waveform could be further investigated to explore the effect of temperature and the pulsating of the waveform. In addition a greater number of shim surface structures should be assessed in an attempt to continue to improve the quality of the seal and reduce the variation in the seal quality. This should include looking at designs that use surface features other than grooves including investigating the effect of dimples or bumps on the surface of the shims in a variety of shapes, orientations and combinations. Additionally the combination shim set should be assessed using grooves of a higher frequency as results within this study suggest this will further improve the performance of the device.

10 References

http://privatewww.essex.ac.uk/~scholp/kw_posthoc.htm [Online]. University of Essex. [Accessed March 2012].

http://www.eureca.de/pdf/optics/schneider/Schneider.pdf [Online]. [Accessed 18th September 2013].

http://www.me.berkeley.edu/~lwlin/me128/FEMNotes.pdf [Online]. Berkeley, University of California. [Accessed 5 December 2013].

http://www.valleylab.com/education/poes/poes_05.html [Online]. [Accessed July 2012].

ASME, ENGINEERS, A. S. O. M., CLASSIFICATION, A. S. O. M. E. S. C. B., QUALITIES, D. O. S. & INSTITUTE, A. N. S. 2010. *Surface Texture: Surface Roughness, Waviness and Lay*, American Society of Mechanical Engineers.

AUTODESK.
http://wikihelp.autodesk.com/Simulation_Mechanical/enu/2013/Help/0031 -Autodesk31/0193-Analysis193/0196-Multiphy196 [Online]. [Accessed February 2013].

Avril, S., Badel, P. and Duprey, A. 2010. Anisotropic and hyperelastic identification of< i> in vitro</i> human arteries from full-field optical measurements. *Journal of Biomechanics,* 43, 2978-2985.

Avril, S., Schneider, F., Boissier, C. and Li, Z.-Y. 2011. In vivo velocity vector imaging and time-resolved strain rate measurements in the wall of blood vessels using MRI. *Journal of Biomechanics,* 44, 979-983.

Badel, P., Genovese, K. and Avril, S. 2012. 3D Residual Stress Field in Arteries: Novel Inverse Method Based on Optical Full-field Measurements. *Strain,* 48, 528-538.

Badel , P., Pierre-Yves R, C. and Avril, S. 2013. Finite Element simulation of buckling-induced vein tortuosity and influence of the wall constitutive properties. *Journal of the Mechanical Behavior of Biomedical Materials*.

Barauskas, R., Gulbinas, A., Vanagas, T. and Barauskas, G. 2008. Finite element modeling of cooled-tip probe radiofrequency ablation processes in liver tissue. *Computers in Biology and Medicine,* 38, 694-708.

Barton, J. 2012. Experimental Mechanics. Southampton University

Becker, A. A. 2004. *An Introductory Guide to Finite Element Analysis*, Professional Engineering Publishing.

Beddoes, E. 2012. Biocompatible Coatings for Electrosurgical Devices. Cardiff: Cardiff University.

Berjano, E. 2006. Theoretical modeling for radiofrequency ablation: state-of-the-art and challenges for the future. *BioMedical Engineering OnLine,* 5, 24.

Berk, K. N., and Carey, P., 2010. *Data Analysis wit Microsoft Excel*, Brooks/ Cole.

Calvo, B., Peña, E., Martinez, M. A., and Doblaré, M. 2007. An uncoupled directional damage model for fibred biological soft tissues. Formulation and computational aspects. *International Journal for Numerical Methods in Engineering*, 69, 2036-2057

Carbonell, A., M,. Joels, C., S., Kercher, K., W,. Matthews, B., D,. Sing, R., F,. and Heiniford, B., T., 2003. A Comparison of Laparoscopic Bipolar Vessel Sealing Devices in the Hemostasis of Small-, Medium-, and Large-Sized Arteries. *Journal of Laparoendoscopic and Advanced Surgical Techniques,* 13, 4.

Chen, H., Navia, J. & Kassab, G. 2009. A Simulation of Vessel–Clamp Interaction: Transient Closure Dynamics. *Annals of Biomedical Engineering,* 37, 1772-1780.

Chuong, C. J. and Fung, Y. C. 1986. On Residual Stresses in Arteries. *Journal of Biomechanical Engineering,* 108, 189-192.

Danpinid, A., Luo, J., Vappou, J., Terdtoon, P. and Konofagou, E. E. 2010. In vivo characterization of the aortic wall stress–strain relationship. *Ultrasonics,* 50, 654-665.

Davis, J. R. and Committee, A. I. H. 2000. *Nickel, Cobalt, and Their Alloys*, ASM International.

Debroy, D. A. N. *http://rsbweb.nih.gov/ij/docs/examples/stained-sections/index.html* [Online]. [Accessed March 2011].

Dilley, A. V., Friend, M.-A. G. and Morris, D. L. 1995. An experimental study of optimal parameters for bipolar electrocoagulation. *Gastrointestinal Endoscopy,* 42, 27-30.

Dodde, R. E., Miller, S. F., Geiger, J. D. and Shih, A. J. 2008. Thermal-Electric Finite Element Analysis and Experimental Validation of Bipolar Electrosurgical Cautery. *Journal of Manufacturing Science and Engineering,* 130, 021015.

Duck, F. A. 1990. *Physical properties of tissue: a comprehensive reference book*, Academic Press.

Evans, S. L. and Holt, C. A. 2009. Measuring the mechanical properties of human skin in vivo using digital image correlation and finite element modelling. *The Journal of Strain Analysis for Engineering Design,* 44, 337-345.

FamaeyY, N., Sommer, G., Vander Sloten, J. and Holzapfel, G. A. 2012. Arterial clamping: Finite element simulation and in vivo validation. *Journal of the Mechanical Behavior of Biomedical Materials,* 12, 107-118.

Famaey, N., Vander Sloten, J. and Kuhl, E. 2013. A three-constituent damage model for arterial clamping in computer-assisted surgery. *Biomechanics and Modeling in Mechanobiology,* 12, 123-136.

Famaey, N., Verbeken, E., Vinckier, S., Willaert, B., Herijgers, P. and Vander Sloten, J. 2010. In vivo soft tissue damage assessment for applications in surgery. *Medical Engineering & Physics,* 32, 437-443.

Farrugia, M., Mcgurgan, P., Mcmillan, L. and O'Donovan, P. 2001. Recent advances in electrosurgery--VERSAPOINT® technology. *Reviews in Gynaecological Practice,* 1, 12-17.

Foschi, D., Cellerino, P., Corsi, F., Taidelli, T., Morandi, E., Rizzi, A. and Trabucchi, E. 2002. The mechanisms of blood vessel closure in humans by the application of ultrasonic energy. *Surgical Endoscopy,* 16, 814-819.

Fung, Y. C. 1983. *What principle governs the stress distribution in living organisms? In: Fung, Y.C., Fukada, E., Wang, J. J. (Eds.), Biomechanics in China, Japan, and USA.,* Beijing, Science Press.

García, A., Peña, E., Laborda, A., Lostalé, F., De Gregorio, M. A., Doblaré, M. and Martínez, M. A. 2011. Experimental study and constitutive modelling of the passive mechanical properties of the porcine carotid artery and its relation to histological analysis: Implications in animal cardiovascular device trials. *Medical Engineering & Physics,* 33, 665-676

Gasser, T. C., Schulze-Bauer, C. A. J. & Holzapfel, G. A. 2002. A Three-dimensional Finite Element Model for Arterial Clamping. *Journal of Biomechanical Engineering,* 124, 355-363.

Genovese, K. 2009. A video-optical system for time-resolved whole-body measurement on vascular segments. *Optics and Lasers in Engineering,* 47, 995-1008.

Ghosh, P. 2008. *Adhesives and Coating Technology,* New Delhi, Tata-McGraw-Hill Publishing

Groves, R. 2012. *Quantifying the mechanical properties of skin in vivo and ex vivo to optimise microneedle device design.* Cardiff University

Gunasekara - Dimunge, A. 2011. Biocompatible Coatings for Electrosurgical Devices. Cardiff: Cardiff University

Gyrus, M. *http://www.gyrusmedical.de/company/produkte/6.html?lang=en* [Online]. [Accessed 17 June 2012].

Hamam, R., Hild, F. and Roux, S. 2007. Stress Intensity Factor Gauging by Digital Image Correlation: Application in Cyclic Fatigue. *Strain,* 43, 181-192.

Harewood, F. and Mchugh, P. 2007. Comparison of the implicit and explicit finite element methods using crystal plasticity. *Computational Materials Science,* 39, 481-494.

Harold, K. L., Pollinger, H., Matthews, B. D., Kercher, K. W., Sing, R. F. and Heniford, B. T. 2003. Comparison of ultrasonic energy, bipolar thermal energy, and vascular clips for the hemostasis of small-, medium-, and large-sized arteries. *Surgical Endoscopy,* 17, 1228-1230.

Harrison, J. D. and Morris, D. L. 1991. Does bipolar electrocoagulation time affect vessel weld strength? *Gut,* 32, 188-190.

Hayashi, K. and Markel, M. D. 2001. Thermal Capsulorrhaphy Treatment of Shoulder Instability: Basic Science. *Clinical Orthopaedics and Related Research,* 390, 59-72.

Holmberg, K. & Matthews, A. 1994. *Coatings Tribology: Properties, Techniques and Applications in Surface Engineering*, Elsevier Science.

Holzapfel, G., Gasser, T. and Ogden, R. 2000. A New Constitutive Framework for Arterial Wall Mechanics and a Comparative Study of Material Models. *Journal of Elasticity,* 61, 1-48.

Holzapfel, G. A. 2000. *Nonlinear Solid Mechanics: A continuum approach for engineering* Wiley.

Holzapfel, G. A. (ed.) 2001. *Biomechanics of Soft Tissue,* Boston Academic Press.

Holzapfel, G. A., Gasser, T. C. and Ogden, R. W. 2004. Comparison of a multi-layer structural model for arterial walls with a fung-type model, and issues of material stability. *Journal of Biomechanical Engineering,* 126, 264-275.

Holzapfel, G. A., Gasser, T. C. and Stadler, M. 2002. A structural model for the viscoelastic behavior of arterial walls: Continuum formulation and finite element analysis. *European Journal of Mechanics - A/Solids,* 21, 441-463.

Jain, A. and Goodison, K. E. 2011. Thermal microdevices for biological and biomedical applications. *Journal of Thermal Biology,* 36, 209-218.

Kato, K., Reich, M., Bühler, K. and Schindler, A. E. 1998. A computer based, temperature controlled bipolar electrocoagulation system: II. optimal temperature and coagulation time. *European Journal of Obstetrics & Gynecology and Reproductive Biology,* 78, 103-107.

Katoh, A., Masuzawa, T., Ozeki, K., Kishida, A., Kimura, T. and Higami, T. 2010. Development of tissue adhesion method using integrated low-level energies. *Medical Engineering & Physics,* 32, 304-311.

Kim, J.-H., Avril, S., Duprey, A. and Favre, J.-P. 2012. Experimental characterization of rupture in human aortic aneurysms using a full-field measurement technique. *Biomechanics and Modeling in Mechanobiology,* 11, 841-853.

Kim, J.-H., Badel, P., Duprey, A., Favre, J.-P. and Avril, S. 2011. Characterisation of failure in human aortic tissue using digital image correlation. *Computer Methods in Biomechanics and Biomedical Engineering,* 14, 73-74.

Kim, J. and Baek, S. 2011. Circumferential variations of mechanical behavior of the porcine thoracic aorta during the inflation test. *Journal of Biomechanics,* 44, 1941-1947.

Klingler, C. H., Remzi, M., Marberger, M. and Janetschek, G. 2006. Haemostasis in Laparoscopy. *European Urology,* 50, 948-957.

Laine, L. 1991. Determination of the optimal technique for bipolar electrocoagulation treatment. An experimental evaluation of the BICAP and Gold probes. *Gastroenterology,* 100, 107-112.

Laine, L. A., Bakos, G. J., Vakharia, O. J., Cunningham, C., ThE, N. D. G. and Long, G. L. 2007. Optimizing Bipolar Electrocoagulation (BPEC) for Endoscopic Hemostasis: Assessment of Factors Influencing Energy Delivery and Coagulation Depth. *Gastrointestinal Endoscopy,* 65, AB122-AB122.

Lally, C., Dolan, F. and Prendergast, P. J. 2005. Cardiovascular stent design and vessel stresses: a finite element analysis. *Journal of Biomechanics,* 38, 1574-1581.

Lee, W. J., Chen, T. C., Lai, I. R., Wang, W. and Huang, M. T. 2003. Randomized clinical trial of Ligasure™ versus conventional surgery for extended gastric cancer resection. *British journal of surgery,* 90, 1493-1496.

Le Gall, M. (2013). Experimentation of different shim's geometries and their modelling for a forceps used in electrosurgery Universite de Franche-Comte.

Levy, B. and Emery, L. 2003. Randomized trial of suture versus electrosurgical bipolar vessel sealing in vaginal hysterectomy. *Obstetrics & Gynecology,* 102, 147-151.

Li, E. B., Tieu, A. K. and Yuen, W. Y. D. 2003. Application of digital image correlation technique to dynamic measurement of the velocity field in the deformation zone in cold rolling. *Optics and Lasers in Engineering,* 39, 479-488.

Maas, S. A., Ateshian, G. A., Weiss, J. A. and Ellis, B. J. 2012. FEBio: Finite Elements for Biomechanics. *Journal of Biomechanical Engineering,* 134, 011005-011005.

Maas, S. A., Rawlins, D, Weiss, J, and Ateshian, G. 2013. FEBio 1.7 Users Manual

Maller, R. R. 1998. Passivation of stainless steel. *Trends in Food Science & Technology,* 9, 28-32.

Massarweh, N. N., Cosgriff, N. and Slakey, D. P. 2006. Electrosurgery: History, Principles, and Current and Future Uses. *Journal of the American College of Surgeons,* 202, 520-530.

Mactra Labs, I. *http://www.mectralabs.com/* [Online]. [Accessed 20th August 2013].

Milson, J., Trencheva, K., Monette, S., Pavoor, R., Shukla, P., Ma, J. and Sonoda, T. 2012. Evaluation of the safety, efficacy, and versatility of a new surgical energy device (THUNDERBEAT) in comparison with Harmonic ACE, LigaSure V, and EnSeal devices in a porcine model. *Journal of Laparoendoscopic & Advanced Surgical Techniques,* 22, 378-386.

Munro, M. G. (2012). Fundamentals of electrosurgery Part I: Principles of radiofrequency energy for surgery. The SAGES Manual on the Fundamental Use of Surgical Energy (FUSE), Springer**:** 15-59.

Novitsky, Y. W., Rosen, M. J., Harrell, A. G., Sing, R. F., Kercher, K. W. and Heniford, B. T. 2005. Evaluation of the Efficacy of the Electrosurgical Bipolar Vessel Sealer (LigaSure) Devices in Sealing Lymphatic Vessels. *Surgical Innovation,* 12, 155-160.

Ogden, R. W. 1972. Large Deformation Isotropic Elasticity - On the Correlation of Theory and Experiment for Incompressible Rubberlike Solids. *Proceedings of the Royal Society of London. A. Mathematical and Physical Sciences,* 326, 565-584.

Perktold, K. and RappitschAPPITSCH, G. 1995. Computer simulation of local blood flow and vessel mechanics in a compliant carotid artery bifurcation model. *Journal of Biomechanics,* 28, 845-856.

Persson, C., Evans, S., Marsh, R., Summers, J. and Hall, R. 2010. Poisson's Ratio and Strain Rate Dependency of the Constitutive Behavior of Spinal Dura Mater. *Annals of Biomedical Engineering,* 38, 975-983.

Petrakis, I. E., Kogerakis, N. E., Lasithiotakis, K. G., Vrachassotakis, N. and Chalkiadakis, G. E. 2004. LigaSure versus clamp-and-tie thyroidectomy for benign nodular disease. *Head & neck,* 26, 903-909.

Pons, Y., Gauthier, J., Ukkola-Pons, E., Clément, P., Roguet, E., Poncet, J.-L. and Conessa, C. 2009. Comparison of LigaSure vessel sealing system, harmonic scalpel, and conventional hemostasis in total thyroidectomy. *Otolaryngology - Head and Neck Surgery,* 141, 496-501.

Presthus, J. B., Brooks, P. G. and Kirchhof, N. 2003. Vessel sealing using a pulsed bipolar system and open forceps. *J Am Assoc Gynecol Laparosc,* 10, 528-33.

Rachev, A. and Greenwald, S. E. 2003. Residual strains in conduit arteries. *Journal of Biomechanics,* 36, 661-670.

Richards, R. 2010. Investigation into the factors affecting the quality of blood vessel seals produced using radio-frequency energy. Cardiff University.

Richter, S., Kollmar, O., Neunhoeffer, E., Schilling, M. K., Menger, M. D. and Pistorius, G. 2006a. Differential response of arteries and veins to bipolar vessel sealing: Evaluation of a novel reusable device. *Journal of Laparoendoscopic & Advanced Surgical Techniques,* 16, 149-155.

Richter, S., Kollmar, O., Schilling, M. K., Pistorius, G. A. and Menger, M. D. 2006b. Efficacy and quality of vessel sealing - Comparison of a reusable with a disposable device and effects of clamp surface geometry and structure. *Surgical Endoscopy and Other Interventional Techniques,* 20, 890-894.

Romo, A., Avril, S., Badel, P., Molimard, J., Duprey, A. and Favre, J. 2012. Mechanical Characterization of the Thoracic Ascending Aorta. *IRCOBI.* Dublin, Ireland.

Sha, D., Connolly, R., Schwaitzberg, S. and Levine, A. 2001. The development of non-sticking, passively cooled electrosurgical instruments. *In:* Bioengineering Conference, 2001. Proceedings of the IEEE 27th Annual Northeast, 2001. 11-12.

Shadwick, R. 1999. Mechanical Design in Arteries. *The Journal of Experimental Biology,* 202, 3305-3313.

Sigel, B. and Acevedo, F. J. 1963. Electrocoaptive union of blood vessels: A preliminary experimental study. *Journal of Surgical Research,* 3, 90-96.

Sigel, B. D., and Marvin, R. 1965. The Mechanism of Blood Vessel Closure By High Frequency Electrocoagulation *Surgical Gynecology and Obstetrics,* 8, 9.

Simon, B. R., Kaufmann, M. V., Mcafee, M. A. and Baldwin, A. L. 1993. Finite element models for arterial wall mechanics. *Journal of Biomechanical Engineering,* 115, 489-496.

Sindram, D., Martin, K., Meadows, J., Prabhu, A., Heath, J., Mckillop, I. and Iannitti, D. 2011. Collagen–elastin ratio predicts burst pressure of arterial seals created using a bipolar vessel sealing device in a porcine model. *Surgical Endoscopy*, 1-9.

Sutton, M. A., Ke, X., Lessner, S. M., Goldbach, M., Yost, M., Zhao, F. and Schreier, H. W. 2008. Strain field measurements on mouse carotid arteries using microscopic three-dimensional digital image correlation. *Journal of Biomedical Materials Research Part A,* 84A, 178-190.

Sutton, M. A., Orteu, J. J. and Schreier, H. W. 2009. *Image Correlation for Shape, Motion and Deformation Measurements: Basic Concepts,Theory and Applications*, Springer.

Taylor, C., Hughes, T. R. and Zarins, C. 1998. Finite Element Modeling of Three-Dimensional Pulsatile Flow in the Abdominal Aorta: Relevance to Atherosclerosis. *Annals of Biomedical Engineering,* 26, 975-987.

TECVAC. *http://www.wallworkht.co.uk/content/cambridge/* [Online]. [Accessed 20th August 2013].

Tian, L., Lammers, S. R., Kao, P. H., Reusser, M., Stenmark, K. R., Hunter, K. S., Qi, H. J. and Shandas, R. 2011. Linked opening angle and histological and mechanical aspects of the proximal pulmonary arteries of healthy and pulmonary hypertensive rats and calves. *American Journal of Physiology - Heart and Circulatory Physiology,* 301, H1810-H1818.

Treloar, L. R. G. 1943. The elasticity of a network of long-chain molecules-II. *Transactions of the Faraday Society,* 39, 241-246.

Tungjitkusolmun, S., Eung J, E, W., Cao, H., Jang-Zern, T., Vorperian, V. R. and Webster, J. G. 2000. Finite element analyses of uniform current density electrodes for radio-frequency cardiac ablation. *Biomedical Engineering, IEEE Transactions on,* 47, 32-40.

Van Kesteren, P. 2005. New haemostatic technologies; has conventional ligation become obsolete? *International Congress Series,* 1279, 189-191.

Vivien, L. (2013). Influence of electrode geometry upon the quality of electrosurgical seals, Universite de Franche-Comte.

Wallwiener, C. W., Rajab, T. K., Krämer, B., Isaacson, K. B., Brucker, S. and Wallwiener, M. 2010. Quantifying Electrosurgery-Induced Thermal Effects and Damage to Human Tissue: An Exploratory Study with the Fallopian Tube as a Novel In-Vivo In-Situ Model. *Journal of Minimally Invasive Gynecology,* 17, 70-77.

Wallwiener, C. W., Rajab, T. K., Zubke, W., Isaacson, K. B., Enderle, M., Schäller, D. and Wallwiener, M. 2008. Thermal Conduction, Compression, and Electrical Current-An Evaluation of Major Parameters of Electrosurgical Vessel Sealing in a Porcine In Vitro Model. *Journal of Minimally Invasive Gynecology,* 15, 605-610.

Weiss, J. A., Maker, B. N. and Govindjee, S. 1996. Finite element implementation of incompressible, transversely isotropic hyperelasticity. *Computer Methods in Applied Mechanics and Engineering,* 135, 107-128.

Winter, H., Holmer, C., Buhr, H.-J., Lindner, G., Lauster, R., Kraft, M. and Ritz, J.-P. 2010. Pilot study of bipolar radiofrequency-induced anastomotic thermofusion–exploration of therapy parameters ex vivo. *International Journal of Colorectal Disease,* 25, 129-133.

Worden, K., Holford, K. M., Pullin, R., Evans, S., Hensman, J. J. and Eaton, M. 2010. Validation of acoustic emission (AE) crack detection in aerospace grade steel using digital image correlation. *Applied Mechanics and Materials,* 24, 221-226.

Wright, N. T. and Humphry, J. D. 2003. Denaturation of Collagen via Heating: An Irreversible Rate Process. *Annual Review of Biomedical Engineering,* 4, 109-128.

WS2 COATINGS, L. *http://www.ws2.co.uk/* [Online]. [Accessed 20th August 2013].

HSU, Y. L., Chiu, S. M., Sung, Y.C., Yang, K.Y., and Chu, C.W., 2010. Anti-sticking Properties of PVD CrWN, CrO and ZrO Coatings on Medical Electrode Application *Defect and Diffusion Forum,* 279-301.

Young, B., and Heath, J.W, 2000. *Wheather's Functional Histology a text and colour atlas*, Harcourt Publishers Limited 2000.

Zhang, D. and Arola, D. D. 2004. Applications of digital image correlation to biological tissues. *Journal of Biomedical Optics,* 9, 691-699.

Zhang, D., Eggleton, C. and Arola, D. 2002. Evaluating the mechanical behavior of arterial tissue using digital image correlation. *Experimental Mechanics,* 42, 409-416.

Zhao, S. Z., Xu, X. Y., Hughes, A. D., Thom, S. A., Stanton, A. V., Ariff, B. and Long, Q. 2000. Blood flow and vessel mechanics in a physiologically realistic model of a human carotid arterial bifurcation. *Journal of Biomechanics,* 33, 975-984.

11 Appendix A Matlab Code

The code presented below was the code used to modify the ASCII files exported from the DIC software, developed to allow surface plots to be produced.

```
Dist=data ( 1 , : ) ;
Data ( 1 , : ) = [ ] ;
For i = 2 : 30 ;
        data ( i , : ) = [ ] ;
        data ( i , : ) = [ ] ;
end
data ( 31 , : ) = [ ] ;
time = ( 0 : 0 . 2 : 5 . 8 ) ;
pcolor ( dist, time, data ) ;
xlabel ( 'Distance (mm)' ) ;
ylabel ( 'Time (seconds)' ) ;
clear
clc
```

12 Appendix B Z displacement of device jaws

Within Chapter 4 the z displacement for the device jaws was presented, the data for the shims not included within Chapter 5 is presented here.

12.1 Displacement changes
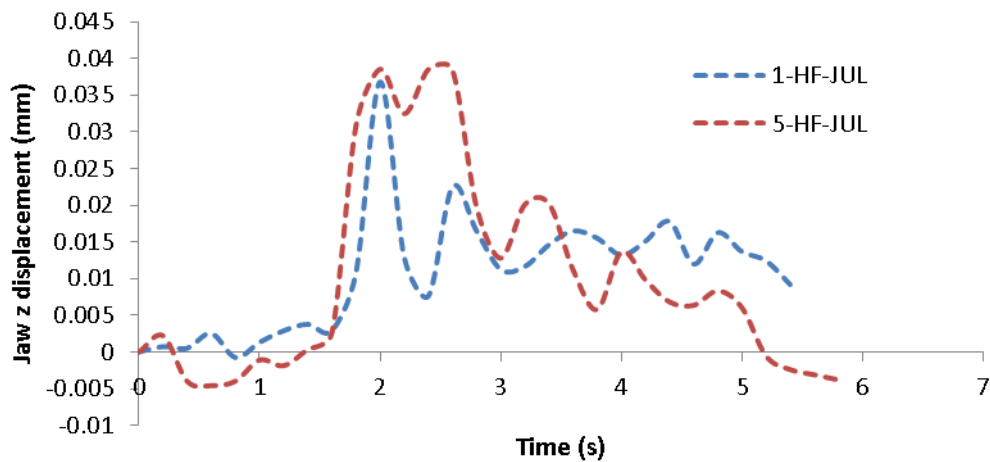
Figure 12-1 The z displacement of the jaws during the sealing process using the HF grooved shim. A positive change in displacement indicates an increase in the shim gap. The different coloured lines refer to different seals performed, with dotted lines referring to specimens sealed at 25mm from the bifurcation and solid lines showing seals performed at 65mm from the bifurcation.
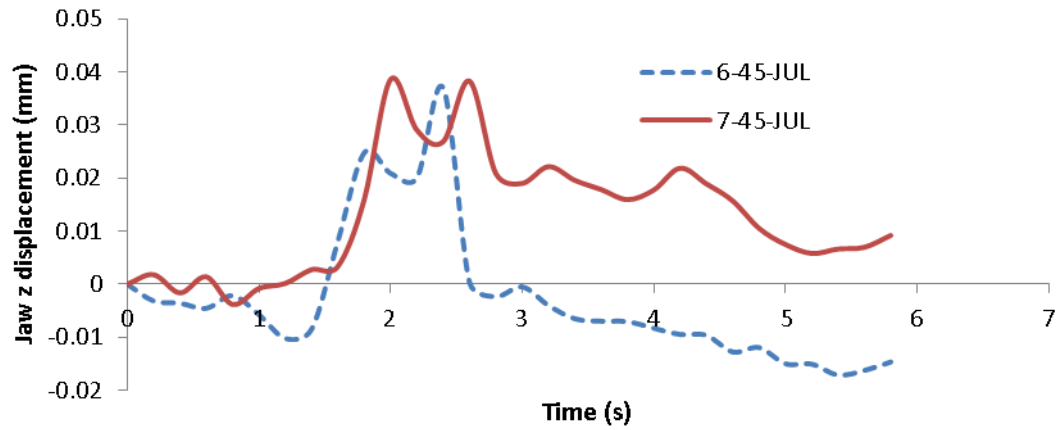
Figure 12-2 The z displacement of the jaws during the sealing process using the 45° grooved shim. A positive change in displacement indicates an increase in the shim gap. The different coloured lines refer to different seals performed, with dotted lines referring to specimens sealed at 25mm from the bifurcation and solid lines showing seals performed at 65mm from the bifurcation.
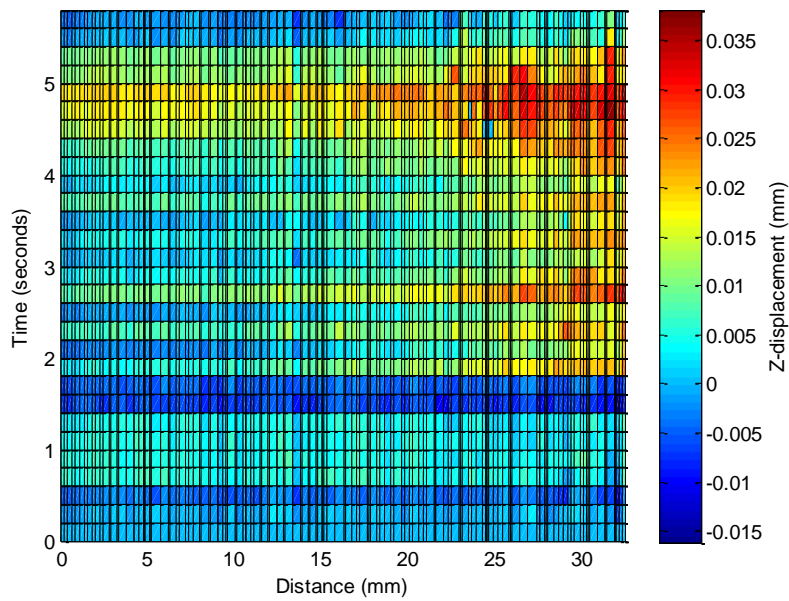
12.2 Surface Plots
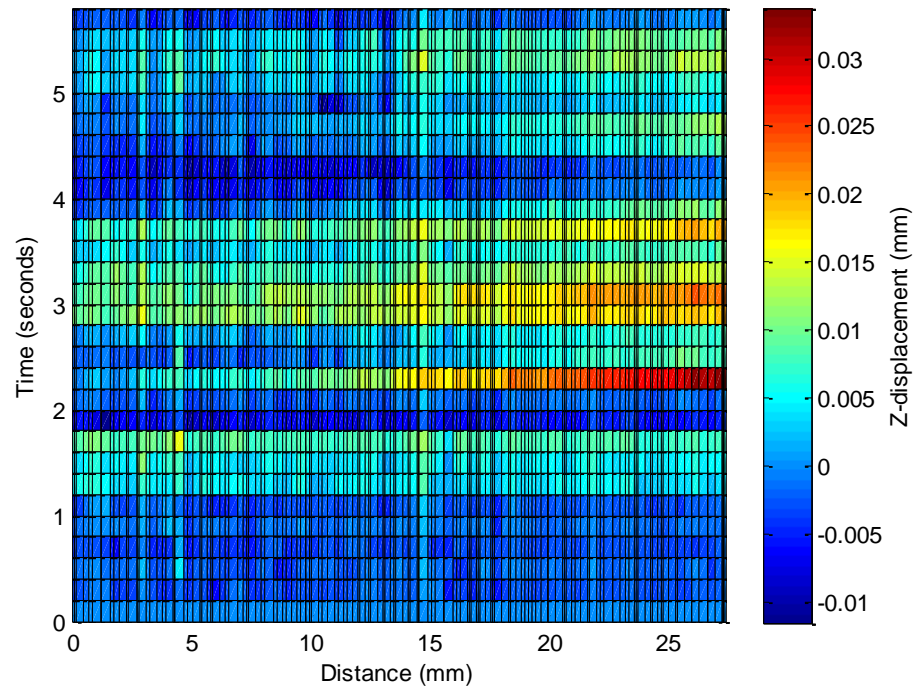
Figure 12-3 Surface plots showing the variation in z displacement along the length of the jaw for the sealing process. Distance refers to the position along the length of the jaw, with 0 indicating the position closest to the handles of the device. Example shown was sealed using the 45° grooved shims, sample number 1-CC-JUL
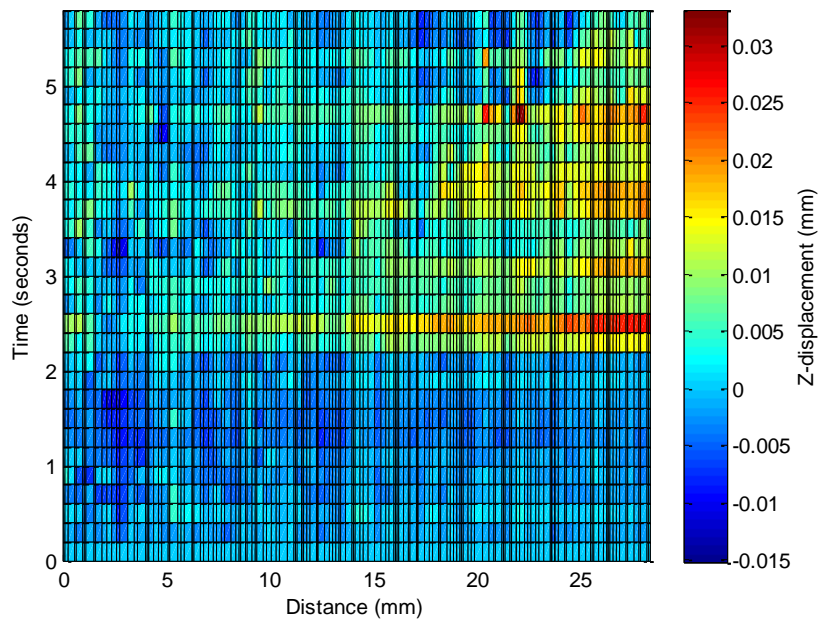
Figure 12-4 Surface plots showing the variation in z displacement along the length of the jaw for the sealing process. Distance refers to the position along the length of the jaw, with 0 indicating the position closest to the handles of the device. Example shown was sealed using the 45° grooved shims, sample number 2-CC-JUL.
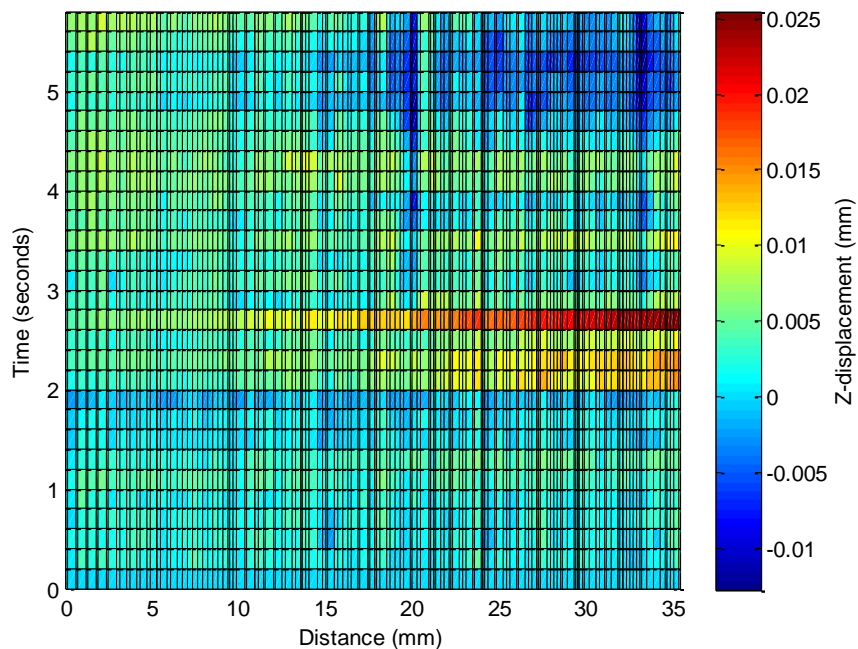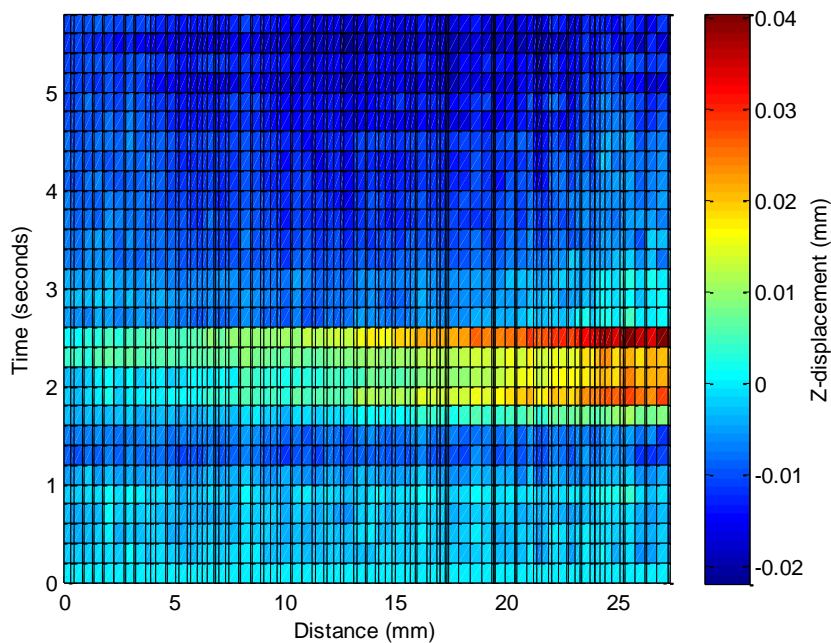

Figure 12-5 Surface plots showing the variation in z displacement along the length of the jaw for the sealing process. Distance refers to the position along the length of the jaw, with 0 indicating the position closest to the handles of the device. Example shown was sealed using the 45° grooved shims, sample number 6-CC-JUL.
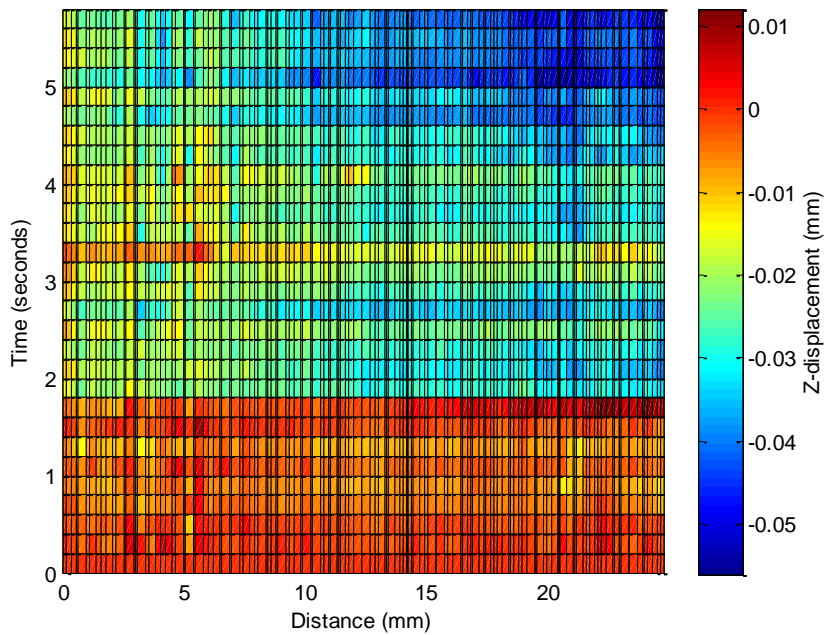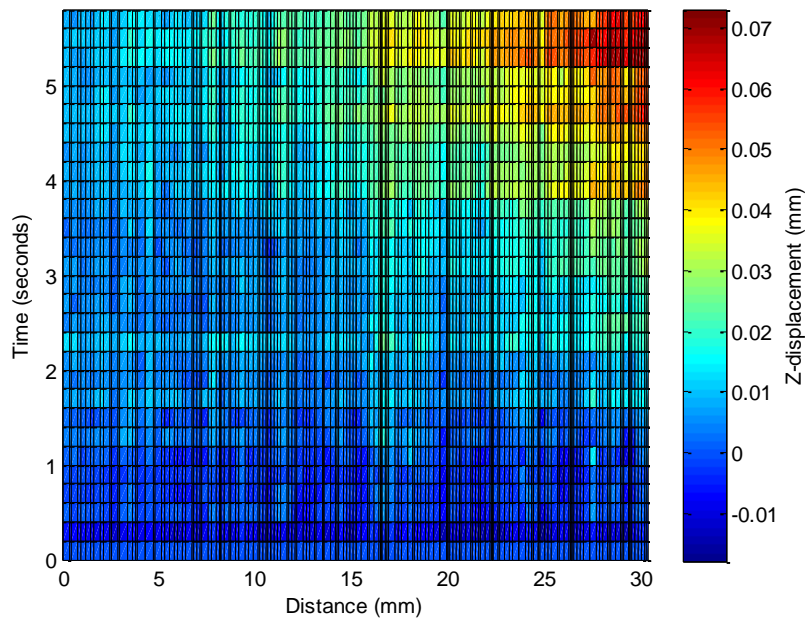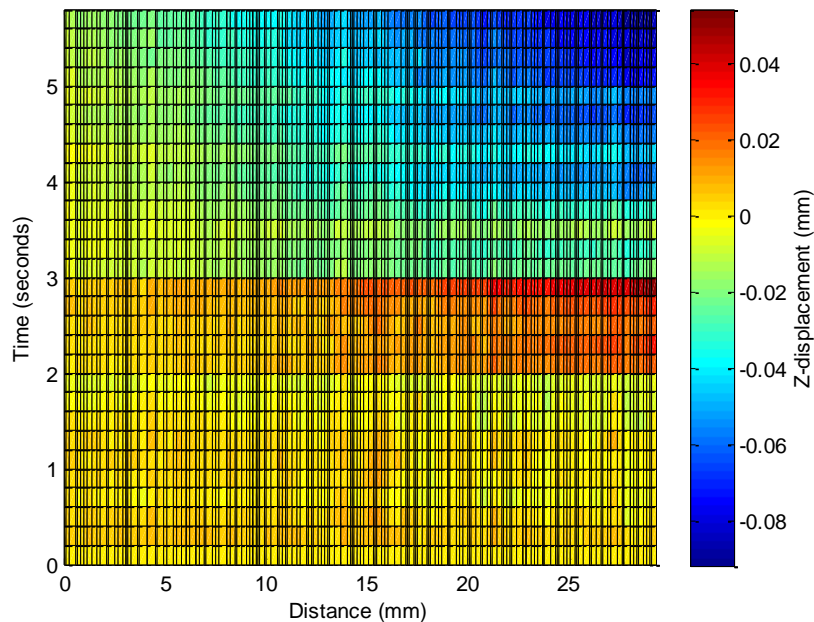
Figure 12-6 Surface plots showing the variation in z displacement along the length of the jaw for the sealing process. Distance refers to the position along the length of the jaw, with 0 indicating the position closest to the handles of the device. Example shown was sealed using the 45° grooved shims, sample number 3-NA-JUL.
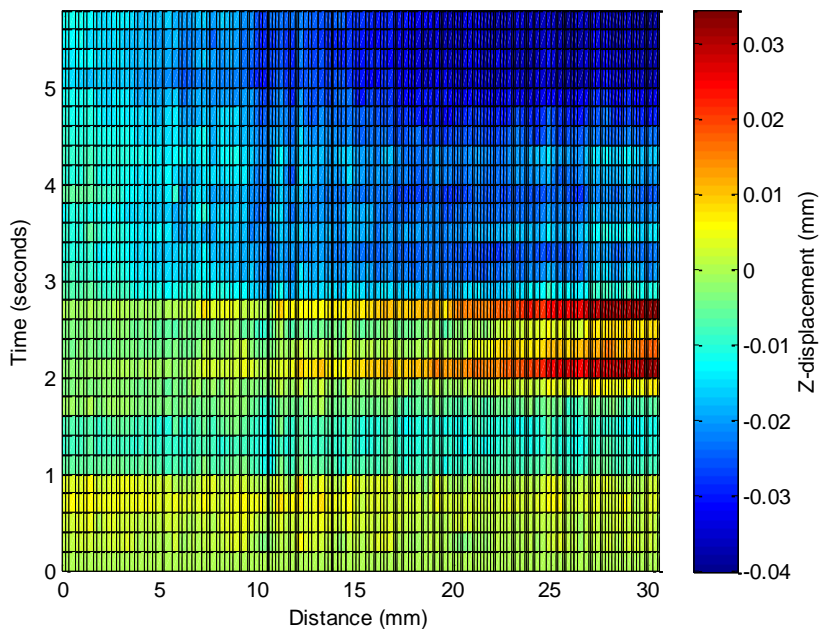
Figure 12-7 Surface plots showing the variation in z displacement along the length of the jaw for the sealing process. Distance refers to the position along the length of the jaw, with 0 indicating the position closest to the handles of the device. Example shown was sealed using the 45° grooved shims, sample number 4-NA-JUL.
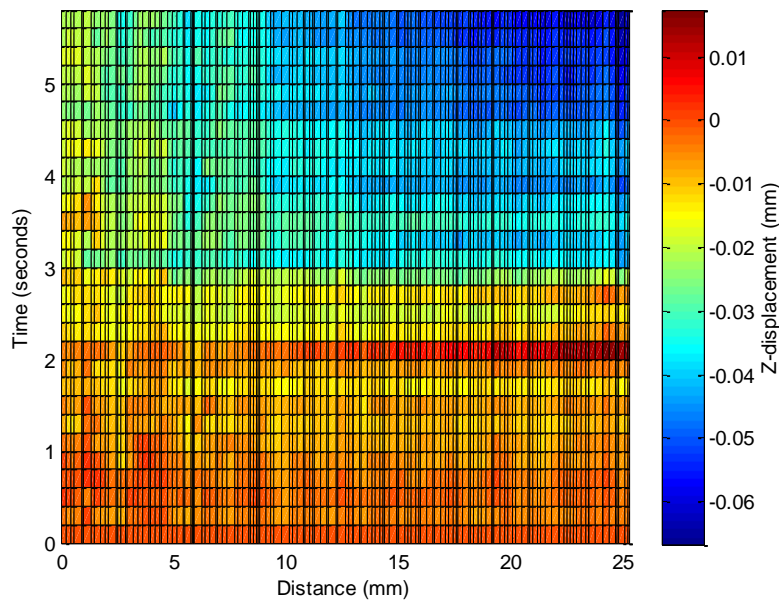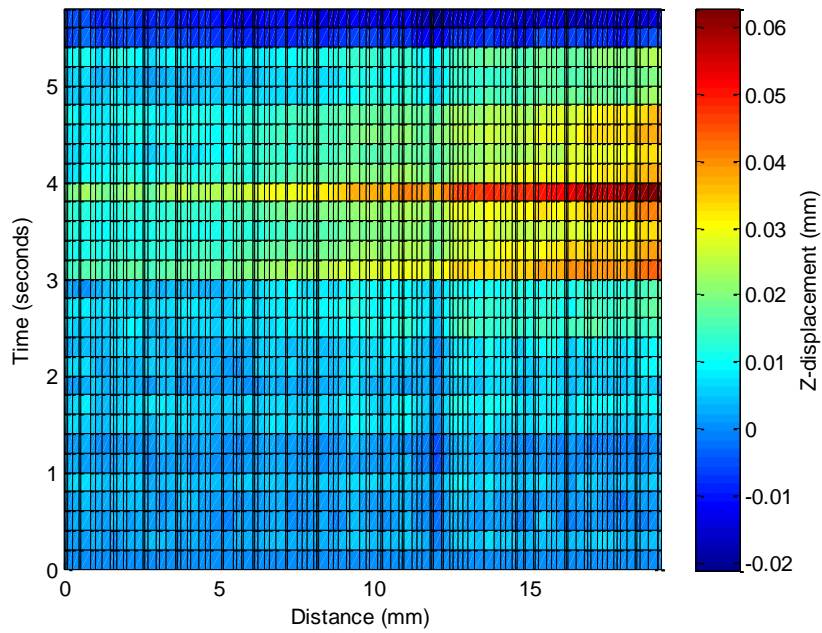
Figure 12-8 Surface plots showing the variation in z displacement along the length of the jaw for the sealing process. Distance refers to the position along the length of the jaw, with 0 indicating the position closest to the handles of the device. Example shown was sealed using the 45° grooved shims, sample number 5-NA-JUL.
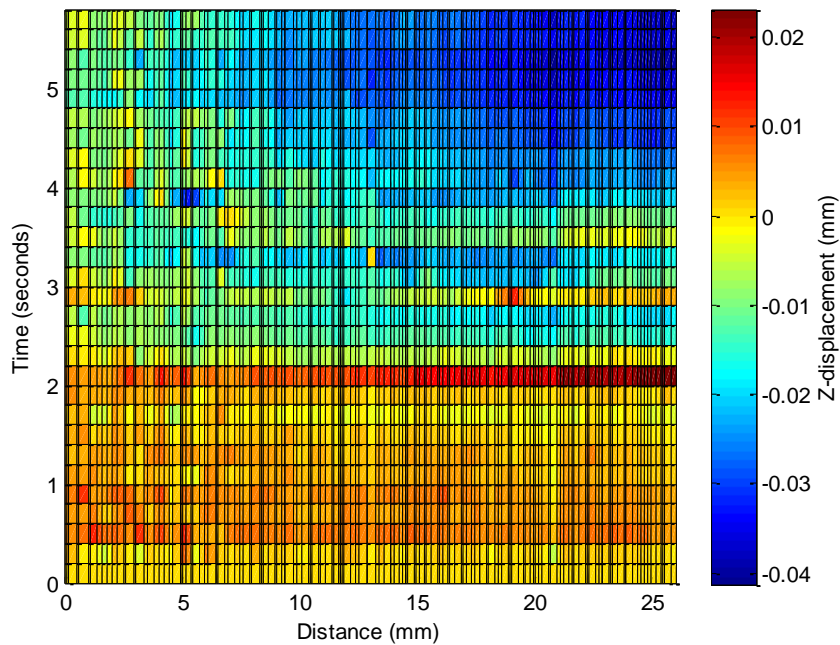
Figure 12-9 A surface plots showing the variation in z displacement along the length of the jaw for the sealing process. Distance refers to the position along the length of the jaw, with 0 indicating the position closest to the handles of the device. Example shown was sealed using the 45° grooved shims, sample number 6-NA-JUL.
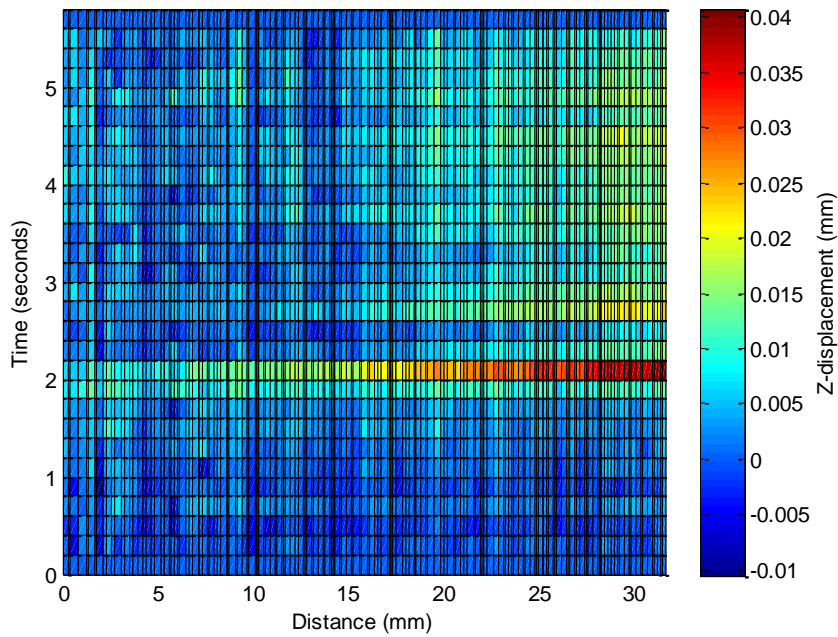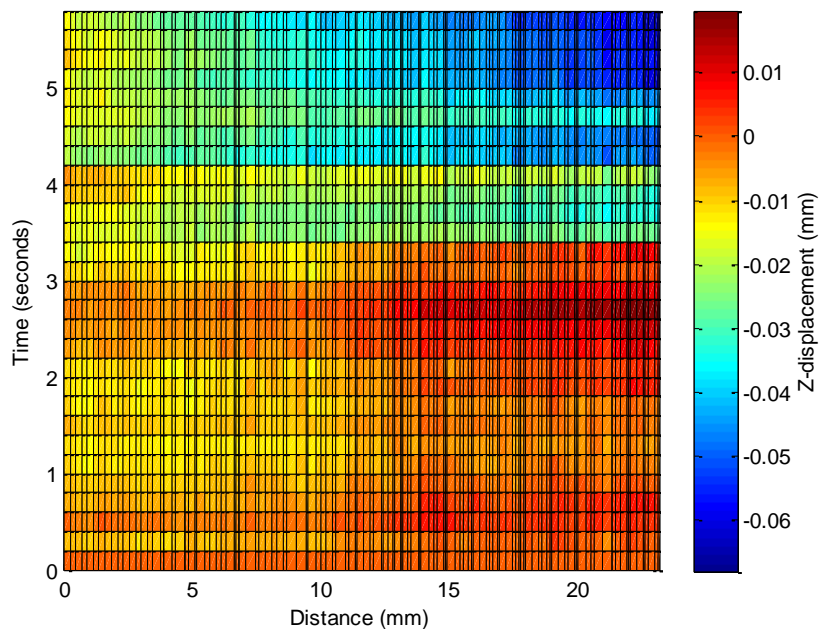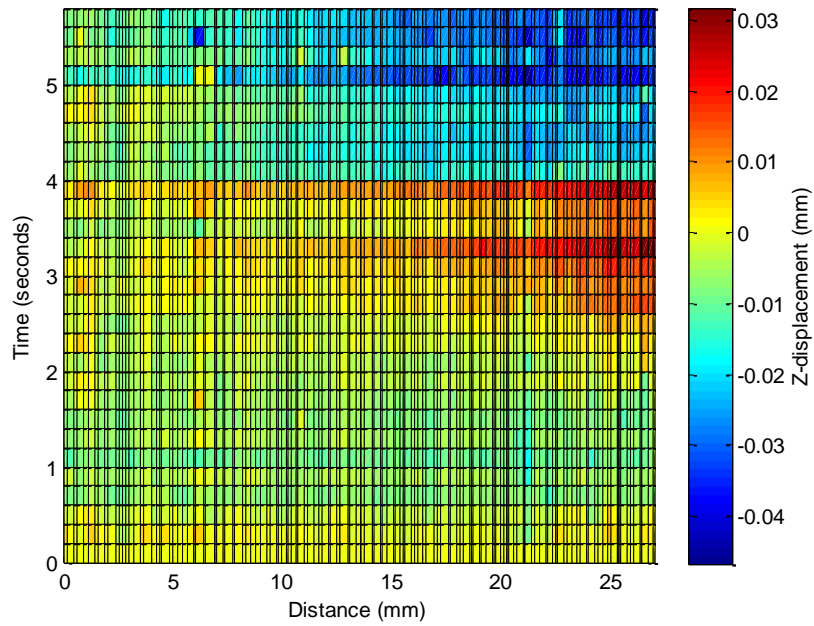
Figure 12-10 Surface plots showing the variation in z displacement along the length of the jaw for the sealing process. Distance refers to the position along the length of the jaw, with 0 indicating the position closest to the handles of the device. Example shown was sealed using the 45° grooved shims, sample number 1-HF-JUL.
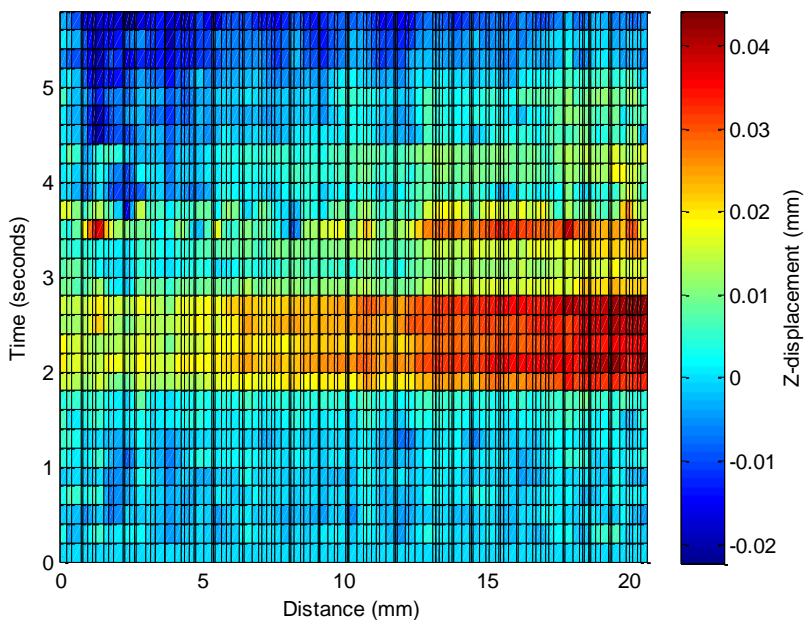
Figure 12-11 Surface plots showing the variation in z displacement along the length of the jaw for the sealing process. Distance refers to the position along the length of the jaw, with 0 indicating the position closest to the handles of the device. Example shown was sealed using the 45° grooved shims, sample number 5-HF-JUL.

Figure 12-12 Surface plots showing the variation in z displacement along the length of the jaw for the sealing process. Distance refers to the position along the length of the jaw, with 0 indicating the position closest to the handles of the device. Example shown was sealed using the 45° grooved shims, sample number 4-45-JUL.


Figure 12-13 Surface plots showing the variation in z displacement along the length of the jaw for the sealing process. Distance refers to the position along the length of the jaw, with 0 indicating the position closest to the handles of the device. Example shown was sealed using the 45° grooved shims, sample number 6-45-JUL.

Figure 12-14 Surface plots showing the variation in z displacement along the length of the jaw for the sealing process. Distance refers to the position along the length of the jaw, with 0 indicating the position closest to the handles of the device. Example shown was sealed using the 45° grooved shims, sample number 1-OR-JUL.


Figure 12-15 Surface plots showing the variation in z displacement along the length of the jaw for the sealing process. Distance refers to the position along the length of the jaw, with 0 indicating the position closest to the handles of the device. Example shown was sealed using the 45° grooved shims, sample number 2-OR-JUL.

Figure 12-16 Surface plots showing the variation in z displacement along the length of the jaw for the sealing process. Distance refers to the position along the length of the jaw, with 0 indicating the position closest to the handles of the device. Example shown was sealed using the 45° grooved shims, sample number 5-OR-JUL.

Figure 12-17 Surface plots showing the variation in z displacement along the length of the jaw for the sealing process. Distance refers to the position along the length of the jaw, with 0 indicating the position closest to the handles of the device. Example shown was sealed using the 45° grooved shims, sample number 6-OR-JUL.

Figure 12-18 Surface plots showing the variation in z displacement along the length of the jaw for the sealing process. Distance refers to the position along the length of the jaw, with 0 indicating the position closest to the handles of the device. Example shown was sealed using the 45° grooved shims, sample number 7-OR-JUL.

13 Appendix C Y displacement of tissue

Within Chapter 4 the y displacement of the tissue was presented, the data is not included as part of that chapter is now presented.

13.1 Displacement Changes
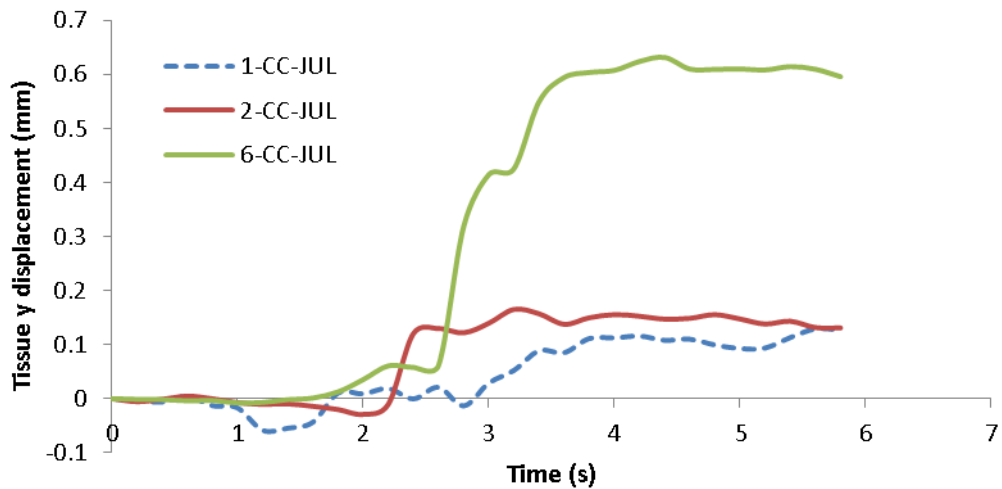
Figure 13-1 The y displacement of the tissue during the sealing process for the combination shims. A positive change in displacement indicates the tissue moving closer to the device. The diff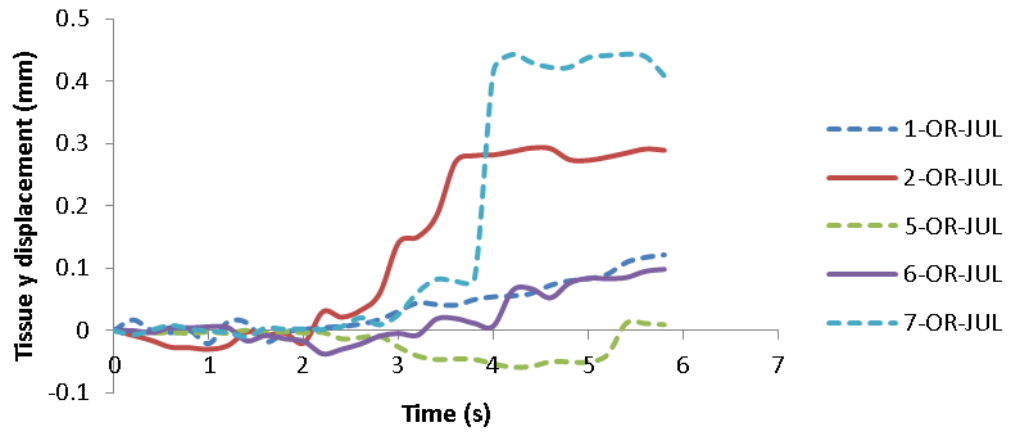erent coloured lines refer to different seals performed, with dotted lines referring to specimens sealed at 25mm from the bifurcation and solid lines showing seals performed at 65mm from the bifurcation.
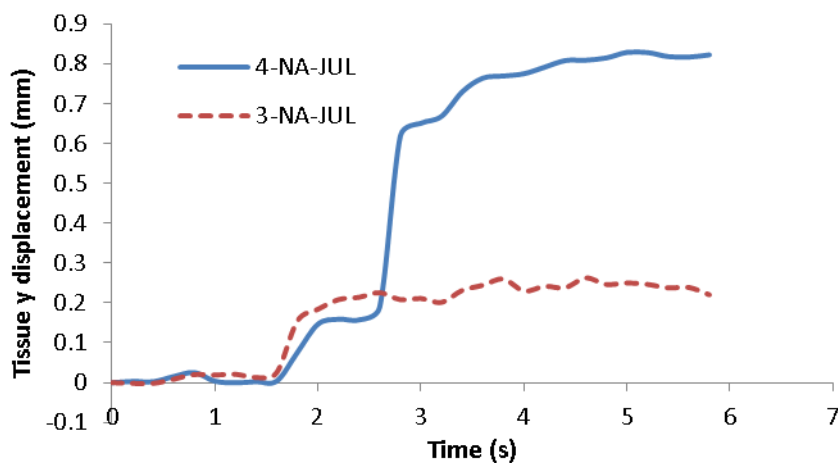

Figure 13-2 The y displacement of the tissue during the sealing process for the narrow grooved shims. A positive change in displacement indicates the tissue moving closer to the device. The different coloured lines refer to different seals performed, with dotted lines referring to specimens

sealed at 25mm from the bifurcation and solid lines showing seals performed at 65mm from the bifurcation.
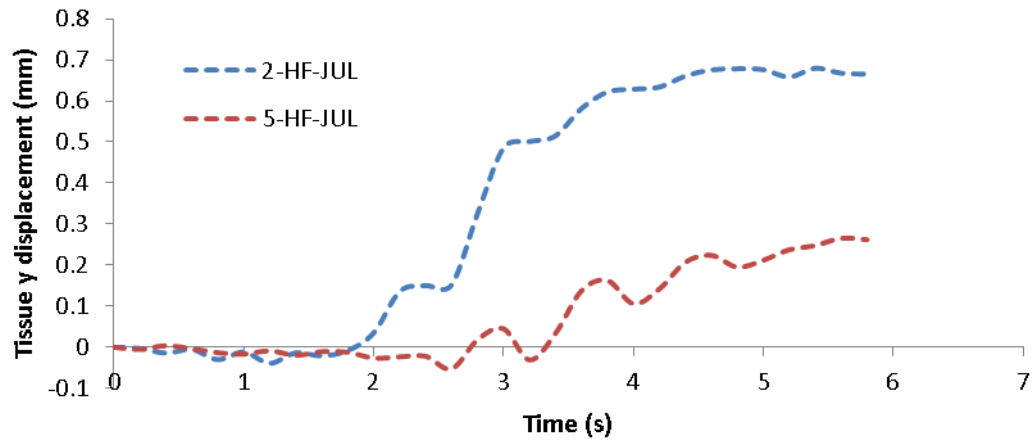

Figure 13-3 The y displacement of the tissue during the sealing process for the HF shims. A positive change in displacement indicates the tissue moving closer to the device. The different coloured lines refer to different seals performed, with dotted lines referring to specimens sealed at 25mm from the bifurcation and solid lines showing seals performed at 65mm from the bifurcation.
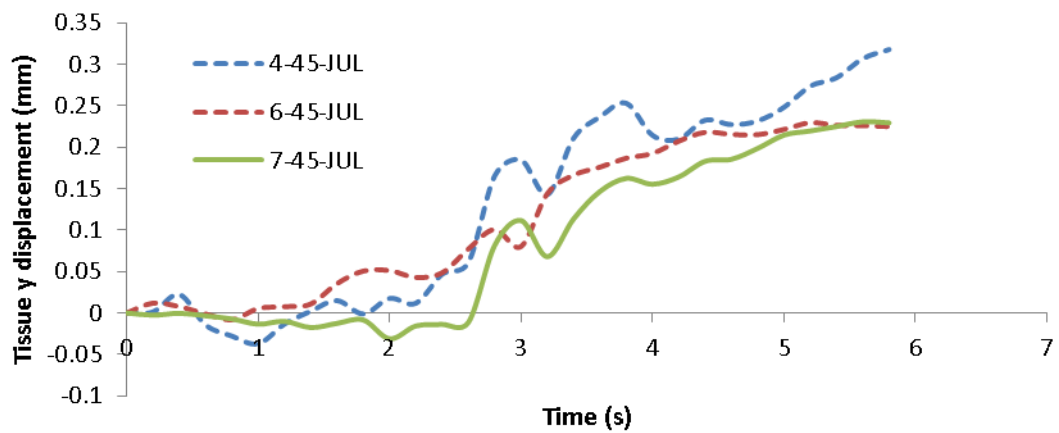
Figure 13-4 The y displacement of the tissue during the sealing process for the 45° grooved shims. A positive change in displacement indicates the tissue moving closer to the device. The different coloured lines refer to different seals performed, with dotted lines referring to specimens sealed at 25mm from the bifurcation and solid lines showing seals performed at 65mm from the bifurcation.

Figure 13-5 The y displacement of the tissue during the sealing process for the original shims. A positive change in displacement indicates the tissue moving closer to the device. The different coloured lines refer to different seals performed, with dotted lines referring to specimens sealed at 25mm from the bifurcation and solid lines showing seals performed at 65mm from the bifurcation.
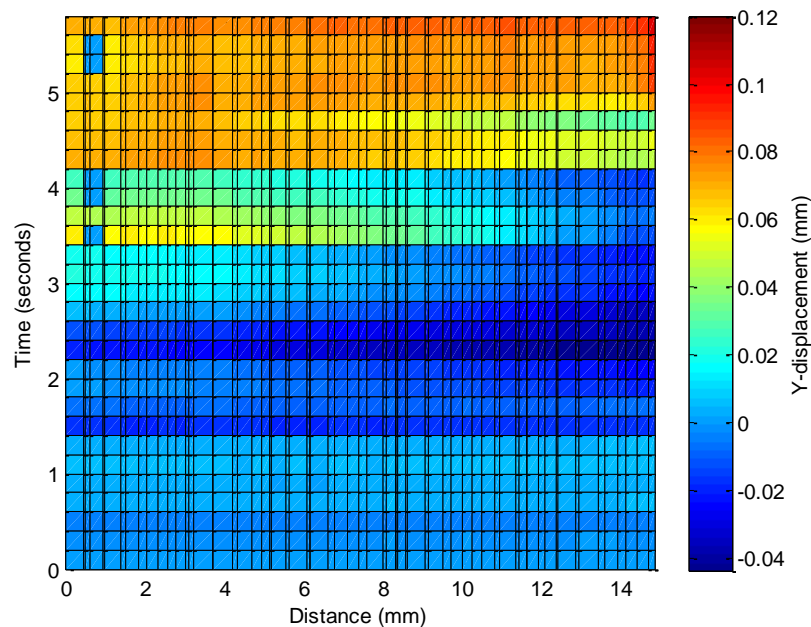
.

13.2 Surface Plots
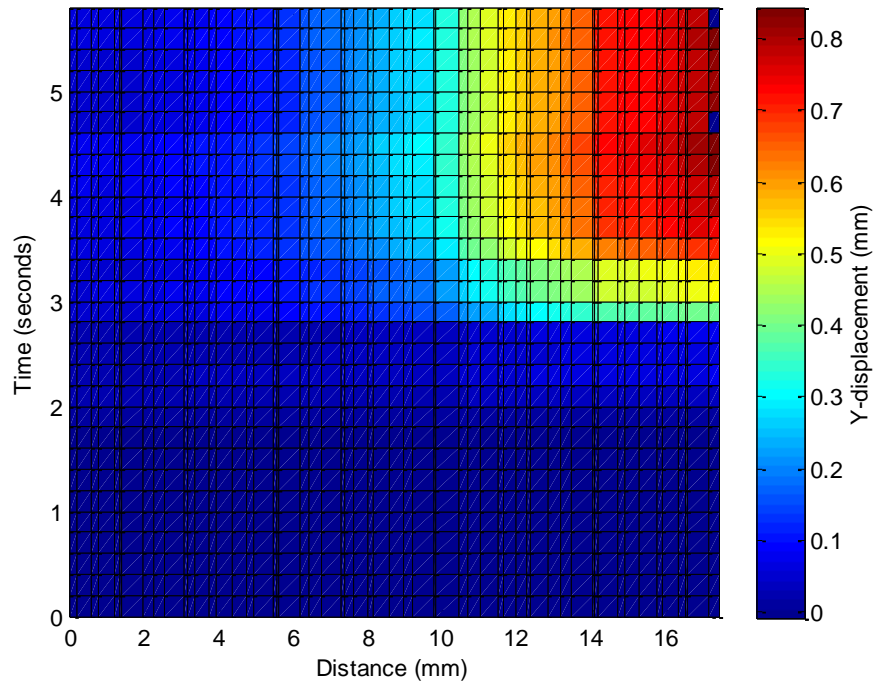
Figure 13-6 Surface plots showing the variation in y displacement along the length of the vessel for the sealing process. Distance refers to the position along the length of the vessel, with 0 indicating the position furthest from the device. Example shown was sealed using the original shims, sample number 6-CC-JUL.
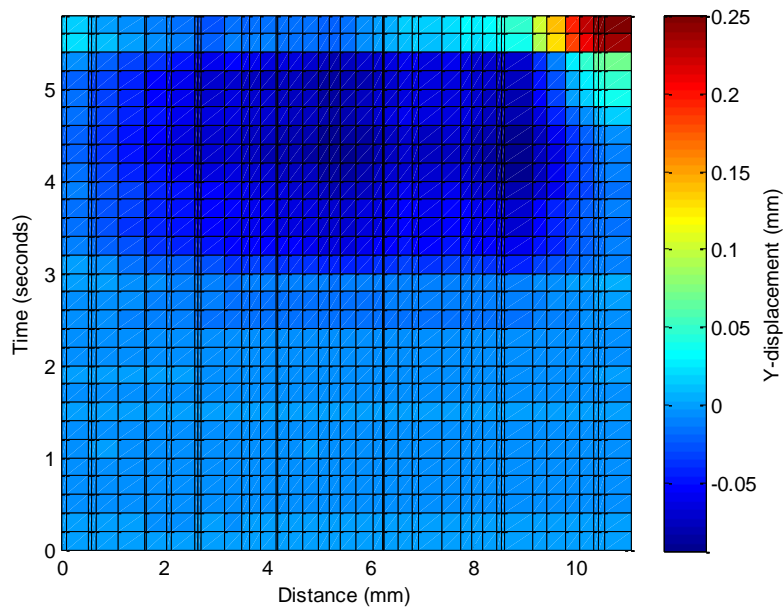
Figure 13-7 Surface plots showing the variation in y displacement along the length of the vessel for the sealing process. Distance refers to the position along the length of the vessel, with 0 indicating the position furthest from the device. Example shown was sealed using the original shims, sample number 5-OR-JUL.

Figure 13-8 Surface plots showing the variation in y displacement along the length of the vessel for the sealing process. Distance refers to the position along the length of the vessel, with 0 indicating the position furthest from the device. Example shown was sealed using the original shims, sample number 6-OR-JUL.

## 14 Appendix D Tissue and jaw displacement

In Chapter 4 the data exploring the relationship between the pulses of the jaws and the pulses of the tissue was presented, the data not included within the results section is now presented.
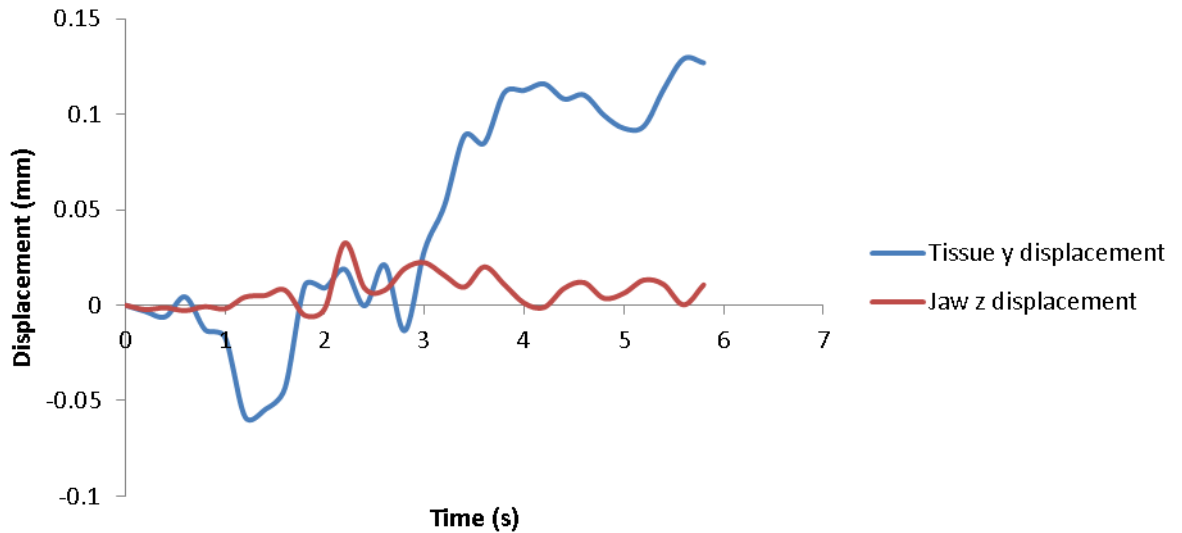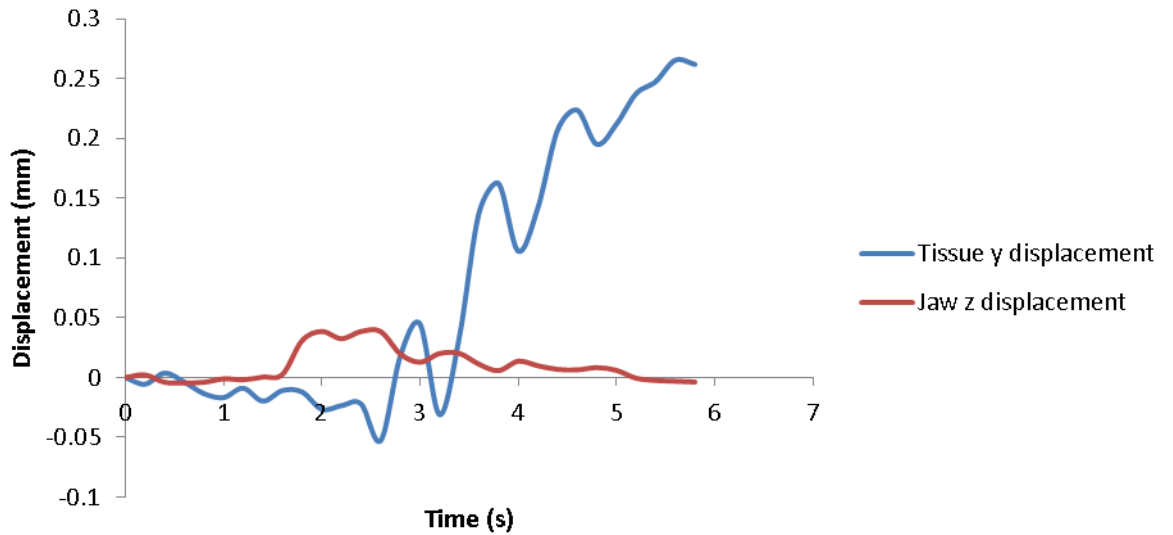

Figure 14-1 The y displacement of the tissue and the z displacement of the jaws during the sealing process for the combination shim, sample 1-CC-JUL. A positive change in tissue displacement indicates the tissue moving closer to the device, and a positive change in jaw displacement indicates an increase in shim gap.
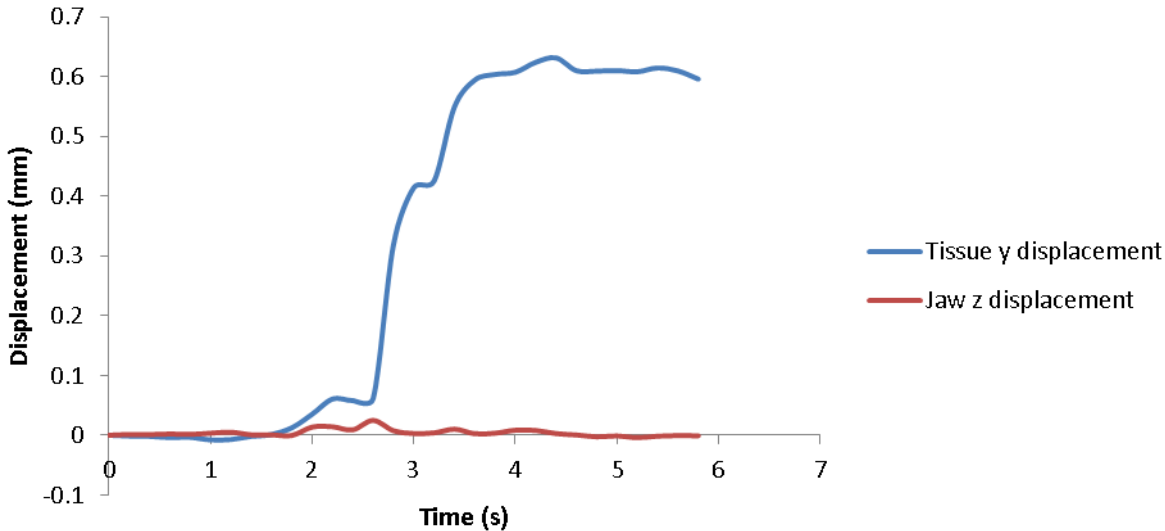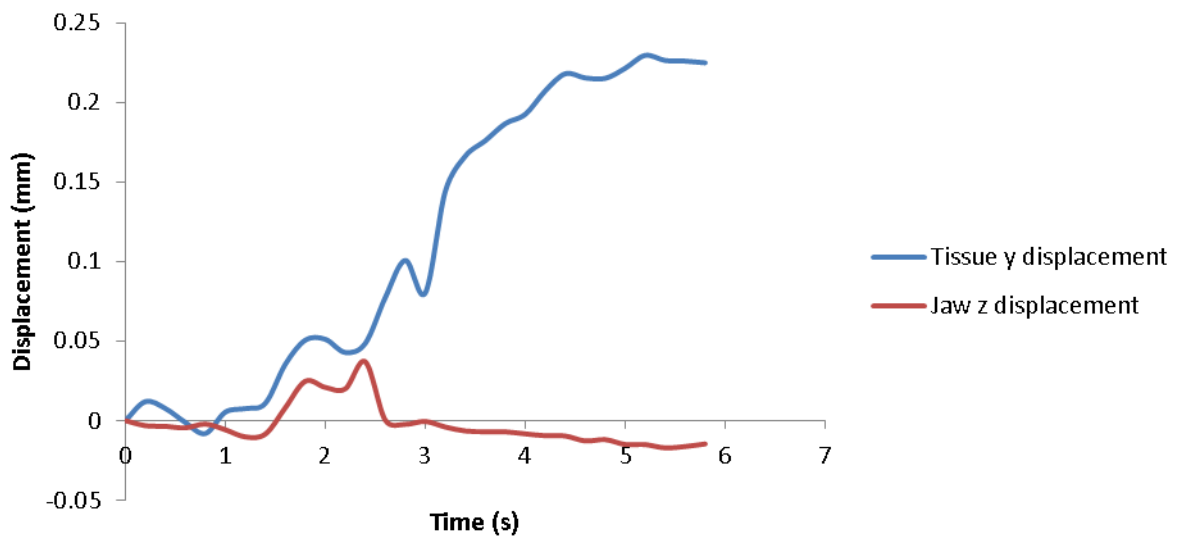
Figure 14-2 The y displacement of the tissue and the z displacement of the jaws during the sealing process for the combination shim, sample 6-CC-JUL. A positive change in tissue displacement indicates the tissue moving closer to the device, and a positive change in jaw displacement indicates an increase in shim gap.
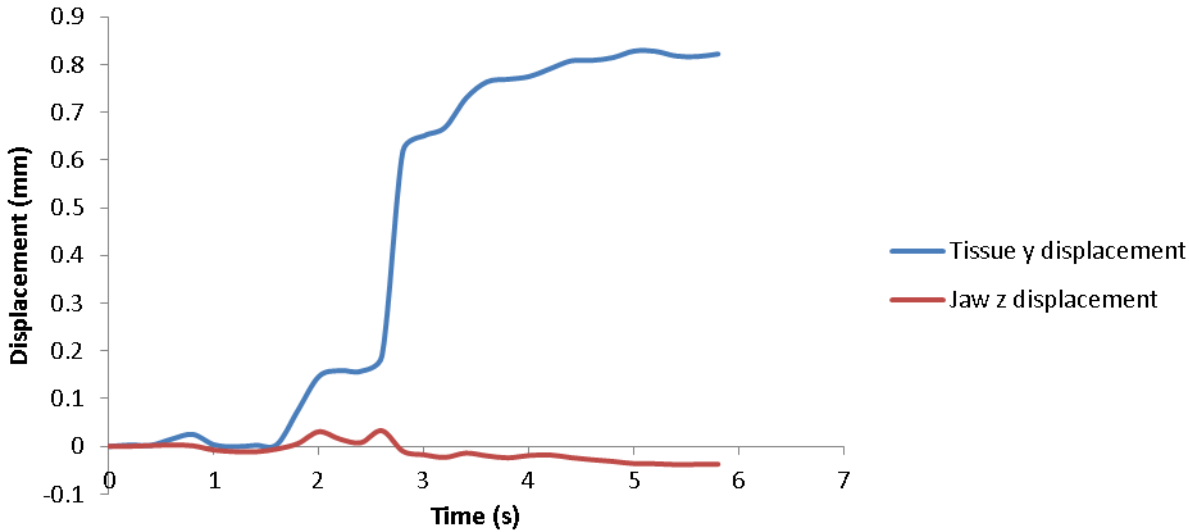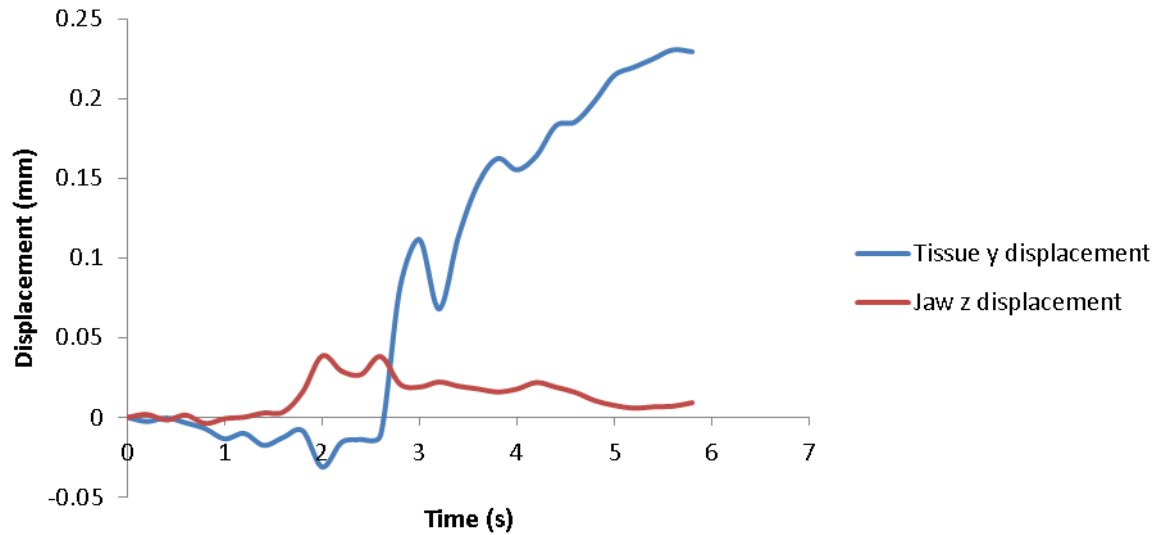

Figure 14-3 The y displacement of the tissue and the z displacement of the jaws during the sealing process for the combination shim, sample 4-NA-JUL. A positive change in tissue displacement indicates the tissue moving closer to the device, and a positive change in jaw displacement indicates an increase in shim gap.
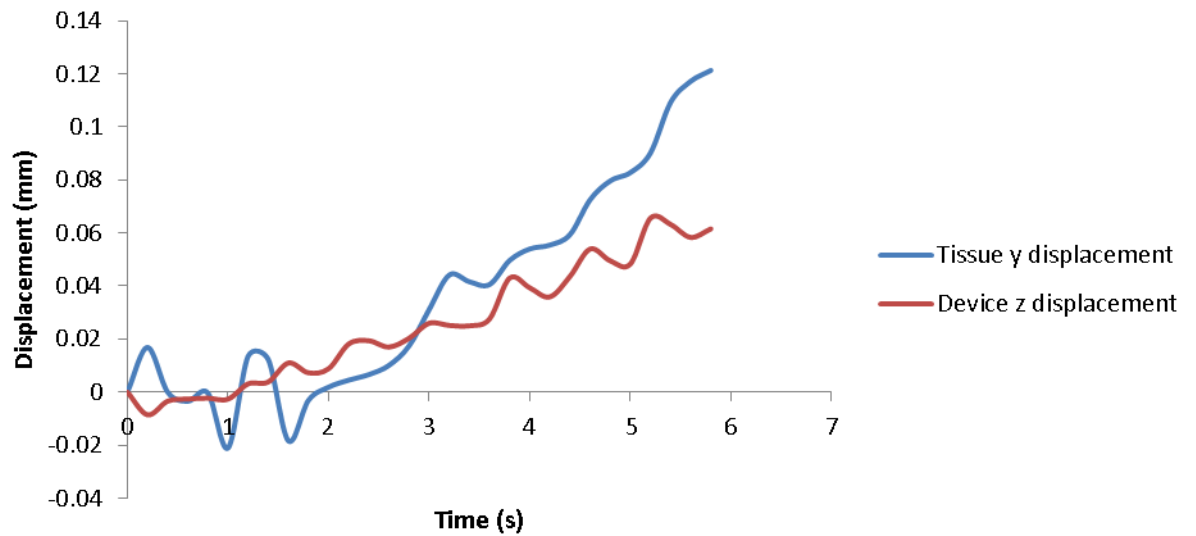
Figure 14-4 The y displacement of the tissue and the z displacement of the jaws during the sealing process for the combination shim, sample 5-HF-JUL. A positive change in tissue displacement indicates the tissue moving closer to the device, and a positive change in jaw displacement indicates an increase in shim gap.
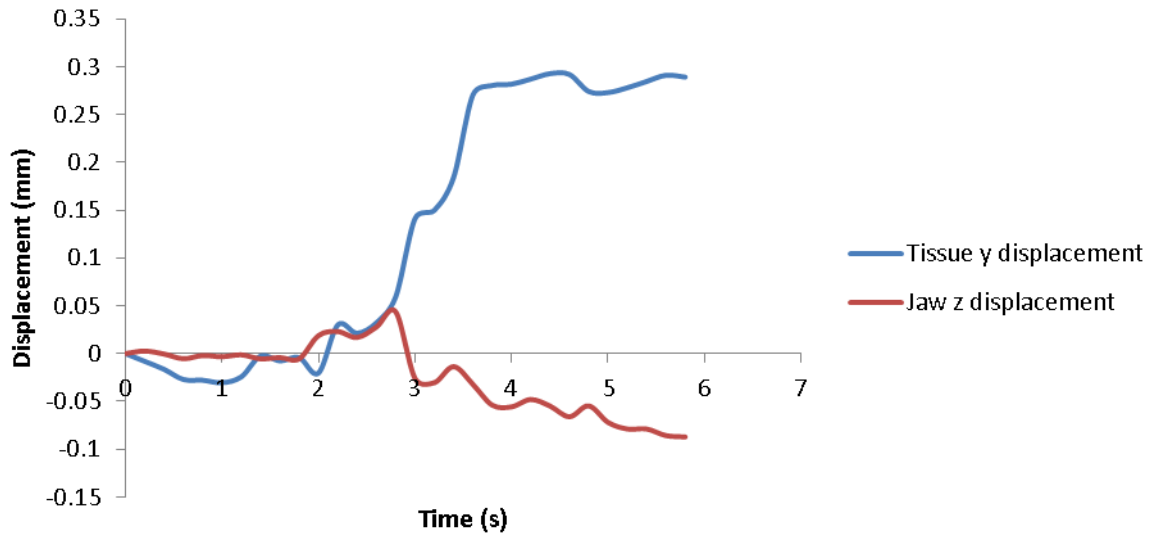

Figure 14-5 The y displacement of the tissue and the z displacement of the jaws during the sealing process for the combination shim, sample 6-45-JUL. A positive change in tissue displacement indicates the tissue moving closer to the device, and a positive change in jaw displacement indicates an increase in shim gap.
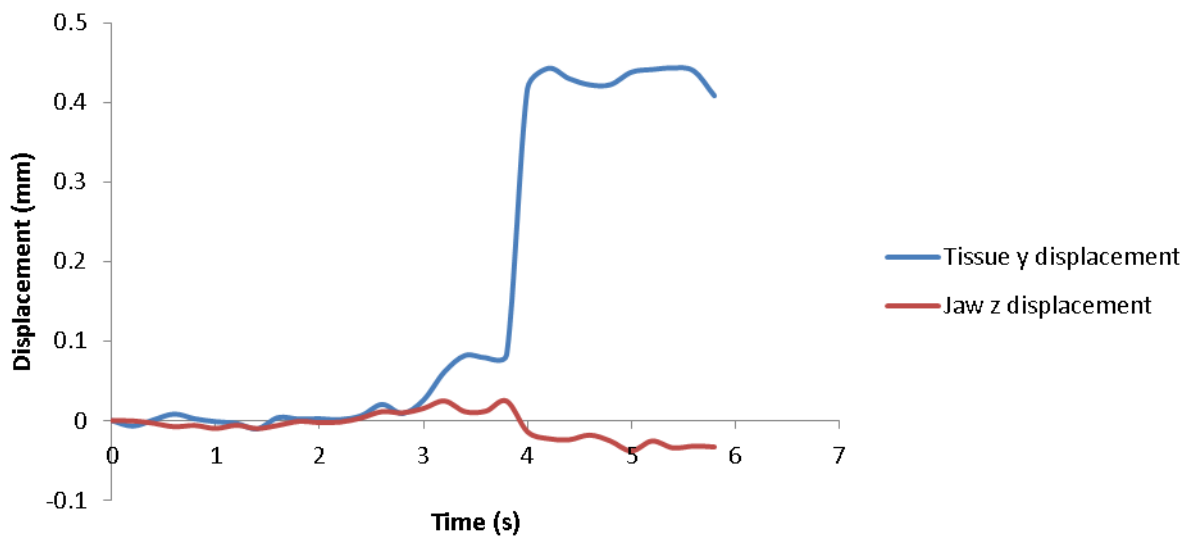
Figure 14-6 The y displacement of the tissue and the z displacement of the jaws during the sealing process for the combination shim, sample 7-45-JUL. A positive change in tissue displacement indicates the tissue moving closer to the device, and a positive change in jaw displacement indicates an increase in shim gap.

Figure 14-7 The y displacement of the tissue and the z displacement of the jaws during the sealing process for the combination shim, sample 1-OR -JUL. A positive change in tissue displacement indicates the tissue moving closer to the device, and a positive change in jaw displacement indicates an increase in shim gap.

Figure 14-8 The y displacement of the tissue and the z displacement of the jaws during the sealing process for the combination shim, sample 2-OR-JUL. A positive change in tissue displacement indicates the tissue moving closer to the device, and a positive change in jaw displacement indicates an increase in shim gap.

Figure 14-9 The y displacement of the tissue and the z displacement of the jaws during the sealing process for the combination shim, sample 7-OR-JUL. A positive change in tissue displacement indicates the tissue moving closer to the device, and a positive change in jaw displacement indicates an increase in shim gap.

15 Appendix E Strain of tissue
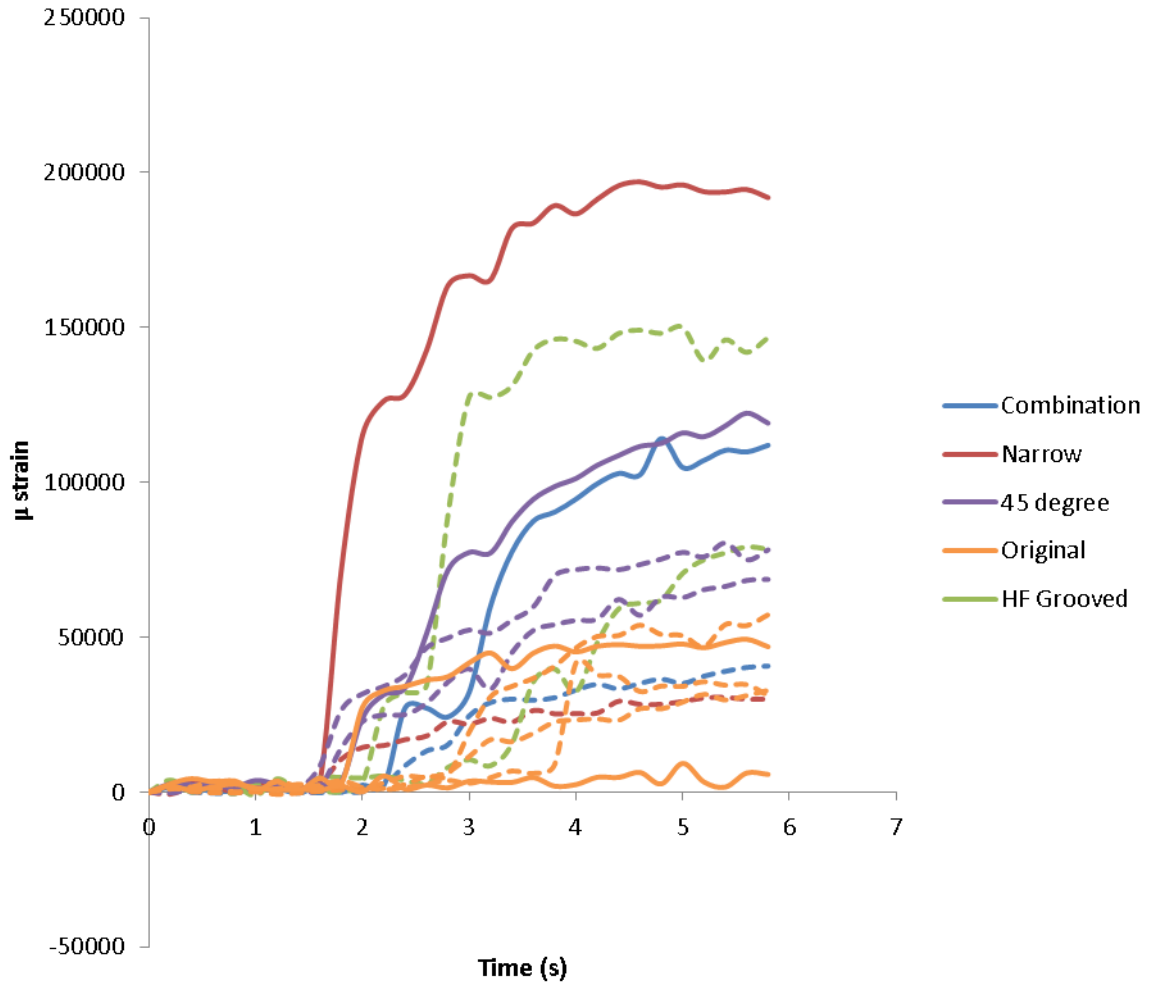
Figure 15-1 The principal strain of the tissue during the sealing process for various shims. A positive change in displacement indicates the tissue moving closer to the device. The different coloured lines refer to different shims tested, with dotted lines referring to specimens sealed at 25mm from the bifurcation and solid lines showing seals performed at 65mm from the bifurcation.